

AD-A198 053

Technical Report 1009

# Structural Dynamics Model of a Cartesian Robot

DTIC  
ELECTE  
AUG 02 1988  
S D

Alfonso Garcia Reynoso

MIT Artificial Intelligence Laboratory

**DISTRIBUTION STATEMENT A**  
Approved for public release;  
Distribution Unlimited

UNCLASSIFIED

SECURITY CLASSIFICATION OF THIS PAGE (When Data Entered)

REPORT DOCUMENTATION PAGE		READ INSTRUCTIONS BEFORE COMPLETING FORM
1. REPORT NUMBER AI-TR 1009	2. GOVT ACCESSION NO.	3. RECIPIENT'S CATALOG NUMBER
4. TITLE (and Subtitle) Structural Dynamics Model of a Cartesian Robot		5. TYPE OF REPORT & PERIOD COVERED technical report
		6. PERFORMING ORG. REPORT NUMBER
7. AUTHOR(s) Alfonso Garcia Reynoso		8. CONTRACT OR GRANT NUMBER(s) N00014-85-K-0124
9. PERFORMING ORGANIZATION NAME AND ADDRESS Artificial Intelligence Laboratory 545 Technology Square Cambridge, MA 02139		10. PROGRAM ELEMENT, PROJECT, TASK AREA & WORK UNIT NUMBERS
11. CONTROLLING OFFICE NAME AND ADDRESS Advanced Research Projects Agency 1400 Wilson Blvd. Arlington, VA 22209		12. REPORT DATE October 1985
		13. NUMBER OF PAGES 218
14. MONITORING AGENCY NAME & ADDRESS (if different from Controlling Office) Office of Naval Research Information Systems Arlington, VA 22217		15. SECURITY CLASS. (of this report)
		15a. DECLASSIFICATION/DOWNGRADING SCHEDULE
16. DISTRIBUTION STATEMENT (of this Report)  Distribution is unlimited.		
17. DISTRIBUTION STATEMENT (of the abstract entered in Block 20, if different from Report)		
18. SUPPLEMENTARY NOTES  None		
19. KEY WORDS (Continue on reverse side if necessary and identify by block number)  vibration response component mode synthesis system modeling		
20. ABSTRACT (Continue on reverse side if necessary and identify by block number)  Methods are developed for predicting vibration response characteristics of systems which change configuration during operation. A cartesian robot, an example of such a position-dependent system, served as a test case for these methods and was studied in detail.  The chosen system model was formulated using the technique of Component Mode Synthesis (CMS). The model assumes that the system is slowly		

DD FORM 1473  
1 JAN 73EDITION OF 1 NOV 65 IS OBSOLETE  
S/N 0:02-014-66011

UNCLASSIFIED

SECURITY CLASSIFICATION OF THIS PAGE (When Data Entered)

Block 20 cont.

varying, and connects the carriages to each other and to the robot structure at the slowly-varying connection points. The modal data required for each component is obtained experimentally in order to get a realistic model. The analysis results in prediction of vibrations that are produced by the inertia forces as well as gravity and friction forces which arise when the robot carriages move with some prescribed motion.

Computer simulations and experimental determinations are conducted in order to calculate the vibrations at the robot end-effector. Comparisons are shown to validate the model in two ways: for fixed-configuration the mode shapes and natural frequencies are examined, and then for changing configuration the residual vibration at the end of the move is evaluated.

A preliminary study was done on a geometrically nonlinear system which also has position-dependency. The system consisted of a flexible four-bar linkage with elastic input and output shafts. The behavior of the rocker-beam is analyzed for different boundary conditions to show how some limiting cases are obtained. A dimensional analysis leads to an evaluation of the consequences of dynamic similarity on the resulting vibration.



Accession For	
NTIS CRA&I	<input checked="checked" type="checkbox"/>
DTIC TAB	<input type="checkbox"/>
Unannounced	<input type="checkbox"/>
Justification	
By	
Distribution /	
Availability Codes	
Dist	Avail and/or Special
A-1	

# Structural Dynamics Model of a Cartesian Robot

by

**Alfonso García Reynoso**

BSME Instituto Tecnológico de Veracruz

(1967)

MSME Instituto Tecnológico y de Estudios Superiores de Monterrey

(1969)

Submitted to the Department of  
Mechanical Engineering in  
Partial Fulfillment of the  
Requirements for the Degree of

**Doctor of Science  
In Mechanical Engineering**

at the


**Massachusetts Institute Of Technology**

October 1985

©Alfonso García Reynoso, 1985

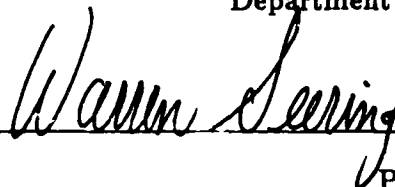
The author hereby grants to M.I.T. permission to reproduce  
and to distribute copies of this thesis document in whole or in  
part.

Signature of Author



Department of Mechanical Engineering  
November 2, 1985

Certified by



Professor Warren P. Seering  
Thesis Supervisor

Accepted by



Ain A. Sonin  
Chairman, Departmental Graduate Committee



## Abstract

Methods are developed for predicting vibration response characteristics of systems which change configuration during operation. A cartesian robot, an example of such a position-dependent system, served as a test case for these methods and was studied in detail.

The chosen system model was formulated using the technique of Component Mode Synthesis (CMS). The model assumes that the system is slowly varying, and connects the carriages to each other and to the robot structure at the slowly-varying connection points. The modal data required for each component is obtained experimentally in order to get a realistic model. The analysis results in prediction of vibrations that are produced by the inertia forces as well as gravity and friction forces which arise when the robot carriages move with some prescribed motion.

Computer simulations and experimental determinations are conducted in order to calculate the vibrations at the robot end-effector. Comparisons are shown to validate the model in two ways: for fixed-configuration the mode shapes and natural frequencies are examined, and then for changing configuration the residual vibration at the end of the move is evaluated.

A preliminary study was done on a geometrically nonlinear system which also has position-dependency. The system consisted of a flexible four-bar linkage with elastic input and output shafts. The behavior of the rocker-beam is analyzed for different boundary conditions to show how some limiting cases are obtained. A dimensional analysis leads to an evaluation of the consequences of dynamic similarity on the resulting vibration.

Thesis Supervisor: Warren P. Seering

Title: Associate Professor of Mechanical Engineering

**Acknowledgment:** This report describes research done at the Artificial Intelligence Laboratory of the Massachusetts Institute of Technology. Support for the laboratory's artificial intelligence research is provided in part by the Advanced Research Projects Agency of the Department of Defense under Office of Naval Research contract N00014-85-K-0124, and in part by CONACYT, COSNET, and the Instituto Tecnológico de Veracruz in Mexico.

## Acknowledgments

I would like to thank all people who contributed to the realization of this research work. First of all my thesis supervisor Prof. Warren P. Seering who gave me strong encouragement, advice, and support, and showed unlimited patience. My thesis committee members, Prof. Stephen H. Crandall, Prof. Steven Dubowsky, and Prof. Richard H. Lyon who gave me valuable advice in many occasions. Among the students, three of them spent considerable time helping me in different phases of my research; they are Ken Pasch, Neil Singer, and Peter Meckl. In the early part of my work, I received considerable help from George Pariseanu, also from Mark Moeller, Charles Thomson, Charles Gedney, Robert Powell, Shawn Burke, and James Slack. Other students in the Artificial Intelligence Lab. who have helped me in several ways are Steve Gordon, Steve Eppinger, Karl Ulrich, Allen Ward, Eric Vaaler, Michael Caine, Michael Benjamin, Dan Frost, Robert Podoloff, Fred MARTins, and Gary Drlik. To all of them I feel grateful.

In the MIT staff I would like to express my gratitude to Mrs. Sandra W. Tepper of the Administrative Office of the Mechanical Engineering Dept. for her orientation, advice, and help. Also I would like to thank Mr. James Galvin of the Student Accounts Office for his special care and help during several economic problems that I experienced during my five years of stay in MIT.

From Mexico I would like to thank CONACYT which gave me economic support for most of the period. Also to Ing. Angel Zamudio Poistan, Director of the Instituto Tecnológico de Veracruz, and Ing. Josué Nieto Metzger, Subdirector, for their support; also to Dr. Alicia Cruz Bazán who helped me in many different ways during all this period. My mother-in-law Mrs. Carmen Lopez Vda. de Portilla, and my brother-in-law Mr. Francisco Ramírez-España Solares who cared about my economic problems. I should also thank Ing Federico Avila Vinay, and Ing Juan Carmona Razcón who helped me when they were Directors of this Institute. I also thank COSNET for their support in the last five months of my program. To all of them I feel infinitely grateful.

I would like to specially thank my wife Diana and my children Alfonso, Manuel, and Miguel Angel for having so much patience and consideration.

Finally, I would like to dedicate this work to the memory of my mother Margarita Reynoso de García, and in honor of my father Alfonso García Núñez.

# Contents

<b>1</b>	<b>INTRODUCTION</b>	<b>10</b>
1.1	Summary . . . . .	10
1.2	Previous Research in Position-Dependent Systems . . . . .	13
1.3	Literature Survey on Component Mode Synthesis . . . . .	15
1.4	Organization of the Thesis . . . . .	19
<b>2</b>	<b>PROPOSED QUASI-STATIC MODEL</b>	<b>20</b>
2.1	Application of Component Mode Synthesis . . . . .	20
2.1.1	Characteristics of the beam . . . . .	24
2.1.2	Characteristics of the 2-degree of freedom system . . . . .	24
2.1.3	Compatibility condition . . . . .	24
2.2	Modal Representation of Components . . . . .	27
2.3	Modal Parameter Identification . . . . .	32
2.4	Physical Connection of the Components . . . . .	36
2.5	CMS Model of Connections . . . . .	40
2.6	Convergence of CMS . . . . .	46
2.7	Conditioning of the Numerical Process . . . . .	51
2.8	Predictions of Quasi-Static Model . . . . .	54
<b>3</b>	<b>PROPOSED DYNAMIC MODEL</b>	<b>56</b>
3.1	A Procedure of Analysis . . . . .	56
3.2	Eigenfunctions . . . . .	57
3.3	Equations of Motion . . . . .	67
3.4	Force Analysis and Prescribed Motion . . . . .	68
3.4.1	Prescribed Motor-rotor Vibration . . . . .	69
3.4.2	Friction Considerations . . . . .	70
3.4.3	Conditioning of the Encoder Motion . . . . .	72
3.5	Solution of the Equations of Motion . . . . .	76
3.6	Some Results of the Dynamic Model . . . . .	79
<b>4</b>	<b>EXPERIMENTS AND RESULTS</b>	<b>82</b>
4.1	Objectives . . . . .	82
4.2	Modal Tests . . . . .	83

4.3	High-Resolution Transfer Functions . . . . .	93
4.4	Modal Variation with Position . . . . .	95
4.5	Vibration of Moving Robot . . . . .	95
4.5.1	Computer-Controlled Tests . . . . .	99
4.5.2	Vibration Results for Motion in X-direction . . . . .	101
4.5.3	Vibration Results for Motion in Y-direction . . . . .	106
4.5.4	Vibration Results for Motion in Z-direction . . . . .	106
4.5.5	Comparison of Simulation and Experimental Results . . . . .	107
<b>5</b>	<b>CONCLUSIONS AND RECOMMENDATIONS</b>	<b>117</b>
5.1	Conclusions . . . . .	117
5.2	Recommendations . . . . .	122
<b>A</b>	<b>MODE SHAPE DATA</b>	<b>133</b>
A.1	Determination of Modal Characteristics . . . . .	133
A.2	Mode Shape Data for Robot Structure . . . . .	144
A.3	Mode Shape Data for Carriages . . . . .	145
A.4	Mode Shapes for Lead Screws . . . . .	145
A.5	Modal Matrices for Data Input . . . . .	156
A.6	Mode shape data . . . . .	165
<b>B</b>	<b>VIBRATION OF MOVING ROBOT</b>	<b>184</b>
B.1	Methods of Analysis . . . . .	184
B.1.1	Prescribed Rigid Body Motion . . . . .	184
B.1.2	Prescribed Motor-Rotor Vibration . . . . .	185
<b>C</b>	<b>PRELIMINARY STUDY OF VIBRATIONS</b>	<b>197</b>
C.1	Preliminary Vibration Analysis . . . . .	197
C.2	Introduction . . . . .	199
C.3	Continuous Parameter Model . . . . .	202
C.3.1	Kinetic co-energies . . . . .	202
C.3.2	Potential Energies . . . . .	203
C.3.3	Generalized Forces . . . . .	203
C.4	Description of Simplified Models . . . . .	207
C.5	Comparison of Models . . . . .	211
C.6	Linearized System Vibration . . . . .	211
C.7	Summary . . . . .	217

# List of Figures

1.1	Picture of Cartesian Robot . . . . .	11
1.2	Simply supported beam with moving 2-dof subsystem . . .	13
2.1	Two-dof subsystem moving on beam . . . . .	23
2.2	Components of cartesian robot . . . . .	28
2.3	Curve fit of transfer function . . . . .	35
2.4	Detail of lead screw and nut . . . . .	36
2.5	Schematic representation of physical connections . . . . .	37
2.6	Cam followers on ways . . . . .	38
2.7	Degrees of freedom of physical connections . . . . .	39
2.8	Box diagram of Component Mode Synthesis . . . . .	41
2.9	triple connection . . . . .	42
2.10	Convergence of 1st natural frequency with number of modes used . . . . .	50
2.11	Redundant degrees of freedom causing ill-condition . . . . .	53
2.12	Synthesized mode shape 1 of robot . . . . .	54
2.13	Synthesized mode shape 2 of robot . . . . .	55
3.1	Linear interpolation of mode shape data . . . . .	58
3.2	Cubic spline interpolation of mode shape data . . . . .	59
3.3	Least-squares curve-fit of mode shape data using Chebyshev polynomials of order 3 . . . . .	61
3.4	Least-squares curve-fit of mode shape data using Chebyshev polynomials of order 5 . . . . .	61
3.5	Modal variation after curve-fitting mode shape data using Chebyshev polynomials of order 3 . . . . .	62
3.6	Modal variation after curve-fitting mode shape data using Chebyshev polynomials of order 5 . . . . .	63
3.7	Two different solutions to the curve-fitting of mode shape data using a beam-like eigenfunction . . . . .	64
3.8	Curve fit of mode shape data using a beam-like eigenfunc- tion, case of good data . . . . .	65
3.9	Curve fit of mode shape data using a beam-like eigenfunc- tion, case of noisy data . . . . .	65

3.10	Modal variation with position for case of equivalent beam eigenfunctions . . . . .	66
3.11	Variation of friction force along x-direction . . . . .	71
3.12	Encoder displacement . . . . .	73
3.13	Unfiltered encoder velocity . . . . .	74
3.14	Unfiltered encoder acceleration . . . . .	75
3.15	Impulse response of digital filter . . . . .	76
3.16	Fourier transform of digital filter . . . . .	77
3.17	Filtered encoder velocity . . . . .	77
3.18	Filtered encoder acceleration . . . . .	78
3.19	Vibration of end-effector in x-direction . . . . .	80
3.20	End vibration in x-direction . . . . .	80
3.21	Fourier transform of end vibration in x-direction . . . . .	81
4.1	Robot configuration for modal test . . . . .	86
4.2	Test set-up for modal analysis . . . . .	87
4.3	Typical transfer function . . . . .	87
4.4	Mode shape no.1 of robot . . . . .	89
4.5	Mode shape no.2 of robot . . . . .	90
4.6	Mode shape no.3 of robot . . . . .	91
4.7	Mode shape no.4 of robot . . . . .	92
4.8	Multimodal curve fit no.1 of transfer function of Z-carriage	94
4.9	Multimodal curve fit no.2 of transfer function of Z-carriage	94
4.10	Test set-up for computer-controlled experiment . . . . .	100
4.11	Actual Velocity Profile followed by Controller. . . . .	101
4.12	Encoder displacement during motion in X-direction . . . . .	102
4.13	Encoder velocity during motion in X-direction . . . . .	102
4.14	Vibration of end-effector during motion in X-direction . . . . .	103
4.15	Vibration at the end of the move for motion in X-direction	104
4.16	Fourier transform of end vibration for motion in X-direction	105
4.17	Encoder displacement during motion in Y-direction . . . . .	106
4.18	Encoder velocity during motion in Y-direction . . . . .	107
4.19	Vibration of end-effector during motion in Y-direction . . . . .	108
4.20	End vibration for motion in Y-direction . . . . .	109
4.21	Fourier transform of end vibration for motion in Y-direction	110
4.22	Encoder displacement during motion in Z-direction . . . . .	111
4.23	Encoder velocity during motion in Z-direction . . . . .	111
4.24	Vibration of end-effector during motion in Z-direction . . . . .	112
4.25	End vibration for motion in Z-direction . . . . .	113
4.26	Fourier transform of end vibration for motion in Z-direction	114
A.1	Test set-up for impact procedure . . . . .	135
A.2	Test set-up for random procedure . . . . .	136

A.3 Mode shapes no.1 (top) and no.2 (bottom) of robot structure as obtained by test . . . . .	137
A.4 Mode shapes no.3 (top) and no.4 (bottom) of robot structure as obtained by test . . . . .	138
A.5 Mode shapes no.5 (top) and no.6 (bottom) of robot structure as obtained by test . . . . .	139
A.6 Mode shapes no.7 (top) and no.8 (bottom) of robot structure as obtained by test . . . . .	140
A.7 Mode shapes no.9 (top) and no.10 (bottom) of robot structure as obtained by test . . . . .	141
A.8 Mode shapes no.11 (top) and no.12 (bottom) of robot structure as obtained by test . . . . .	142
A.9 Mode shape no.13 of robot structure as obtained by test . . . . .	143
A.10 Drive-point transfer function of robot structure . . . . .	144
A.11 Mode shapes no.1 (top) and no.2 (bottom) of X-carriage as obtained by test . . . . .	146
A.12 Mode shapes no.3 (top) and no.4 (bottom) of X-carriage as obtained by test . . . . .	147
A.13 Mode shapes no.1 (top) and no.2 (bottom) of Y-carriage as obtained by test . . . . .	148
A.14 Mode shapes no.3 (top) and no.4 (bottom) of Y-carriage as obtained by test . . . . .	149
A.15 Mode shapes no.5 (top) and no.6 (bottom) of Y-carriage as obtained by test . . . . .	150
A.16 Mode shapes no.7 (top) and no.8 (bottom) of Y-carriage as obtained by test . . . . .	151
A.17 Mode shapes no.9 (top) and no.10 (bottom) of Y-carriage as obtained by test . . . . .	152
A.18 Mode shapes no.1 (top) and no.2 (bottom) of Z-carriage as obtained by test . . . . .	153
A.19 Mode shapes no.3 (top) and no.4 (bottom) of Z-carriage as obtained by test . . . . .	154
A.20 Mode shape no.5 of Z-carriage as obtained by test . . . . .	155
A.21 Drive-point transfer function of Z-carriage . . . . .	155
A.22 Model of motor-rotor and lead-screw . . . . .	156
A.23 mode shape no. 1 of robot . . . . .	166
A.24 mode shape no. 2 of robot . . . . .	167
A.25 mode shape no. 3 of robot . . . . .	168
A.26 mode shape no. 4 of robot . . . . .	169
A.27 mode shape no. 5 of robot . . . . .	170
A.28 mode shape no. 6 of robot . . . . .	171
A.29 mode shape no. 7 of robot . . . . .	172

A.30 mode shape no. 8 of robot . . . . .	173
A.31 mode shape no. 9 of robot . . . . .	174
A.32 mode shape no. 10 of robot . . . . .	175
A.33 mode shape no. 11 of robot . . . . .	176
A.34 mode shape no. 12 of robot . . . . .	177
A.35 mode shape no. 13 of robot . . . . .	178
A.36 mode shape no. 14 of robot . . . . .	179
A.37 mode shape no. 15 of robot . . . . .	180
A.38 mode shape no. 16 of robot . . . . .	181
A.39 mode shape no. 17 of robot . . . . .	182
 B.1 Flexible system . . . . .	 186
B.2 Two substructures A,B . . . . .	190
B.3 Assembled A-B . . . . .	193
B.4 Response at $x_2$ to impulse-response input at $x_1$ , calculated (top) and expected (bottom) . . . . .	195
B.5 Response at $x_2$ to step-response input at $x_1$ , calculated (top) and expected (bottom) . . . . .	196
 C.1 Continuous parameter model of the system . . . . .	 198
C.2 Behavior of $a$ vs. $K_1$ for various values of $K_2$ . . . . .	207
C.3 Lumped parameter model of the system . . . . .	208
C.4 Variation of three natural frequencies with crank position for quasi-static case . . . . .	210
C.5 Comparison of behavior of first natural frequency in bending obtained from the continuous and the lumped models. Case of $\frac{K_4}{K_3} = 0.1$ . . . . .	212
C.6 Comparison of behavior of first natural frequency in bending obtained from the continuous and the lumped models. Case of $\frac{K_4}{K_3} = 10$ . . . . .	213
C.7 Frequency response of two members of a family of mecha- nisms. The original data corresponds to ordinate 2 . . . . .	216



# Chapter 1

## INTRODUCTION

### 1.1 Summary

A position-dependent system in vibration analysis is defined as a system whose vibration characteristics are changing as its components change their relative positions. Machines and structures such as cranes and bridges are examples of such systems. One such system which motivated the present analysis, is a cartesian robot (seen in Figure 1.1) as a structure with moving carriages) whose dynamic performance needs to be predicted accurately during the motion of the carriages.

The importance of the present analysis comes from the fact that this is a precision assembly robot and any residual vibration at the end of the move can badly affect assembly operations with small tolerances. So, it would be desirable to have a good mathematical model of how the vibrations evolve during the motion so that these vibrations could be actively controlled. It could also be used as a design model.

The mathematical model to be developed should be accurate and fast to execute when implemented in a computer. The approach followed to develop this model was based on Component Mode Synthesis which is a



Figure 1.1: Picture of Cartesian Robot

method to connect substructures to predict the dynamic behavior of an assembly based on the dynamic behavior of each substructure. This method (CMS), traditionally applied to connect parts that form a time-invariant system can be extended to position-dependent systems under the following assumption: that the system is of slowly-varying coefficients; that is, that any appreciable change in the system coefficients occurs after many cycles of vibration.

Experimental modal analyses were performed to determine the dynamic behavior of each substructure. We used these results applying CMS to develop the mathematical model. There were difficulties to be overcome. First was the problem of parameter identification to accurately scale the eigenvectors of each substructure so that they were orthonormal. This involved special curve-fitting techniques applied to transfer functions obtained by test. Another important difficulty was to realize that an ill-condition may be present when we use several points to connect 2 substructures, so we developed a method to detect this problem and to aid in correcting it.

The model had to be validated by test, and it was done for two different aspects: the quasi-static case and the dynamic case. For the quasi-static case we fixed the position of the carriages so that the problem became time-invariant and then we compared the modal characteristics as obtained by testing the complete robot with the modal data calculated by the model. The average error in natural frequencies for the first 17 modes was 6.9%. The second aspect of the validation involved running the carriages according to a given velocity profile at the motor end, and recording the vibration at the end effector of the robot; this was compared to the prediction of the model when a prescribed motion at the motor end (equal to the one obtained in the test) was imposed. These results showed an acceptable agreement between the predicted results and the test results.

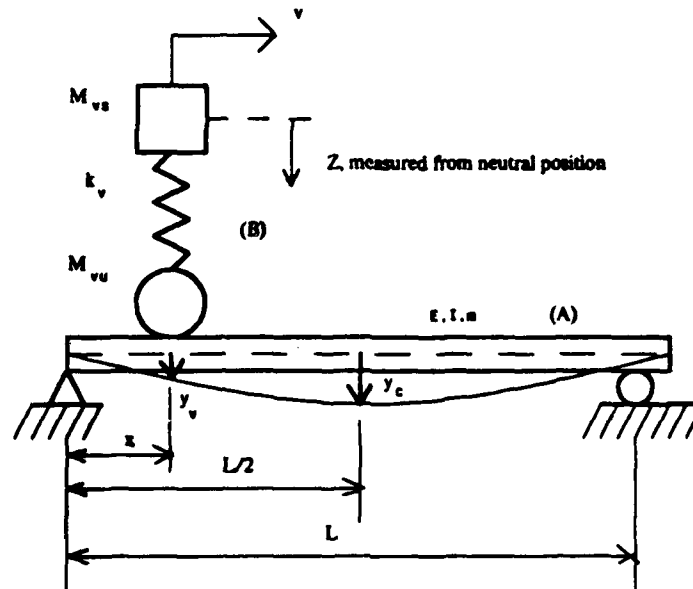


Figure 1.2: Simply supported beam with moving 2-dof subsystem

## 1.2 Previous Research in Modeling of Position-Dependent Systems

The problem of studying the vibrations of a position-dependent system involves dealing with systems of continuous-parameter elements which are described by partial differential equations with changing boundary conditions as the elements change position. This situation, already difficult to solve for the case of ideal elements, becomes worse when the elements are real, that is, when there are all kinds of non-uniformities present. Then, an exact solution is very cumbersome and for practical purposes we should use a method that gives a fast and accurate solution.

One practical approach adopted by civil engineers in the case of the bridge problem is explained by Biggs [9], where it is tacitly assumed that the system is slowly varying, and they use one point of connection to model the contact between the bridge and the vehicle. The analysis simplifies the

single-span bridge structure by taking it as a simply-supported beam; the vehicle is taken as a 2-degree of freedom system. To derive the equations of motion, assuming one mode of the beam only, the method uses the modal equation of motion for the beam  $\ddot{A}_n + \omega_n^2 A_n = \frac{F \phi_n(z)}{\int_0^l m |\phi_n(z)|^2 dz}$ . The term  $F$ , the force between the beam and the 2-degree of freedom subsystem is expressed as a function of the acceleration of the mass in contact with the beam ( $\ddot{y}_v$ ), (see figure 1.2) the acceleration of the second mass ( $\ddot{z}$ ) and the spring force ( $k(z - y_v)$ ) in the 2-degree of freedom subsystem. A coupled set of differential equations in  $y_v$  and  $z$  results.

Since the problem in hand, as in many other manipulators, can be studied under the assumption of slowly-varying coefficients as is explained later, we can extend the idea behind the approach for the bridge problem. We first notice that in the method mentioned above (bridge problem), the dynamics of the 2-degree of freedom subsystem are introduced to the beam equation through the condition of equilibrium of forces at the point of connection. This idea is broadly used in methods of connection of two or more substructures, namely the Impedance method [61] and the Component Mode Synthesis method [33], where the starting point is the specification that the vibration of any two points of connection should be the same. Then, the Impedance method substitutes for the motion, a frequency function whereas the Component Mode Synthesis method uses a function of time. These methods have several advantages over that of Biggs [9]. They can handle several points of connection between parts and they can work in 3-D in a more convenient way than the previous approach. In addition to that, they can use data obtained experimentally, which may lead to a more realistic model.

For the more general case of position-dependent systems, where the coefficients may quickly vary during the vibration, the solution may be found

if a pattern of vibration is repeated for each cycle of the oscillating system. In this case there is extensive literature. A section of this literature is related to the vibration of linkages, and for some simple cases the differential equations of motion reduce to Hill's equation or to Mathew's equation. One example is the research done by Capellen [13].

A method for analyzing the complete behavior of industrial robotic manipulators with flexible links and including the control systems is presented by Sunada and Dubowsky [73] in which they use finite element models to analyze the links. The method is made computationally efficient through the use of Component Mode Synthesis.

For the case of the robot where each component remains invariant but the boundary conditions are changing with position, the method of Component Mode Synthesis may be more adequate for giving a mathematical model which can run fast in the computer since it requires extensive processing of the experimental data to be done beforehand. It uses only the modal results for the components in the model.

### 1.3 Literature Survey on Component Mode Synthesis

The use of modal characteristics of each component to derive the approximate dynamic behavior of the assembled structure may be accomplished in different ways as summarized by Hart, Hurty and Collins [34]. These methods can be grouped in three categories. The first is Free-free Modal Synthesis which is based on free-free modes of the components. Hou [33] reviews these methods and introduces a new approach which is adequate for handling experimentally determined mode shapes. This procedure is applied in this study to develop the mathematical model of the robot. The second

is Component Mode Synthesis which uses boundary-fixed mode shapes and boundary displacement functions. This method was pioneered by Hurty [36] where natural modes and frequencies of structural systems are determined by an energy method, synthesized from admissible mode functions selected for the component mode members of the system. The synthesis is accomplished by using equations of constraint that follow from conditions of force equilibrium and deflection compatibility at the junctions. Other authors have introduced variations to the method [34],[16],[3]. All these methods are very effective in reaching convergence when only a few modes of the components are available. The third category is Component Mode Substitution which uses free-free modal displacements and interface loading at the attachment points. It was introduced by Benfield and Hruda [4], and it has the advantage of improving the accuracy obtained by the free-free procedure.

The accuracy of the model for the free-free case depends on the number of modes used. We have found that for this particular application the number of modes required to get a good convergence index can be easily obtained by test (10 to 16 modes for each component including the rigid body modes).

Other authors have surveyed the existing literature on Component Mode Synthesis, Greif and Wu [26] summarize the work done from 1980 to 1983. Craig [17] surveys some of the many variations to the basic procedure of CMS which have been extensively developed during the past 20 years for application in the modal analysis of complex structures. He points out that further research on damping synthesis and the use of experimental data to either verify or formulate CMS mathematical models should be conducted.

A technique for modeling a structure using a severely truncated mode set is developed by Hintz [32] where in order to improve convergence he uses

modes (constraint modes and attachment modes) based upon a static analysis of the component structure response due to imposed interface forces and displacements. MacNeal [52] uses statically determined deflection influence coefficients as well as residual flexibility of the higher, truncated modes to improve accuracy. Rubin [67] introduces a method that employs an incomplete set of free-boundary normal modes each adjusted to account for the contribution of residual(neglected) modes. This method adds residual inertia and dissipative effects to the residual flexibility introduced by MacNeal.

On the use of attachment modes in substructure coupling, Craig and Chang [18] make an evaluation of the methods that employ attachment modes, and they develop a generalized substructure coupling procedure which has good convergence characteristics. Hale [27] increases accuracy by an iterative procedure for generating improved substructure trial state vectors.

Regarding damping synthesis, there are a few analytical studies. Kana and co-workers [43],[44],[45],[46] developed three methods for calculating proportional substructure damping matrices from test data. Hasselman [30], [31] used diagonal and off-diagonal terms to develop system damping matrices that involve various substructure coupling procedures.

The use of experimental data to develop CMS mathematical models and the experimental verification of the simulations has been reported in a few papers. Klosterman and Lemon [47] present a building block approach to do substructure coupling using either experimentally obtained data or modal data obtained by Finite Element analysis. They applied the method to complex mechanical machinery consisting of 5 components, and used 6-7 elastic normal modes for the most flexible ones. They emphasized that the higher modes that were left out in the truncation had a residual



flexibility which had a considerable influence on the system frequencies, so they included this effect by calculating the residual flexibility subtracting from the modal response representation, near the antiresonances, the contribution of the resonant modes. Then, they added an element with an equivalent stiffness derived from the above residual flexibility to the rest of the components. Another paper by Klosterman [48] applies this method to a complex automotive system.

Among other works on the use of experimental data we can mention the one by Thoren [75] that describes a technique by which orthonormal modal vectors computed from dynamic response data, are used to derive mass, stiffness and damping matrices for a discrete model of a distributed elastic system. The same problem is solved by Berman, Wei and Rao [7], and by Berman and Nagy [6]. Ibrahim [40] presents a technique to use a set of *identified complex modes together with an analytical mathematical model* of a structure under test to compute improved mass, stiffness and damping matrices, this based on the orthogonality condition. Berman [8] extends the method of incomplete models and uses it to obtain dynamic equations of motion of a helicopter transmission gearbox from shake test data. Goyder [25] deals with structures of high modal density and reviews methods of mathematical modeling. Ewins and Sainsbury [22] develop techniques for obtaining multidirectional mobility data which must be sufficiently accurate and complete for vibration analysis of an assembly of connected structures.

Considerable attention has been given to the topic of convergence of CMS and mode selection. Hurty [37],[38],[39] developed a first-order perturbation technique to determine the contribution of truncated modes in the natural frequencies of the assembled system as obtained by his method of CMS. Morosow and Abbott [55] determined weighting factors to assess which component modes should be included.

## 1.4 Organization of the Thesis

The thesis introduction describes the problem we are dealing with and the approach followed to solve it, as well as the experiments and calculations performed. It discusses the existing literature on the topic as well.

The second chapter, Proposed Quasi-static Model of a Cartesian Robot, introduces details about the method of Component Mode Synthesis and explains how the mathematical model was developed for the homogeneous case, that is, with no forcing terms. It then focuses on predicting modal results for a given configuration of the robot. It also explains the difficulties encountered with the orthonormalization of the eigenvectors and with the ill-conditioning that may be present .

The following chapter, Proposed Dynamic Model of a Cartesian Robot introduces the forcing terms in the model which are due to the inertia forces associated with the acceleration of the carriages and to the gravity forces acting on a changing system. At this point, the model can predict the vibration of any of the test points in the structure.

Then we show, in the chapter of Experiments and Results, the experiments that have been done to validate the model and the degree of correlation obtained with the model used.

Finally we include three appendices to give more detail about the data and results. Appendix A deals with the mode shape data obtained for each of the robot components as well as for the assembled robot. Appendix B gives detail about the vibrations of the moving robot, in particular about the method followed to derive the forcing function. Appendix C shows a preliminary analysis done by this author. This work gave knowledge and insights on how to deal with problems of systems that change their configuration.

## Chapter 2

# PROPOSED QUASI-STATIC MODEL OF A CARTESIAN ROBOT

### 2.1 Application of Component Mode Synthesis

The free-free modal synthesis procedure [33] which we have used in the analysis and referred to as CMS from now on, can be summarized as follows:

Suppose that we have 2 components A and B whose natural frequencies  $[\omega_a]$ ,  $[\omega_b]$  and mode shapes  $[\phi_a]$ ,  $[\phi_b]$  are known. These components can be either free in space or fixed, but the interfaces must be free when obtaining their mode shapes. Assuming that the eigenvectors are orthonormal (unit modal mass) we have two sets of decoupled equations to represent both systems:

$$\begin{aligned}\{\ddot{p}_a\} + [\omega_a^2] \{p_a\} &= [\phi_a]^t \{f_a\} \\ \{\ddot{p}_b\} + [\omega_b^2] \{p_b\} &= [\phi_b]^t \{f_b\}\end{aligned}\tag{2.1}$$

where the actual vibration would be

$$\begin{aligned}\{x_a\} &= [\phi_a] \{p_a\} \\ \{x_b\} &= [\phi_b] \{p_b\}\end{aligned}\quad (2.2)$$

If we enforce compatibility at the interfaces, then we have for the connection points  $\{x_{a_c}\} = \{x_{b_c}\}$  or  $[\phi_{a_c}]\{p_a\} = [\phi_{b_c}]\{p_b\}$  where the subindex  $c$  indicates that only the interface points are being used. If we apply these compatibility conditions, the original generalized coordinates  $\{p_a\}$  and  $\{p_b\}$  are overconstrained and we have to reduce the order of the system so that we end up with a set of linearly independent coordinates  $\{q\}$ . We can partition these vectors and the modal matrices as well

$$\{p_a\} = \begin{Bmatrix} \{p_a^I\} \\ \{p_a^D\} \end{Bmatrix} = \begin{Bmatrix} \{q_a\} \\ \{p_a^D\} \end{Bmatrix} \quad (2.3)$$

$$\{p_b\} = \begin{Bmatrix} p_b^I \end{Bmatrix} = \begin{Bmatrix} q_b \end{Bmatrix} \quad (2.4)$$

$$[\phi_{a_c}] = \begin{bmatrix} [\phi_{a_c}^I] & [\phi_{a_c}^D] \end{bmatrix} \quad (2.5)$$

$$[\phi_{b_c}] = [\phi_{a_c}^I] \quad (2.6)$$

where the superscripts  $I$  and  $D$  stand for independent and dependent.

Then,

$$\begin{bmatrix} [\phi_{a_c}^I] & [\phi_{a_c}^D] \end{bmatrix} \begin{Bmatrix} q_a \\ p_a^D \end{Bmatrix} = [\phi_{b_c}^I] \{q_b\} \quad (2.7)$$

Rearranging we have

$$\{p_a^D\} = \begin{bmatrix} -[\phi_{a_c}^D]^{-1} [\phi_{a_c}^I] & [\phi_{a_c}^D]^{-1} [\phi_{b_c}^I] \end{bmatrix} \begin{Bmatrix} q_a \\ q_b \end{Bmatrix} \quad (2.8)$$

Finally if we include the complete vector  $\{p\}$  we have

$$\begin{Bmatrix} p_a^I \\ p_a^D \\ p_b^I \end{Bmatrix} = \begin{bmatrix} I & 0 \\ -[\phi_{a_c}^D]^{-1} [\phi_{a_c}^I] & [\phi_{a_c}^D]^{-1} [\phi_{b_c}^I] \\ 0 & I \end{bmatrix} \begin{Bmatrix} q_a \\ q_b \end{Bmatrix} \quad (2.9)$$

or  $\{p\} = [T]\{q\}$ . This matrix  $[T]$  is the transformation matrix that connects A and B.

To obtain the equations of motion of the assembled system we first combine the two parts as follows:

$$\begin{Bmatrix} \ddot{p}_a \\ \ddot{p}_b \end{Bmatrix} + \begin{bmatrix} [\omega_a^2] & 0 \\ 0 & [\omega_b^2] \end{bmatrix} \begin{Bmatrix} p_a \\ p_b \end{Bmatrix} = \begin{bmatrix} [\phi_a]^t & 0 \\ 0 & [\phi_b]^t \end{bmatrix} \begin{Bmatrix} f_a \\ f_b \end{Bmatrix} \quad (2.10)$$

Substituting  $\{p\} = [T]\{q\}$  and then premultiplying by  $[T]^t$  we get:

$$[T]^t [T] \{\ddot{q}\} + [T]^t \begin{bmatrix} [\omega_a^2] & 0 \\ 0 & [\omega_b^2] \end{bmatrix} [T] \{q\} = [T]^t \begin{bmatrix} \phi_a^t & 0 \\ 0 & \phi_b^t \end{bmatrix} \begin{Bmatrix} f_a \\ f_b \end{Bmatrix} \quad (2.11)$$

These equations are now coupled and after solving the eigenvalue problem of this pseudosystem we get  $\{\omega'\}$  and  $[\psi]$ . Finally for the assembled system we have that  $\omega$  and  $\phi$  are given by

$$\{\omega\} = \{\omega'\} \quad (2.12)$$

and

$$[\phi] = \begin{bmatrix} [\phi_a] & 0 \\ 0 & [\phi_b] \end{bmatrix} [T] [\psi] \quad (2.13)$$

Notice that the name free-free for this method does not imply that the components have to be tested on a free-free condition(floating), but rather that the points of connection of the components should be free during the test(as opposed to the fixed-boundary case), while the other points can be either fixed or free.

One important characteristic of this method (CMS) is that it can either use mode shapes for each component as obtained by a finite-element technique or the mode shapes can be obtained experimentally. There are complicated cases where we may be better off using test results as data for CMS in order to get a good model. Another important advantage of CMS is that it handles data in matrix form. This allows us to tackle complicated

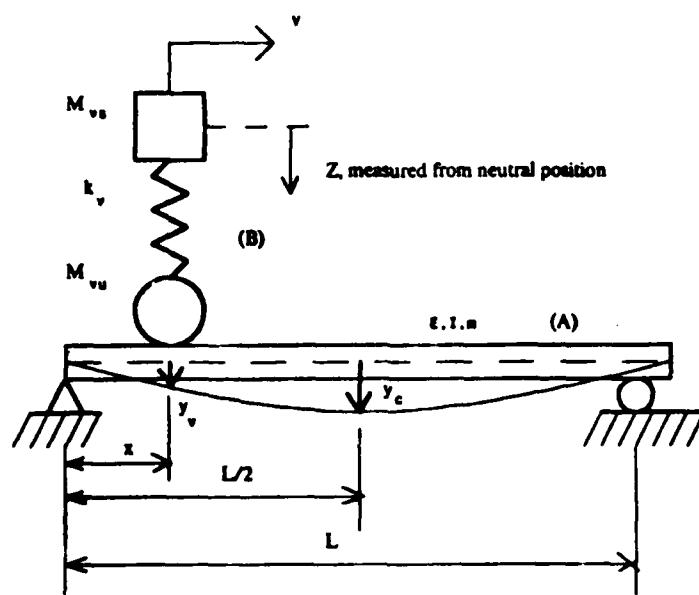


Figure 2.1: Two-dof subsystem moving on beam

problems with many degrees of freedom at the connections and in 3-D with ease. This CMS approach works well for time-invariant cases, that is, when the points of connection are always the same and each component remains invariant. This approach can be extended to the case of position-dependent systems for the case of slowly-varying coefficients as shown below.

Consider the following example: Suppose we have a bridge problem as explained by Biggs [9] and illustrated in Figure 2.1. We will here develop the equations of motion for this system using CMS methods and then we will compare the results with those obtained by Biggs through use of another method. The bridge is modeled as a beam and the vehicle as a 2-degree of freedom system traveling at constant velocity as shown in Figure 2.1.

Assume that  $M_{vu}$  slides without friction and always in contact with the beam. Assume also that the time  $\tau_1 = \frac{L}{v}$ , required to travel the distance  $L$ , is much larger than a natural period of oscillation  $t_n$ :  $\tau_1 \gg t_n$ . We can conceive two time scales in this problem; a fast time  $t$  that follows each

cycle of vibration and a slow time  $\tau$  that follows the rigid body motion of the carriages. This variable  $\epsilon$  is defined as the ratio of the slow time  $\tau$  to the fast time  $t$ :  $\epsilon = \frac{\tau}{t}$ , and for the beam problem its formula is

$$\epsilon = \frac{\frac{2\pi}{\omega_1}}{\frac{2L}{v}} \quad (2.14)$$

or in other words  $\epsilon$  is the ratio of the period of the dominant mode of oscillation to twice the travel time.

Assume  $\tau = \epsilon t$ , then  $x = v\tau = v\epsilon t$ .

### 2.1.1 Characteristics of the beam

Consider the first mode only for a simply supported beam:  $\omega_A^2$ ,  $\phi_A = \sqrt{\frac{2}{mL}} \sin \frac{\pi x}{L}$ ,  $f_A = 0$ .

### 2.1.2 Characteristics of the 2-degree of freedom system

The 2-degree of freedom subsystem, free in a 1-D space has the following natural modes:  $\omega_{B_1}^2 = 0$ ,  $\omega_{B_2}^2 = k_v \left( \frac{M_{vu} + M_{us}}{M_{vu}M_{us}} \right)$

$$[\phi_B] = \begin{bmatrix} C_1 & C_2 \\ C_1 & -C_2 \frac{M_{us}}{M_{vu}} \end{bmatrix} \quad (2.15)$$

where  $C_1 = \frac{1}{\sqrt{M_{us} + M_{vu}}}$ , and  $C_2 = \sqrt{\frac{M_{vu}}{M_{us}(M_{us} + M_{vu})}}$

$$[f_B] = \begin{Bmatrix} M_{vu}g \\ (M_{vu} + M_{us})g \end{Bmatrix} \quad (2.16)$$

### 2.1.3 Compatibility condition

At the connection point we have  $y_{v_A} = y_{v_B}$  or

$$[\phi_A] \{p_A\} = [\phi_B] \begin{Bmatrix} p_{B_1} \\ p_{B_2} \end{Bmatrix}$$

Substituting we get

$$\sqrt{\frac{2}{mL}} \sin \frac{\pi v t \epsilon}{L} \{p_A\} = \begin{bmatrix} C_1 & -C_2 \frac{M_{vs}}{M_{vu}} \end{bmatrix} \begin{Bmatrix} p_{B_1} \\ p_{B_2} \end{Bmatrix} \quad (2.17)$$

eliminate  $p_{B_2}$  to get

$$\begin{Bmatrix} p_A \\ p_{B_1} \\ p_{B_2} \end{Bmatrix} = [T] \begin{Bmatrix} p_A \\ p_{B_1} \end{Bmatrix} \quad (2.18)$$

where

$$[T] = \begin{bmatrix} 1 & 0 \\ 0 & 1 \\ -\sqrt{\frac{2}{mL} \frac{M_{vs}}{M_{vu}}} (M_{vu} + M_{vs}) \sin \frac{\pi v t \epsilon}{L} & \sqrt{\frac{M_{vs}}{M_{vu}}} \end{bmatrix}$$

With this transformation matrix  $[T]$  we can form the equations of motion of the assembled system in terms of the remaining generalized coordinates

$$\{q\} = \begin{Bmatrix} p_A \\ p_{B_1} \end{Bmatrix} \text{ to get}$$

$$[m]\{\ddot{q}\} + [k]\{q\} = \{F\} \quad (2.19)$$

where

$$[m] = [T]^t [T], \quad [k] = [T]^t \begin{bmatrix} \omega_A^2 & 0 & 0 \\ 0 & 0 & 0 \\ 0 & 0 & \omega_{B_2}^2 \end{bmatrix} [T],$$

$$\{F\} = [T]^t \begin{bmatrix} \sqrt{\frac{2}{mL}} \sin \frac{\pi v t \epsilon}{L} & 0 \\ 0 & C_1 \\ 0 & -C_2 \frac{M_{vs}}{M_{vu}} \end{bmatrix} \begin{Bmatrix} 0 \\ (M_{vs} + M_{vu})g \end{Bmatrix}$$



Substituting the expression for  $[T]$  the equations of motion become:

$$\begin{aligned}
 & \left[ \begin{array}{cc} 1 + \frac{2}{mL} \frac{M_{vu}}{M_{vs}} (M_{vu} + M_{vs}) \sin^2 \frac{\pi v t \epsilon}{L} & - \frac{M_{vu}}{M_{vs}} \sqrt{\frac{2}{mL}} (M_{vu} + M_{vs}) \sin \frac{\pi v t \epsilon}{L} \\ \text{symmetric} & 1 + \frac{M_{vu}}{M_{vs}} \end{array} \right] \begin{Bmatrix} \ddot{q}_1 \\ \ddot{q}_2 \end{Bmatrix} \\
 & + \left[ \begin{array}{cc} \omega_A^2 + \frac{2k_v}{mL} \frac{1}{M_{vs}^2} (M_{vu} + M_{vs})^2 \sin^2 \frac{\pi v t \epsilon}{L} & - \frac{k_v}{M_{vs}^2} \sqrt{\frac{2}{mL}} (M_{vu} + M_{vs}) \sin \frac{\pi v t \epsilon}{L} \\ \text{symmetric} & k_v \frac{M_{vu}}{M_{vs}^2} \end{array} \right] \\
 & \begin{Bmatrix} q_1 \\ q_2 \end{Bmatrix} = \begin{Bmatrix} g (M_{vs} + M_{vu}) \sqrt{\frac{2}{mL}} \sin \frac{\pi v t \epsilon}{L} \\ 0 \end{Bmatrix}
 \end{aligned} \quad (2.20)$$

To compare this solution with the one provided by Biggs we must determine  $y_c$ , the vibration at the midspan of the beam, and  $z$ , the vibration of the mass  $M_{vs}$ . These are obtained by

$$\begin{Bmatrix} y_c \\ z \end{Bmatrix} = [\phi][T][q] \quad (2.21)$$

Substituting the expression for  $[T]$  and solving for  $q$  we get:

$$\begin{Bmatrix} q_1 \\ q_2 \end{Bmatrix} = \sqrt{\frac{mLM_{vs}^2}{2(M_{vu} + M_{vs})}} \begin{bmatrix} \sqrt{\frac{M_{vu} + M_{vs}}{M_{vs}^2}} & 0 \\ \frac{M_{vu}}{M_{vs}} \sqrt{\frac{2}{mL}} \sin \frac{\pi v t \epsilon}{L} & \sqrt{\frac{2}{mL}} \end{bmatrix} \begin{Bmatrix} y_c \\ z \end{Bmatrix} \quad (2.22)$$

Also, the second time derivative of  $q$  is given by:

$$\begin{aligned}
 & \begin{Bmatrix} \ddot{q}_1 \\ \ddot{q}_2 \end{Bmatrix} = \sqrt{\frac{mLM_{vs}^2}{2(M_{vu} + M_{vs})}} \left( \begin{bmatrix} \sqrt{\frac{M_{vu} + M_{vs}}{M_{vs}^2}} & 0 \\ \frac{M_{vu}}{M_{vs}} \sqrt{\frac{2}{mL}} \sin \frac{\pi v t \epsilon}{L} & \sqrt{\frac{2}{mL}} \end{bmatrix} \begin{Bmatrix} \ddot{y}_c \\ \ddot{z} \end{Bmatrix} + \right. \\
 & \epsilon \begin{bmatrix} 0 & 0 \\ \frac{M_{vu}}{M_{vs}} \sqrt{\frac{2}{mL}} \frac{\pi v}{L} \cos \frac{\pi v t \epsilon}{L} & 0 \end{bmatrix} \begin{Bmatrix} \dot{y}_c \\ \dot{z} \end{Bmatrix} \Bigg) + \\
 & \epsilon^2 \begin{bmatrix} 0 & 0 \\ -\frac{M_{vu}}{M_{vs}} \sqrt{\frac{2}{mL}} \left( \frac{\pi v}{L} \right)^2 \sin \frac{\pi v t \epsilon}{L} & 0 \end{bmatrix} \begin{Bmatrix} y_c \\ z \end{Bmatrix}
 \end{aligned} \quad (2.23)$$

Substituting these expressions for  $q$  and  $\ddot{q}$  and premultiplying by

$$\begin{bmatrix} 1 & \frac{M_{vu}}{M_{vs}} \frac{2}{mL} \sin \frac{\pi v t \epsilon}{L} \\ 0 & 1 \end{bmatrix} \quad (2.24)$$

we decouple the mass matrix and finally get

$$\begin{aligned}
 & \begin{bmatrix} 1 + \frac{2}{mL} M_{vu} \sin^2 \frac{\pi vt}{L} & 0 \\ 0 & M_{vs} \end{bmatrix} \begin{Bmatrix} \ddot{y}_c \\ \ddot{z} \end{Bmatrix} + \left( \begin{bmatrix} \omega_A^2 + \frac{2k_v}{mL} \sin^2 \frac{\pi vt}{L} & -\frac{2k_v}{mL} \sin \frac{\pi vt}{L} \\ -k_v \sin \frac{\pi vt}{L} & k_v^2 \end{bmatrix} \right. \\
 & + \epsilon^2 \begin{bmatrix} 0 & 0 \\ -M_{vu} (\frac{\pi v}{L})^2 \sin \frac{\pi vt}{L} & 0 \end{bmatrix} \left. \right) \begin{Bmatrix} y_c \\ z \end{Bmatrix} + \epsilon \begin{bmatrix} 0 & 0 \\ M_{vu} \frac{\pi v}{L} \cos \frac{\pi vt}{L} & 0 \end{bmatrix} \begin{Bmatrix} \dot{y}_c \\ \dot{z} \end{Bmatrix} = \\
 & \begin{Bmatrix} \frac{2g}{mL} (M_{vs} + M_{vu}) \sin \frac{\pi vt}{L} \\ 0 \end{Bmatrix}
 \end{aligned} \tag{2.25}$$

These equations are the same as the ones obtained by Biggs when we neglect all terms in  $\epsilon$ . So, the method of CMS gives the right answer when  $\epsilon \ll 1$  which is the case for systems with slowly-varying coefficients.

## 2.2 Modal Representation of the Robot Components

In order to use CMS, each component of the robot must be represented by its rigid body and elastic modes, and these modes must be tridimensional.

The robot components are seven as can be seen in Figure 2.2. They are called *STR*, *X*, *Y*, *Z*, *MX*, *MY*, *MZ* whose description is given below. The cartesian robot is mounted in the Artificial Intelligence Laboratory of MIT in building NE43. It was designed and built by a team of students under the supervision of Prof. Warren P. Seering.

**STR:** The component *STR* is formed by the structure that holds the carriages and it also includes the dynamics of the floor on which it is mounted, that is the 9th floor of Building NE43 of MIT. This structure has on its top part two parallel ways which guide the Y-carriage when it moves. This structure is formed by 6 pieces joined together by

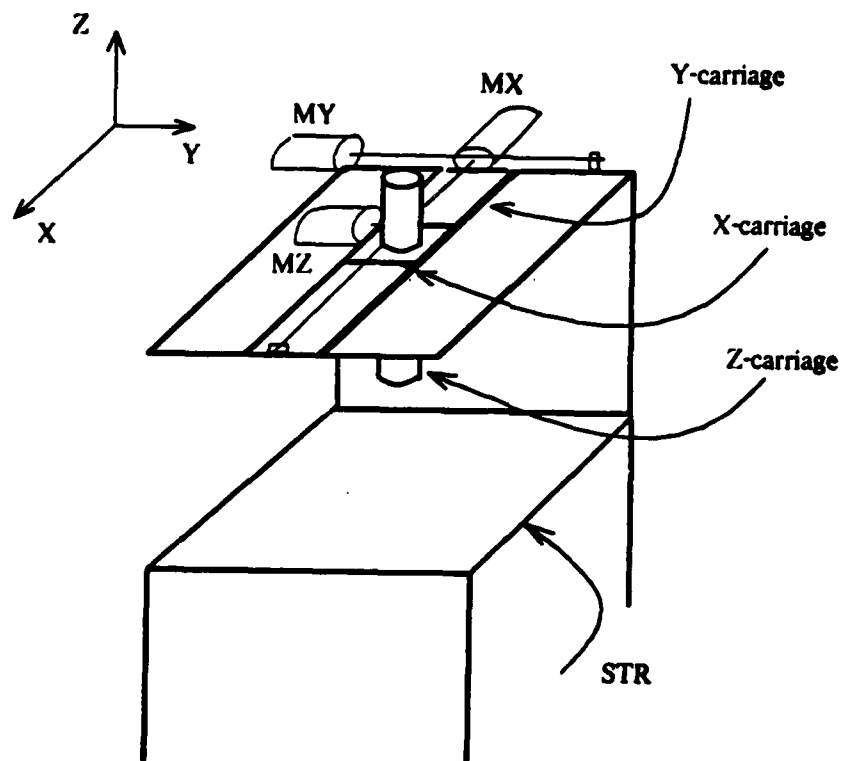


Figure 2.2: Components of cartesian robot

long and thick bolts so that a large torque can be applied to tighten them, thus avoiding any creep-friction problem that would introduce nonlinearities in the vibration analysis.

**Component X:** The component X is the X-carriage which moves in the X-direction; it is supported by the ways of the Y-carriage and it supports, in turn, the Z-carriage. When it moves it is acted upon by the motor MX through a lead screw.

**Component Y:** The component Y is the Y-carriage which moves in the Y-direction; it is supported by STR and it supports, in turn, the X-carriage. It is acted upon by the motor MY through a lead screw.

**Component Z:** The Z-component is the Z-carriage which moves in the Z-direction and is supported by the X-carriage. It is acted upon by the MZ motor through a rack and pinion transmission.

The component STR being fixed to the floor does not have rigid body modes, but the rest of the components do have, and to calculate them it is necessary to know the mass and inertia properties which are shown in Table 2.1.

Before calculating the rigid body modes, it is necessary to specify the points on the structure to be measured. These points must include at least the connection points of the components, and for the case of the parts that have ways that slide, we take as many points along the ways as possible.

The rigid body modes are six in general, three rigid body translations along X,Y, and Z directions and three rigid body rotations about those 3 axes. It can be shown that these modes produce translations in the  $x,y$

and  $z$  directions which are given by the following formula:

$$\begin{Bmatrix} \phi_{x_n} \\ \phi_{y_n} \\ \phi_{z_n} \end{Bmatrix} = \begin{bmatrix} \frac{1}{\sqrt{M}} & 0 & 0 & 0 & \frac{(Z - Z_{cg})}{\sqrt{I_x}} & -\frac{(Y - Y_{cg})}{\sqrt{I_x}} \\ 0 & \frac{1}{\sqrt{M}} & 0 & -\frac{(Z - Z_{cg})}{\sqrt{I_y}} & 0 & \frac{(X - X_{cg})}{\sqrt{I_y}} \\ 0 & 0 & \frac{1}{\sqrt{M}} & \frac{(Y - Y_{cg})}{\sqrt{I_z}} & -\frac{(X - X_{cg})}{\sqrt{I_z}} & 0 \end{bmatrix} \begin{Bmatrix} \delta_{1n} \\ \delta_{2n} \\ \delta_{3n} \\ \delta_{4n} \\ \delta_{5n} \\ \delta_{6n} \end{Bmatrix} \quad (2.26)$$

where  $M$  is the mass of the component,  $I_x$  is the moment of inertia about its center of gravity ( $X_{cg}, Y_{cg}, Z_{cg}$ ) with respect to the X-axis and so forth.  $\phi_{x_n}$  represents the mode shape value of a point with coordinates  $(X, Y, Z)$  along the X-direction for mode  $n$ .  $\phi_{y_n}$  corresponds to direction Y, and so forth.  $\delta_{1n}$  to  $\delta_{6n}$  are Kronecker deltas which have the value of zero unless  $n$  coincides with the first subscript, in which case they take the value of one.

The above formulas are correct when the principal axes of the component are aligned with the X, Y, and Z axes but if they are not, then one way to correct this is by calculating the mode shape values along the principal axes first, and then rotating them to coincide with X, Y, and Z.

The mass, moment of inertia and position of the center of gravity can be either calculated or determined by test. For the moments of inertia we can swing the component as a pendulum and measure the period of oscillation  $T_0$ , and from it we can calculate the moment of inertia by means of  $I_{cg} = \frac{1}{4\pi^2} M g L T_0^2 - M L^2$ , where  $L$  is the distance from CG to the center of rotation. This method seems to be simple to use but it is very sensitive to errors when  $L$  is short and the position of the center of gravity is not precisely determined. Another procedure consists in using flexible strings to obtain a rocking motion as well as a translational motion from which the moment of inertia can be determined. The way we proceeded was to

do analytical calculations of the moments of inertia.

With regard to the elastic modes, each of the components, with the exception of STR, was tested on a free-free condition, that is, "floating" by mounting it on soft foam pads; then the Impact Test was applied to a series a test points(the same used for rigid body modes), and the mode shapes obtained. These mode shapes can be expressed as arrays where the number of rows is the number of degrees of freedom (3 for each point times the number of points) and the number of columns is the number of modes.

$$\begin{bmatrix} \phi_{11} & . & \phi_{1n} \\ . & . & . & . \\ \phi_{m1} & . & . & \phi_{mn} \end{bmatrix}$$

A pictorial representation of these modes (in three dimensions) was obtained in a Structural Dynamics Analyzer to check continuity and compatibility of the modes (to find out if there were bad measurements).

The structure STR was tested differently since it was attached to the floor. Here the modes were obtained by a random excitation test using an electrodynamic shaker. The test points along the ways were marked at 1-inch apart to have good resolution, since the Y-carriage runs over them.

The frequency range for each of the main components varied since each one had its own frequency interval and we wished to have a minimum of 5 elastic modes of each component. Table 2.2 shows the natural frequencies determined for each of the main components. The mode shapes can be seen in Appendix A .

The components MX and MY which are motors coupled to lead screws were treated in a special way. MY is mounted on STR and its dynamics, other than torsion, were already included in the test done on STR. Similarly, MX is mounted on the Y-carriage and it was tested already, except for torsion. So, all we needed was to calculate the torsional modes of MX and

MY. These were as shown in Table 2.3. The component MZ has a short shaft with a pinion at the end, and it was modeled as being rigid in torsion.

The modal analysis method employed by the Structural Dynamics Analyzer involves curve fitting the transfer functions to determine the modal parameters of the component. This technique, which calculates eigenvectors by assuming the existence of only one mode at a time, is not very accurate, that is, it does not give correct absolute values of the mode shapes. The relative values it predicts are probably more reliable.

In order to normalize the elastic mode shapes (for unit modal mass), a convenient step when formulating the equations of motion based on experimental data, we proceeded as explained in the next section.

## 2.3 Modal Parameter Identification

When a modal test is performed on a structure, we obtain the natural frequencies and some scaled version of the mode shapes. This information represents a family of dynamically similar structures, and it is not until we determine the right scaling factor to normalize the mode shapes that we have really identified the particular structure under test. This normalization factor is difficult to obtain with accuracy, when working experimentally, because we have to make assumptions about the modal damping in the structure when we use transfer function measurements. So, even though there are many algorithms to curve fit the measured transfer functions as discussed below, the calculated mode shape values (or scaling factors for normalization) will depend on the algorithm used, and there is an important variance in the results. This in turn results in an uncertainty in the predicted results of CMS.

There are a number of ways that people have proceeded to normalize

the mode shapes based on experimental data. One simple approach used in exact analysis of continuous systems, which may work for structures of simple geometry (like a uniform beam for example) consists of applying the formula for normalization of a continuous beam:  $C = \frac{1}{\sqrt{\int_0^l \psi^2 \rho dz}} \approx \frac{1}{\sqrt{\sum_{i=1}^n \psi_i^2 \rho_i \Delta x_i}}$  where  $C$  would be the scaling factor to get the correct mode shape  $\{\phi\} = C\{\psi\}$ . This formula can be extended to other simple shapes where we integrate over the contour:  $C \approx \frac{1}{\sqrt{\sum_{i=1}^n \psi_i^2 \rho_i \Delta A_i}}$

Another procedure to find the correct mode shape values is based on multi-excitation of the structure [66], in which the structure is excited at several points simultaneously in such a way as to excite one single mode of vibration; then the vibration is measured at each of the test points and that vibration gives the mode shape directly. This method which implies having more sophisticated equipment was not used in our laboratory.

The most common method used is based on a drive-point transfer function measurement [77], which in our case was obtained with high frequency resolution, and then a curve-fitting technique was applied to it to extract from each mode its modal parameters. One of the formulas for the drive-point transfer function is :

$$H(\omega) = A\omega^2 + B + \sum_{k=1}^n \frac{-\phi_{kk}^2 (\frac{\omega}{\omega_k})^2}{1 - (\frac{\omega}{\omega_k})^2 + 2j\zeta_k \frac{\omega}{\omega_k}} \quad (2.27)$$

where  $\omega$  is the frequency,  $A$  and  $B$  are parameters appearing in  $A\omega^2$  which represents the contribution of the higher modes, and  $B$  which is the contribution of the lower modes. Each mode has three parameters:  $\omega_k$  is the natural frequency in rad/sec,  $\zeta_k$  is the modal damping ratio, and  $\phi_{kk}$  is the true mode shape value at the drive-point. This formula assumes the following idealizations:

- Damping is linear and viscous.
- Damping is proportional.



In order to get these modal parameters, different algorithms that curve-fit the experimental data have been prepared, some of them assume there is one dominant mode only, and they compensate for the other modes assuming these are far apart. In this single mode group of techniques we can mention the circle fit to the Nyquist polar plot (real part vs imaginary part with frequency as a parameter), the quadrature picking, and the rational fraction least squares [11].

Another group of techniques make multimodal curve fits to the transfer function. In general they involve a large number of iterations. They may also have problems of convergence since these are nonlinear parametric fits (linear in  $\phi_{kk}^2$ , nonlinear in  $\omega_k$  and  $\zeta_k$ ), and an iterative procedure is necessary. Among these methods we can mention the method of rational fraction polynomials [11], the Marquardt Algorithm [54], and Global Fitting [24]. Brown, Allemang, and Zimmerman [11] describe parameter estimation techniques that can be used to determine modal parameters from experimentally measured frequency response or unit impulse response with particular details on multidegree of freedom techniques. Moré [54] discusses an efficient implementation of the Levenberg-Marquardt algorithm and shows that it has very strong convergence properties.

The way we proceeded, which was easy to use and readily available, was to utilize a Simplex technique that minimizes the sum of the squares of the residuals (or the differences between the data and the corresponding calculated values based on successively improved parameters). Caceci and Cacheris [12] present this technique of curve fitting and discuss its application, advantages and disadvantages. The Simplex program used for curve-fitting admits any function, linear or nonlinear, whose coefficients are the parameters to be determined. We used equation 2.27 with the modal parameters to be adjusted  $\omega_k$ ,  $\zeta_k$ , and  $\phi_{kk}$  with  $n$  varying from 5 to 13

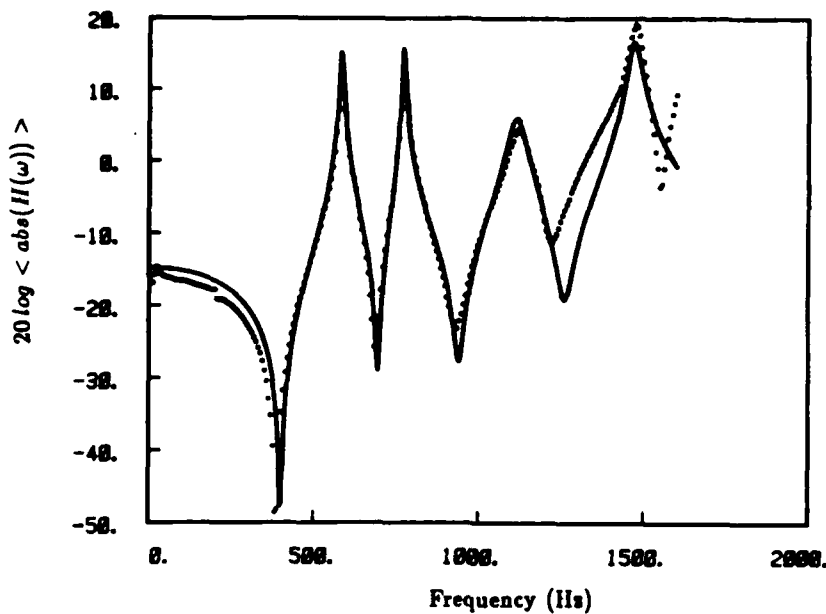


Figure 2.3: Curve fit of transfer function

according to the component. We first tried to determine all parameters simultaneously, which are  $3n$ , but the process was converging so slowly (if at all) that we could not proceed. Then, taking as initial values for these parameters the values obtained by a single-mode curve-fitting technique, we applied the Simplex method to the determination of three parameters at a time (for one mode), but using equation 2.27 with all the modes of interest. Here convergence was achieved in a small number of iterations. Then we proceeded in the same way with each of the subsequent modes, each time updating the corresponding parameters. This procedure tended to converge a little faster. One of the results of the curve fits is shown in Figure 2.3.

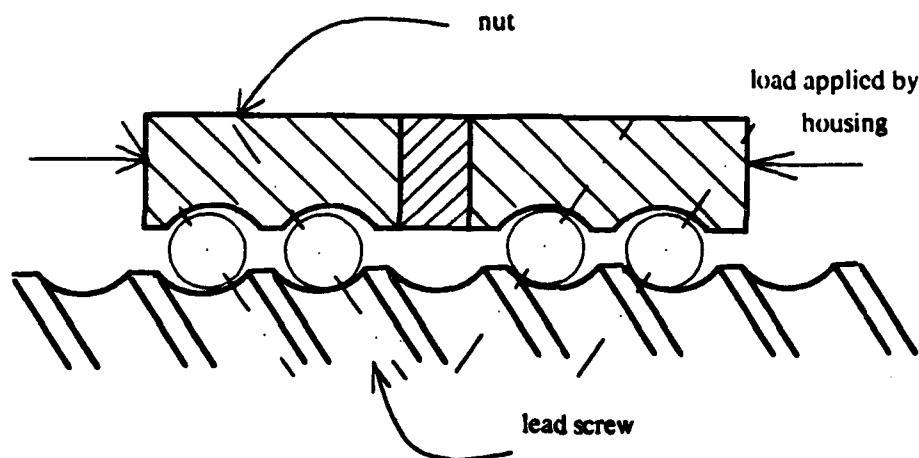


Figure 2.4: Detail of lead screw and nut

## 2.4 Physical Connection of the Components

Before applying CMS we have to define the degrees of freedom of each connection, that is, the vectors representing the motion of the points of connection. This depends on how the components are physically connected.

When the carriages are constructed to form the cartesian robot, they are connected by means of preloaded cam followers that run on straight bars or ways as illustrated in Figure 2.6 . There are a number of these connections between each mating pair of components as can be seen in Figure 2.5. With regard to the connection of the lead screws, there is a special nut mounted on the component to be moved, with lubricated balls inside, thus transforming the rotation of the lead screw into a translation of the carriage. (see Figure 2.4).

Since the cam follower acting on the way exerts a normal force (if friction is neglected), we can consider as the degree of freedom in that connection

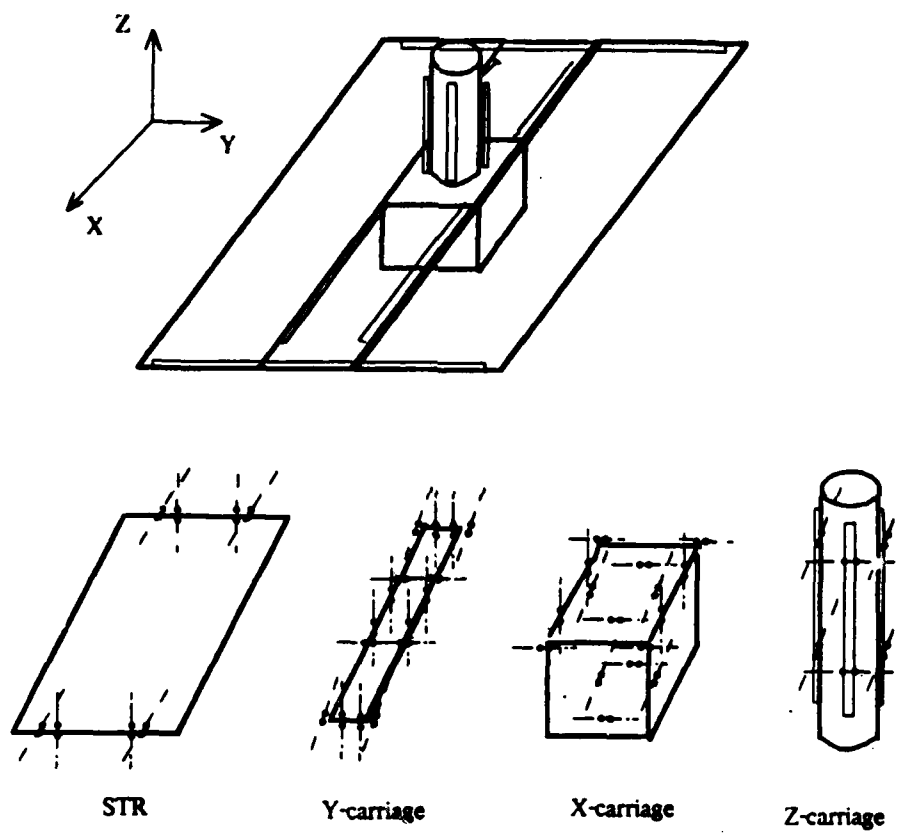


Figure 2.5: Schematic representation of physical connections

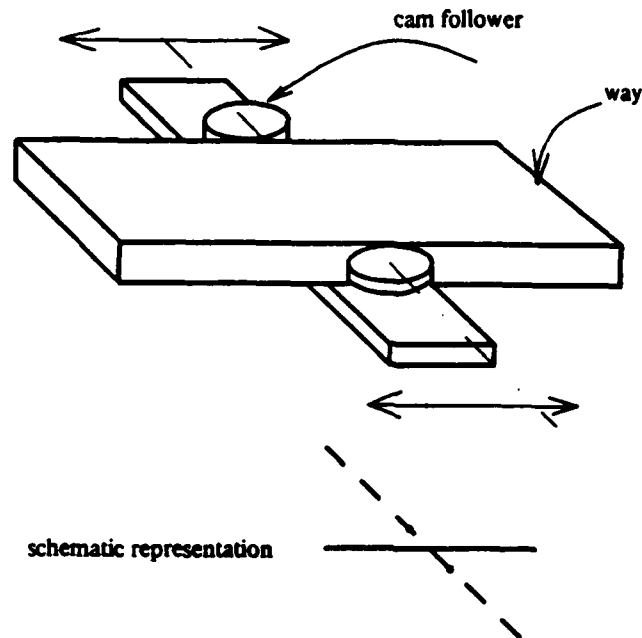
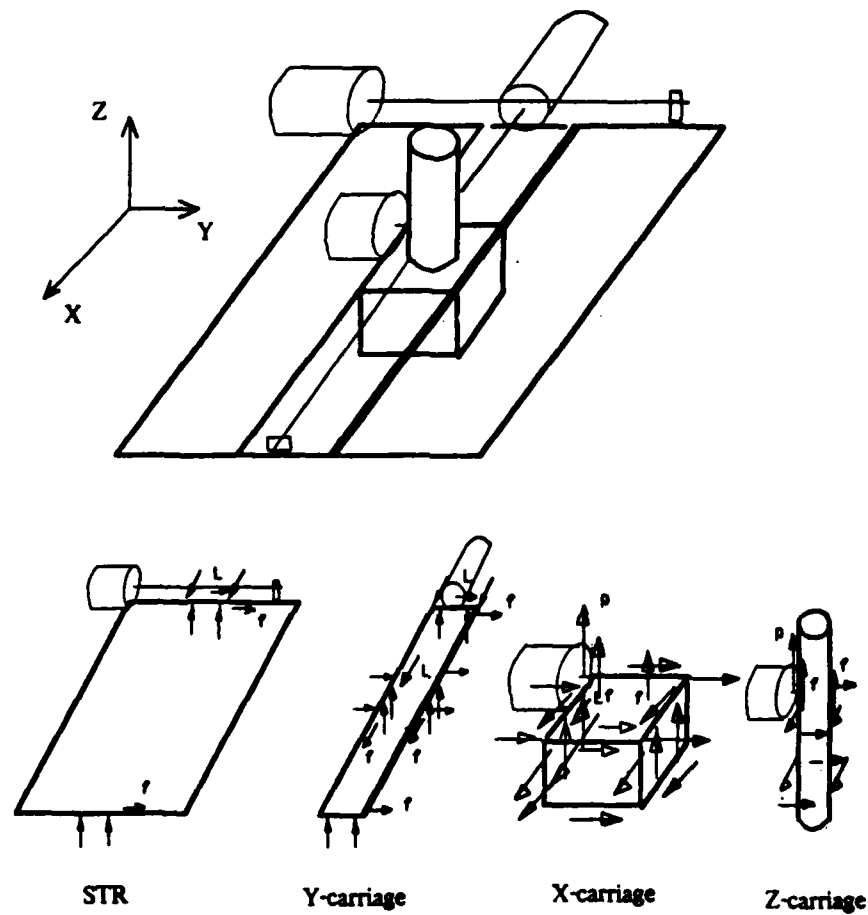


Figure 2.6: Cam followers on ways

one coordinate or vector perpendicular to the way. Friction is accounted for by putting (in selected positions only) one vector (degree of freedom) parallel to the way. The nut that connects to the lead screw is represented by a vector (degree of freedom) parallel to the lead screw axis. So, the degrees of freedom of all these robot connections are defined as schematically represented in Figure 2.7. Notice that we use translational degrees of freedom, but not rotational ones. Bending moments and torques are transmitted between two components by using several degrees of freedom in the connection.

Friction was included as a friction degree of freedom because the predicted mode shapes of the synthesized robot (without friction degrees of



L - lead screw-nut degree of freedom

f - friction degree of freedom

p - rack-pinion degree of freedom

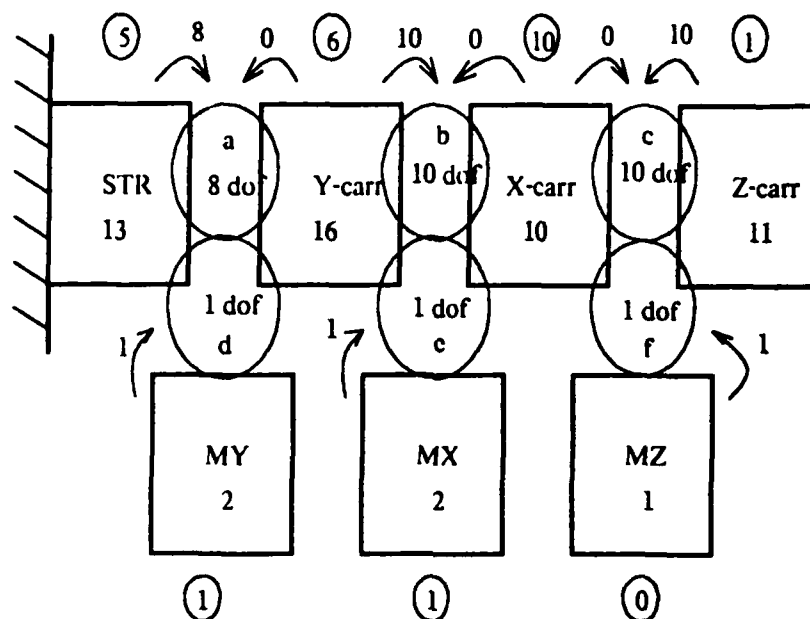
Figure 2.7: Degrees of freedom of physical connections

freedom) showed a relative motion between the parts which was not observed in the experimental mode shapes. There is also a more fundamental reason for including the friction degrees of freedom; a Coulomb friction force opposes motion and tries to equilibrate forces until it saturates, that is, when its static limit is reached. This saturation makes its behavior nonlinear as opposed to a linear spring, for example, which ideally never saturates. So, if we assume that the forces never reach saturation, and that is because the cam-followers are preloaded against the ways, then we can say that the friction effect is like a bolt joint which does not allow slide motion during a cycle of vibration. Nevertheless, to avoid redundancies we introduced only a selected number of these friction degrees of freedom just to prevent some relative motions between components based on experimental results.

## 2.5 CMS Model of Connections

After deciding what distribution of degrees of freedom can represent component connections and having the modal representation of those individual components, we can use CMS to establish the compatibility conditions at the interfaces and end up with a prediction of the dynamic behavior of the robot. Figure 2.8 shows a schematic view of the connections illustrated in Figure 2.5 by representing each component with a box and each connection with an ellipse. The numbers inside the ellipses are the numbers of degrees of freedom used, whereas the numbers inside the boxes are the number of modes used.

The compatibility condition is the starting point for CMS. It says that the points of connection of two adjacent components have to move together in the same way, that is,  $x_{A_1} = x_{D_1}$ . A slightly different condition is used



no. inside box: total no. of component modes

no. above arrow: no. of generalized coordinates chosen to be dependent

encircled no.: no. of generalized coordinates chosen to be independent

Figure 2.8: Box diagram of Component Mode Synthesis

when we describe the assemblies MX and MY (motor and lead screw). Here, the motion of the component that is moved by the lead screw is equal to the sum of the motion of the supporting component plus the translational motion of the nut caused by rotation of the screw, that is  $x_{A_i} = x_{D_i} + x_{L_i}$ . For example, in Figure 2.9 we show the case of MY, STR and Y. Here, if Y moves to the right, it may happen that only MY rotates, or only STR translates, or both move. But in any case the sum of motions of STR and MY must be equal to the motion of the Y-carriage. Something similar happens between the Z-carriage and X and MZ.

The mode shape data of the components can be defined as in table 2.4.



Component	Mass(Kg)	CG(mm)	$I_{x_{cg}} (Kg - m^2)$	$I_{y_{cg}}$	$I_{z_{cg}}$
X-carriage	17.556	$x = 359$ $y = 451$ $z = 130$	0.3846	0.18006	0.25495
Y-carriage	25.4016	$x = 185$ $y = 471$ $z = 74$	0.8060	2.0194	2.1081
Z-carriage	12.2458	$x = 368$ $y = 542$ $z = -160$	0.7404	0.7404	0.0234

Table 2.1: Mass and Inertia properties of Robot Carriages

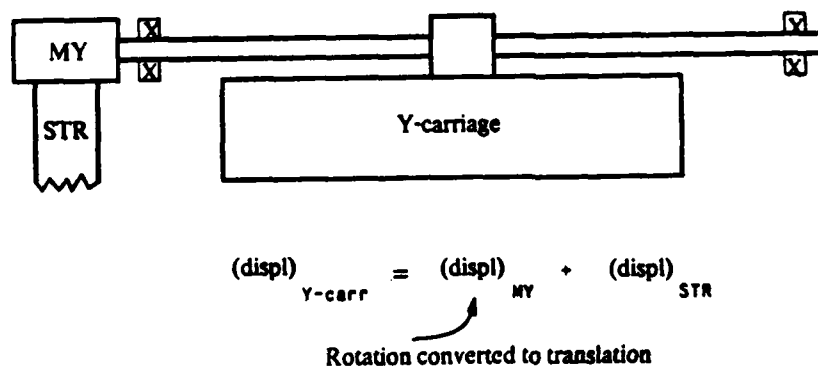


Figure 2.9: triple connection

Mode No.	STR	X-carriage	Y-carriage	Z-carriage
1	14.67	168	121	587
2	21.77	218	140	623
3	36.87	431	150	772
4	46.89	606	181	1115
5	51.78	-	200	1471
6	62.62	-	234	-
7	81.81	-	356	-
8	96.95	-	393	-
9	128.37	-	415	-
10	136.26	-	506	-
11	156.82	-	-	-
12	176.83	-	-	-
13	193.90	-	-	-

Table 2.2: Natural Frequencies(Hz) of Main Components

Mode	$f_n(\text{Hz}), \text{MX}$	$\phi_n(x), \text{MX}$	$f_n(\text{Hz}), \text{MY}$	$\phi_n(x), \text{MY}$
1	0	259.56	0	254.98
2	1321	$346 \cos(2.734E - 4\omega_n x)$	993	$298 \cos(2.734E - 4\omega_n x)$
3	3963	$354 \cos(2.734E - 4\omega_n x)$	2979	$307 \cos(2.734E - 4\omega_n x)$

Table 2.3: Natural Modes in Torsion of MX, MY.

Each component has at least one joint (with several degrees of freedom) and for each of this joints there is an associated modal matrix for which the number of rows is the number of degrees of freedom, and the number of columns is the number of modes. Notice that these modal matrices are partitioned in such a way that the first submatrix (suffix  $R$ ) corresponds to the independent generalized coordinates, and the second submatrix (suffix  $O$ ) corresponds to the dependent ones. The number of generalized coordinates for each component can be seen in Figure 2.8. The encircled numbers above the top boxes, and the ones below the bottom boxes are the number of independent generalized coordinates.

Based on these compatibility conditions we can establish the following matrix equation:  $Ap^D = Bp^I$ , where  $[A]\{p^D\}$  is

$$\begin{bmatrix} FSTRO1 & -FYA1O & 0 & 0 & 0 & 0 \\ 0 & FYA2O & 0 & 0 & 0 & 0 \\ 0 & 0 & -FZTO1 & 0 & 0 & 0 \\ FSTRO2 & -FYA3O & 0 & FMY1O & 0 & 0 \\ 0 & -FYA4O & 0 & 0 & -FMX1O & 0 \\ 0 & 0 & FZTO2 & 0 & 0 & -FMZ1O \end{bmatrix} \begin{Bmatrix} p_{STR}^D \\ p_Y^D \\ p_Z^D \\ p_{MY}^D \\ p_{MX}^D \\ p_{MZ}^D \end{Bmatrix} \quad (2.28)$$

and  $[B]\{p^I\}$  is

$$\begin{bmatrix} -FSTRR1 & 0 & FYA1R & 0 & 0 & 0 \\ 0 & FXA1R & -FYA2R & 0 & 0 & 0 \\ 0 & -FXA2R & 0 & FZTR1 & 0 & 0 \\ -FSTRR2 & 0 & FYA3R & 0 & -FMY1R & 0 \\ 0 & -FXA3R & FYA4R & 0 & 0 & FMX1R \\ 0 & FXA4R & -FZTR2 & 0 & 0 & 0 \end{bmatrix} \begin{Bmatrix} p_{STR}^I \\ p_X^I \\ p_Y^I \\ p_Z^I \\ p_{MY}^I \\ p_{MX}^I \end{Bmatrix} \quad (2.29)$$

From this equation we get the dependent elements of the generalized coordinates  $p^D$  as a function of the independent ones  $p^I$ . Then, the transformation

Component	Modal matrix	Size	Connection (Figure 2.8)
Fixed structure (STR)	[FSTRR1 FSTRO1]	8 x 13	a
	[FSTRR2 FSTRO2]	1 x 13	d
X-carriage	[FXA1R]	10 x 10	b
	[FXA2R]	10 x 10	c
	[FXA3R]	1 x 10	e
	[FXA4R]	1 x 10	f
Y-carriage	[FYA1R FYA1O]	8 x 16	a
	[FYA2R FYA2O]	10 x 16	b
	[FYA3R FYA3O]	1 x 16	d
	[FYA4R FYA4O]	1 x 16	e
Z-carriage	[FZT1R FZT1O]	10 x 11	c
	[FZT2R FZT2O]	1 x 11	f
Ball screw-motor, X-direction	[FMX1R FMX1O]	1 X 2	e
Ball screw-motor, Y-direction	[FMY1R FMY1O]	1 X 2	d
Ball screw-motor, Z-direction	[FMZ1O]	1 X 1	f

Table 2.4: Modal Matrices of Robot Components.

matrix which is implicitly defined by

$$\begin{Bmatrix} p^D \\ p^I \end{Bmatrix} = [T] \{p^I\} \quad (2.30)$$

can be formed. So, by following the procedure already described in section 2.1 we can obtain the equations of motion of the cartesian robot, which for the homogeneous case have a solution described in terms of the natural modes of vibration. These modes were synthesized in the computer on the base of the previous analysis and then transmitted to a Structural Dynamics Analyzer in order to take advantage of its display capabilities; thus we were able to see a 3-D representation of each mode shape on the analyzer screen, the comparison of experimentally determined with synthesized mode shapes could be conveniently done. Before showing some of these results, we should discuss some issues about convergence and conditioning of this CMS process.

## 2.6 Convergence of CMS

As it has been pointed out by several authors, among them Bathe [2], the technique of CMS makes use of the Rayleigh-Ritz analysis [2] in the sense that it takes as the Ritz-basis vectors the eigenvectors of the individual components and then through a linear combination of them, it gives the best solution available that corresponds to those basis vectors. This is only an approximation since we are not using all the modes of each component but rather we have truncated by establishing a finite frequency range of study.

To understand why CMS is considered a Rayleigh-Ritz analysis and under what conditions this is true, we perform the following analysis. Suppose we somehow know the complete mass and stiffness matrices of the assem-

bled system formed by the substructures A and B, but suppose that the eigenvalue problem is too large to be solved:

$$[K][\Phi] = \lambda[M][\Phi] \quad (2.31)$$

We want to reduce the system order from  $m$  to  $s$  by using the Ritz-basis vectors  $\phi$  ( $m \times s$ ). In so doing, we are trying to get an approximation to  $\Phi$ , call it  $\bar{\phi}$ . Put  $[\bar{\phi}] = [\phi][x]$  where  $[x]$  are the Ritz coordinates to be calculated.

Then form the Rayleigh quotient

$$\rho(\bar{\phi}) = \frac{[\bar{\phi}]^T [K] [\bar{\phi}]}{[\bar{\phi}]^T [M] [\bar{\phi}]} \quad (2.32)$$

which becomes after substitution of  $[\bar{\phi}]$

$$\rho(\bar{\phi}) = \frac{\sum_{i=1}^s \sum_{j=1}^s x_i x_j \tilde{k}_{ij}}{\sum_{i=1}^s \sum_{j=1}^s x_i x_j \tilde{m}_{ij}} \quad (2.33)$$

where  $[\tilde{K}] = [\phi]^T [K] [\phi]$  and  $[\tilde{M}] = [\phi]^T [M] [\phi]$ .

Minimize the Rayleigh quotient:

$$\frac{\partial \rho(\bar{\phi})}{\partial x_i} = \frac{2\tilde{m} \sum_{j=1}^s x_j \tilde{k}_{ij} - 2\tilde{k} \sum_{j=1}^s x_j \tilde{m}_{ij}}{\tilde{m}^2} = 0 \quad (2.34)$$

Use  $\rho = \frac{\tilde{k}}{\tilde{m}}$  to get

$$\sum_{j=1}^s x_j (\tilde{k}_{ij} - \rho \tilde{m}_{ij}) = 0 \text{ for } i = 1, 2, \dots, s \quad (2.35)$$

This is equivalent to the eigenvalue problem  $[\tilde{K}][x] = \rho[\tilde{M}][x]$  of reduced order  $s$  which we suppose we can solve. This process parallels the CMS process as illustrated in Table 2.5.

From this analysis we conclude the following:

- The Ritz coordinates  $[x]$  are the same as the product  $[T][\psi]$  in CMS.

Concept	Component Mode Synthesis	Rayleigh-Ritz Analysis
Original equations	$[\ddot{p}_A] + [\omega_A^2]\{p_A\} = \{0\}$ $[\ddot{p}_B] + [\omega_B^2]\{p_B\} = \{0\}$ <p>only <math>n</math> modes are known</p>	$[K][\bar{\phi}] = \lambda[M][\bar{\phi}]$ <p><math>[K], [M]</math> are known, but not <math>[\bar{\phi}]</math>. Problem too big to solve</p>
Choose Ritz-basis vectors $[\phi]$	$[\phi] = [\phi_A \phi_B]$	$[\phi]$ , a guess
Apply physical principles	<p>compatibility:</p> $[\phi_{A_c}]\{p_A\} = [\phi_{B_c}]\{p_B\}$ <p>Eliminate overconstraining: <math>\{p\} \rightarrow \{q\}</math> through <math>\{p\} = [T]\{q\}</math></p>	<p>assume <math>[\bar{\phi}] = [\phi][x]</math>, minimize <math>\rho(\bar{\phi})</math>, or minimize potential energy.</p>
Reduced system of order $s$	$[T]^t[T]\{\ddot{q}\} + [T]^t[\omega_n^2][T]\{q\} = \{0\}$	$[\tilde{K}][x] = \rho[\tilde{M}][x]$
Solve eigenvalue problem	get $\rho_i, [\psi]$	get $\rho_i, [x]$
Approximation to eigenvalues	$\hat{\omega}_i^2 = \rho_i$	$\hat{\omega}_i^2 = \rho_i$
Approximation to eigenvectors	$[\bar{\phi}] = [\phi][T][\psi]$	$[\bar{\phi}] = [\phi][x]$

Table 2.5: Comparison of CMS and Rayleigh-Ritz Methods

- While the Rayleigh-Ritz analysis uses any set of Ritz-basis vectors to get an approximation to the eigenvalues and eigenvectors with a precision that varies according to the good choice of the basis vectors, CMS uses, in most of the cases, the most adequate vectors (a set that includes the first  $n$  modes of each component), although the use of a truncated set precludes getting the exact solution.
- As the number of modes used in the analysis increases, CMS converges monotonically from above in one of the fastest ways possible since each addition of a Ritz-basis vector is one of the best vectors that can be added.
- In the Rayleigh-Ritz analysis, the use of a complete mass and stiffness matrix to get the reduced system, and then the application of a minimization process to the Rayleigh quotient is equivalent to applying compatibility conditions in CMS. Both methods lead to the reduced system of equations whose eigenvalue problem solution gives the Ritz coordinates  $[x] = [T][\psi]$ .
- If the Rayleigh-Ritz analysis uses as basis vectors the eigenvectors of the substructures, then it leads to the same answer obtained by CMS.
- In practical cases  $[K]$  and  $[M]$  are not known, so we do not apply Rayleigh-Ritz analysis, but its principle is implicitly used in CMS.

The results obtained for the eigenvalues and eigenvectors of the assembled robot are approximations to the real values, and it has been shown for the Rayleigh-Ritz analysis [2] that the convergence is monotonic from above, that is, the more modes we use from the components, the closer we get to the real results. But this method always yields eigenvalues that are higher than the exact ones. The rate of convergence can be determined



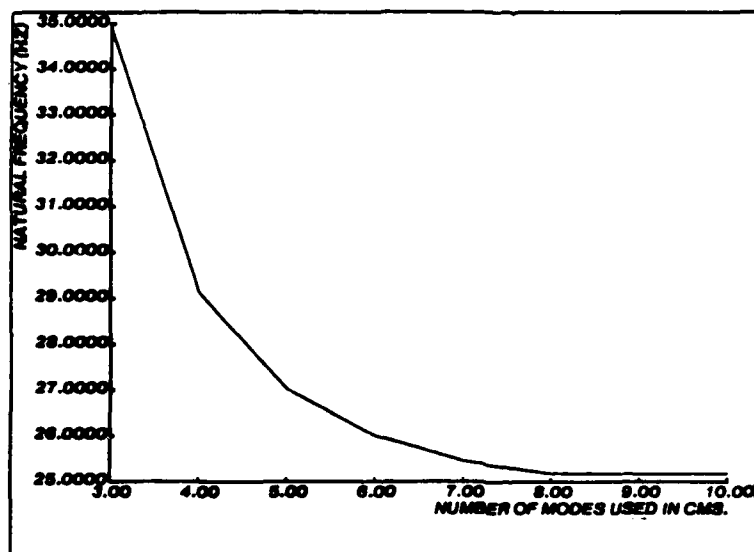


Figure 2.10: Convergence of 1st natural frequency with number of modes used

numerically by simply comparing two sets of eigenvalues, one obtained with a given number of modes and the other obtained with one mode less for any of the components; then we can determine whether the convergence is satisfactory or which component needs more modes. To illustrate this convergence rate, consider the case of a free-free beam whose modes are known (see Table 2.6). If we connect it to a fixed support near the end to have a pinned-pinned-free beam, and we compare the first natural frequency of this so supported beam as obtained by CMS to that obtained from its formula (see Blevins [10]), we can see the effect of using more and more modes of the free-free beam as is shown in Figure 2.10.

We should point out that this monotonic convergence from above can only be seen when the modes of the original component are correctly normalized. This can be done exactly in theory, but in practice, as we have discussed before (section 2.3), there is always an uncertainty on the nor-

malization. Therefore this convergence pattern may be different, that is, the convergence may be towards a set of eigenvalues other than the true values.

## 2.7 Conditioning of the Numerical Process

When applying CMS to connect two or more structures, and when more than one point of connection is used, an ill-condition may arise. Ill conditioning is a situation in which a slight change in the data produces a big change in the results.

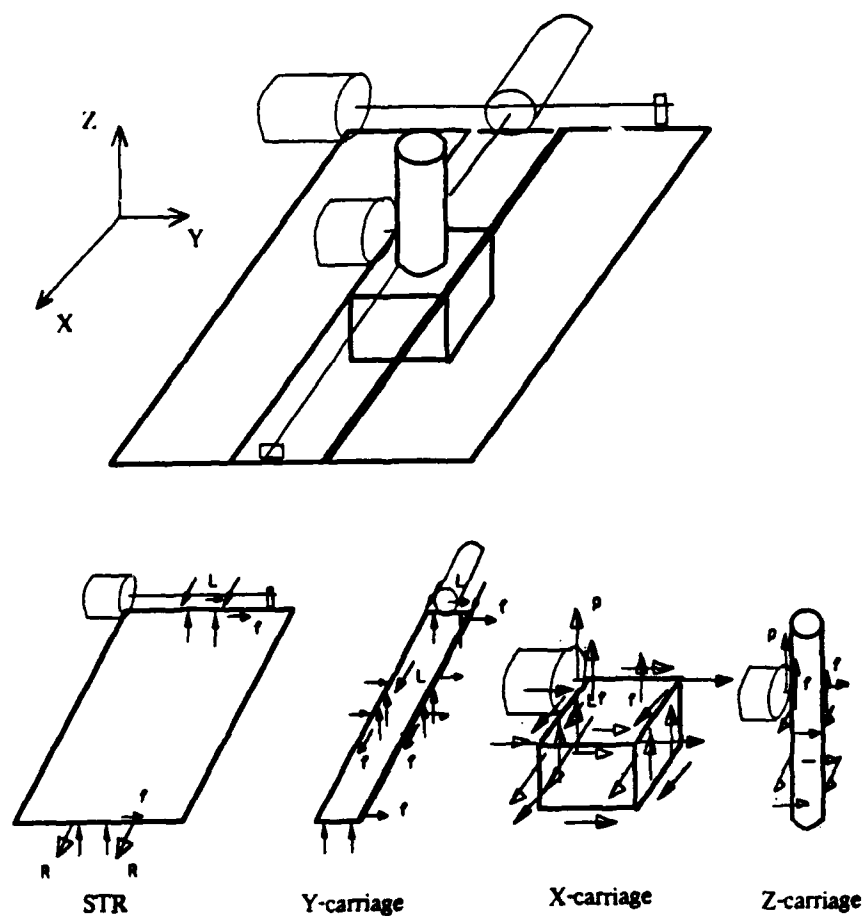
The numerical process in CMS includes the inversion of a matrix (see equation 2.28) plus the solution of an eigenvalue problem, and either of the two or both operations may be ill-conditioned. To detect this problem we follow the procedure described below.

Turing [76] describes a way to determine the conditioning for matrix inversion; that is, given the problem  $[A]\{x\} = \{b\}$ , we want to know what effect a slight change in  $\{b\}$  produces in the result  $\{x\}$ . It is found that  $\Delta x_i = \frac{\partial x_i}{\partial b_j} \Delta b_j = (A^{-1})_{ij} \Delta b_j$ , so the biggest element in  $[A]^{-1}$  determines the condition number. For the case of CMS, where we have  $\{p^D\} = [A]^{-1}([B]\{p^I\})$ , we proceed as follows:

- Run original case and get eigenvalues.
- Find most sensitive degree of freedom in  $b = Bp^I$  by finding  $j$  for biggest  $\frac{\partial p^{-1D}}{\partial (Bp^I)_j} = (A^{-1})_{ij}$ .
- Alter mode shape value for most sensitive degree of freedom of  $B$  by 1 % and get the new eigenvalues.
- Compare corresponding eigenvalues.

This problem of ill-conditioning was present for an early model of the robot joints as shown in Figure 2.11. Two of the degrees of freedom in the X-direction were redundant, and when connecting the robot components, the first resultant two modes of the robot were unexpectedly high. By applying the above procedure we found that the alteration of 1 % in the most sensitive degree of freedom produced 2.07 % and 1.47 % change in these two first modes respectively. The problem disappeared when two degrees of freedom in the X-direction were removed (two from the front). Then the change in the two modes was -0.04 % and 0.03 % and the natural frequencies were reasonable as expected. This elimination of two degrees of freedom in the X-direction did not affect the predicted robot eigenvalues appreciably, at least in the frequency range of interest.

In order to identify possible redundant degrees of freedom we can proceed as follows. In 3-D there are at least 6 degrees of freedom to be used since that is the minimum required to connect two rigid bodies. The way these degrees of freedom are distributed can not be arbitrary since they have to prevent any possible relative motion (translation or rotation) between the connecting parts. If the bodies are flexible, we can start adding more degrees of freedom and here is where a redundant combination may give problems. The most sensitive degree of freedom as indicated by the largest element of  $A^{-1}$  is a good candidate at which to start looking for redundancies. In the case of the robot, an explanation of why an ill-condition was present is that the first two mode shapes (the ill-conditioned modes) are like a rigid body rocking on torsional springs at the floor, but when we connect the carriages on the top of the structure, we are trying to infer from a distant section (top of the robot) what this addition of inertia (of the carriages) will produce, and this addition is introduced redundantly since only two degrees of freedom in X-direction are necessary.



L - lead screw-nut degree of freedom  
 f - friction degree of freedom  
 p - rack-pinion degree of freedom  
 R - pair of redundant degrees of freedom

Figure 2.11: Redundant degrees of freedom causing ill-condition

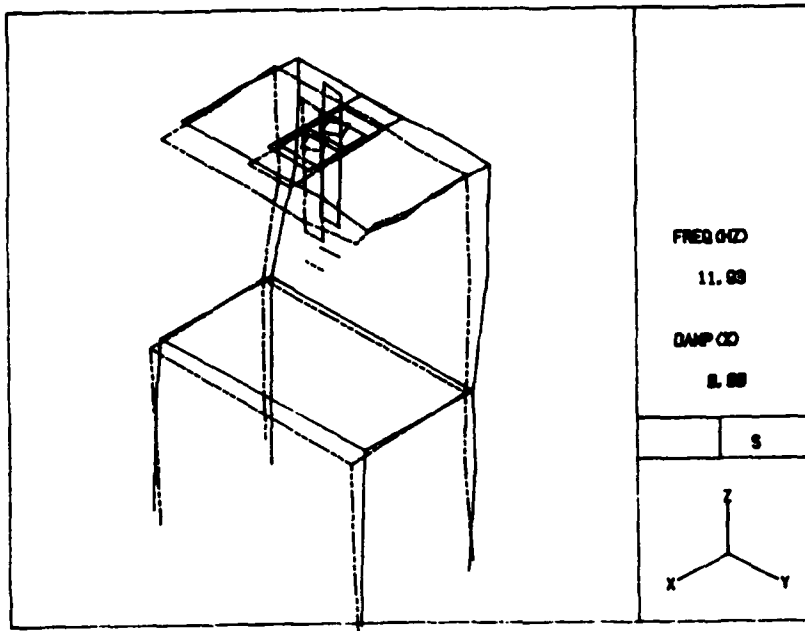


Figure 2.12: Synthesized mode shape 1 of robot

## 2.8 Predictions of Quasi-Static Model

For a given configuration, that is, for a fixed position of the carriages, vibration can be described by means of the natural modes of the system. Our model of CMS can predict those modes and the Structural Dynamics Analyzer can display the motions. Some of the results are shown in Figure 2.12 and Figure 2.13. For more detail and comparison between predicted and measured mode shapes, see Chapter 4 and Appendix A.

Mode No.	$f_n$ (Hz)
1	0
2	0
3	135
4	373
5	731
6	1209
7	1806
8	2522
9	3358
10	4313

Table 2.6: Natural Modes of a Free-Free Beam

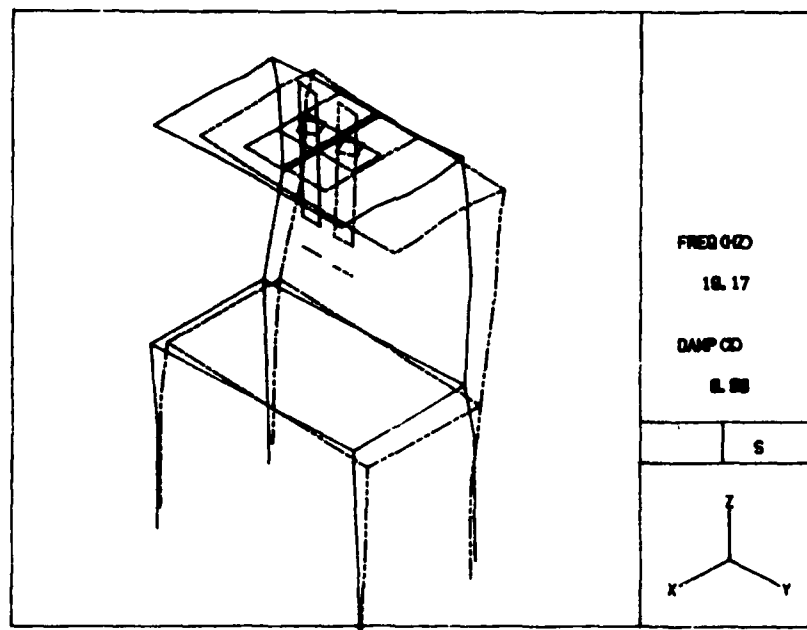


Figure 2.13: Synthesized mode shape 2 of robot

## Chapter 3

# PROPOSED DYNAMIC MODEL OF A CARTESIAN ROBOT

### 3.1 A Procedure to Analyze Systems of slowly-varying configuration

Here we discuss the possibility of extending the method of CMS to systems which have equations with slowly varying coefficients, which is the case of this and many other robots as discussed below. We apply this method to the case of a simply supported beam with a 2-degree of freedom system traveling on the beam at a constant speed. Based on this simple example, we attempt to justify the use of this method for analysis of a cartesian robot and we discuss the significance of the errors resulting from the associated approximations.

As discussed in Chapter 2, in the example of a moving two-degree of freedom system on a simply supported beam, our goal is to apply CMS

to connect the robot components in such a way as to take into account that some of the points of connection may be slowly changing with time. We do this by putting as the argument of the eigenfunctions of the linear bearing surfaces (ways) some function of time that describes how the points of connection are moving. This procedure, as it was applied to the beam problem is valid when  $\epsilon \ll 1$ , that is when we can neglect some terms in  $\epsilon$  in the general equations of motion. For a typical bridge the value of  $\epsilon$  falls in the range of 0.10 to 0.20. In the case of the robot, these parameters depend on which direction the carriages are traveling; for each of three directions X,Y,Z the results are as shown in Table 3.1. Since  $\epsilon$  is small, we can classify the cartesian robot as a slowly-varying system; so, besides the fact that we can neglect some terms in  $\epsilon$  and apply CMS directly to derive the equations of motion, we can make further use of the slowly varying characteristics (if desired) to find approximate solutions to the equations in an efficient way.

There is a well developed set of techniques for solving such problems in close form, as explained by Nayfeh [57]. The problems may be multi-degree of freedom and can contain forcing terms. Nevertheless, the most straightforward technique to solve the equations is by numerical integration, and that is what we have chosen to do since we first want to verify that the model can represent the real system with reasonable precision.

## 3.2 Determination of Continuous Eigenfunctions

As mentioned before, the relative motion between carriages is constrained by preloaded cam followers that run on linear bearing surfaces or ways, and physically speaking this motion is continuous. On the other hand



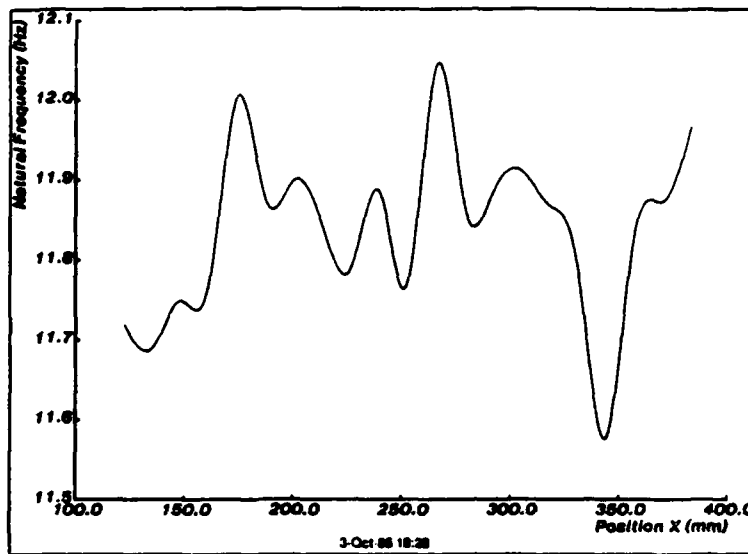


Figure 3.1: Linear interpolation of mode shape data

the test points that describe the eigenfunctions of these ways are discrete although they are closely spaced. This situation makes it necessary either to interpolate between points or to curve-fit using some suitable functions.

We first tried the interpolation techniques because they are easy to use. The interpolation assumes that the test points give exact values for the eigenfunctions; that is, that there is no error involved in the measurements. This of course is not the case. We used linear interpolation and cubic spline interpolation for calculating the mode shape values at the connection points, and to evaluate these techniques we looked at the resulting variation of the 1st natural frequency of the robot with position; this variation should be smooth and could be checked experimentally. So, we found that the linear interpolation gave an irregular modal variation as shown in Figure 3.1, as did the cubic spline interpolation (see Figure 3.2). From these results we conclude that the problem must involve the presence of measurement errors.

Direction	Dominant $f_n$ (Hz)	Ways Length (m)	max. speed(m/s)	value of $\epsilon$
X	12.4	.279	1.27	0.18
Y	18.9	.584	1.27	0.06
Z	48.4	.152	1.27	0.08

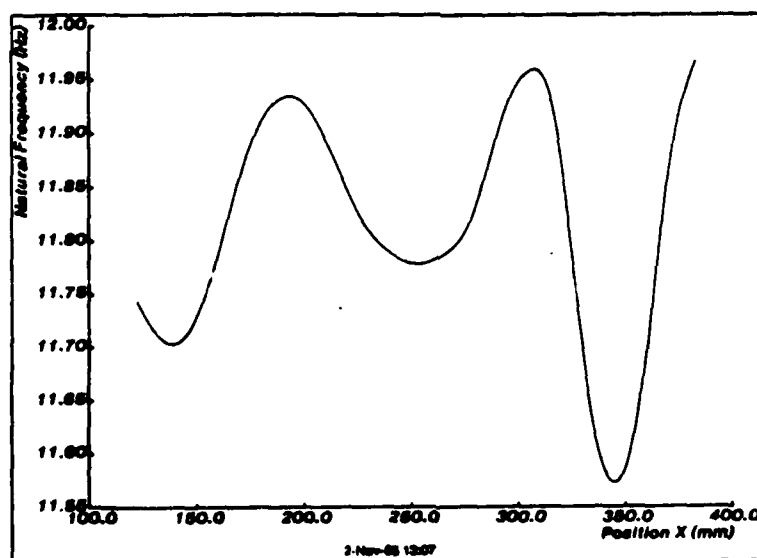
Table 3.1: Typical Values of  $\epsilon$  for Cartesian Robot

Figure 3.2: Cubic spline interpolation of mode shape data

Next we tried curve-fitting the eigenfunctions over the test points on the ways, in the least squares sense, in order to smooth out the errors. One attempt was to use Chebyshev polynomials of different orders. These polynomials are defined by:

$$\begin{aligned} T_0(x) &= 1 \\ T_1(x) &= x \\ T_{n+1}(x) &= 2xT_n(x) - T_{n-1} \end{aligned} \quad (3.36)$$

and they are orthogonal polynomials with some convenient properties for curve-fitting. Figure 3.3 and Figure 3.4 show the curve fits for orders 3 and 5 for a particular case. The corresponding modal variations are shown in Figure 3.5 and Figure 3.6. One observation on the use of Chebyshev polynomials is that they give more weight to the end points of the ways which is an undesirable characteristic because good data may be difficult to get at these ends. Examination of the results showed that the modal variation is very sensitive to choice of the order of the polynomial fit chosen. This is a clear indication that the method is not robust.

Therefore, we chose to proceed by developing a method to fit beam-like eigenfunctions in a least squares sense to experimental data collected on the ways. The ways can be considered as beams whose boundary conditions have to be defined. If the beam is uniform, the eigenfunction is defined by:

$$\phi(x) = C_1 \sin(\beta x) + C_2 \cos(\beta x) + C_3 \sinh(\beta x) + C_4 \cosh(\beta x) + C_5 \quad (3.37)$$

where the parameters  $C_1$  to  $C_5$  and  $\beta$  depend on the end conditions of the beam and  $x$  is a coordinate along the beam (see Appendix C for details). Curve-fitting this function to the data, in order to find the parameters, involves doing a nonlinear parametric fit (nonlinear in  $\beta$ ) which may have multiple solutions depending on the initial guesses for the parameters. The method used was again based on the Simplex technique, where we specify any function we want and the sum of the square of the residuals is

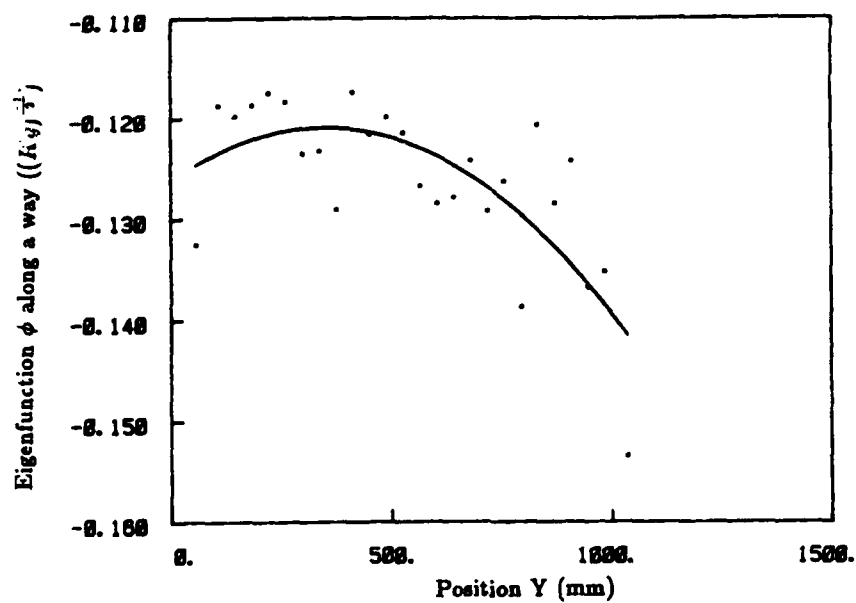


Figure 3.3: Least-squares curve-fit of mode shape data using Chebyshev polynomials of order 3

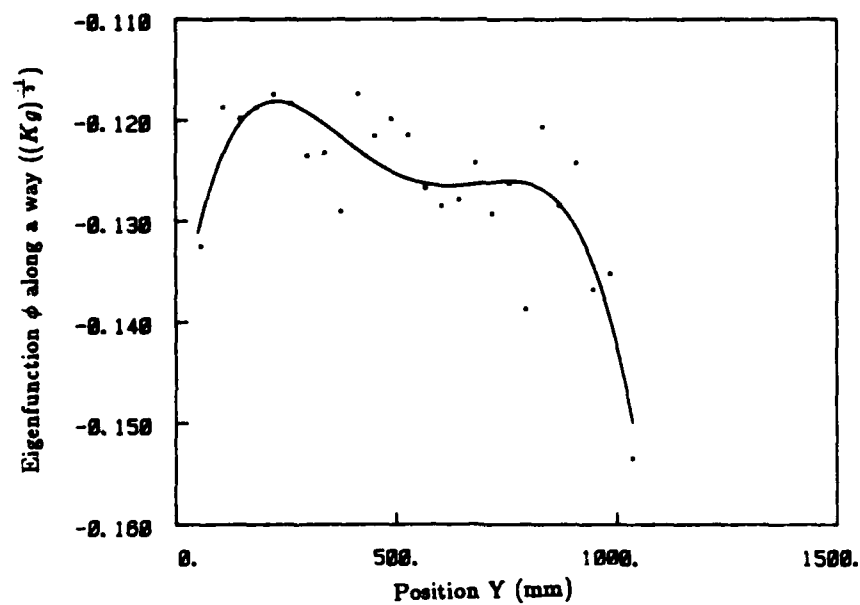


Figure 3.4: Least-squares curve-fit of mode shape data using Chebyshev polynomials of order 5

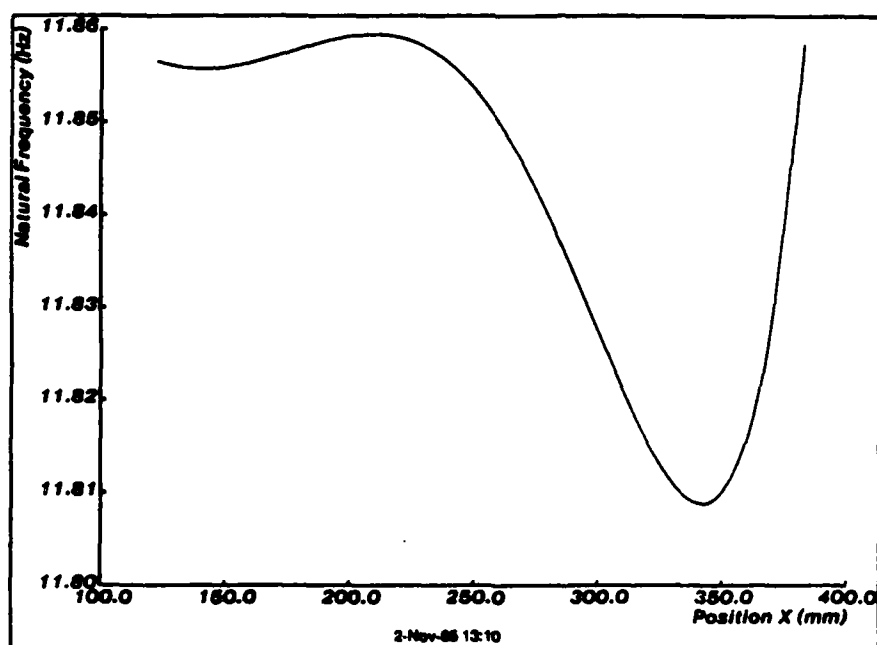


Figure 3.5: Modal variation after curve-fitting mode shape data using Chebyshev polynomials of order 3

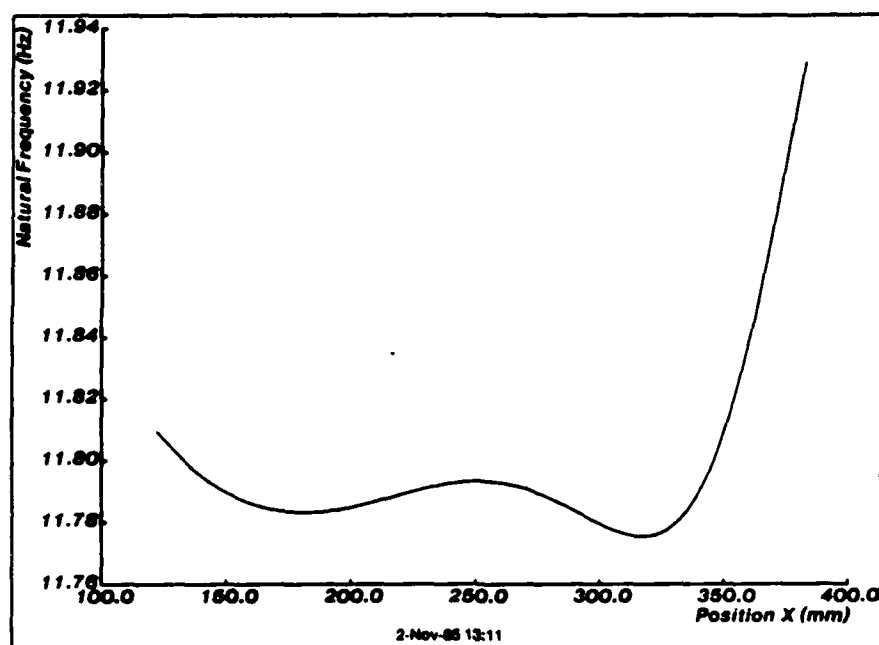


Figure 3.6: Modal variation after curve-fitting mode shape data using Chebyshev polynomials of order 5

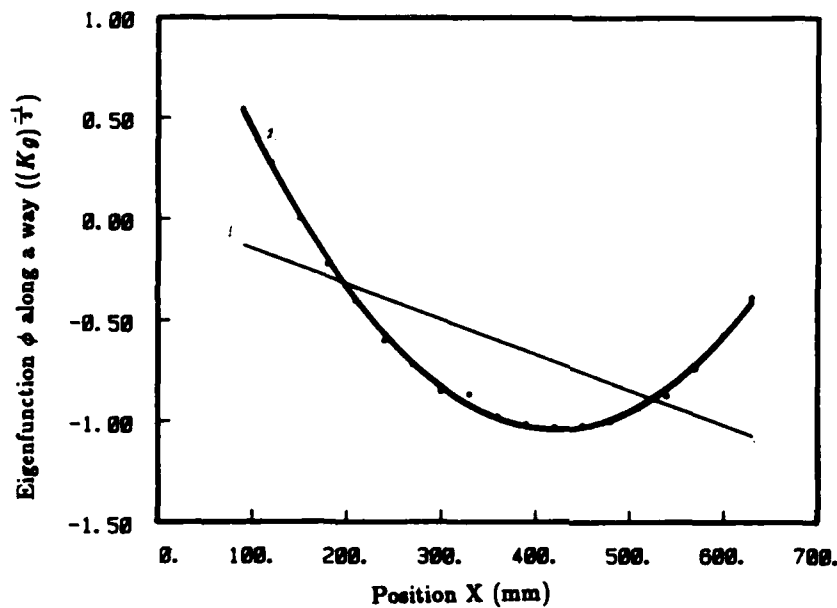


Figure 3.7: Two different solutions to the curve-fitting of mode shape data using a beam-like eigenfunction

minimized. To find a good solution we have to do several curve-fitting calculations using different initial values of the parameters each time, and then choose one result that has the minimum standard deviation. Figure 3.7 shows two different solutions to the curve-fitting of one case; notice that the best fit has a standard deviation of  $5.3E-3$  whereas the bad fit has  $9.6E-2$ . Figure 3.8 shows another case where the data is generally good and Figure 3.9 shows the case where there is noisy data. So, the idea of the equivalent beam smoothes out the errors and at the same time introduces the physics into the problem. When these beam-like curve fits are used to connect the components of the robot, the modal variation looks reasonable as expected (see Figure 3.10).

This curve-fitting technique that assumes an equivalent beam was only used for the cases where a motion normal to the ways would occur. For example, if the axis is positioned along the Y-direction, then only  $\phi(x)$  and

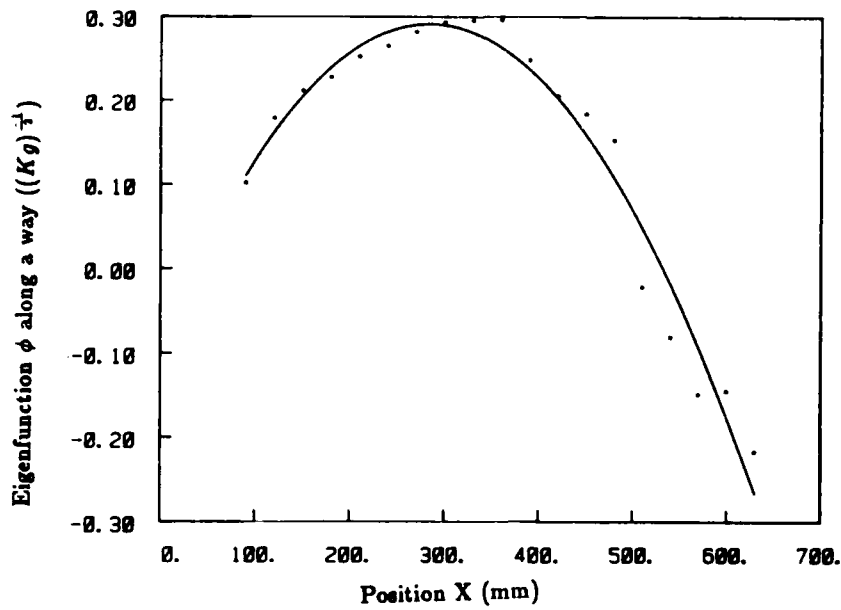


Figure 3.8: Curve fit of mode shape data using a beam-like eigenfunction, case of good data

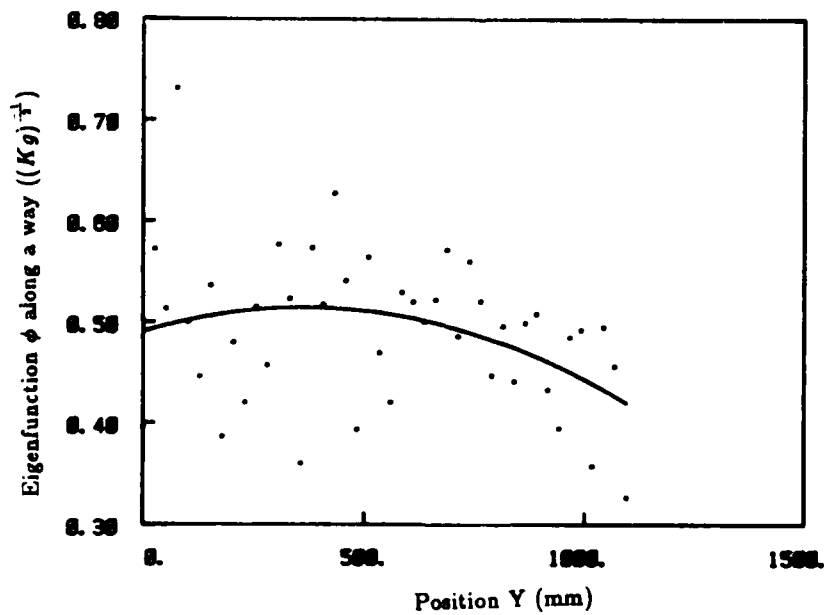


Figure 3.9: Curve fit of mode shape data using a beam-like eigenfunction, case of noisy data



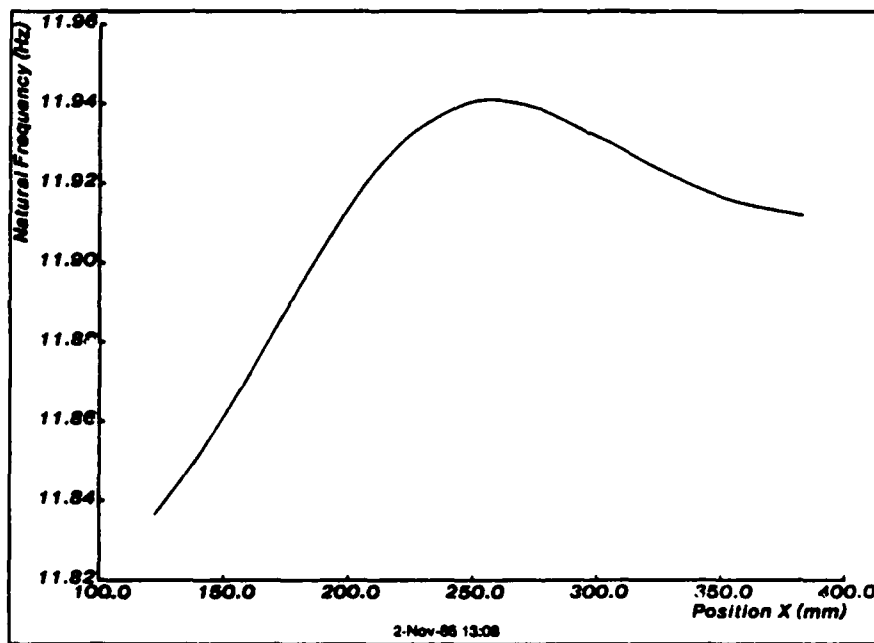


Figure 3.10: Modal variation with position for case of equivalent beam eigenfunctions

$\phi(z)$  would be curve-fitted with beam-like eigenfunctions, and  $\phi(y)$  would be done with a straight line which would be a good model for tension or compression of a uniform bar. The number of curve fits done for the robot was as shown in Table 3.2.

### 3.3 Equations of Motion

There are four different levels of equations involved in the vibration analysis of the robot. These are:

$$[M]\{\ddot{x}\} + [C]\{\dot{x}\} + [K]\{x\} = \{F\} \quad (3.38)$$

$$\{\ddot{p}\} + [2\zeta_n\omega_n]\{\dot{p}\} + [\omega_n^2]\{p\} = [\phi]^t\{F\} \quad (3.39)$$

$$[m]\{\ddot{q}\} + [c]\{\dot{q}\} + [k]\{q\} = [T]^t[\phi]^t\{F\} \quad (3.40)$$

$$\{\ddot{r}\} + [2\zeta_n\omega_n]\{\dot{r}\} + [\omega_n^2]\{r\} = [\psi]^t[T]^t[\phi]^t\{F\} \quad (3.41)$$

The first level or equation 3.38 represents the real vibrations  $\{x\}$  of the robot before it is connected; that is, when each component vibrates separately in an isolated way. The second level, or equation 3.39 is obtained from equation 3.38 by operating with the modal matrix  $[\phi]$  which decouples the equations. Equation 3.40 represents the connected robot and it is obtained by using the transformation matrix  $[T]$  that operates on equation 3.39 to connect the components since it contains the compatibility conditions (see chapter 2). These equations are coupled again. Finally, level 4 is the decoupled set of equations 3.41 that is obtained from equations 3.40 by operating with the modal matrix  $[\psi]$ . To transform back to  $\{x\}$  when we know  $\{r\}$  we can use the following equation:

$$\{x\} = [\phi][T][\psi]\{r\} \quad (3.42)$$

Before describing the procedure followed for the solution of these equations, we shall discuss the driving functions.

### 3.4 Force Analysis and Prescribed Motion

So far in this thesis we have dealt with the left-hand side of the equations, that is, the part that describes the homogeneous solution of the system. The right-hand side which contains the forcing terms that excite the system are described now. When the carriages move, the inertia forces and the gravity forces acting on a system that changes configuration tend to excite vibrations on the structure, and so the forcing terms are associated with the motion of the carriages.

In order to leave out the control system that causes the motion, and consider only the structural vibrations, we measure the motion of the motor rotor including torsional vibration during a prescribed robot motion and use this information as prescribed motion at the motor rotor to drive the equations of motion.

With regard to the interface between the carriages and structure in the model we can do the simulations in two different ways:

1. At a given instant the carriages can be assumed not have relative motion, so they are pinned to the ways, but those pins are slowly changing with time. Here we subtract the rigid body mode by assuming that the carriages are rigid and calculating the reaction forces that occur due to an acceleration equal to the rigid body acceleration. These reaction forces are then used to drive the equations of motion.
2. The carriages can be assumed not to be pinned to the ways so that they can slide in the direction of motion. However they have to overcome a friction force which acts as an external force whose value we know. Then, at the end of the move we set this force to zero.

Since this second alternative does not require knowledge of the rigid body acceleration, which strictly speaking is not known, we have chosen to

do the simulations of the robot vibrations using this second method.

### 3.4.1 Prescribed Motor-rotor Vibration

In this procedure we eliminate the forces exerted by the motors from the equations of motion in favor of the prescribed vibration which acts as a "forcing" function to drive the system.

The problem, besides being position-dependent presents limitations in the available data, that is, all we know are the natural modes of each component and a series of complex frequency responses from which the modes were calculated. The problem may be solved in several ways as explained in Appendix B, but the one that we consider the most suitable for the characteristics of this cartesian robot is a time-domain technique which is not restricted to time-invariant systems.

As we have discussed in Chapter 2, the application of the compatibility conditions in the CMS method leads to a set of coupled differential equations (equation 2.11 ). These equations represent the complete cartesian robot, and they are driven by forces exerted by the motors in the presence of friction and gravity forces. These equations can be decoupled first for convenience and then manipulated to eliminate the motor forces by simple multiplications by constants and adding together different rows of the system, since the motor forces appear in linear form. In doing this elimination, the equations become coupled again, and we reduce the number of equations by the number of motor forces eliminated (maximum of 3 forces, one for  $MX$ , one for  $MY$ , and one for  $MZ$ ). Consequently we must add new equations, and these come from the relations between the variables  $r$  of the assembled system and the real encoder positions  $x_{MX}$ ,  $x_{MY}$ , or  $x_{MZ}$  as follows

$$x_{MX} = [\phi_{MX}][T][\psi]\{r\}, \text{ etc.} \quad (3.43)$$

where  $\{\phi_{MX}\}$  is a row vector coming from the modal matrix evaluated at the motor shaft.

So, by adding these equations we again have the number of equations required for the number of unknowns ( $\{r\}$ ). The resulting equations can be represented by

$$\begin{bmatrix} (m_c) \\ (\phi_{MX})(T)(\psi) \\ (\phi_{MY})(T)(\psi) \\ (\phi_{MZ})(T)(\psi) \end{bmatrix} \begin{Bmatrix} \ddot{r}_1 \\ \ddot{r}_2 \\ . \\ \ddot{r}_n \end{Bmatrix} + \begin{bmatrix} (C_c) \\ 0 \\ 0 \\ 0 \end{bmatrix} \begin{Bmatrix} \dot{r}_1 \\ \dot{r}_2 \\ . \\ \dot{r}_n \end{Bmatrix} + \begin{bmatrix} (K_c) \\ 0 \\ 0 \\ 0 \end{bmatrix} \begin{Bmatrix} r_1 \\ r_2 \\ . \\ r_n \end{Bmatrix} = \begin{Bmatrix} \{f_c\} \\ x_{MX} \\ x_{MY} \\ x_{MZ} \end{Bmatrix} \quad (3.44)$$

where  $f_c$  contains the system external forces other than motor forces. These equations can now be integrated directly to find  $\{r\}$ , and from there the vibration at any point  $x$  can be obtained from  $\{x\} = [\phi][T][\psi]\{r\}$ .

Notice that we have differentiated equation 3.43 twice with respect to time in order to obtain a mass matrix which remains non-singular. This is a convenient situation to have for numerical integration of the equations. This differentiation of equation 3.43 assumes that the terms in  $\dot{\phi}$  and  $\ddot{\phi}$  are negligible compared to the terms in  $\dot{r}$  and  $\ddot{r}$  respectively which is correct for a slowly-varying system. For the vibration analysis of the moving robot we moved it always in one single direction (X,Y, or Z) to simplify the mathematical manipulations.

### 3.4.2 Friction Considerations

The friction force plays an important role in the robot vibrations. This force is high due to preload in the cam followers; it normally represents about 15 percent of the total motor force during motion.

The friction force has been measured by Benjamin [5] who did a computer-controlled experiment on the cartesian robot to determine the values of the

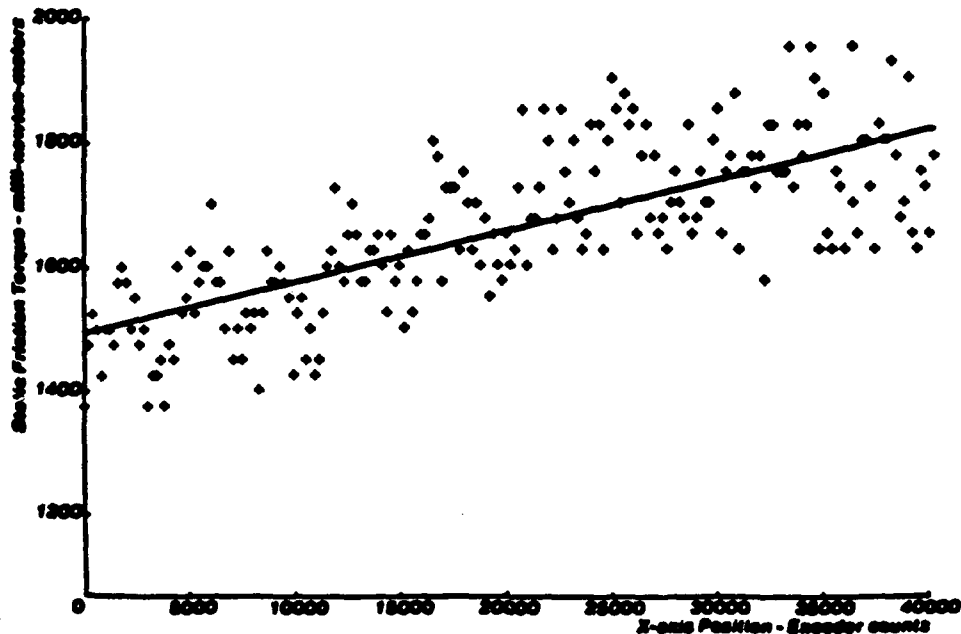


Figure 3.11: Variation of friction force along x-direction

friction force along the X-direction of the robot for different positions of the X-carriage. He modeled this force variation by a straight line which was fitted to a number of points obtained experimentally. His results are reproduced in Figure 3.11. For the Y-direction and Z-direction he did not report any results.

A simple static test measuring the force required to start motion was done to get approximate values of the friction force for four different positions along the ways for each direction. From these values we approximate a position-dependent function that describes the friction force for any of the three principal directions.

These forces are used in the model in an attempt to simulate what

physically happens during the motion. We assume that the friction force is equal to the saturation value of friction (follows the straight line variation) as long as there is relative motion between carriages and ways. It may happen that the friction forces reverse sign, and that is when the difference in displacement between two sliding parts changes sign. This occurs for the case of motion in x-direction when :  $[\phi_{X-carriage}][T][\psi] - [\phi_{Y-carriage}][T][\psi]$  changes sign, where  $\phi_{X-carriage}$  is the mode shape value at the instantaneous slide point of the X-carriage, and  $\phi_{Y-carriage}$  is the corresponding value of the Y-carriage. The program has to monitor this difference and adjust the sign of the friction force accordingly.

As soon as the motion stops, the friction force is assumed to be always fluctuating between the - saturation value and the + saturation value while not allowing any relative motion. Under these circumstances the force is no longer known. To cope with this we pin the carriage to the ways using friction pins. This means that we modify the model by connecting the carriages to the ways at the end of a simulated move. This gives a slightly different dynamic behavior of the structure. In practice we noticed better correlation with the experimental results when we simply set the friction force to a constant value during the move and zero at the end of the move; this suggests that perhaps there is a little backlash in the nut-lead screw connection.

### 3.4.3 Conditioning of the Encoder Motion

The encoder motion is used as a prescribed motion at the motor rotor to drive the equations of motion. The optical encoder used gives a displacement (rotation) function which is stepwise continuous as shown in Figure 3.12. This displacement when used without any conditioning to calculate velocity and acceleration gives strong discontinuities mainly in

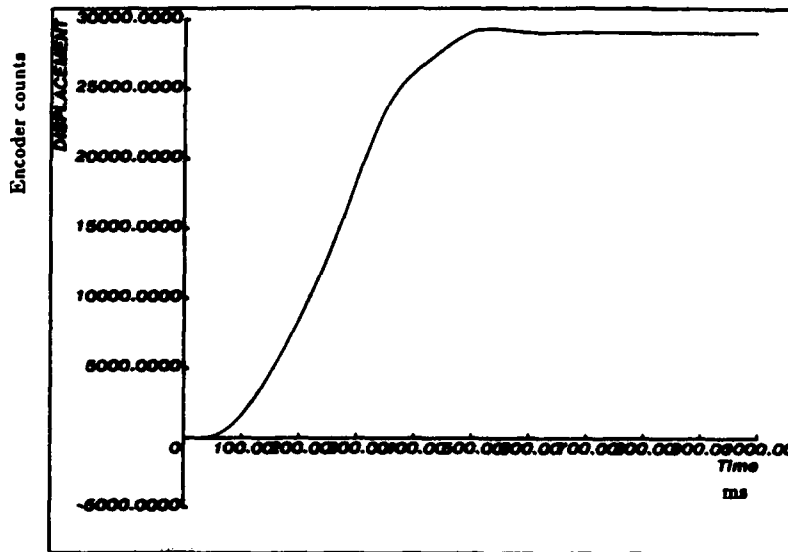


Figure 3.12: Encoder displacement

the acceleration function because the encoder provides discrete rather than continuous information (see Figure 3.13 and Figure 3.14). To avoid these problems we have to filter out the stepwise characteristic of the encoder measurements; one way is by using a digital filter.

The filter considered is a differentiating, low-pass filter with zero phase-shift which besides differentiating the encoder displacement, filters out the undesired higher harmonics.

This digital filter is a non-recursive type filter because the filter output  $g_m$  is calculated explicitly from the input  $f_m$  by means of

$$g_m = \sum_{n=-N}^N b_n f_{m-n} \quad (3.45)$$

where  $b_n$  are the filter coefficients. This summation is an approximation to the convolution integral where the set of  $b_n$  constitutes the impulse response of the filter. These coefficients have to be calculated so that the frequency-domain effects of this process come out as desired, that is, the desired



Component	No. of ways	No. of modes	No. of fits
STR	2	13	78
Y	2	10	60
Z	4	5	60

Table 3.2: Number of Curve Fits for Ways

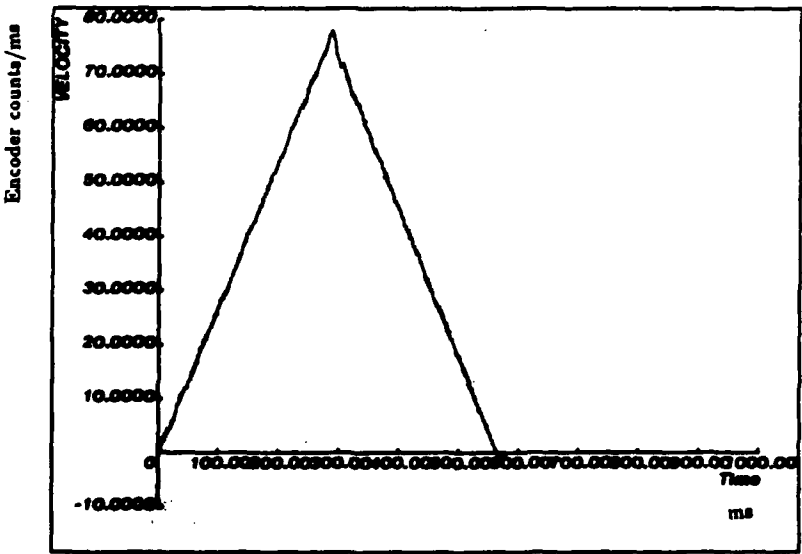


Figure 3.13: Unfiltered encoder velocity

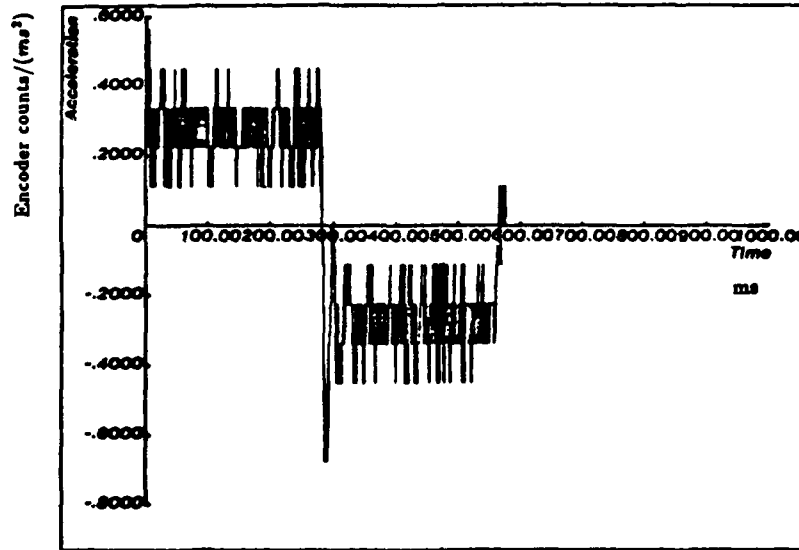


Figure 3.14: Unfiltered encoder acceleration

transfer function of the filter  $H_d(j\omega)$  can be approximated by some  $\tilde{H}(j\omega)$  through a least squares process. In this way we find  $b_n$  for  $n$  in the interval  $[-N, N]$ .

The general formula for the coefficients, as given by Stearns [72] is

$$b_n = \frac{T}{2\pi} \int_{-\frac{\pi}{T}}^{\frac{\pi}{T}} H_d(j\omega) e^{jn\omega T} d\omega, -N < n < N \quad (3.46)$$

We chose to design a filter which would eliminate all frequencies above 130 Hz (this limit being set by the first 10 modes of the robot), and differentiate the displacement history twice as well. An algorithm developed by McClellan, Parks and Rabiner [51] can do this linear phase filter design, although its differentiation is of first order, so we have to do the process twice starting with displacement to get acceleration. The number of points( $N$ ) was 63.

The impulse response obtained for this filter is shown in Figure 3.15 and the corresponding Fourier transform is shown in Figure 3.16, where

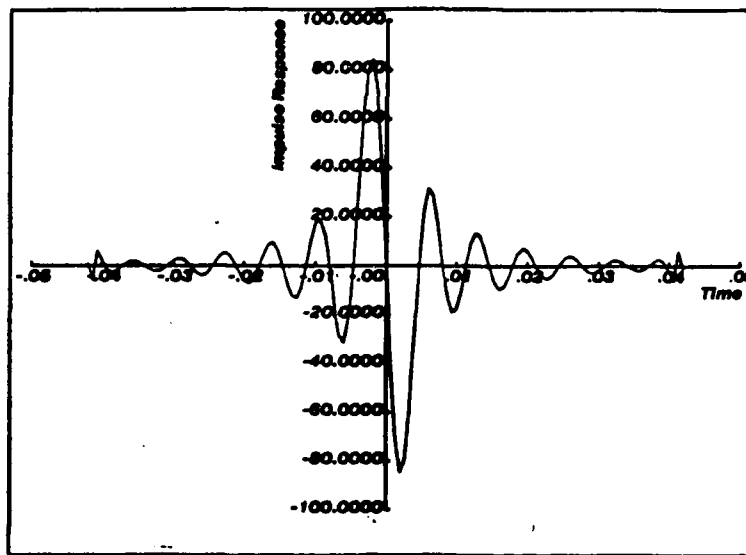


Figure 3.15: Impulse response of digital filter

the Nyquist frequency is  $F = 1500$  Hz which corresponds to the sampling time  $t = 0.67$  ms of the computer-controlled experiment.

The application of the digital filter to the encoder data gives the velocity and acceleration shown in Figure 3.17 and Figure 3.18 respectively. These data were collected during a move in the X-direction. Note the component of acceleration at 87.5 Hz which corresponds to the dominant 8th mode of vibration (see Appendix A).

### 3.5 Solution of the Equations of Motion

In order to calculate the time history  $z$  of vibrations at any of the test points of the robot we can integrate equation 3.41, truncating to a convenient number of modes if we want, and then using equation 3.42 we can transform back to real coordinates. This transformation has to be done at each step since the matrices involved in the calculation are position-dependent. Now,

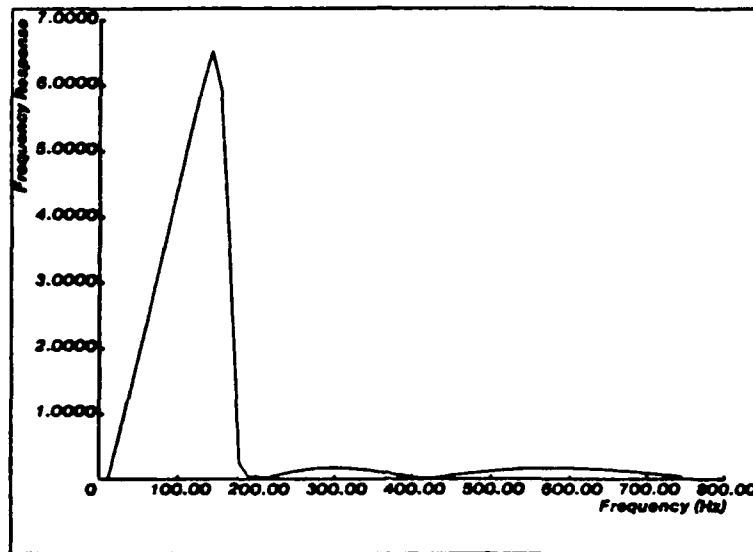


Figure 3.16: Fourier transform of digital filter

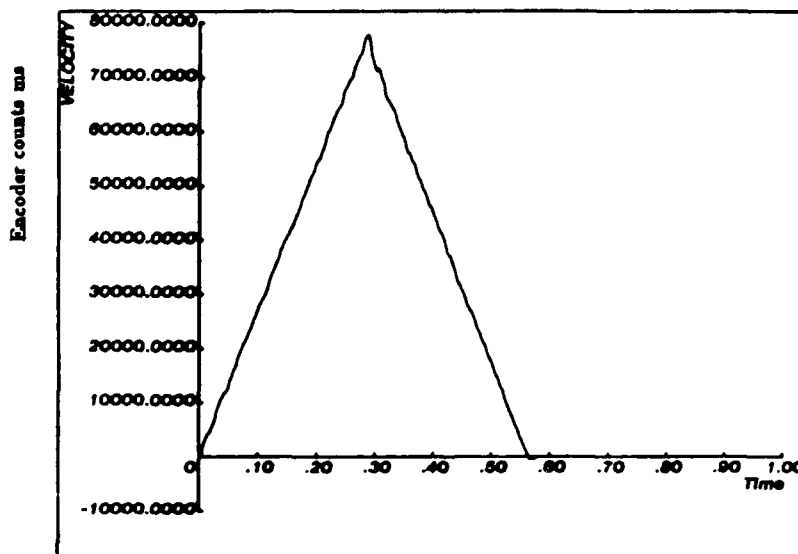


Figure 3.17: Filtered encoder velocity

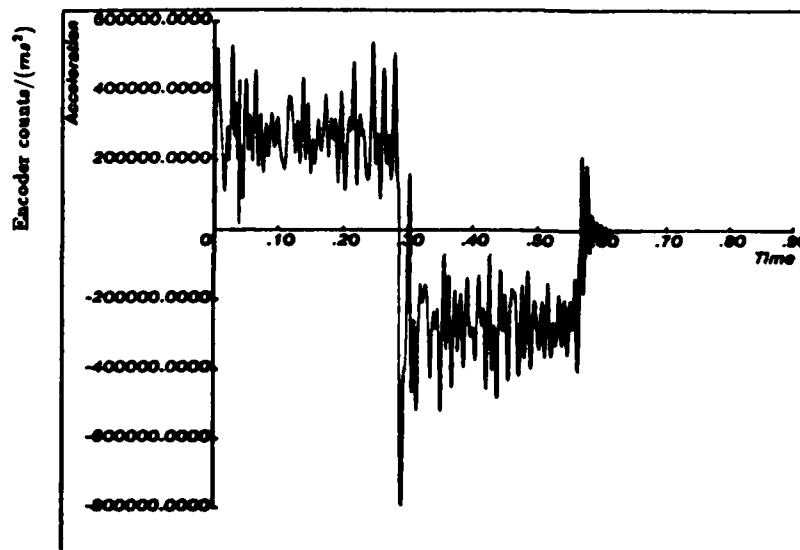


Figure 3.18: Filtered encoder acceleration

if we want to have a fast computer model to integrate these equations, we have to do all the work that can be done prior to the integration, so that the integration itself is fast and can hopefully be done in real time. For this purpose, three computer programs were prepared to solve the equations as described below:

- The first program calculates the modal parameters at discrete points along the path, say at every 10 mm.
- The second program smoothes the modal parameters using cubic splines to calculate these parameters at each time step. These two programs can be run prior to the integration.
- The last program integrates the equations by using the parameters derived above at each time step. It integrates equation 3.41 with a 4th order Runge-Kutta-Merson algorithm. Then it transforms  $r$  to  $x$  to generate a time history at the desired test points.

This scheme was implemented on a VAX 11/750 computer and the ratio of computation time to real time was 40 to 1 when we integrated over the first 10 modes of equation 3.41. To improve this speed for real time control purposes we could proceed in a number of ways, for example using a faster computer or trying to use fewer equations in equation 3.41, or even trying to get asymptotic approximations to these equations with slowly-varying coefficients, but this is beyond the scope of the present work.

### 3.6 Some Results of the Dynamic Model

To test the model, a series of experiments were conducted on the robot which are explained in detail in chapter 4. From these tests, the motion at the motor-rotor for the cases of motion along the X-direction, or Y-direction, or Z-direction could be determined, and it is from this data that we can prescribe the motion of the carriages to run the dynamic model. Figure 3.19 shows the vibration at the end-point (test point 144) of the robot when the carriages are moved in the X-direction. This curve is a time domain representation and covers the whole motion, that is from  $t = 0$  to  $t = 0.57$  s. Figure 3.20 shows the robot tip residual vibration ( $t = 0.57$  to  $t = 0.89$  s). Figure 3.21 shows the frequency content of this end vibration. For the case of the Y-direction and Z-direction see Chapter 4 where we compare these simulation results to the test results.

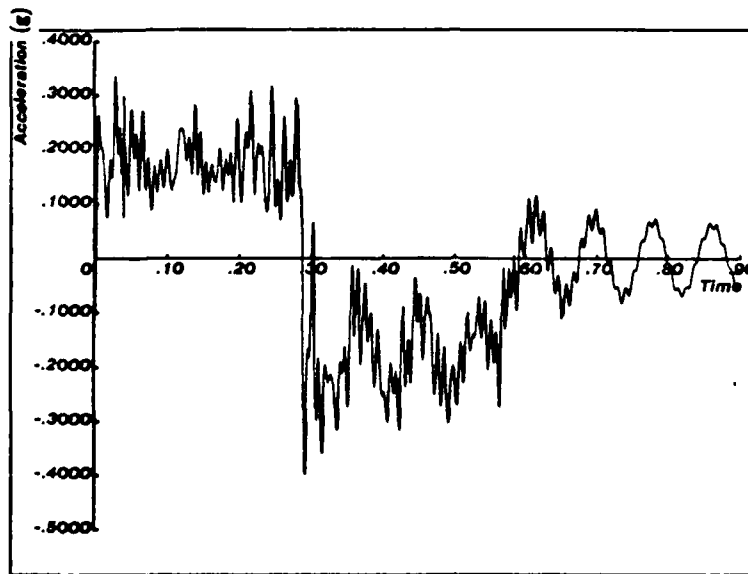


Figure 3.19: Vibration of end-effector in x-direction

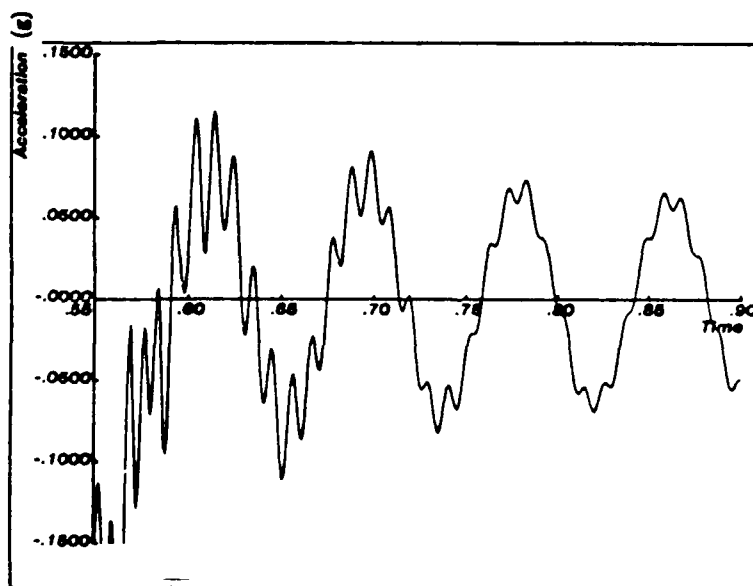


Figure 3.20: End vibration in z-direction

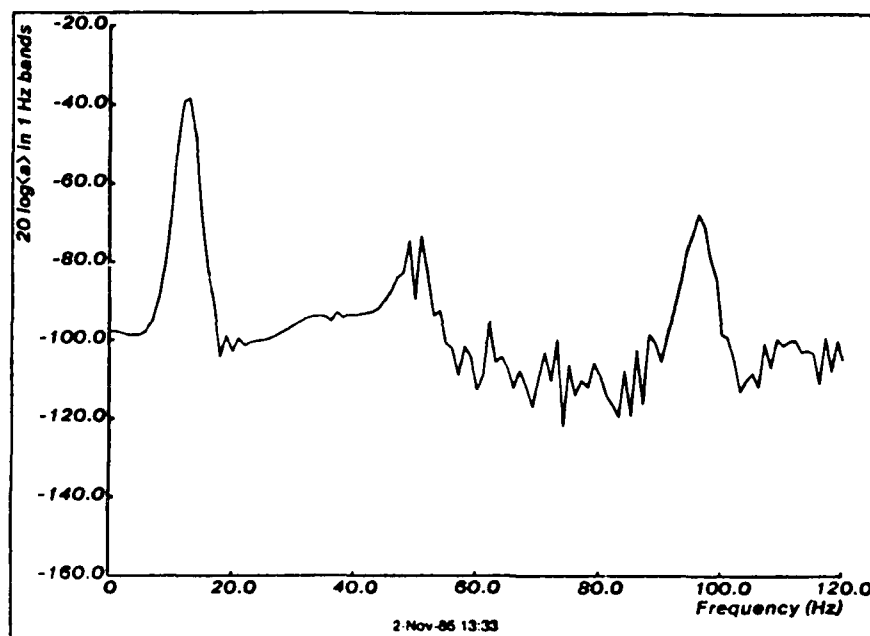


Figure 3.21: Fourier transform of end vibration in x-direction



## Chapter 4

# EXPERIMENTS AND RESULTS

### 4.1 Objectives

We are trying to understand how a time-dependent system vibrates in order to be able to control the vibration and/or design the system in a better way. For this purpose we have developed a mathematical model which must then be validated by test.

There are two classes of objectives for the tests described in this thesis, one is that we need modal data from each of the robot components to be used as input to the mathematical model. The other class of objectives is the mathematical model validation which should evaluate the accuracy of this model. The modal tests which were done to gather input data are briefly mentioned in this chapter, but fully described in Appendix A. In contrast, the validation tests are explained with more detail here, and a comparison with the predicted results from the mathematical model is presented.

We will discuss four different types of tests. The first two provided data

for the model; the last two were used in verification. The tests included

- Modal tests to determine natural frequencies, modal damping and mode shapes.
- High-resolution transfer function measurements for orthonormalization of eigenvectors.
- Measurements of modal variation with position of the carriages.
- Measurements of robot vibration when the carriages are moving.

## 4.2 Modal Tests

The theory of modal analysis deals with two kinds of modes, normal modes and complex modes. The type of modes depends on the damping behavior of the structure. Caughey [14] presents an analysis of the conditions under which a damped linear system possesses classical normal modes. He concludes that the damping matrix must be diagonalized by the same transformation that uncouples the undamped systems. Meirovitch [53] gives a modal analysis procedure designed to handle the general case of damping. The modal analysis as is done in the laboratory with the use of digital equipment may utilize either of the two methods, although in general real structures should be analyzed using complex mode theory. Ibrahim [40] explains the errors involved in the normal mode approximation to complex modes, concluding that even for lightly damped structures this approximation may lead to large errors. Potter [62] and Potter and Richardson [63] explain the theory of complex modal analysis showing how to calculate modal vectors from a measured transfer matrix.

With regard to vibration tests, Mustain [56] shows the results of a survey of modal vibration test/analysis techniques in the USA. Favour, Mitchell,

and Olson [23] discuss the historical development of transient test techniques utilizing a digital computer. Halvorsen and Brown [28] describe the impact procedure, its theory, applications and limitations. Ramsey and Richardson [65] present a brief review of modal analysis based upon the identification of modal parameters from measured transfer functions. They point out the advantages of a band selectable Fourier transform (zoom transform) for obtaining increased accuracy, resolution and dynamic range in the measurements. Richardson and Kniskern [66] present an algorithm that reduces error in the mode vector when using more than one simple row or column of residue data (more than one excitation point when using a shaker, or more than one response point when using a hammer). Okubo [59] analyzes the effect of nonlinearities on transfer function measurements with impact excitations. With regard to nonlinearities in Structural Dynamics, Crandall [19] discusses the nature of nonlinear structural models and surveys a variety of nonlinear response phenomena which can be predicted by such models.

For the modal tests, we have in the Acoustics and Vibration Laboratory an HP-5423A Structural Dynamics Analyzer. In conjunction with measuring instruments to determine acceleration and force, and with excitation means like an electrodynamic shaker or an instrumented hammer, the Analyzer provides adequate facilities for our purposes. This Analyzer assumes proportional damping when doing modal analysis calculations.

The vibration tests performed on the robot components to obtain input data for the mathematical model are explained in detail in Appendix A. Basically we obtain from 4 to 10 elastic modes for each component, which in addition to the corresponding 6 rigid body modes, give a sufficient number of modes for the model to provide convergence.

Of more interest in this chapter is the validation test performed on the

completely assembled robot which was tested in the configuration shown in Figure 4.1. Here the X-carriage and Y-carriage are in the middle of their respective way paths, and the Z-carriage is all the way down. The test set-up is shown in Figure 4.2. A Bruel and Kjaer electrodynamic shaker type 4801 with mode study head type 4814 was used to excite the structure at the test point no. 145 in the -Z direction while a triaxial accelerometer B & K type 4340 was used to transmit acceleration to the analyzer via a charge preamplifier B & K type 2628. The force was measured by a Wilcoxon impedance head attached between the shaker and the structure. For each of the test points where the accelerometer was attached, and for each direction (X,Y, or Z) a transfer function made of 50 to 80 averages was calculated and stored in the analyzer. The frequency range was 0-200 Hz in the first set of measurements, and 0-25 Hz in the second set with a total number of measurements of 405 for each test.

A typical transfer function is shown in Figure 4.3, and the natural frequencies and modal damping factors are shown in table 4.1. Here in this table we also show the corresponding predicted values obtained by the mathematical model. The first 4 mode shapes as obtained by test are shown in the top part of Figures 4.4- 4.7 whereas the corresponding predicted modes are shown in the bottom part.

Comparing the experimental and synthesized results we notice that the average error in the first 17 natural frequencies is 6.9 %. The mode shapes show the same type of tridimensional motion for both sets of results.

We believe that this agreement is close enough and that the mathematical model can also predict the modal characteristics for any other configuration with comparable accuracy.

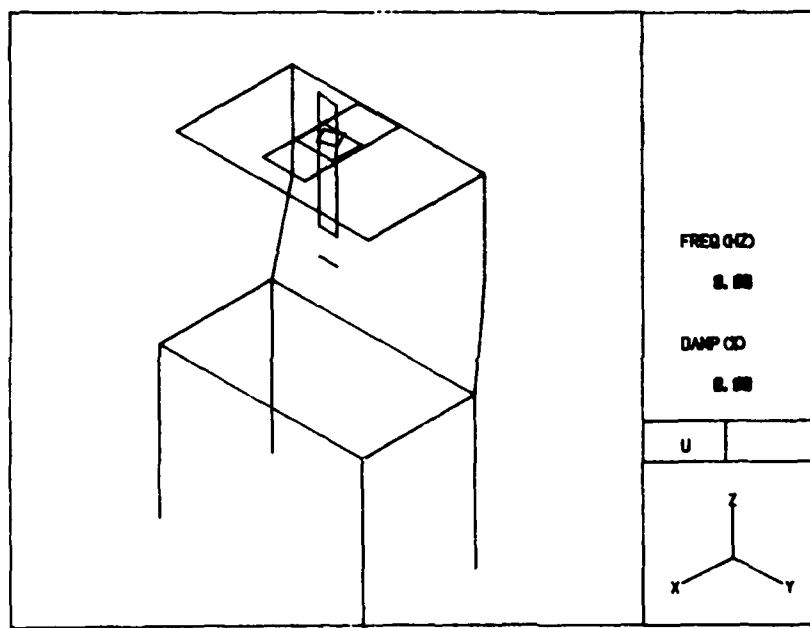


Figure 4.1: Robot configuration for modal test

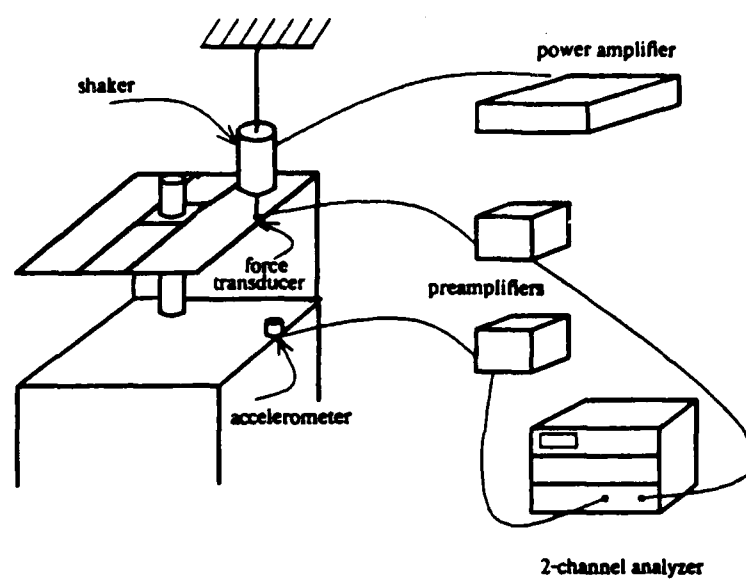


Figure 4.2: Test set-up for modal analysis

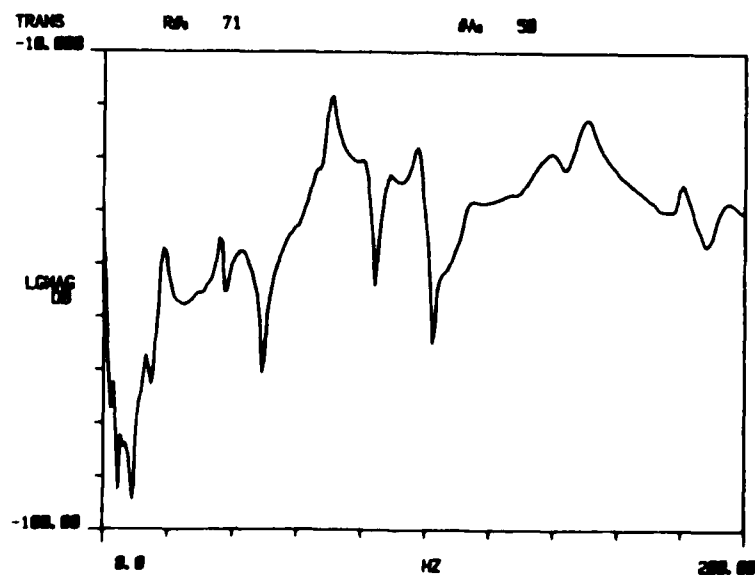


Figure 4.3: Typical transfer function

Mode No.	Measured		Predicted	
	$f_n$ (Hz)	$\zeta_n$ (%)	$f_n$ (Hz)	$\zeta_n$ (%)
1	12.36	1.98	11.93	1.45
2	18.85	1.65	19.17	1.45
3	36.36	1.42	36.87	0.78
4	42.83	9.52	46.34	3.30
5	47.83	4.90	49.53	2.54
6	60.51	3.24	61.38	1.45
7	70.72	0.89	75.06	1.82
8	81.47	1.95	96.47	0.63
9	86.67	1.74	101.75	1.41
10	97.70	1.17	123.39	1.30
11	112.52	7.39	126.84	1.06
12	126.27	0.10	128.72	0.75
13	139.43	2.62	141.05	1.16
14	149.85	1.00	145.68	2.86
15	152.34	0.66	148.23	2.76
16	178.12	1.79	169.39	1.04
17	184.37	0.01	179.06	1.11

Table 4.1: Natural Frequencies and Modal Damping Factors.

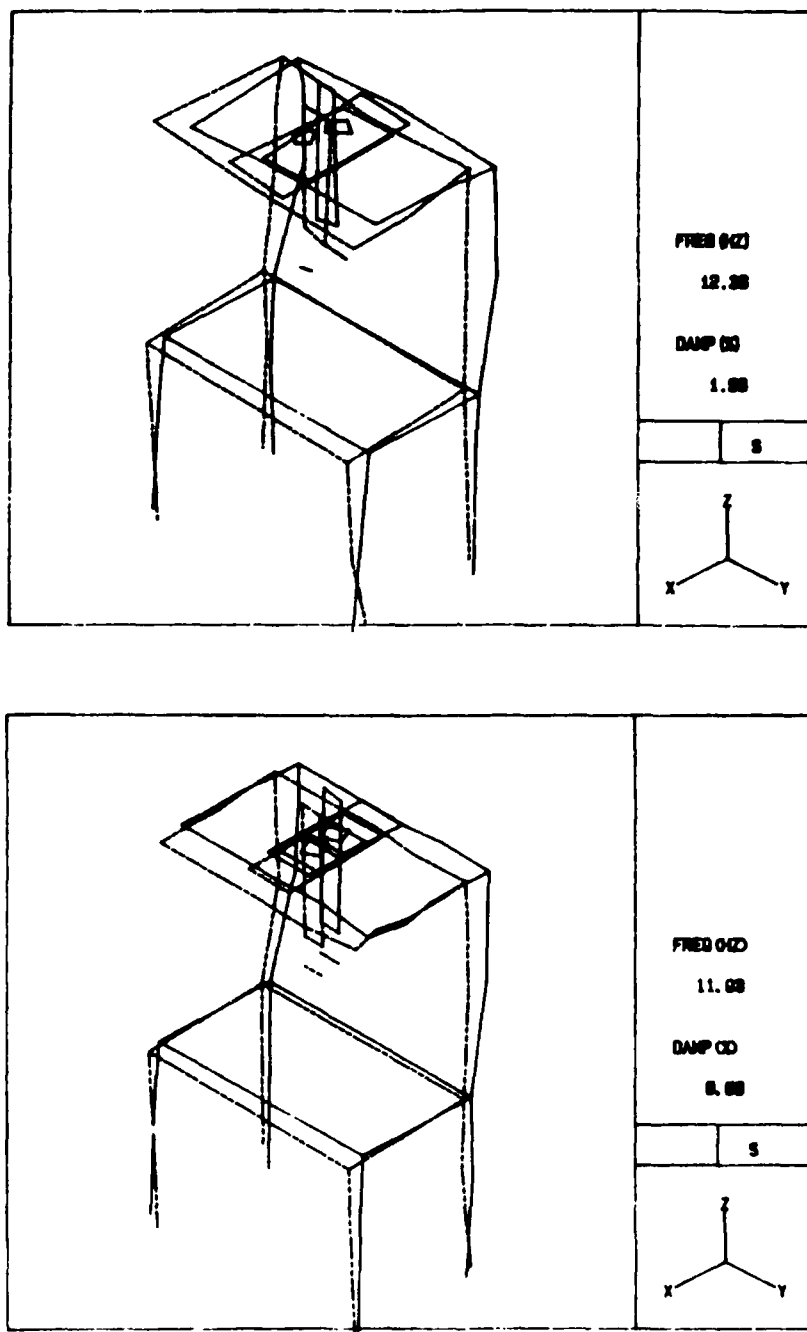


Figure 4.4: Mode shape no.1 of robot as obtained by test (top) and by synthesis (bottom)



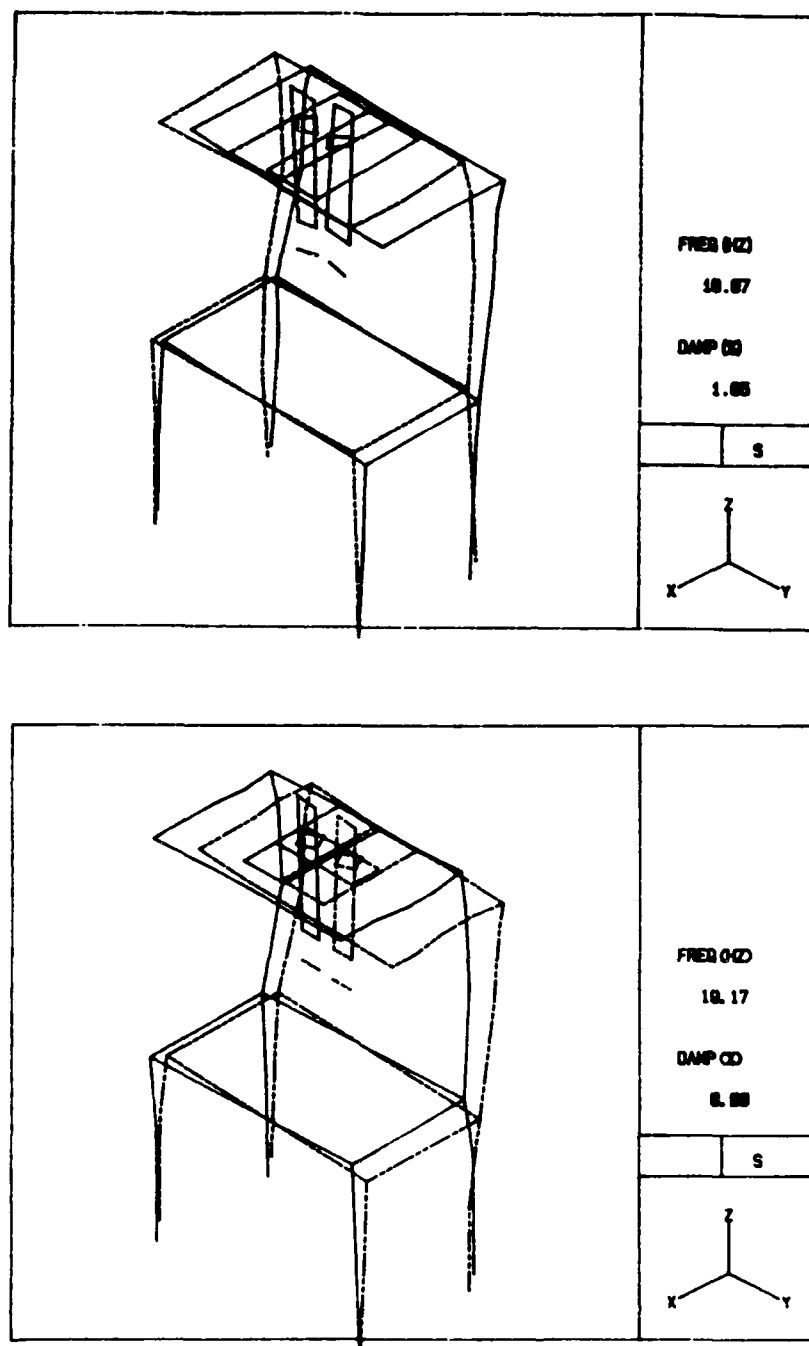


Figure 4.5: Mode shape no.2 of robot as obtained by test (top) and by synthesis (bottom)

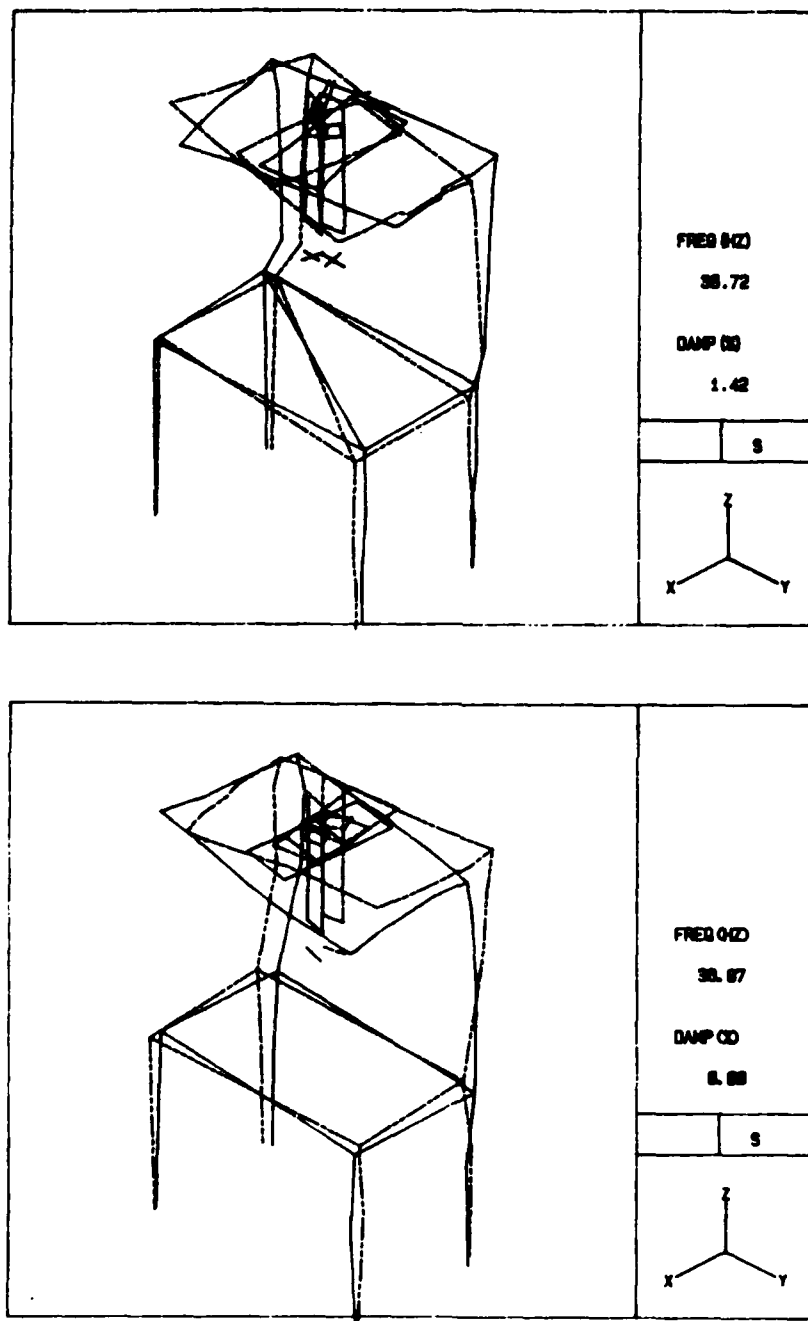


Figure 4.6: Mode shape no.3 of robot as obtained by test (top) and by synthesis (bottom)

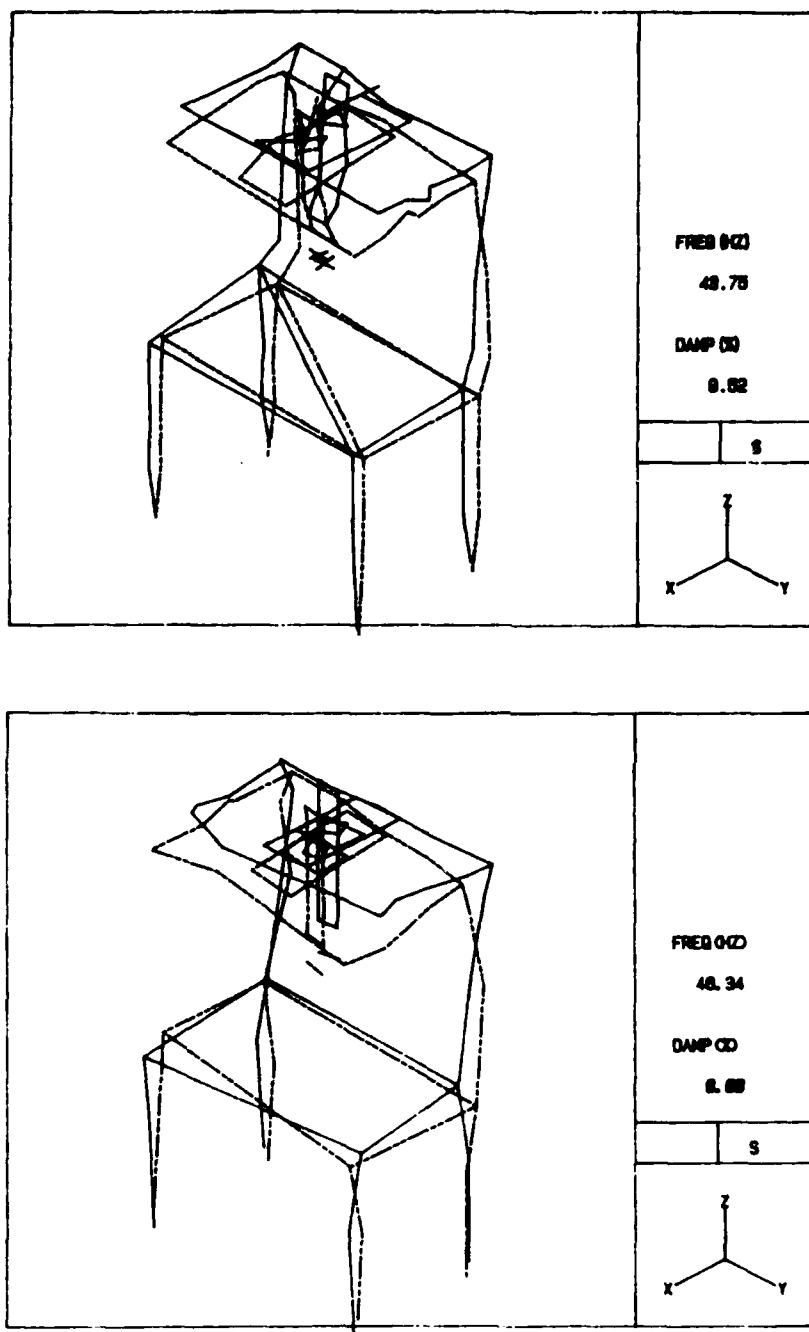


Figure 4.7: Mode shape no.4 of robot as obtained by test (top) and by synthesis (bottom)

### 4.3 High-Resolution Transfer Functions

The HP analyzer calculates transfer functions using 256 complex numbers for equally spaced frequencies in the specified frequency bandwidth. This resolution can be increased by repeating the test with different center-frequencies, and so, ending up with several transfer functions that can later be collected into one single plot outside of the analyzer, in a computer. We transmitted these transfer functions to a PDP11/44 computer through a GPIB interface. The resultant high-resolution transfer function which contains detailed information around each mode of interest can be used to get more accurate estimates of the modal parameters, particularly the mode shape value for orthonormal eigenvector as explained in chapter 2.

Two of the robot components were tested for these high-resolution transfer functions; the robot structure (without the carriages) attached to the floor, and the Z-carriage. Details of the test are given in Appendix A. One of these curve-fits for the Z-carriage is shown in Figure 4.8. As was discussed in chapter 2, the results may seem accurate but there is an important variance when we apply different curve-fitting methods. For example, if we change the initial conditions of this nonlinear parametric fit we get the curve fit shown in Figure 4.9 which may seem a very similar result but the mode shape values differ from 5 to 25 percent depending on the mode, and that happens because damping changes as well in such a way that the combination of  $\phi_{kk}$ ,  $\omega_k$ , and  $\zeta_k$  gives another solution of the nonlinear problem. Therefore, this difficulty in the system parameter identification may preclude good accuracy of the mathematical model.

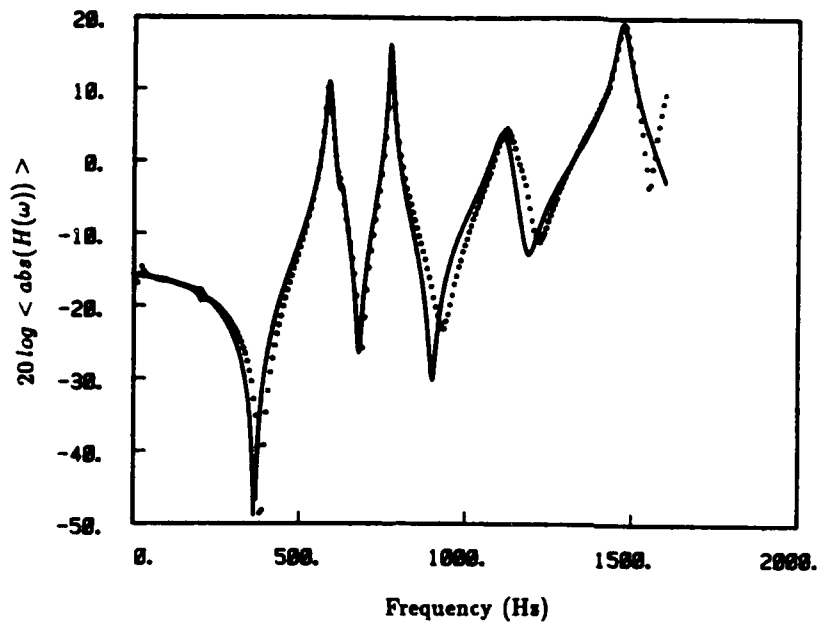


Figure 4.8: Multimodal curve fit no.1 of transfer function of Z-carriage

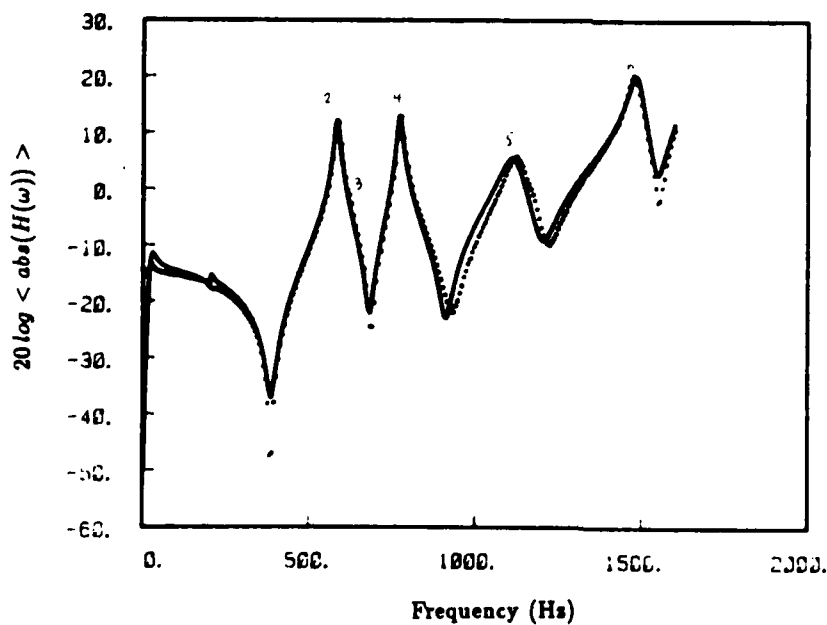


Figure 4.9: Multimodal curve fit no.2 of transfer function of Z-carriage

## 4.4 Modal Variation with Position

A position-dependent system changes its modal characteristics as it changes configuration. The cartesian robot shows slight changes when the relative position of the carriages change. In order to partially evaluate these changes, the robot was tested in different configurations obtaining for each one a single transfer function which may show at least the variation in natural frequencies. Table 4.2 shows these variation for the 1st mode as well as the corresponding calculated value from the mathematical model. Table 4.3 shows similar results for the second mode.

These tables (4.2 and 4.3) and the set of mode shape plots show in general good agreement between experimental and calculated results. Based on this and on the results of section 4.1 we can generalize the validity of the model to the whole work space of the cartesian robot. Table 4.4 shows the variation of the first ten natural frequencies along the Y-direction for different positions in the X and Z directions (calculated from the model). The values of Y (mm) represent the position of the Y-carriage as measured in the global system of coordinates.

## 4.5 Vibration of Moving Robot

The final objective of this thesis is to be able to predict the vibrations of any part of the robot as the carriages move, and the experimental results described in this section permit evaluation of the model simulations. Three different experiments were carried out:

- Motion of the carriages in the X-direction only.
- Motion in Y-direction.
- Motion in Z-direction.

Position of carriages	$f_1$ (Hz) measured	$f_1$ (Hz) predicted)
$X_{front}, Y_{middle}, Z_{down}$	11.80	11.98
$X_{front}, Y_{left}, Z_{down}$	11.22	11.70
$X_{middle}, Y_{middle}, Z_{down}$	12.36	12.05
$X_{middle}, Y_{left}, Z_{down}$	10.94	11.75
$X_{middle}, Y_{middle}, Z_{up}$	11.49	12.27

Table 4.2: Modal Variation with Position, first Mode.

Position of carriages	$f_2$ (Hz) measured	$f_2$ (Hz) predicted)
$X_{front}, Y_{middle}, Z_{down}$	18.90	19.09
$X_{front}, Y_{left}, Z_{down}$	19.03	19.23
$X_{middle}, Y_{middle}, Z_{down}$	18.85	19.17
$X_{middle}, Y_{left}, Z_{down}$	17.97	19.31
$X_{middle}, Y_{middle}, Z_{up}$	18.82	19.15

Table 4.3: Modal Variation with Position, second Mode.

Table 4.4: Variation of Natural Frequencies (Hz) with Position for the First Ten Modes, according to the model.

X back Z top

Y= 422.28: 12.1 19.3 36.9 47.9 49.9 61.1 69.9 88.7 101.9 105.4

Y= 578.07: 12.4 19.2 36.9 48.3 49.8 61.6 71.0 91.0 102.1 110.4

Y= 733.85: 12.5 19.1 36.9 47.9 49.9 61.8 72.0 92.5 101.1 106.8

Y= 889.64: 12.7 19.1 36.9 47.6 50.0 62.0 72.5 93.1 100.4 107.8

Y=1006.48: 12.9 19.0 36.9 47.2 50.1 62.1 72.9 93.5 99.8 108.1

X back Z middle

Y= 422.28: 12.1 19.3 36.9 47.7 49.9 61.2 69.5 90.1 101.6 119.2

Y= 578.07: 12.4 19.2 36.9 48.0 49.9 61.7 70.8 92.7 106.1 121.5

Y= 733.85: 12.6 19.1 36.9 47.6 50.0 61.9 71.8 93.7 101.8 122.9

Y= 889.64: 12.9 19.1 36.9 47.3 50.2 62.1 72.7 94.2 102.0 123.4

Y=1006.48: 13.0 19.0 36.9 46.9 50.3 62.2 73.2 94.3 101.7 122.5

X back Z down

Y= 422.28: 11.6 19.3 36.9 47.5 49.4 61.0 67.3 89.5 99.7 121.3

Y= 578.07: 11.8 19.2 36.9 47.8 49.6 61.4 68.7 91.8 103.9 124.2

Y= 733.85: 11.9 19.1 36.9 47.4 49.7 61.6 69.7 92.2 100.5 126.2

Y= 889.64: 12.1 19.1 36.9 47.0 49.9 61.7 70.5 92.4 100.7 126.9

Y=1006.48: 12.2 19.0 36.9 46.6 50.0 61.8 71.1 92.3 100.4 125.6

X middle Z top

Y= 422.28: 11.9 19.3 36.9 47.3 49.2 60.9 74.7 89.5 100.6 118.0

Y= 578.07: 12.2 19.2 36.9 47.4 49.3 61.4 75.9 92.3 101.2 121.1

Y= 733.85: 12.3 19.1 36.9 47.0 49.4 61.6 76.5 94.3 101.6 120.5

Y= 889.64: 12.4 19.1 36.9 46.6 49.5 61.7 76.9 95.4 101.4 119.6

Y=1006.48: 12.5 19.0 36.9 46.2 49.6 61.8 77.1 95.6 101.0 119.8



Table 4.4: continued

X middle Z middle

Y= 422.28: 12.2 19.3 36.9 47.2 49.5 61.1 74.1 92.2 100.7 121.8

Y= 578.07: 12.5 19.2 36.9 47.3 49.6 61.5 75.5 95.4 102.6 122.3

Y= 733.85: 12.6 19.2 36.9 47.0 49.7 61.7 76.4 97.0 102.3 122.3

Y= 889.64: 12.9 19.1 36.9 46.5 49.8 61.9 77.0 97.5 102.7 121.9

Y=1006.48: 13.0 19.0 36.9 46.1 49.9 62.0 77.4 97.1 103.1 121.6

X middle Z down

Y= 422.28: 11.8 19.3 36.9 46.9 49.2 60.9 73.0 92.4 100.9 121.3

Y= 578.07: 11.9 19.2 36.9 46.9 49.3 61.3 74.4 95.0 103.3 122.3

Y= 733.85: 12.0 19.2 36.9 46.5 49.5 61.5 75.4 96.4 103.0 122.0

Y= 889.64: 12.2 19.1 36.9 46.1 49.6 61.6 76.1 96.1 102.9 121.6

Y=1006.48: 12.3 19.0 36.9 45.7 49.6 61.6 76.5 95.4 103.2 121.4

X front Z top

Y= 422.28: 11.5 19.2 36.8 46.1 48.7 60.5 75.0 87.6 101.2 117.2

Y= 578.07: 11.6 19.1 36.9 46.1 49.0 60.9 76.1 90.8 101.9 120.5

Y= 733.85: 11.7 19.1 36.9 45.8 49.1 61.1 76.3 93.1 102.4 121.9

Y= 889.64: 11.7 19.0 36.8 45.3 49.2 61.1 76.7 93.9 102.1 123.1

Y=1006.48: 11.8 18.9 36.8 44.9 49.2 61.2 76.9 94.0 101.7 123.4

X front Z middle

Y= 422.28: 11.9 19.2 36.9 46.3 48.9 60.8 75.4 89.9 102.2 115.2

Y= 578.07: 12.1 19.1 36.9 46.2 49.1 61.2 76.8 93.8 102.8 119.1

Y= 733.85: 12.2 19.1 36.9 45.9 49.2 61.3 77.0 96.2 102.6 120.1

Y= 889.64: 12.4 19.0 36.9 45.5 49.3 61.4 77.4 97.2 102.8 121.3

Y=1006.48: 12.5 19.0 36.8 45.1 49.4 61.5 77.6 96.9 102.9 121.7

X front Z down

Y= 422.28: 11.7 19.2 36.8 46.1 48.7 60.6 75.1 89.4 92.1 113.3

Y= 578.07: 11.9 19.2 36.8 46.0 48.9 61.1 76.6 89.4 95.7 116.7

Y= 733.85: 12.0 19.1 36.8 45.7 49.1 61.2 76.8 89.2 97.8 117.4

Y= 889.64: 12.1 19.0 36.8 45.2 49.2 61.3 77.4 88.2 99.2 118.3

Y=1006.48: 12.2 19.0 36.8 44.8 49.2 61.3 77.6 87.5 99.6 118.5

Each test gives out two results, the vibration of the end-effector as measured with an accelerometer, and the motor-rotor displacement as measured with an optical encoder.

The dynamic model which was discussed in the previous chapter may now use this motor motion as input to simulate the robot vibrations, and therefore an evaluation can be done by comparing the experimental to the simulated results. This comparison is shown in detail below.

#### 4.5.1 Computer-Controlled Tests

In order to get information about the robot vibration as the carriages are moving, we made use of the PDP11/23 computer which controls the robot to interact with the rest of the instrumentation as depicted in Figure 4.10. This set-up is the same used by Singer [71]. The motion specified to the carriage motor (one at a time) is controlled by a PWM pulse width modulated amplifier which is driven by the computer trying to follow a velocity profile (linearly increasing during the first half and linearly decreasing in the second half). The amplifier drives the motor and receives feedback from it to correct for deviations to the specified motion. The real velocity profile (Figure 4.11) for a test along X-direction shows the corrections done when compared with the specified profile.

The torsional rigid body motion and superimposed vibration for any of the three motors MX, MY, or MZ are measured by an incremental optical encoder HP type HEDS-6010 BO8 which transmits data to a microcomputer connected to the main computer. These data can then be transmitted to a bigger computer (VAX11/750) to form a data file.

The acceleration at the end-point (or any other of the test points) is received by the HP analyzer in the usual way, but the trigger is again controlled by the computer through a D/A converter.

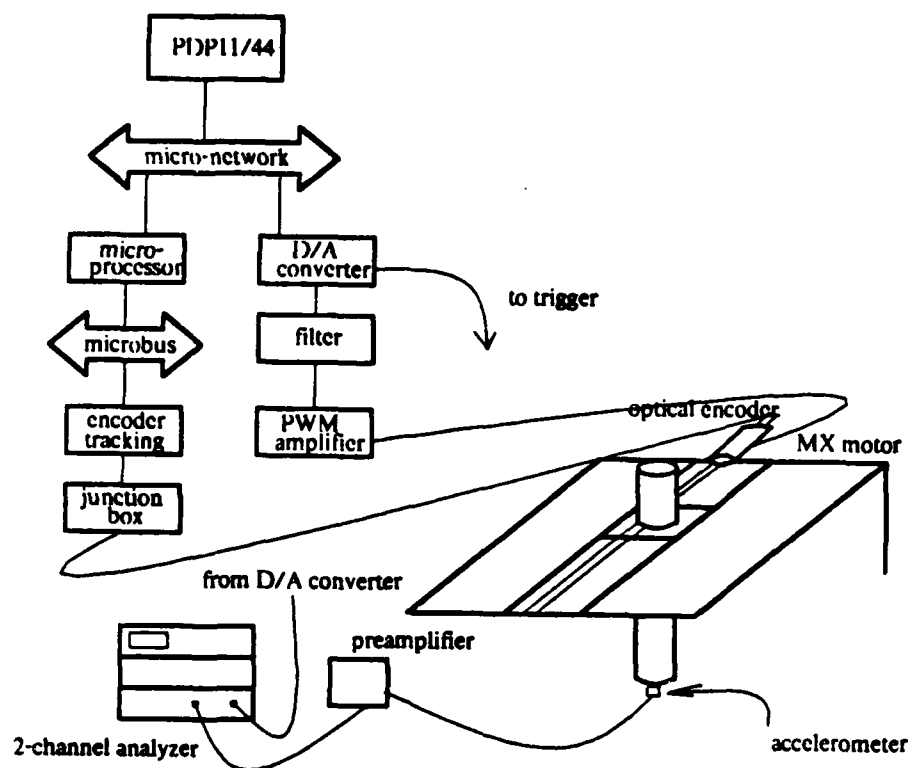


Figure 4.10: Test set-up for computer-controlled experiment

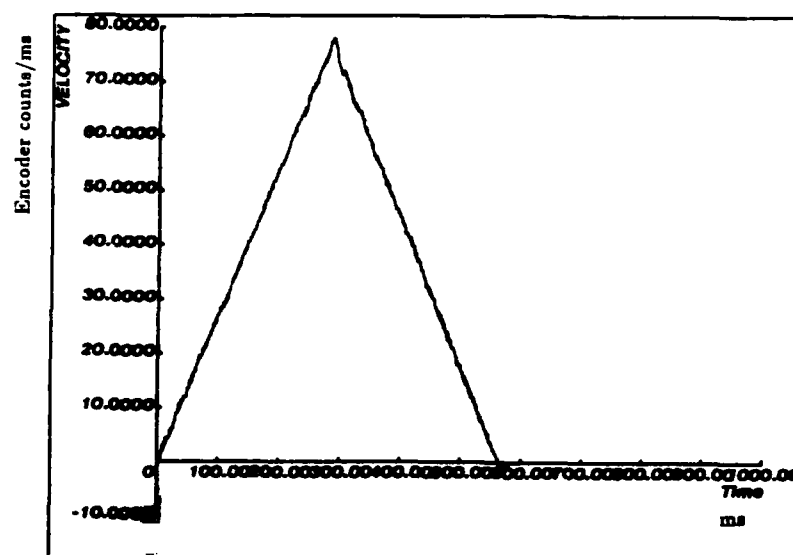


Figure 4.11: Actual Velocity Profile followed by Controller.

#### 4.5.2 Vibration Results for Motion in X-direction

With the Y-carriage in the middle and the Z-carriage down we ran the MX motor along the X-direction from  $X_1 = 154$  mm to  $X_2 = 291$  mm with an average acceleration of  $0.176g$  and an average deceleration of  $0.181g$ . The resulting motor displacement is shown in Figure 4.12, and the corresponding velocity after being filtered is given in Figure 4.13.

The end-point vibration as measured by an accelerometer pointing along the X-direction is shown in the top part of Figures 4.14 and 4.15 (complete vibration and vibration at the end of the move, respectively). The linear spectrum of the end vibration is shown in the top part of Figure 4.16. The corresponding results as obtained with the mathematical model are shown in the bottom part of the same figures.

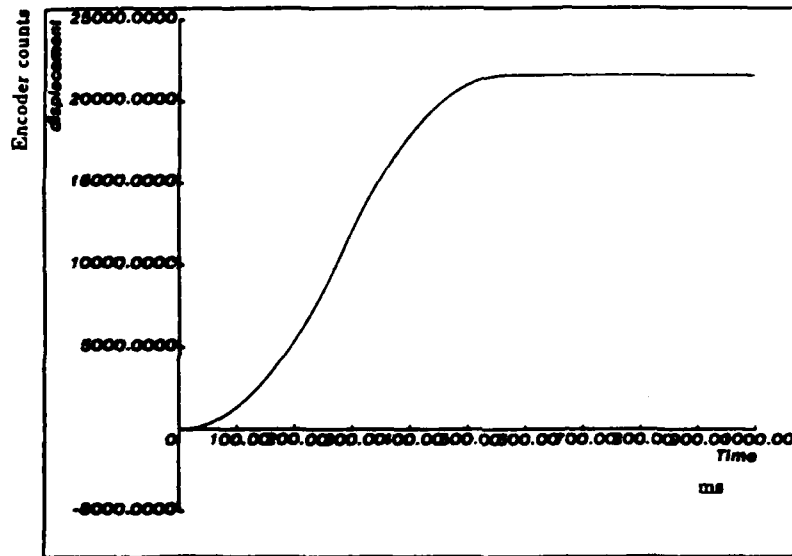


Figure 4.12: Encoder displacement during motion in X-direction

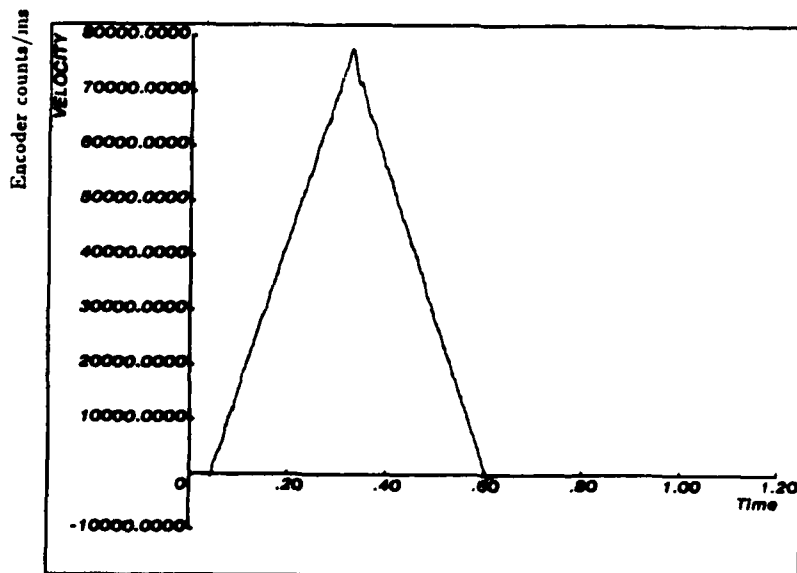


Figure 4.13: Encoder velocity during motion in X-direction

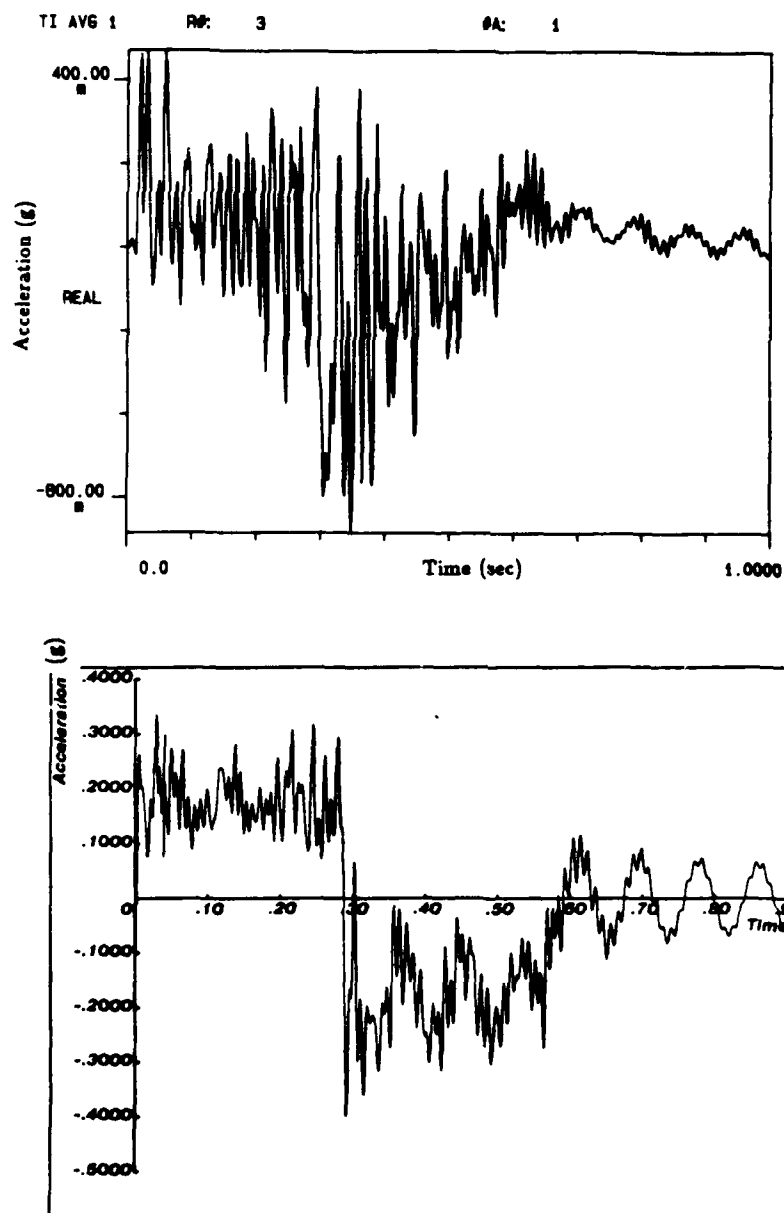


Figure 4.14: Vibration of end-effector during motion in X-direction as obtained by test (top) and by simulation (bottom)

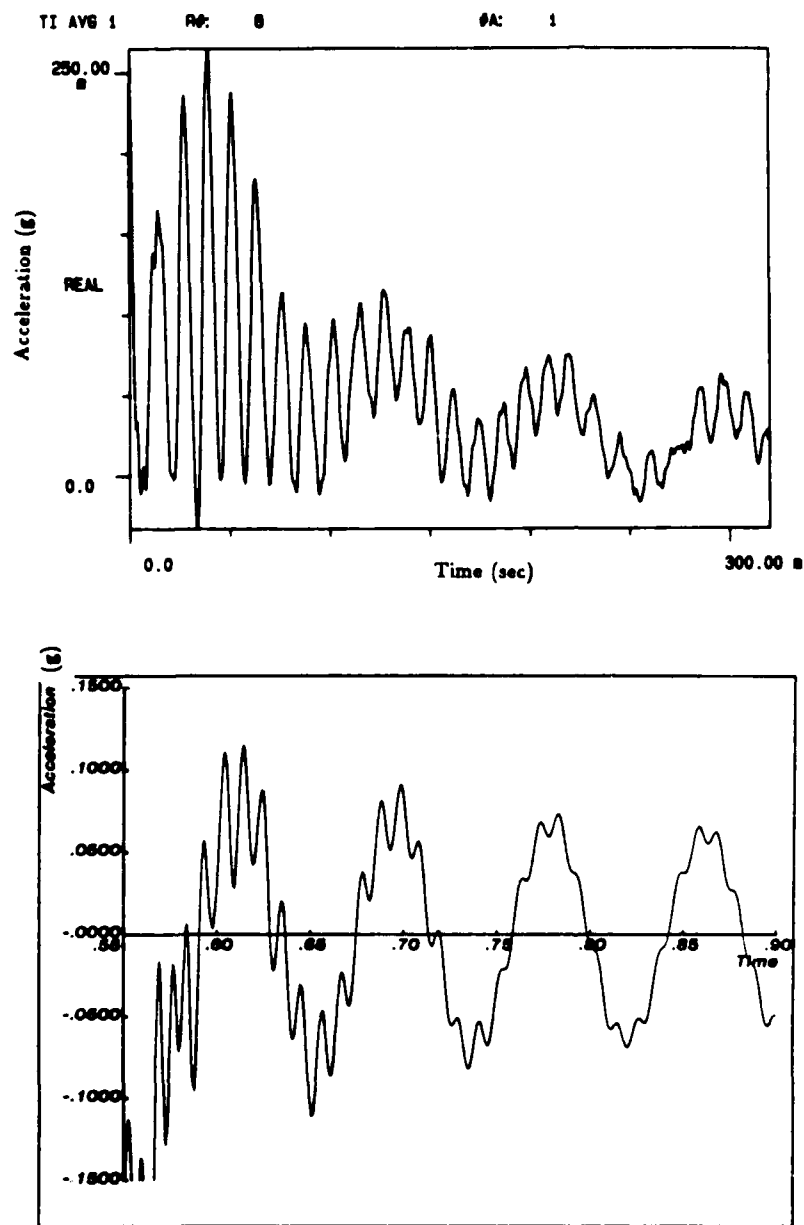


Figure 4.15: Vibration of end-effector at the end of the move for motion in X-direction as obtained by test (top) and by simulation (bottom)

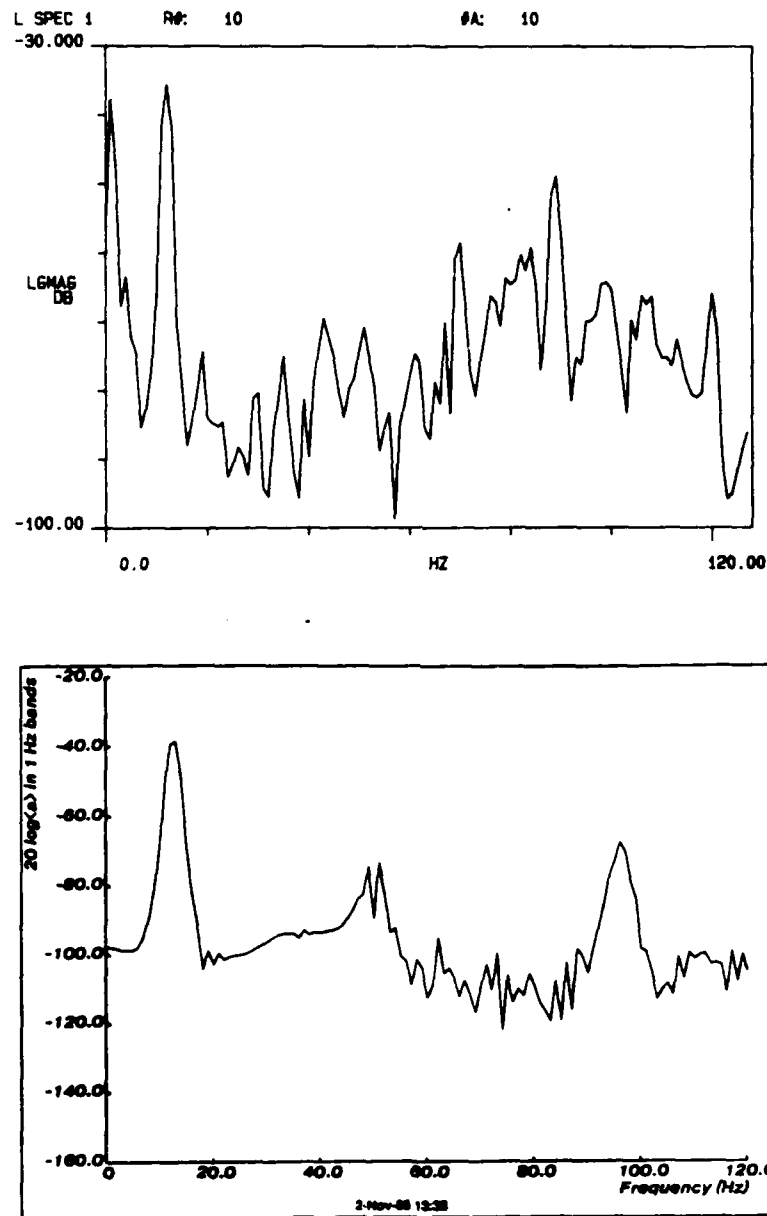


Figure 4.16: Fourier transform of vibration of end-effector at the end of the move for motion in X-direction as obtained by test (top) and by simulation (bottom)



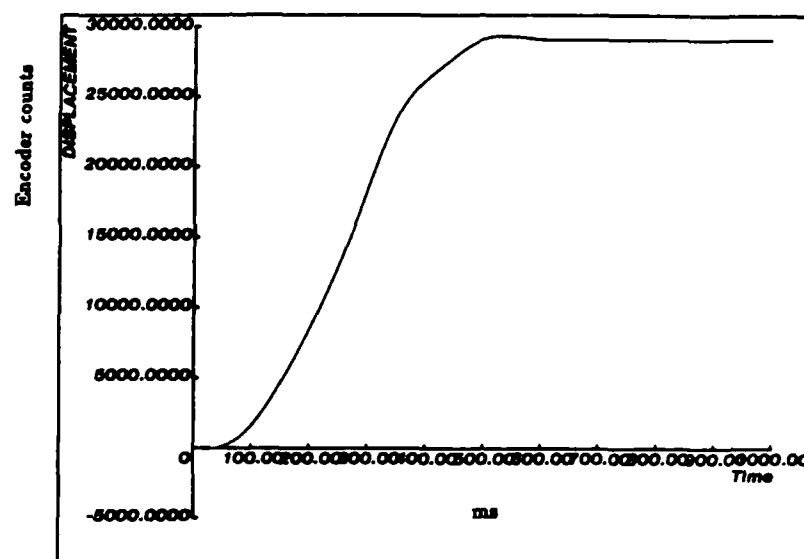


Figure 4.17: Encoder displacement during motion in Y-direction

### 4.5.3 Vibration Results for Motion in Y-direction

The X-carriage was positioned in the middle and the Z-carriage down when the carriages were run in the Y-direction from  $Y_1 = 498$  mm to  $Y_2 = 683$  mm with an average acceleration of  $0.25g$ , and an average deceleration of  $0.32g$ . The motor displacement and velocity are shown in Figure 4.17 and Figure 4.18 respectively. The vibration results as obtained by test are shown in the top part of Figures 4.19 to 4.21. The corresponding results for the model are shown in the bottom part.

### 4.5.4 Vibration Results for Motion in Z-direction

With the X-carriage and Y-carriage positioned in the middle we ran the Z-carriage from  $Z_1 = -486$  mm to  $Z_2 = -372$  mm with an average acceleration of  $1.51g$ , and an average deceleration of  $0.76g$ . The motor displacement and velocity are shown in Figure 4.22 and Figure 4.23 respectively. Here

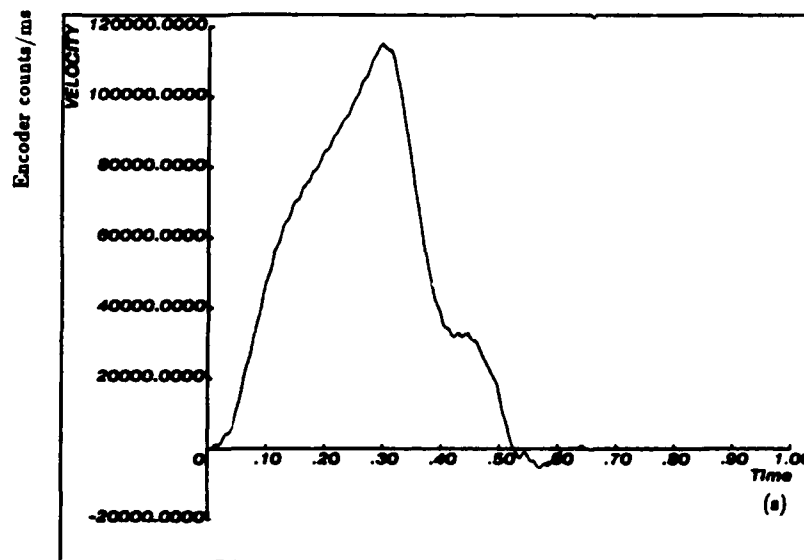


Figure 4.18: Encoder velocity during motion in Y-direction

the encoder displacement was filtered using a cut-off frequency of 270 Hz because the test was of shorter duration and the analyzer could sample the resulting vibration with a larger frequency bandwidth. The vibration results as obtained by test are shown in the top part of Figures 4.24 to 4.26. The corresponding results of the model simulation are shown in the bottom part.

#### 4.5.5 Comparison of Simulation and Experimental Results

The final test of the mathematical model is in these dynamic experiments where the robot carriages are run in all three directions and several measurements are taken at the robot end-effector. A careful study of these results as compared to the model results gives the following general observations.

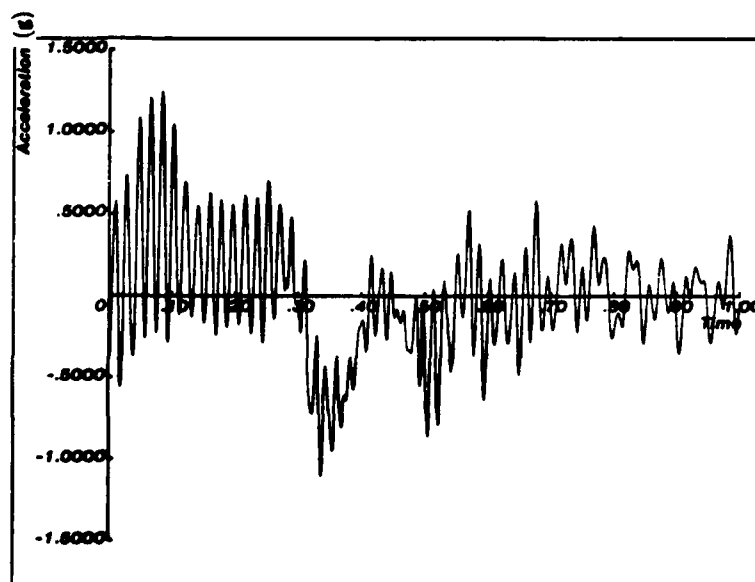
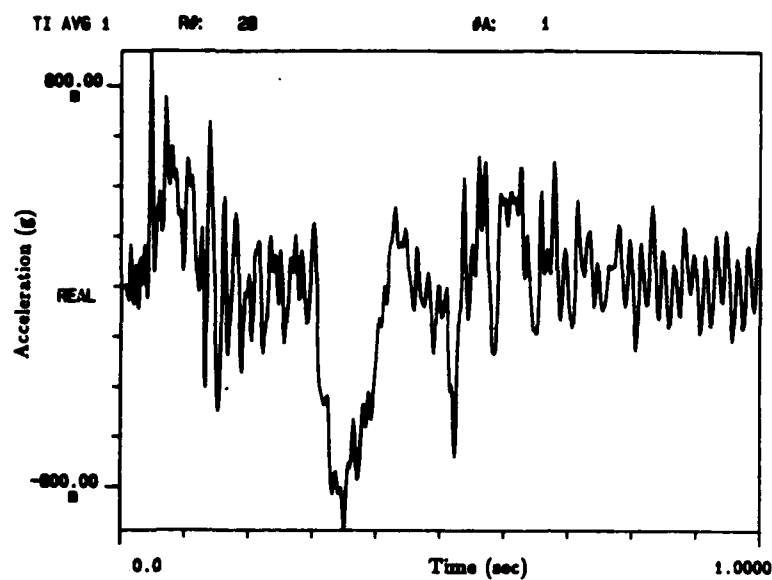


Figure 4.19: Vibration of end-effector during motion in Y-direction as obtained by test (top) and by simulation (bottom)

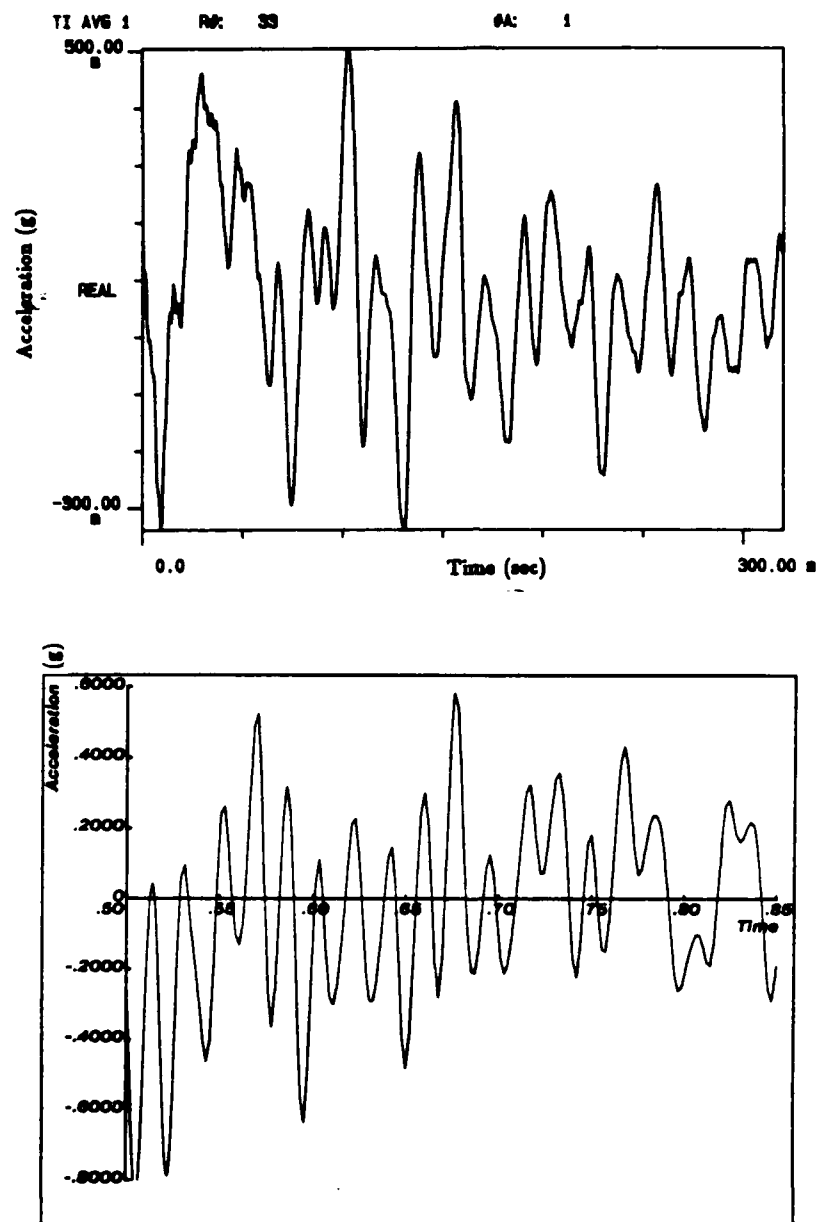


Figure 4.20: Vibration of end-effector at the end of the move for motion in Y-direction as obtained by test (top) and by simulation (bottom)

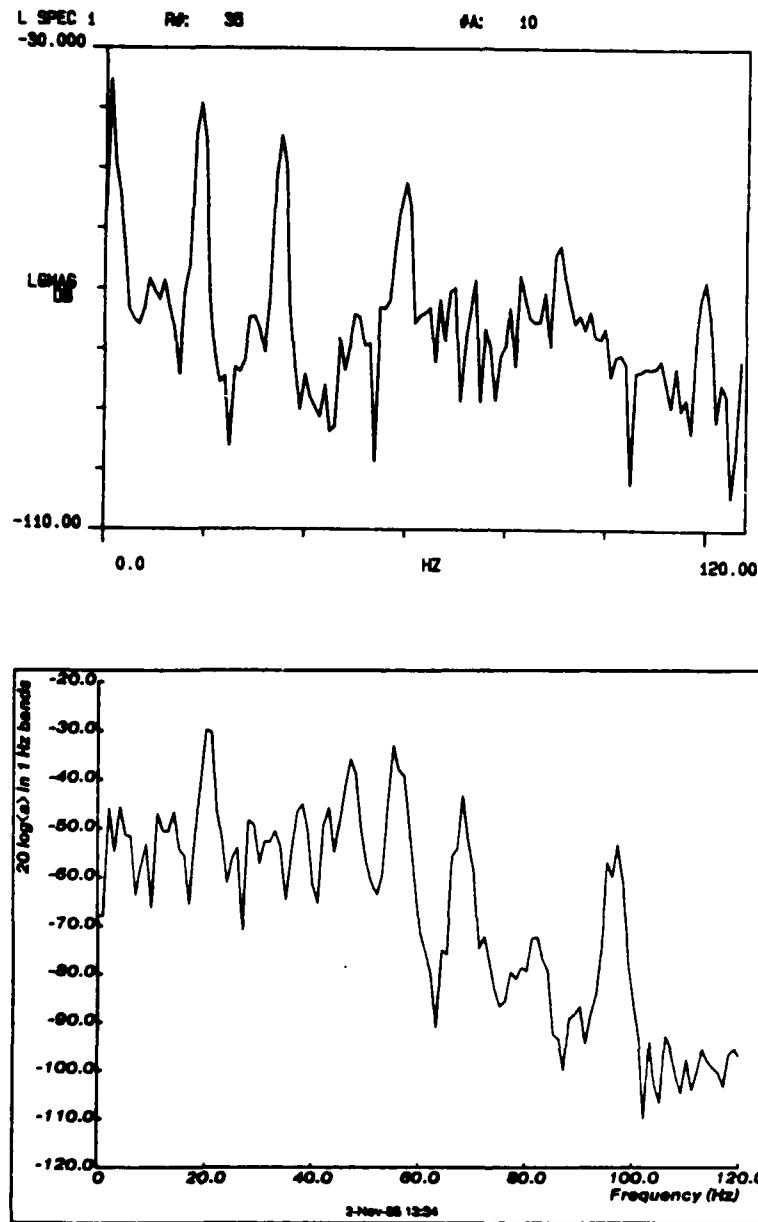


Figure 4.21: Fourier transform of vibration of end-effector at the end of the move for motion in Y-direction as obtained by test (top) and by simulation (bottom)

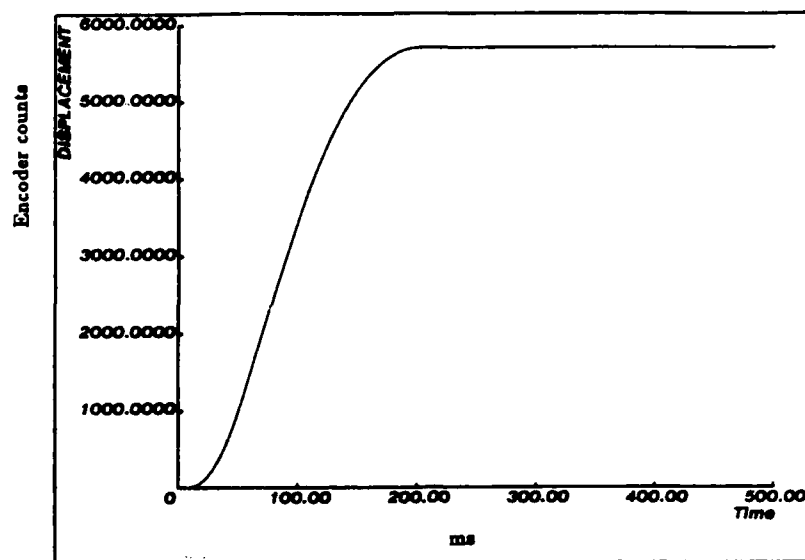


Figure 4.22: Encoder displacement during motion in Z-direction

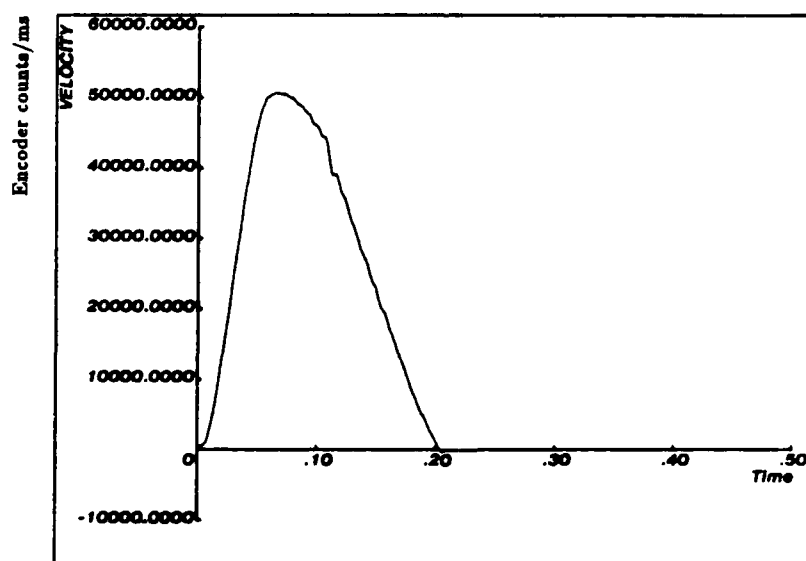


Figure 4.23: Encoder velocity during motion in Z-direction

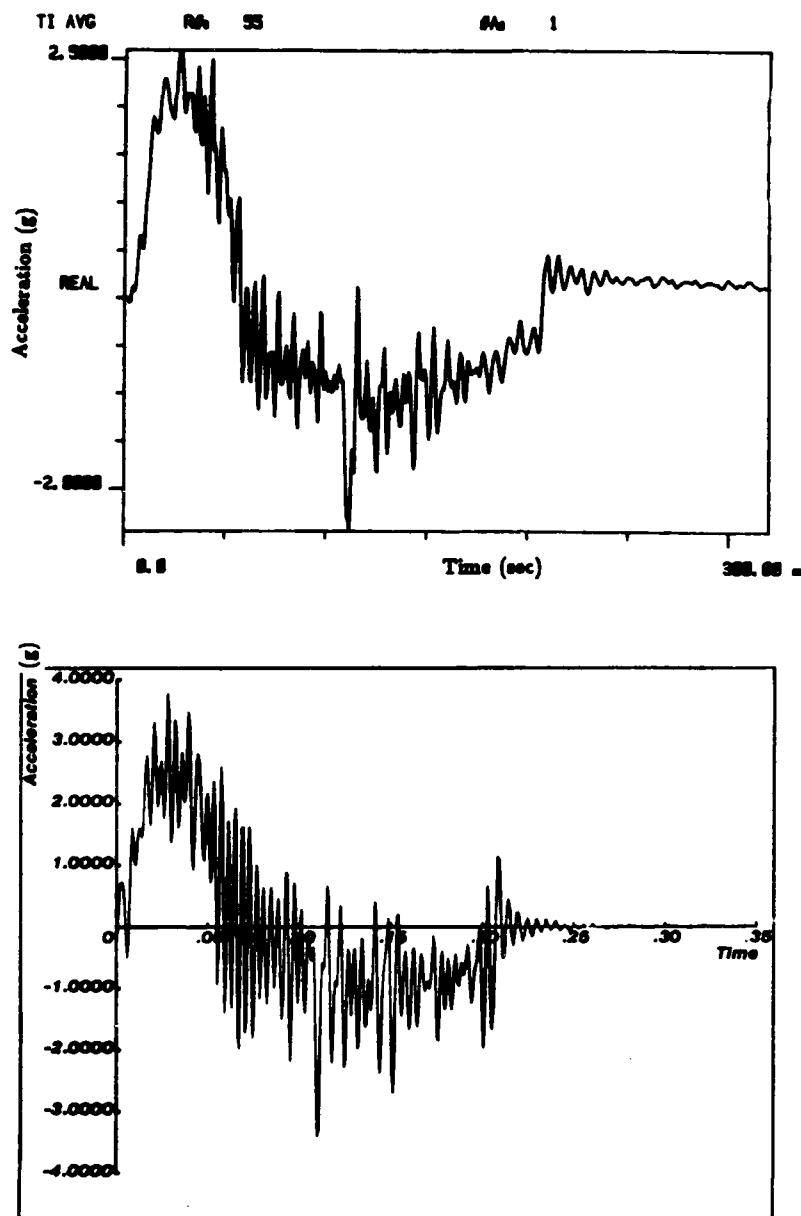


Figure 4.24: Vibration of end-effector during motion in Z-direction as obtained by test (top) and by simulation (bottom)

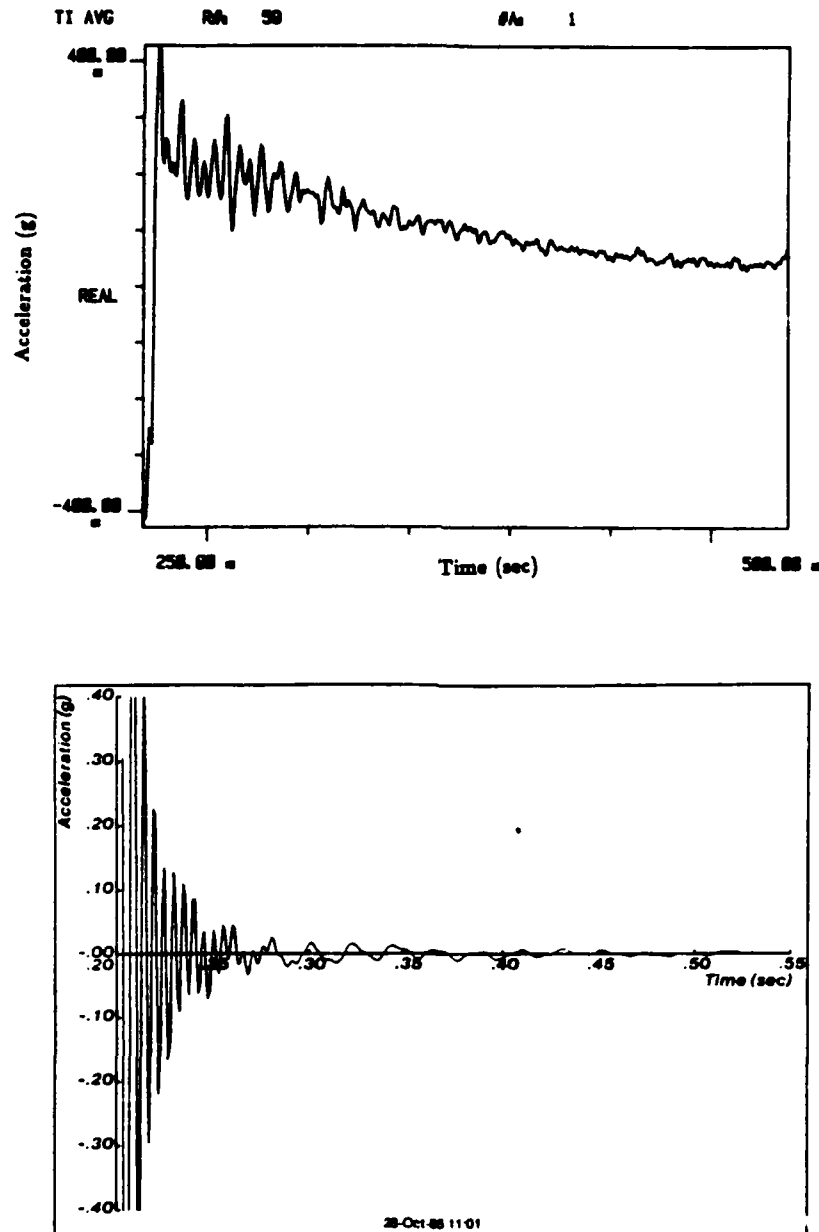


Figure 4.25: Vibration of end-effector at the end of the move for motion in Z-direction as obtained by test (top) and by simulation (bottom)



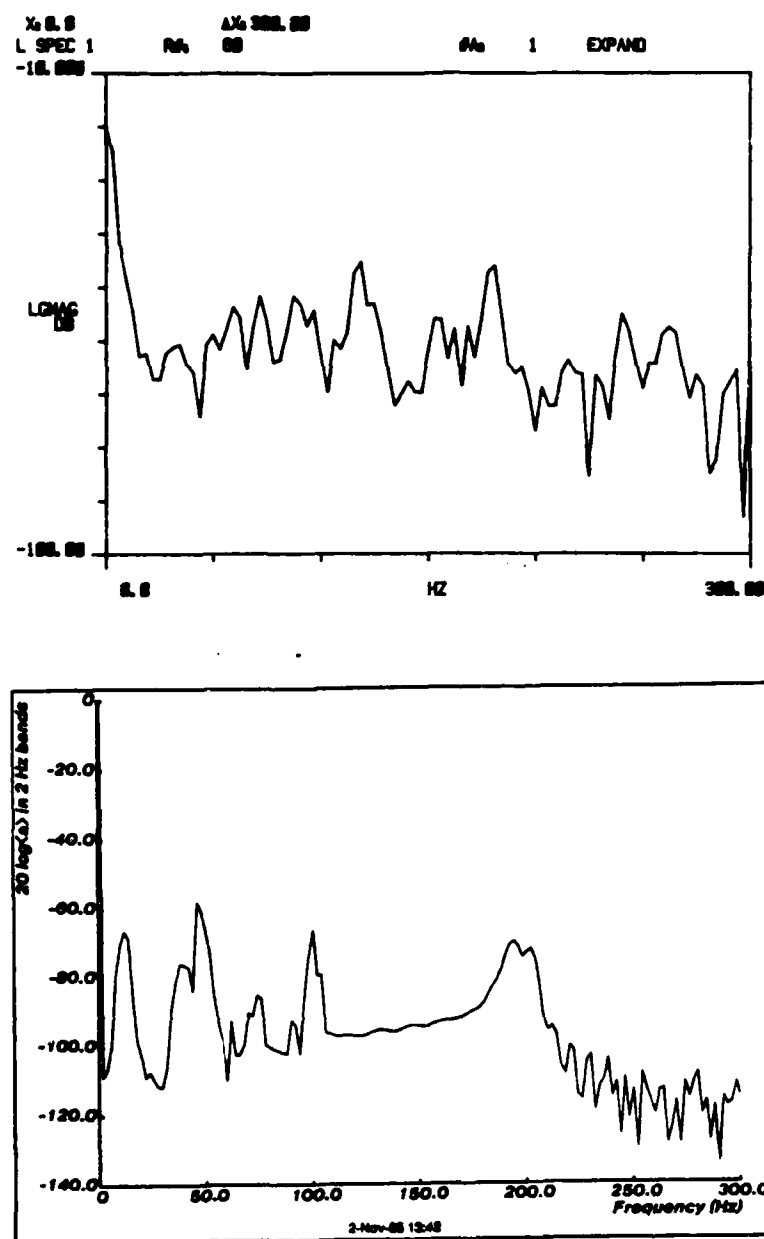


Figure 4.26: Fourier transform of vibration of end-effector at the end of the move for motion in Z-direction as obtained by test (top) and by simulation (bottom)

- The model predicts the same order of magnitude of the results and the same dominant harmonics in the spectra.
- The encoder acceleration, after being filtered, contains the dominant harmonics which are excited by the motor, harmonics which in turn reflect back to the excitation when the motor tries to maintain a given velocity profile.
- The system responds not only with the first two or three modes, but rather with a broad band of frequencies which may be excited.
- The vibration that occurs during the move, in the direction of motion, follows very closely that of the motor rotor. The end vibration however, has its own characteristics which are in part due to the motor whose forces remain active in order to fix the rotor.

A more specific discussion about each of the motion directions is given now:

#### Motion in X-direction

- The vibration during the move and the end vibration as measured by the accelerometer shows some drift which if corrected would make the plot of experimental data look more like the calculated vibration.
- The end vibration has a peak-to-peak amplitude of approximately 0.30 g for the test case and 0.24 g for the calculated one.
- There are two dominant frequencies, one at 12.3 Hz and another at 88 Hz which correspond to the robot modes no.1 and no.8 as shown in Figures ?? and ??. These modes are clearly excited because of their predominant X-direction component of end point motion.

- The relative amplitude of these harmonics as seen in the frequency spectra of Figure 4.16 tend to agree for both cases, experimental and simulated.

#### Motion in Y-direction

- The vibration during the move shows the same general shape for both cases with a peak-to-peak envelope amplitude of 2.0 g for the test case, and 2.5 g for the model.
- The end vibration shows for the test case an envelope of 0.85 g, and for the model case an envelope of 1.2 g.
- The dominant frequencies for both cases have the same general tendency as shown in Figures 4.19 and 4.20. The two most important harmonics occur at 19 Hz and 36 Hz, and correspond to the robot modes no.2 and no.3.

#### Motion in Z-direction

- The vibration during the move has an envelope of 5.0 g for the test case, and 7.0 g for the model case, the difference being that the model responds more at the higher dominant harmonic of 230 Hz.
- The end vibration as obtained by test shows more drift here than in the previous tests. Damping decay is also more visible in this direction.
- The first two dominant frequencies in the end vibration are 115 Hz and 176 Hz (perhaps multiples of the line frequency, 60 Hz), but in general all harmonics are rather uniform in amplitude as seen in Figure 4.26. The spectra in both cases look similar.

## Chapter 5

# CONCLUSIONS AND RECOMMENDATIONS

### 5.1 Conclusions

1. The basic idea behind the present vibration analysis of the cartesian robot is the connection of substructures which remain time-invariant, and whose modal characteristics and transfer functions can be readily determined either experimentally or analytically. For analytically determined data, we normally use a finite element analysis procedure to connect the substructures, but CMS can also be used. For experimentally determined data, the classical way of connecting substructures is the Impedance method, although CMS can be used here also. For this particular problem, the position dependency eliminates the possibility of application of the Impedance method, and for the slowly-varying case CMS and FE can be used. The relatively complex structure of each component and the physical availability of the prototype point towards the use of experimental data for getting a more realistic model. Therefore, the use of CMS becomes logical.

2. The fact that CMS uses modal data as input permits us to process all experimental data separately, and input the processed data to the model which can then perform fewer operations to predict the robot vibrations in a fast way. The matrix handling features of CMS are very convenient when a relatively large number of degrees of freedom are to be used to connect the substructures, as in the case of the robot.
3. The extension of CMS to the case of slowly-varying systems can be done when the speed at which the carriages move is such that the time spent in traveling all along the ways is much bigger than a typical natural period of oscillation. This situation allows us to neglect terms in  $\dot{\phi}$  and  $\ddot{\phi}$  and permits a simple manipulation of the data. The example of a traveling 2-degree of freedom system on a simply supported beam analyzed with two time scales in Chapter 3 gives an illustration of the validity of these approximations.
4. When connecting substructures through multiple degrees of freedom it may happen that a singularity or an ill-condition is present. Since the CMS process involves both the inversion of a matrix  $A$  that incorporates the compatibility conditions, and the solution of an eigenvalue problem, a bad distribution of degrees of freedom causes the eigenvalues to vary significantly from expected values. Furthermore a slight change in the data may cause a large variation in some eigenvalues. This can be avoided by detecting those redundant degrees of freedom and eliminating them or changing the distribution. A technique has been developed in this Thesis to detect and solve these problems.
5. Modal parameter identification has been an issue when we want high precision evaluation of the modal parameters based on experimen-

tal data. When curve fitting from a transfer function, the modeling technique, no matter how precise, has to assume a kind of damping behavior since modal damping is one of the parameters that has to be determined. This damping behavior is difficult to assess with precision and this is where we have an important source of error. The procedure developed here consists in taking a very high resolution drive point transfer function by zooming about each mode of interest, and then curve fitting by applying the nonlinear formula of the multimodal transfer function to a linear programming technique (Simplex) that minimizes the square of the residuals.

6. The compatibility conditions used to connect structures normally establish simple relations like  $x_A = x_B$ , but for some cases where we have a motor with lead screw, or just a motor  $M$  that is supported on one component  $A$  to drive another component  $B$ , we then use another relation which is  $x_A + x_M = x_B$ . This relation enforces the system kinematic relations and the force equilibrium as well.
7. The use of the GPIB interface to establish communication between the HP analyzer and the PDP 11/44 computer really enhances the capabilities to do 3-dimensional analysis since it allows among other things use of an animated display of the computer predicted mode shapes.
8. The eigenfunctions, determined experimentally for a number of discrete points along the ways on which the carriages slide, are subject to error and that adds bumps to the simulated ways. To smooth this we curve fit a beam-like eigenfunction to these data to get in addition to smoothness, a continuous function that permits a faster calculation of the mode shape value at the point of connection (eliminating the

need for interpolation in real time).

9. The use of the optical encoder motion that monitors the motor-rotor displacement during the robot operation to drive the equations of motion permits us to disregard the control system in the vibration analysis. After a computer-controlled experiment gives the encoder motion as well as the real vibration characteristics of the end effector, a computer simulation that utilizes the proposed mathematical model can be run using as input this encoder motion.
10. A dynamic model for the system vibrations that normally contains as a forcing term the motor force can be manipulated to eliminate the unknown force in favor of the encoder motion (displacement, velocity, and acceleration) and have this encoder motion drive the resulting system of coupled differential equations. This process is not restricted to time-invariant systems because it is done in the time domain, and it is simple to use for slowly-varying systems. The elimination of the unknown force which appears in every equation of the originally decoupled system is performed by combination of equations that involve multiplication by constants (from eigenvectors) and additions, plus the incorporation of an extra equation involving the encoder motion.
11. The arrangement of computer programs to do the analysis is such that the simulation program receives the data in its simplest form, having already being processed by previous programs so that the real-time simulation can run efficiently. This fast program however is still 40 times slower than the real-time process when running on a computer VAX/750 using 10 natural modes of vibration.
12. The results of the mathematical model for fixed configuration show

that the eigenvalues and eigenvectors correlate relatively well with the experimental values. The difference in natural frequencies for the range 0 to 200 Hz is 6.89 % average, and this error is not so much affected by the convergence rate of the CMS which behaves like a regular Ritz analysis, but it is more affected by the errors in the modal parameter estimation, particularly in the scaling of the eigenvectors.

13. The results of the mathematical model for the case of the moving robot show that the vibration follows very closely the encoder acceleration, and this in turn contains in its harmonics (among other harmonics introduced by the control system) those natural modes of the robot that are excited by the motion. A comparison of experimental and calculated vibrations show in general good correlation in magnitude and in frequency content.
14. With regard to the preliminary work of the four-bar linkage, one analysis that illustrates the nature of the position-dependent problems, or in other words, of changing boundary conditions is the rocker-beam analysis. Here we studied the behavior of the first natural frequency as the boundary conditions changed, having obtained the limiting cases of cantilever beam, pinned-pinned, clamped-pinned and free-pinned beams.
15. Another result of the four-bar linkage problem, the linearization of the equations of motion by neglecting higher order terms leads to a parallel analysis in the moving 2-degree of freedom system on a beam which allowed extending the method of CMS to position-dependent problems.
16. Finally, the dimensional analysis for the four-bar linkage illustrates



that dynamically similar systems behave in the same way, and therefore, in the normalization of the mode shapes for the robot problem we have to distinguish the right member of the family which belongs to the data obtained in order to properly identify the system.

## 5.2 Recommendations

1. An improved technique for modal parameter identification should be pursued to more closely evaluate the modal parameters, particularly the orthonormal mode shape value since that determines most importantly the precision of the final simulation results. Different damping patterns should be examined, and solution of the convergence problems of multimodal curve fits should be tried.
2. Another study should be to incorporate the control system to the mathematical model in order to have a complete representation of the dynamic system. Again CMS may be used to connect the mechanical system to the control system through the motors.
3. Another study which would make the model more precise would be to add corrections to first order to the differential equations by restoring some of the neglected terms.
4. To make the program faster, one approach that could be tried is the asymptotic approximations to the solution of the differential equations by curve-fitting first the appropriate data and then apply standard techniques to approximately solve differential equations with slowly-varying coefficients. The solution would be expressed as a function of position and of the motion parameters.
5. Another study should correct the mathematical model to account

for torque reactions that occur at the motor base. These reactions may affect the simulation of cross vibrations (vibrations that occur perpendicular to the direction of motion).

## Bibliography

- [1] Baruch, M., and Itzhack, I.Y.B., "Optimal Weighted Orthogonalization of Measured Modes", J.AIAA, Vol.16, No.4, 1977, pp.346-351.
- [2] Bathe, K.J., "Finite Element Procedures in Engineering Analysis", Prentice Hall Press, 1982.
- [3] Bejan, R.L., and Feng, C.C., "Free Vibration Analysis by the Modal Substitution Method", AAS Paper 68-8-1, July 1968.
- [4] Benfield, W.A., and Hruda, R.F., "Vibration Analysis of Structures by Component Mode Substitution", J.AIAA, Vol.9, No.7, July 1971, pp.1255-1261.
- [5] Benjamin, M.H., ME Thesis, 1985, M.S. thesis, Massachusetts Institute of Technology.
- [6] Berman, A. and Nagy, E.J., "Improvement of a Large Dynamic Analytical model Using Ground Vibration Test Data", AIAA 82-0743, pp.301-306.
- [7] Berman, A., Wei, F.S., and Rao, K.V., "Improvement of Analytical Dynamic Models Using Modal Test Data", AIAA 80-0800, pp.809-814.
- [8] Berman, A., "System Identification of a Complex Structure", AIAA paper no.75-809, pp.1-6.

- [9] Biggs, J.M., "Introduction to Structural Dynamics", McGraw-Hill, 1964
- [10] Blevins, R.D., "Formulas for Natural Frequencies and Mode Shape", Van Nostrand Reinhold, 1979.
- [11] Brown, D.L., Allemang, R.J., Zimmerman, R., and Mergeay, M., "Parameter Estimation Techniques for Modal Analysis", SAE paper 790221, pp.828-846.
- [12] Caceci, M.S., and Cacheris, W.P., "Fitting Curves to Data", Byte, May 1984, pp 340-362.
- [13] Capellen, M., "Torsional Vibrations in the Shafts of Linkage Mechanisms". ASME trans. Feb 1967, pp.126-136
- [14] Caughey, T.K., "Classical Normal Modes in Damped Linear Dynamic Systems", J. of Applied Mechanics, Transactions of the ASME, June 1960, pp.269-271.
- [15] Chen, J.C., Analytical Model Accuracy Requirements for Structural Dynamic Systems", AIAA 82-0734, pp.521-529.
- [16] Craig, R.R., and Bampton, M.C.C., "Coupling of Substructures for Dynamic Analysis", J. AIAA, Vol.6, No.7, July 1968, pp.1313-1319.
- [17] Craig, R.R. Jr., "Methods of Component Mode Synthesis", Shock and Vibration Digest, 9 (11) 1977, pp.3-10.
- [18] Craig, R.R., and Chang, C.J., "On the use of Attachment Modes in Substructure Coupling for Dynamic Analysis", Paper No. 77-405, AIAA/ASME 18th Struct., Struc. Dyn. and Materials Conf., San Diego, 1977, pp.89-99.

- [19] Crandall, S.H., "Nonlinearities in Structural Dynamics", Shock and Vibration Digest, V6, No.8, 1974.
- [20] Crandall, Karnopp, Kurtz and Pridmore-Brown, "Dynamics of Mechanical and electromechanical Systems." Mc Graw-Hill, 1968.
- [21] Erdman, A.G., Sandor, G.N., and Oakberg, R.G., "A General Method for Kineto-Elastodynamic Analysis and Synthesis of Mechanisms." ASME trans. Nov 1972, pp.1193-1205
- [22] Ewins, D.J., and Sainsbury, M.G., "Mobility Measurements for the Vibration Analysis of Connected Structures", Shock and Vibration Bulletin, No.42, Pt.1, Jan 1972, pp.105-122.
- [23] Favour, J.D., Mitchell, M.C., and Olson, N.L., "Transient Test Techniques for Mechanical Impedance and Modal Survey Testing", Shock and Vibration Bulletin, 42 Pt1, Jan 1972, pp.71-82.
- [24] Giménez, J.G., and Carrascosa, L.I., "Global Fitting, an Efficient Method of Experimental Modal Analysis of Mechanical Systems", Proceedings of the 1st International Modal Analysis Conference, Orlando, Fla. 1982.
- [25] Goyder, H.G.D., "Methods and Application of Structural Modelling From Measured Structural Frequency Response Data", J. Sound and Vibration (1980) 68(2), pp.209-230.
- [26] Greif, R., and Wu, L., "Substructure Analysis of Vibrating Systems", Shock and Vibration Digest, 1983 15(1), pp.17-24.
- [27] Hale, A.L., "On Substructure Synthesis and its Iterative Improvement for Large Nonconservative Vibratory Systems", AIAA paper no.82-0772, pp.582-593.

- [28] Halvorsen, W.G., and Brown, D.L., "Impulse Technique for Structural Frequency Response Testing", *Sound and Vibration*, November 1977, pp.8-21.
- [29] Hartog, Den, "Mechanical Vibrations." Mc Graw-Hill. 1956
- [30] Hasselman, T.K., "A Matrix Method For Synthesis of Structural Damping from Substructure Test Results", *Symp. Substruc. testing and Synthesis*, NASA Marshall Space Flight Center, 1972.
- [31] Hasselman, T.K., "Damping Synthesis from Substructure Tests", *J.AIAA*, 14 (10), 1976, pp.1409-1418.
- [32] Hintz, R.M., "Analytical Methods in Component Modal Synthesis", *J.AIAA*, Vol.13, No.8, August 1975, pp.1007-1016.
- [33] Hou, S.N., "Review of Modal Synthesis Techniques and a New Approach", *The Shock and Vibration Bulletin*, No.40, Pt.4 Naval Research Lab., Washington, D.C., December 1969, pp.25-39.
- [34] Hurty, W.C., Collins, J.D., and Hart, G.C., "Dynamic Analysis of Large Structures by Modal Synthesis Techniques", *Computers and Structures*, Vol 1 Dec 1971, pp535-563.
- [35] Hurty, W.C., "Dynamic Analysis of Structural Systems Using Component Modes", *J. AIAA*, Vol.3, No.4, April 1965, pp.678-685.
- [36] Hurty, W.C., "Vibrations of Structural Systems by Component Mode Synthesis", *J. Engineering Mechanics Division*, *Proceedings ASCE*, August 1960 pp.51-69.
- [37] Hurty, W.C., "A Criterion for Selecting Realistic Natural Modes of a Structure", *Tech.Memo.33-364*, Jet Propulsion Lab., Pasadena, CA. 1967.

- [38] Hurty, W.C., "Truncation Errors in Natural Frequencies as Computed by the Method of Component Mode Synthesis", Proc. First Conf. Matrix Meth. in Struc. Mech., Wright-Patterson AFB, OH, AFFDL-TR-66-80, pp.803-821 1966.
- [39] Hurty, W.C., "Introduction to Modal Synthesis Techniques", Synthesis of Vibrating Systems, ASME, pp.1-13, 1971.
- [40] Ibrahim, S.R., "Determination of Normal Modes from Measured Complex Modes", Shock and Vibration Bulletin, No.52, 1982, pp.13-17.
- [41] Ibrahim, S.R., "Dynamic Modeling of Structures from Measured Complex Modes", AIAA 82-0770, pp.564-573.
- [42] Imam, I., Sandor, G.N., and Kramer, S.N., "Deflection and Stress analysis in High Speed Planar Mechanisms with Elastic Links." ASME trans. May 1973, pp.541-548
- [43] Kana, D.D., and Huzar, S., "Synthesis of Shuttle Vehicle Damping Using Substructure Test Results", Interim Report, Southwest Research Institute, San Antonio, TX, 1972.
- [44] Kana, D.D., and Unruh, J.F., "Prediction of Shuttle Vehicle Damping from Component Test Results", Final Rep., Southwest Research Institute, San Antonio, TX, 1973.
- [45] Kana, D.D., and Huzar, S., "Prediction of Shuttle Vehicle Damping Using Substructure Test Results", Symp. Substruc. Testing and Synthesis, NASA Marshall Space Flight Center, 1972
- [46] Kana, D.D., and Huzar, S., "Synthesis of Shuttle Vehicle Damping Using Substructure Test Results", J. Spacecraft and Rockets, 10 (12),

- 1973, pp.790-797. Testing and Synthesis, NASA Marshall Space Flight Center, 1972
- [47] Klosterman, A.L., and Lemon, J.R., "Dynamic Design Analysis Via the Building Block Approach", Shock and Vibration Bulletin, No.42, Pt.1, Jan 1972, pp.97-104.
- [48] Klosterman, A.L., "A combined Experimental and Analytical Procedure for Improving Automotive System Dynamics", SAE paper 720093, pp.343-353.
- [49] Klosterman, A.L., and McClelland, W.A., "Combining Experimental and Analytical Techniques for Dynamic System Analysis", 1973 Tokyo, Seminar Finite Element Anal., Japan (1973), pp.339-356.
- [50] Kohli,D., Hunter,D., and Sandor,G.N., "Elastodynamic Analysis of a Completely Elastic System." ASME trans. Aug 1977, pp.604-609
- [51] McClellan, J.H., Parks, T.W., and Rabiner, L.R., "FIR Linear Phase Filter Design Program".
- [52] MacNeal, R.H., "A Hybrid Method of Component Mode Synthesis", Computers and Structures, Vol.1, 1971, pp.581-601.
- [53] Meirovitch, L., "Analytical Methods in Vibrations", The MacMillan Co., New York, 1967.
- [54] Moré, J.J., "The Levenberg-Marquardt Algorithm: Implementation and Theory", Lecture Notes in Mathematics No.630, 1977, pp.105-116.
- [55] Morosow, G., and Abbott, P., "Mode Selection", Synthesis of Vibrating Systems, ASME, 1971, pp.72-77.



- [56] Mustain, R.W., "Survey of Modal Vibration Test/Analysis Techniques", SAE prepr 760870, 16p.
- [57] Nayfeh, A.H., "Perturbation Methods", John Wiley and Sons, 1973.
- [58] O'Hara, G.J., "Mechanical Impedance and Mobility Concepts", J. Acoustical Society of America, Vol.41, No.5, 1967, pp.1180-1184.
- [59] Okubo, C., "The Effect of Non-Linearity on Transfer Function Measurement", Sound and Vibration, November 1982, pp.34-39.
- [60] Paul, Burton, "Kinematics and Dynamics of Planar Machinery." Prentice Hall. 1979
- [61] Plunkett, R., "Colloquium on Mechanical Impedance Methods for Mechanical Vibrations", ASME Annual Meeting, New York, N.Y., December 2, 1958.
- [62] Potter, R., "A General Theory of Modal Analysis for Linear Systems", Shock and Vibration Digest, November 1975, pp.3-11.
- [63] Potter, R., and Richardson, M., "Mass, Stiffness, and Damping Matrices from Measured Modal Parameters", International Instrumentation-Automation Conference, New York, Oct 1974, pp.1-5.
- [64] Potter and Foss, "Fluid Mechanics". Wiley. 1975
- [65] Ramsey, K.A., and Richardson, M., "Effective Transfer Function Measurements for Modal Analysis, Part I", Sound and Vibration, Vol.1, No. 11, 1975.
- [66] Richardson, M., and Kniskern, J., "Identifying Modes of Large Structures from Multiple Input and Response Measurements", SAE prepr 760875, 9p.

- [67] Rubin, S., "Improved Component-Mode Representation for Structural Dynamic Analysis", J.AIAA, Vol.13, No.8., August 1975, pp.995-1006.
- [68] Sadler, J.P., and Sandor, G.N., "A Lumped Parameter Approach to Vibration and Stress analysis of Elastic Linkages." ASME trans. May 1973, pp.549-557
- [69] Sadler, J.P. and Sandor, G.N., "Nonlinear Vibration Analysis of Elastic Four-Bar Linkages." ASME trans. May 1974, pp.411-419
- [70] Sanders, J.R., and Tesar, D. "The Analytical and Experimental Evaluation of Vibratory Oscillations in Realistically Proportioned Mechanisms." ASME Trans., Vol 100 Oct 1978, pp.762-768.
- [71] Singer, N.C., ME Thesis, 1985, M.S. thesis, Massachusetts Institute of Technology.
- [72] Stearns, S.D., "Digital Signal Analysis", Hayden Press, 1975.
- [73] Sunada, W.H., and Dubowsky, S., "On the Dynamic Analysis and Behavior of Industrial Robotic Manipulators with Elastic Members", Transactions of the ASME, Vol.105, March 1983, pp.42-51.
- [74] Sutherland, G.H., "Analytical and Experimental Investigation of a High-Speed Elastic-Membered Linkage." ASME trans. Aug 1976, pp.788-794
- [75] Thoren, A.R., "Derivation of Mass and Stiffness Matrices from Dynamic Test Data", AIAA paper 72-436, 13th Structures, Structural Dynamics and Materials Conference, San Antonio, Tex., April 12, 1972, pp.1-5.
- [76] Turing, A.M., "Rounding-Off Errors in Matrix Processes", Quart. J. Mech. Appl. Math., 1, 1948, pp.287-308.

- [77] Union College, Schenectady, N.Y., "Proceedings of the 1st International Modal Analysis Conference", Orlando, Fla., 1982.

# Appendix A

## MODE SHAPE DATA

### A.1 Determination of Modal Characteristics

The vibration analysis to be performed on the cartesian robot requires the *determination of the natural frequencies and mode shapes* of a number of structures and components, some of them being rather complicated in shape. These parts were already described in Chapter 2 and include the robot structure, the carriages, and the lead screws. As mentioned before, the carriages were tested in a free condition (floating) by suspending them on soft foam-pads, and the impact test was applied to a number of test points. Also, the robot structure was tested while bolted to the floor by exciting it with an electrodynamic shaker which was suspended from the ceiling with a flexible string. Finally, the torsional modes of the lead screws were obtained analytically. These conditions are summarized in Table A.1.

The random test using a shaker is more precise than the impact test when we need a calibrated measurement, and for the case of the robot structure attached to the floor, this was required in order to normalize the eigenvectors. For the Z-carriage we required more precision than for the other carriages since its modal characteristics tend to affect more the robot

vibrations. Also, its modes occur at higher frequencies when tested in free-free condition, and the impact test can not give good results above 800 Hz due to the roll-off of the impulse force spectrum.

The test set-up for the impact procedure is shown in Figure A.1. The accelerometer is kept fixed at one convenient test point and the structure is marked at each of the test points. The instrumented hammer is used to impact on each of the test points while the analyzer collects a series of transfer functions. This process can be repeated for a different position of the accelerometer to get a new set of data which added to previous set could provide a more complete analysis; that is, the second set could show some of the modes more clearly than the first set. But strictly speaking, one set of tests is sufficient. The analyzer can then process all these data with an algorithm that determines the mode shape values at the test points.

The test set-up for the random test is shown in Figure A.2. Here the shaker is kept fixed to a convenient test point while the accelerometer has to be moved around for each new transfer function.

The algorithm used by the analyzer (HP 5423A Structural Dynamics Analyzer) presents two options to the user, quadrature picking and rational fraction least squares, both for the single degree of freedom case. The quadrature picking or line-method is useful when damping is low and the modes are closely spaced since it only uses the transfer function value at the mode peak. The rational fraction least squares or band-method curve-fits a band of the transfer function that includes the mode being analyzed, and it is more precise when the modes are well separated.

For the cases of very simple geometry, like the lead screws in torsion, we can analyze them by the theory of continuous-parameter models, particularly when we have one or two uniform elements. Then the analysis is simple and accurate.

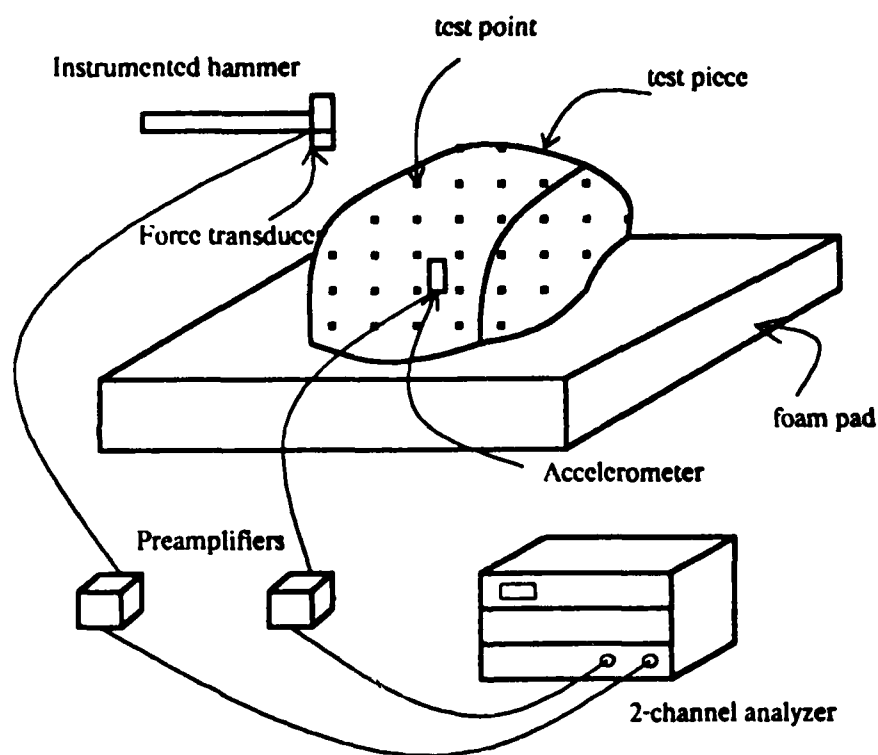


Figure A.1: Test set-up for impact procedure

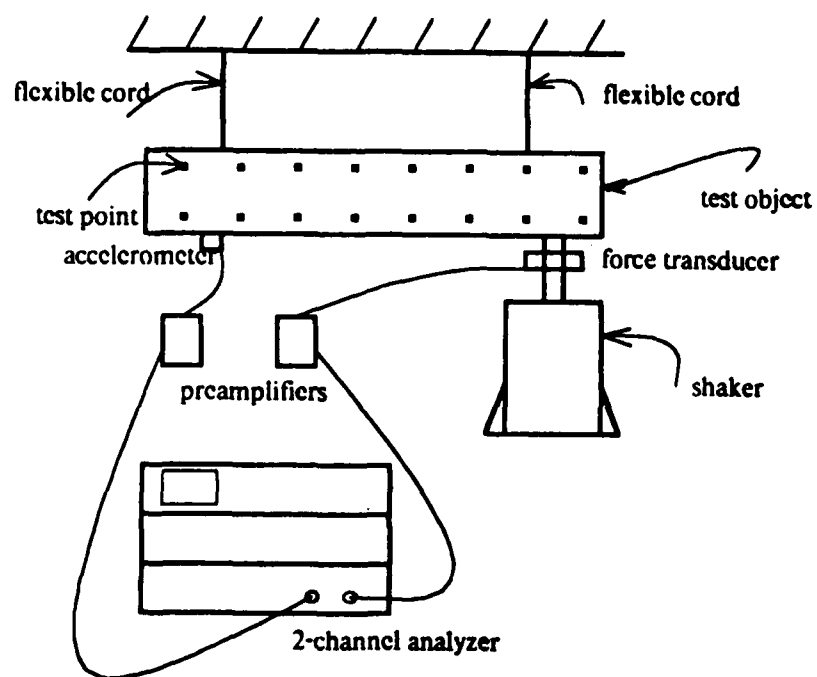


Figure A.2: Test set-up for random procedure

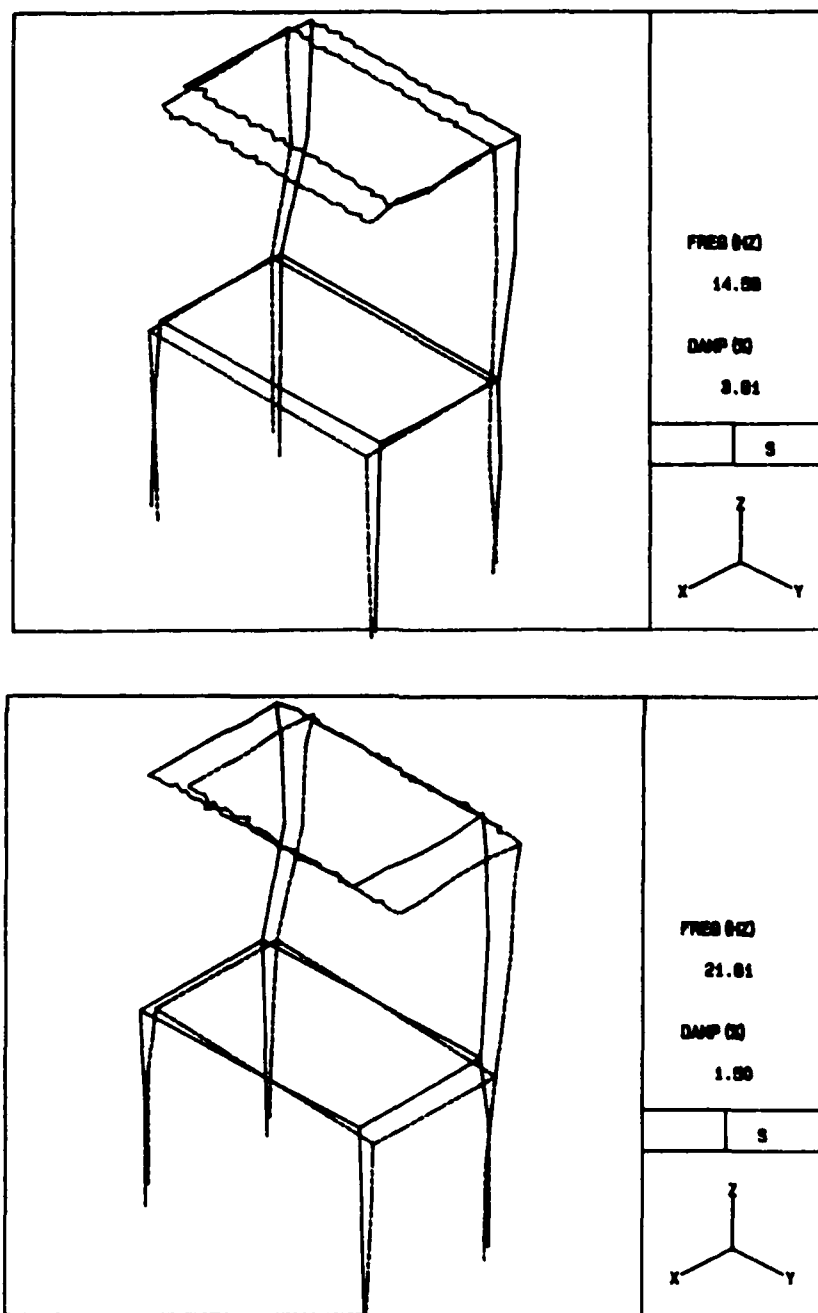


Figure A.3: Mode shapes no.1 (top) and no.2 (bottom) of robot structure as obtained by test



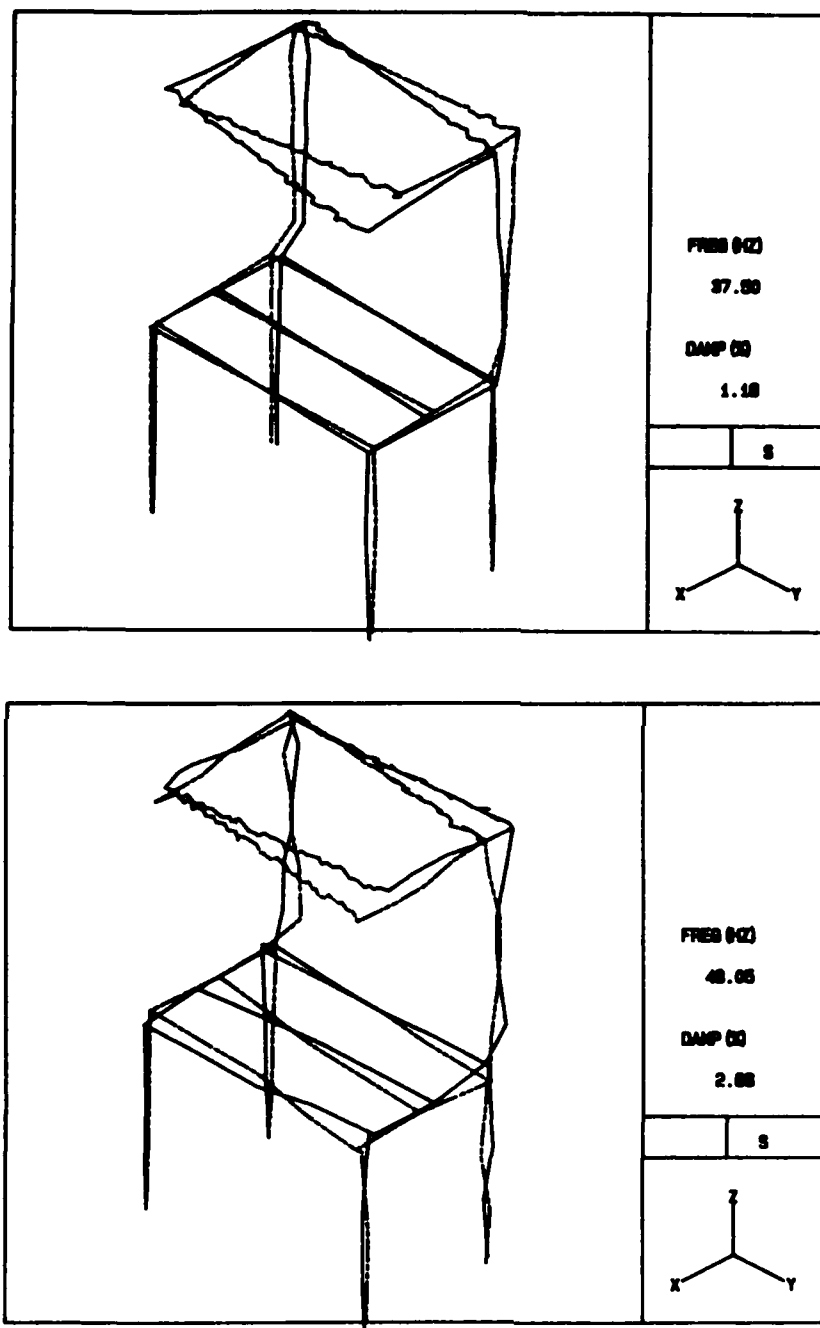


Figure A.4: Mode shapes no.3 (top) and no.4 (bottom) of robot structure as obtained by test

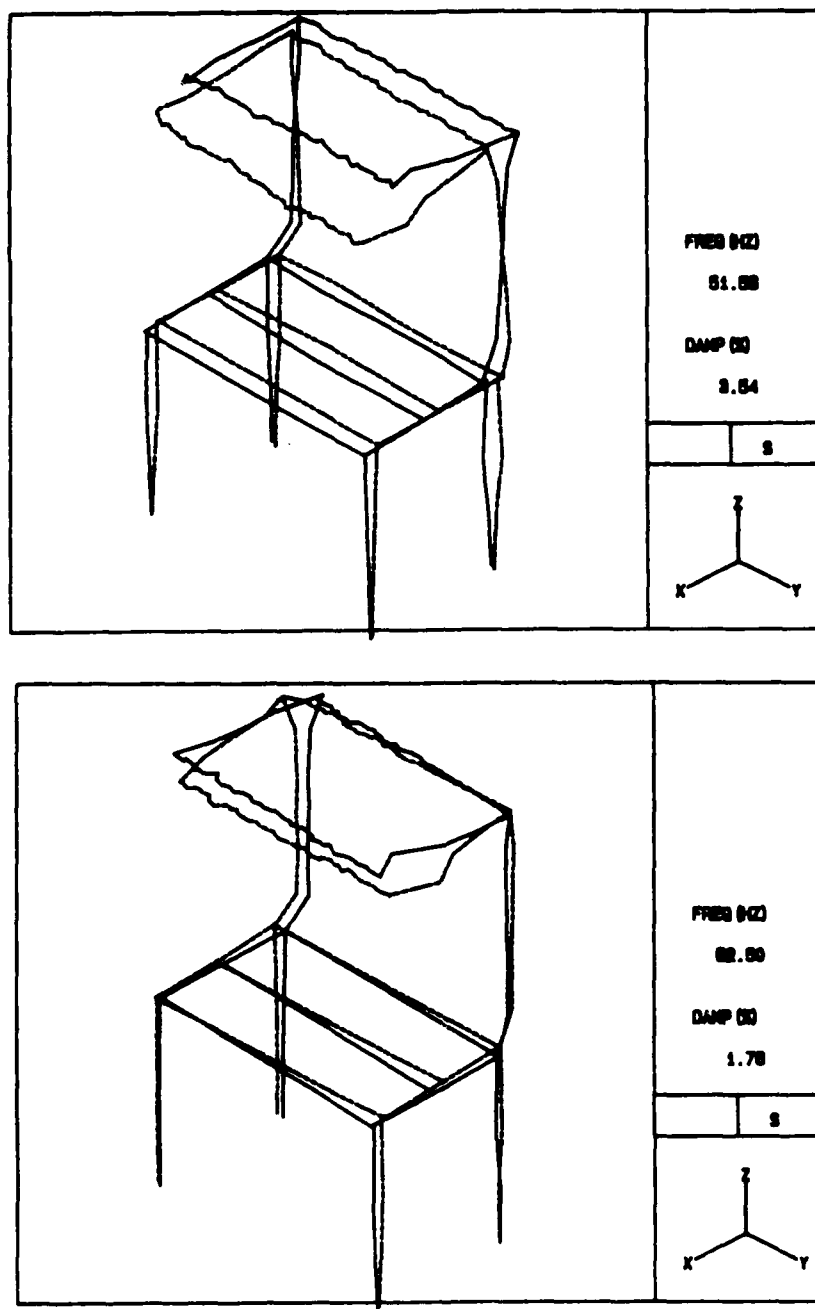


Figure A.5: Mode shapes no.5 (top) and no.6 (bottom) of robot structure as obtained by test

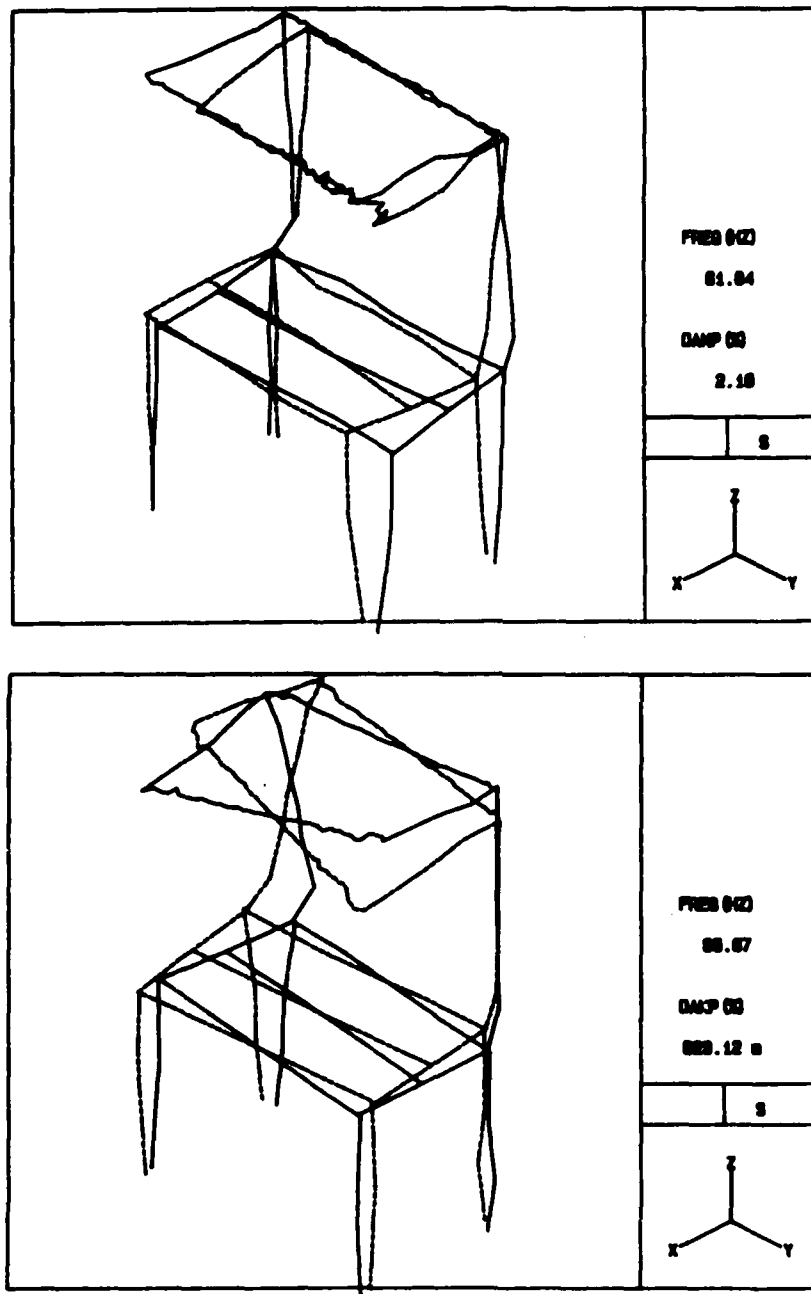


Figure A.6: Mode shapes no.7 (top) and no.8 (bottom) of robot structure as obtained by test

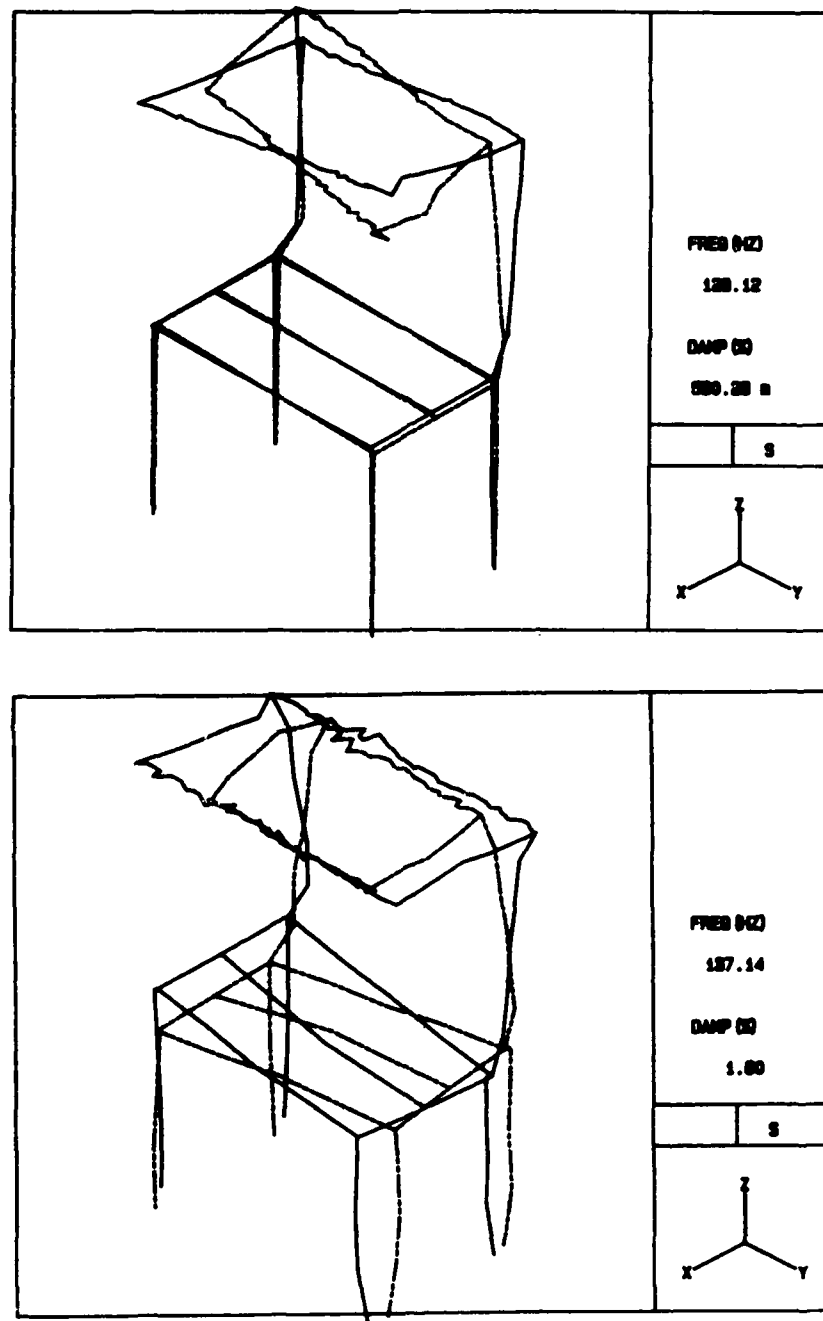


Figure A.7: Mode shapes no.9 (top) and no.10 (bottom) of robot structure as obtained by test

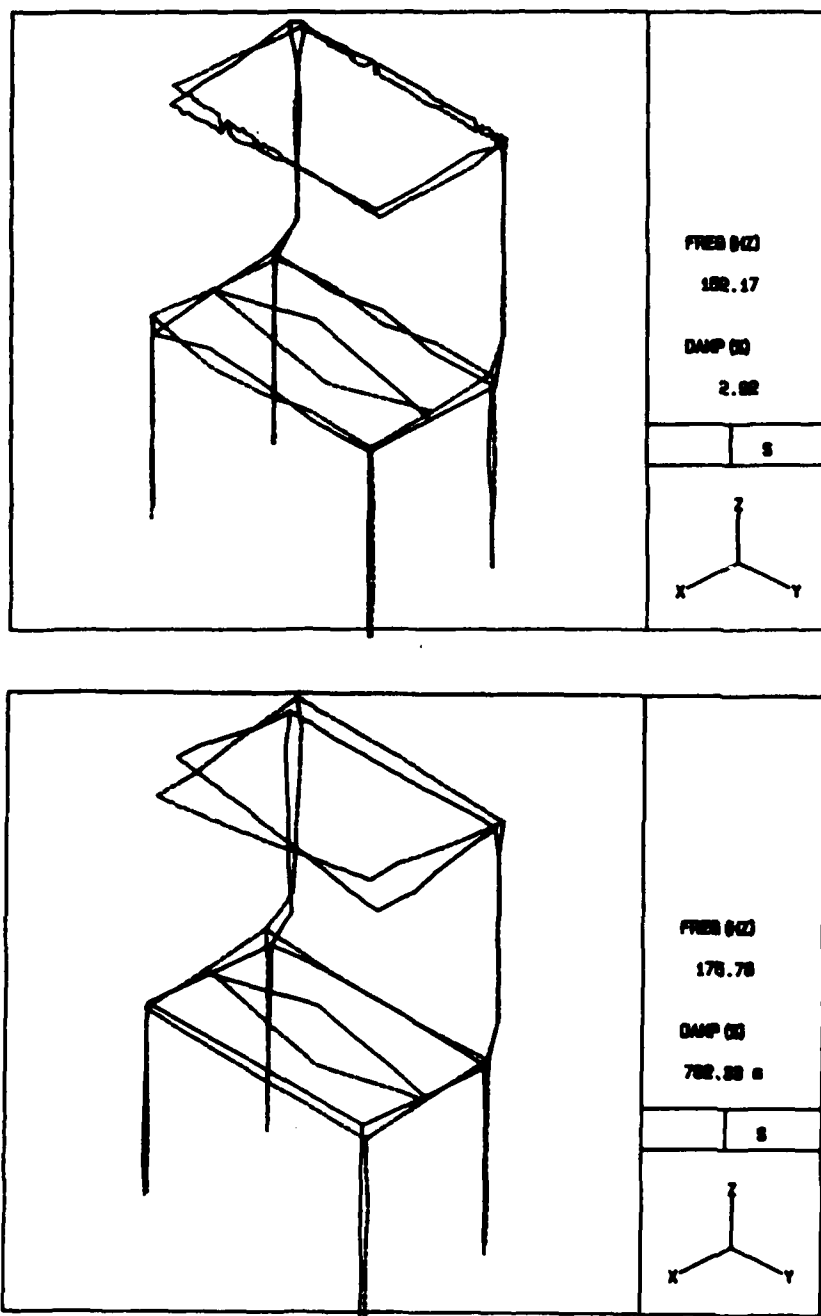


Figure A.8: Mode shapes no.11 (top) and no.12 (bottom) of robot structure as obtained by test

Component	Test	Support Cond.	test points	BW (Hz)	Elastic modes
Structure	random	fixed-free	146	0-200	13
X-carriage	impact	free-free	66	0-610	4
Y-carriage	impact	free-free	92	0-510	10
Z-carriage	random	free-free	54	0-1500	5
MX-lead screw	analytical	free-free	continuous	-	1
MY-lead screw	analytical	free-free	continuous	-	1
MZ	analytical	free-free	continuous	-	0

Table A.1: Conditions of experimental tests.

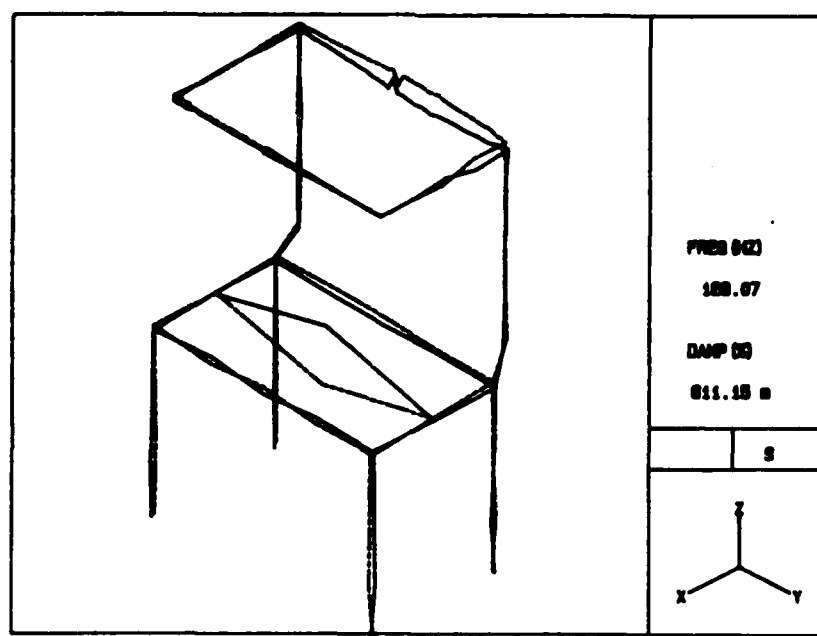


Figure A.9: Mode shape no.13 of robot structure as obtained by test

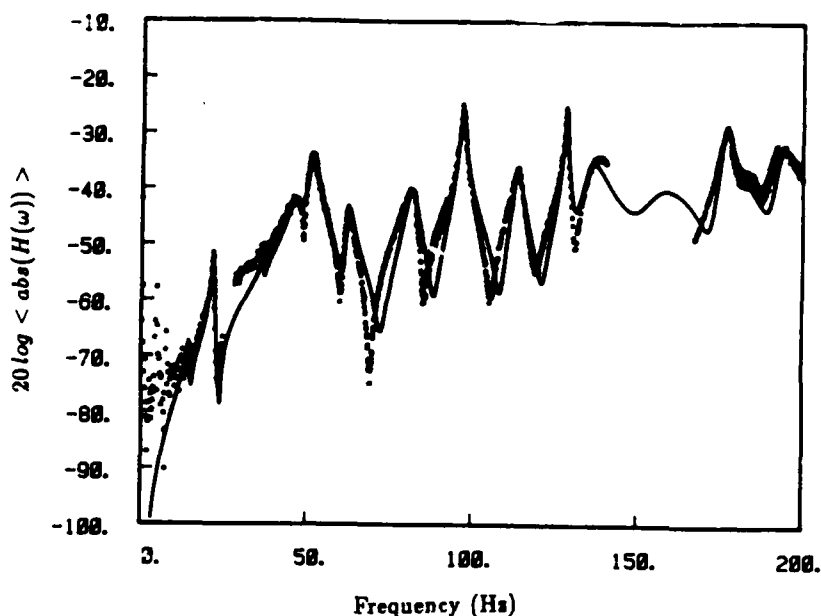


Figure A.10: Drive-point transfer function of robot structure

## A.2 Mode Shape Data for Robot Structure

The robot structure attached to the floor and without carriages gives the following 13 natural modes of vibration in the frequency range of 0 to 200 Hz (see Figures A.3- A.9). The drive-point transfer function which was used for normalization of the eigenvectors was obtained by zooming about each of the modes and then collecting all these transfer functions to make one single plot (see Figure A.10). This figure shows a collection of nearly 2000 points which give the transfer function absolute values with enough frequency resolution about each mode of interest. The curve fitting of these data was already discussed in section 2.3, and the curve fit is shown as a solid line in the same figure. From this curve fit we determine the modal parameters in a more precise way than in the standard modal analysis, and they are used then to normalize the eigenvectors.

### A.3 Mode Shape Data for Carriages

All three carriages were tested separately in a free condition to get the elastic mode shapes shown in Figures A.11- A.20. The rigid body modes were calculated as explained in Chapter 2 .

The normalization was carried out in two different ways according to the modal test used. For the Z-carriage we used the random test and from it we got the drive-point transfer function shown in Figure A.21 which is a collection of zoom transfer functions about each mode. We then curve-fit the modal parameters as explained in section 2.3.

The X-carriage and Y-carriage were tested by the impact procedure (un-calibrated) and, then to normalize we used the mass distribution according to a formula of Chapter 2.

### A.4 Mode Shapes for Lead Screws

These mode shapes in torsion were obtained analytically by modeling each lead screw as a uniform shaft with an inertia (motor rotor) attached to one end, as shown in Figure A.22. The natural frequencies for this system are given by the transcendental equation

$$\frac{J\omega}{GI_p} \sqrt{\frac{G}{\rho}} = -\tan(\omega L \sqrt{\frac{\rho}{G}}) \quad (\text{A.47})$$

and the eigenfunctions are given by

$$a(x) = C_1 \cos(\omega x \sqrt{\frac{\rho}{G}}) + C_2 \sin(\omega x \sqrt{\frac{\rho}{G}}) \quad (\text{A.48})$$

To normalize we use orthogonality of the normal modes to get

$$\int_0^L \rho I_p a_n^2(x) dx + J a_n^2(L) = 1 \quad (\text{A.49})$$



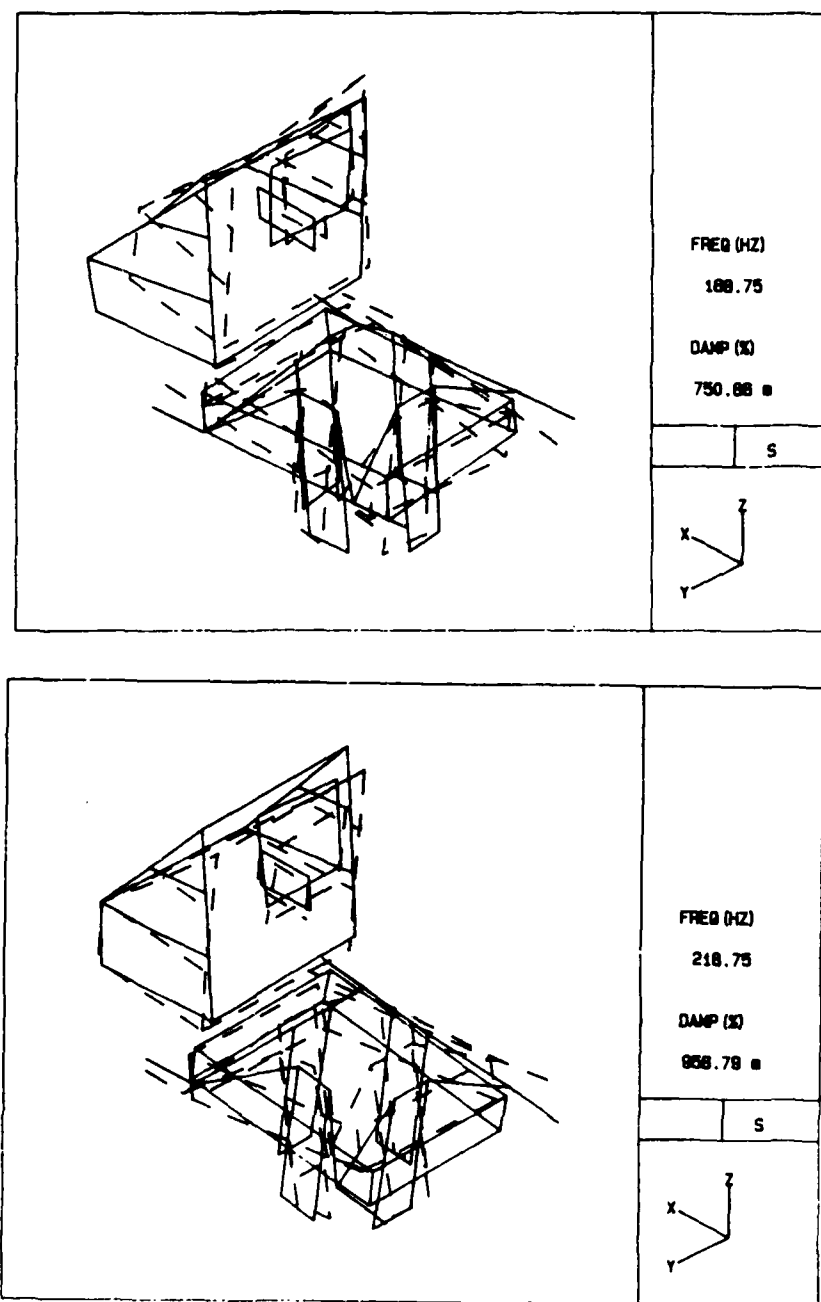


Figure A.11: Mode shapes no.1 (top) and no.2 (bottom) of X-carriage as obtained by test

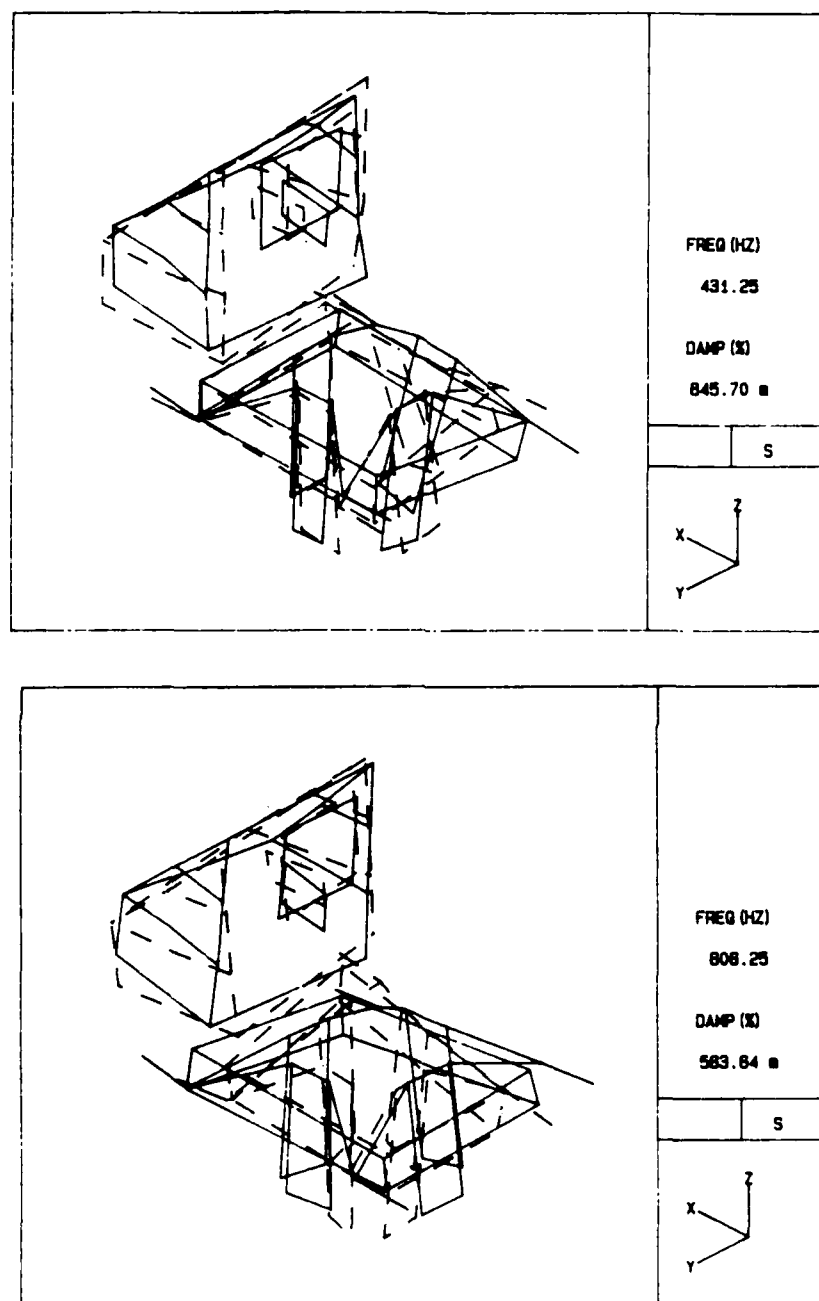


Figure A.12: Mode shapes no.3 (top) and no.4 (bottom) of X-carriage as obtained by test

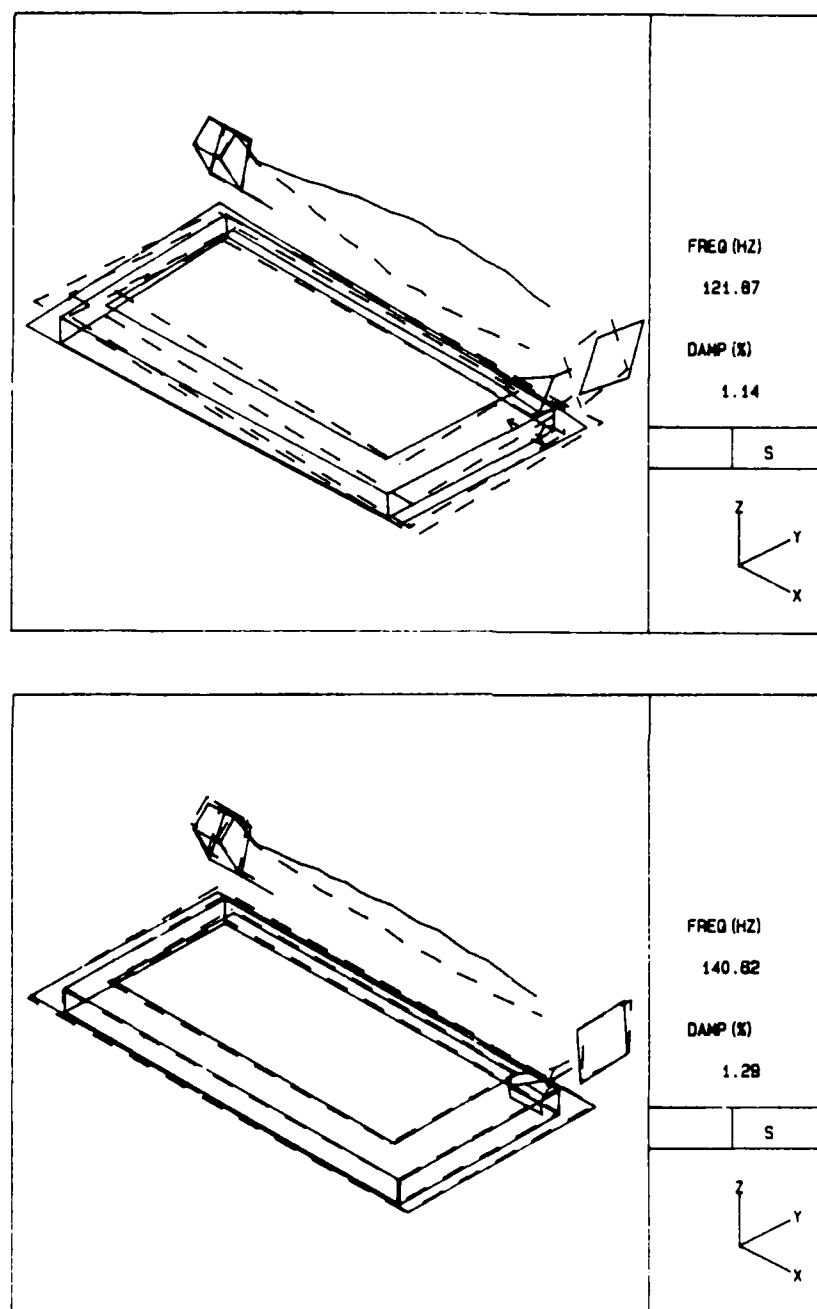


Figure A.13: Mode shapes no.1 (top) and no.2 (bottom) of Y-carriage as obtained by test

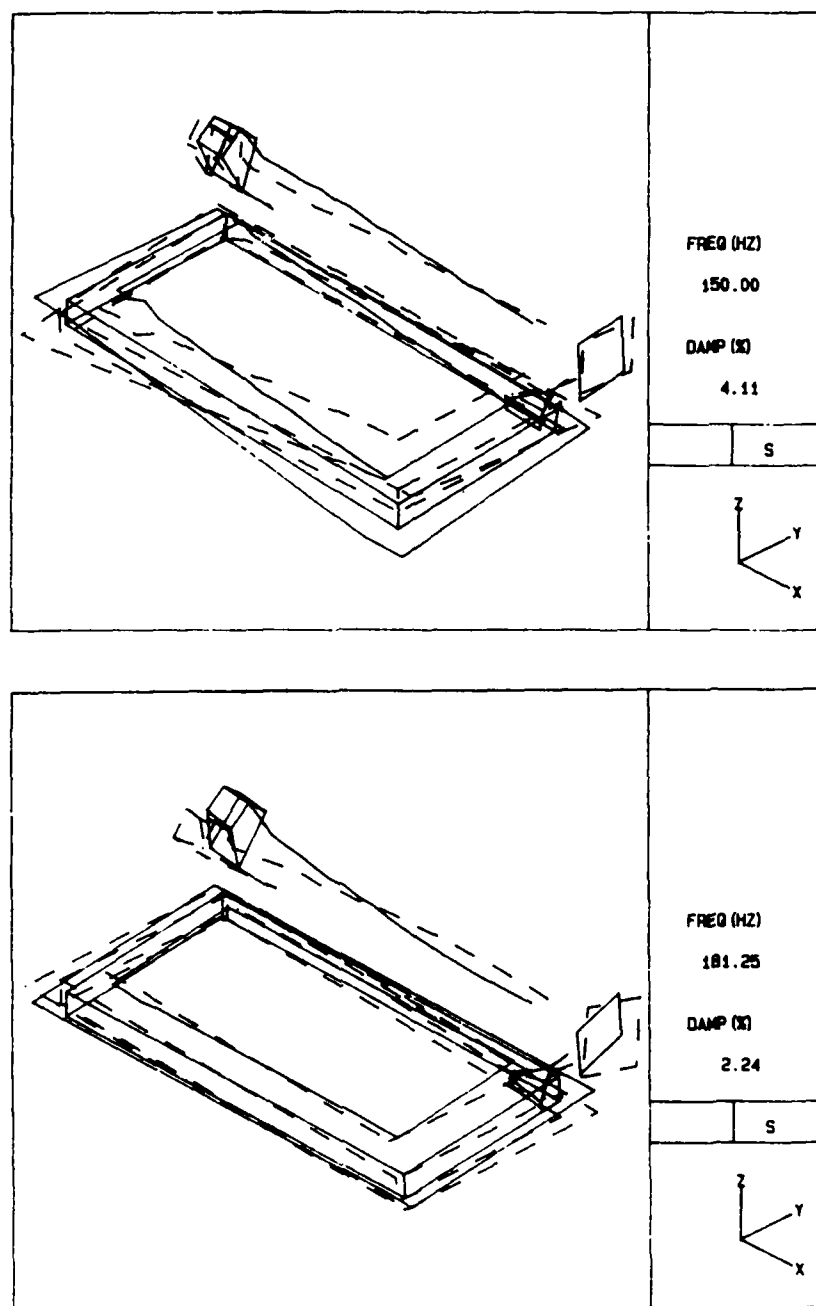


Figure A.14: Mode shapes no.3 (top) and no.4 (bottom) of Y-carriage as obtained by test

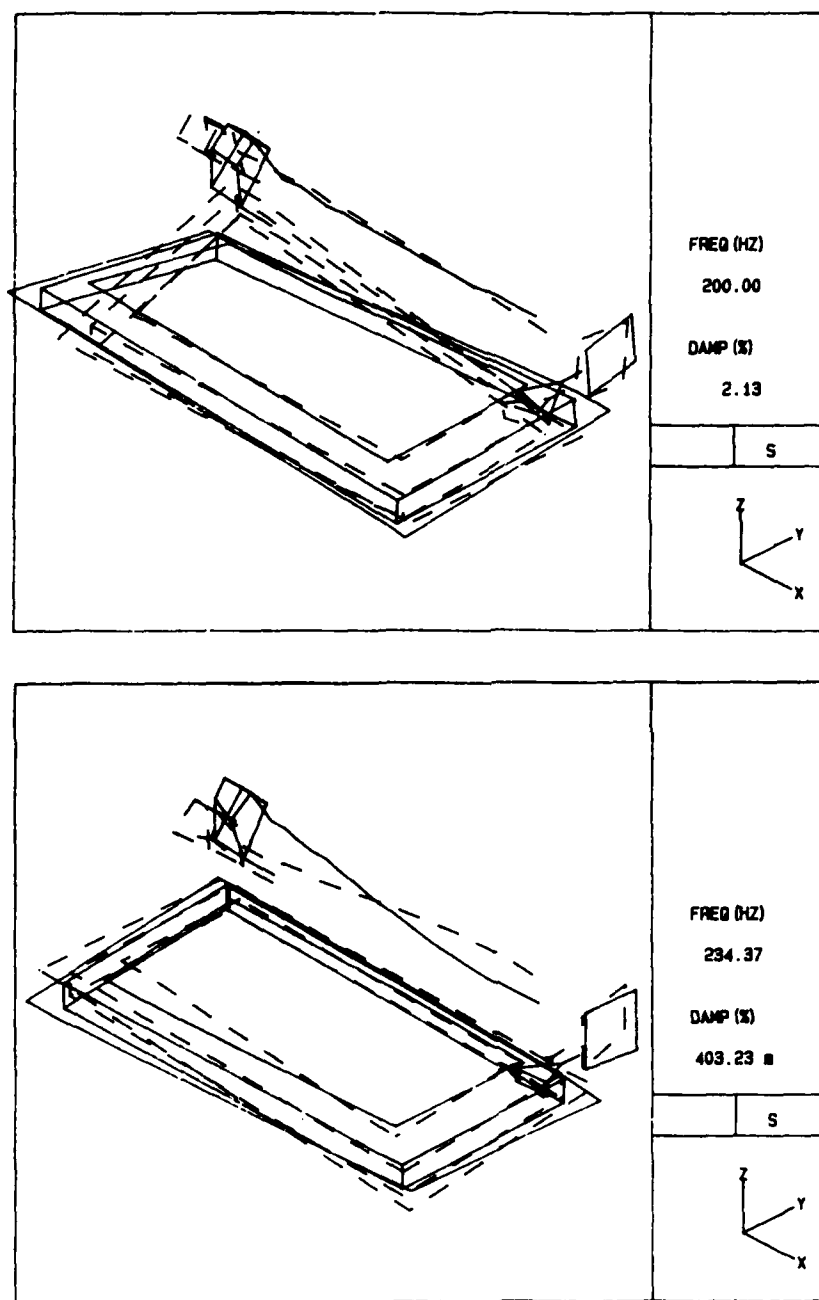


Figure A.15: Mode shapes no.5 (top) and no.6 (bottom) of Y-carriage as obtained by test

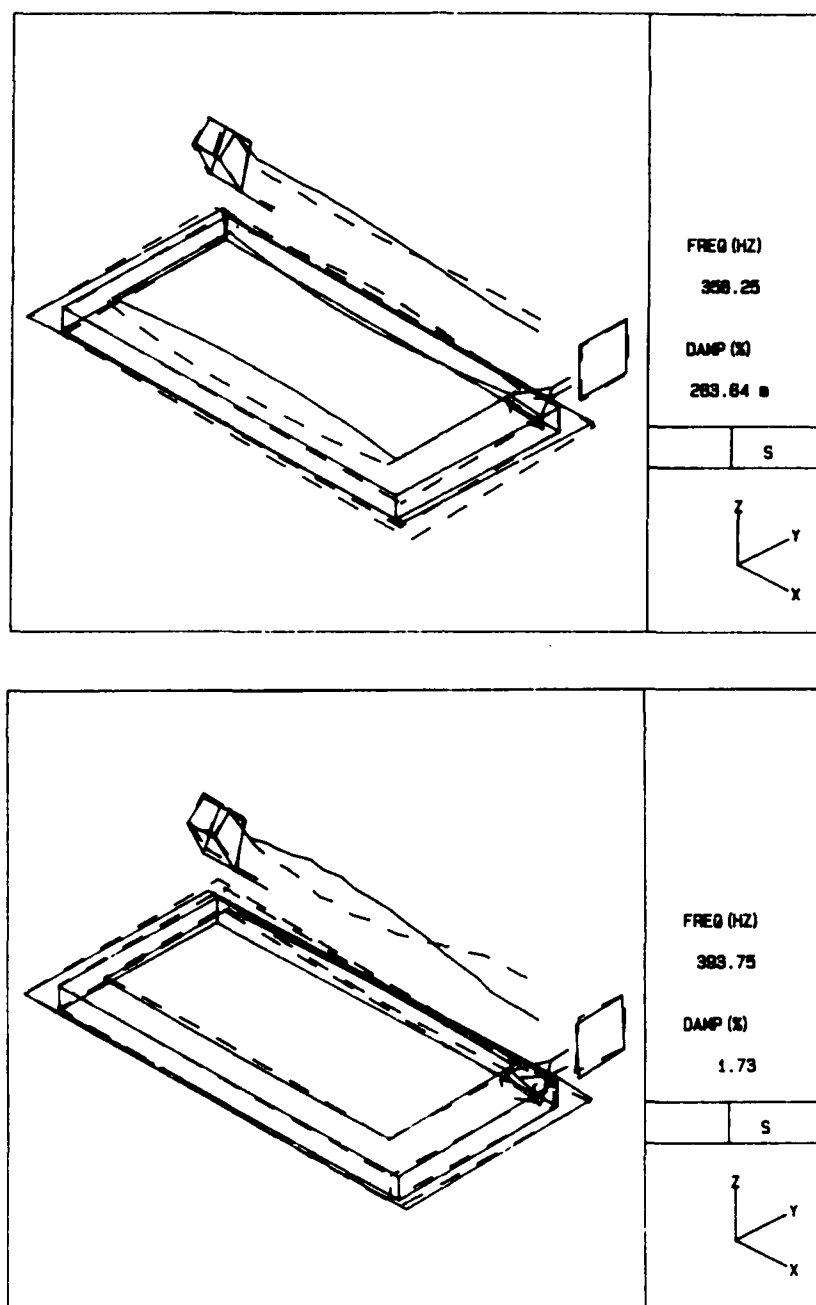


Figure A.16: Mode shapes no.7 (top) and no.8 (bottom) of Y-carriage as obtained by test

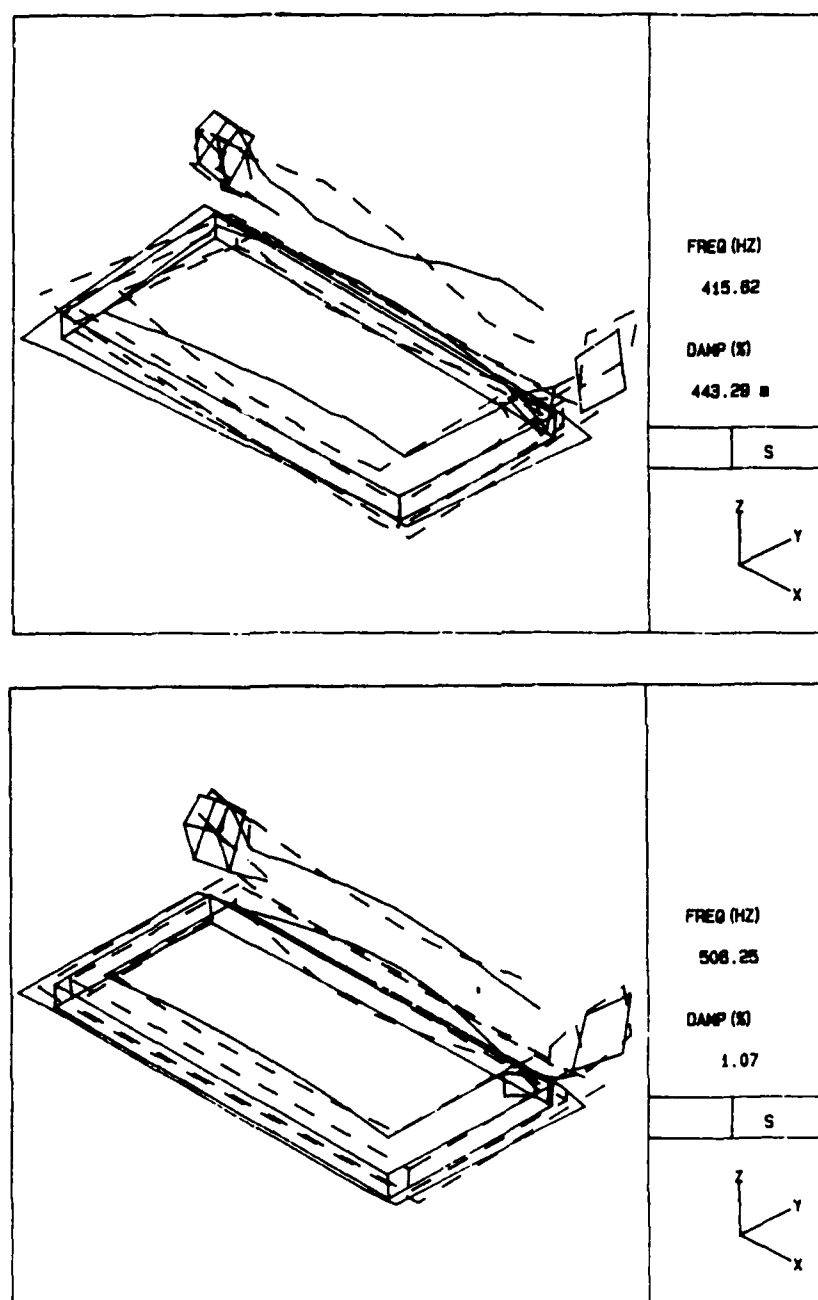


Figure A.17: Mode shapes no.9 (top) and no.10 (bottom) of Y-carriage as obtained by test

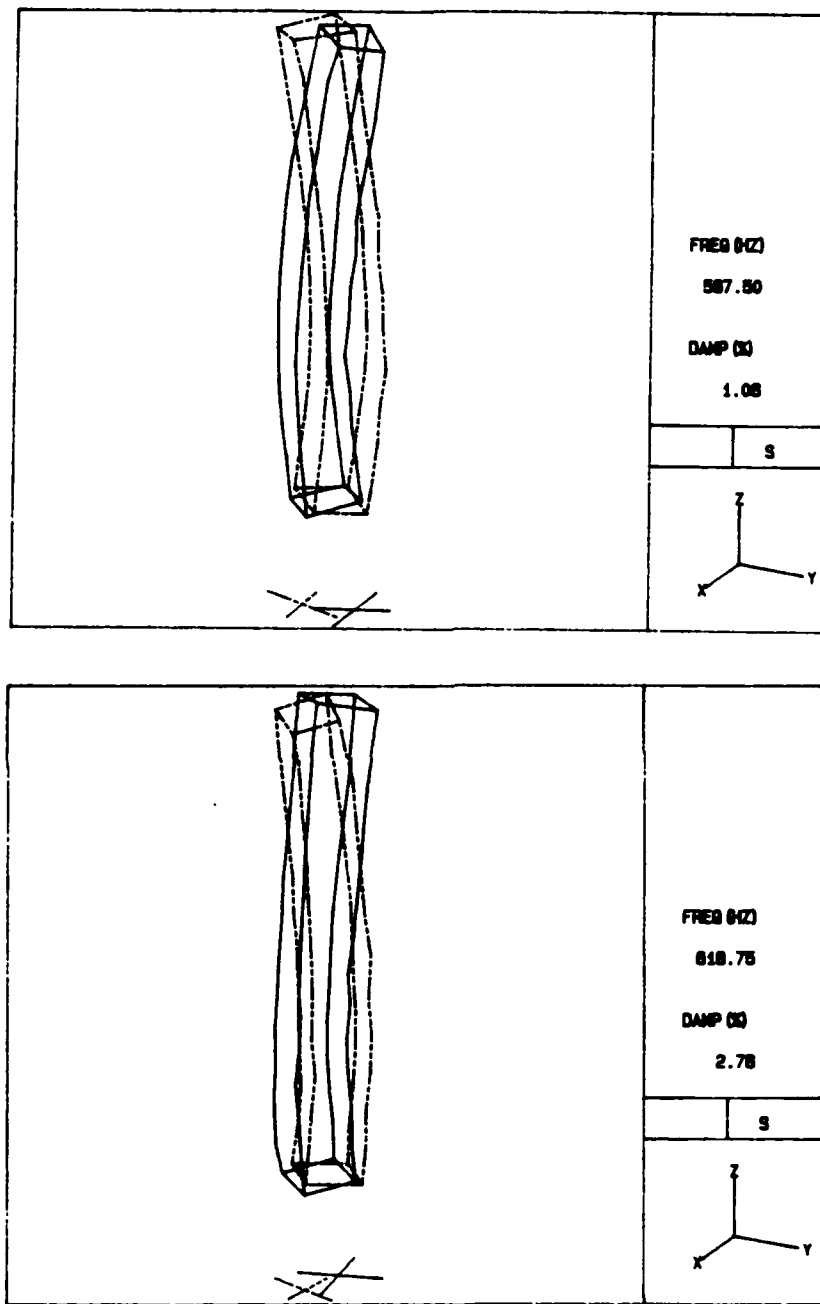


Figure A.18: Mode shapes no.1 (top) and no.2 (bottom) of Z-carriage as obtained by test



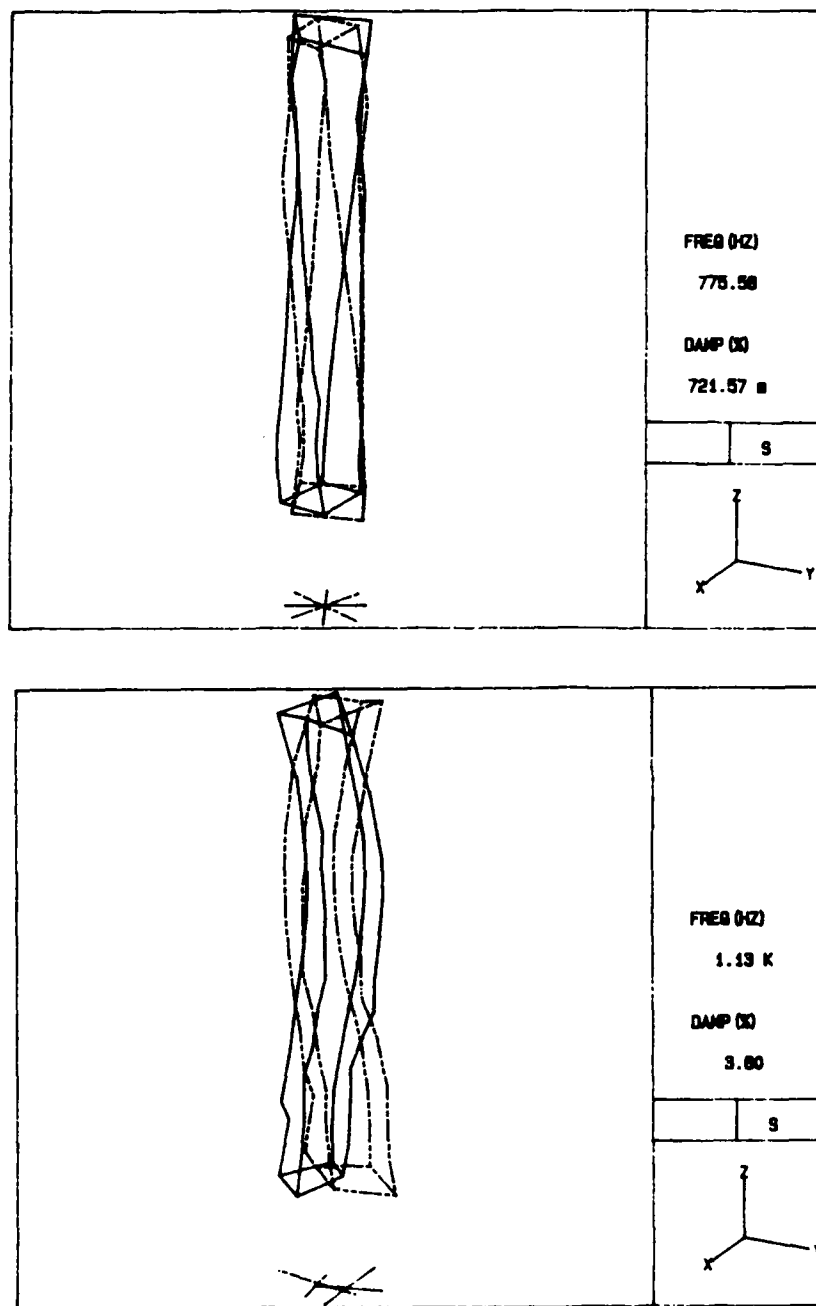


Figure A.19: Mode shapes no.3 (top) and no.4 (bottom) of Z-carriage as obtained by test

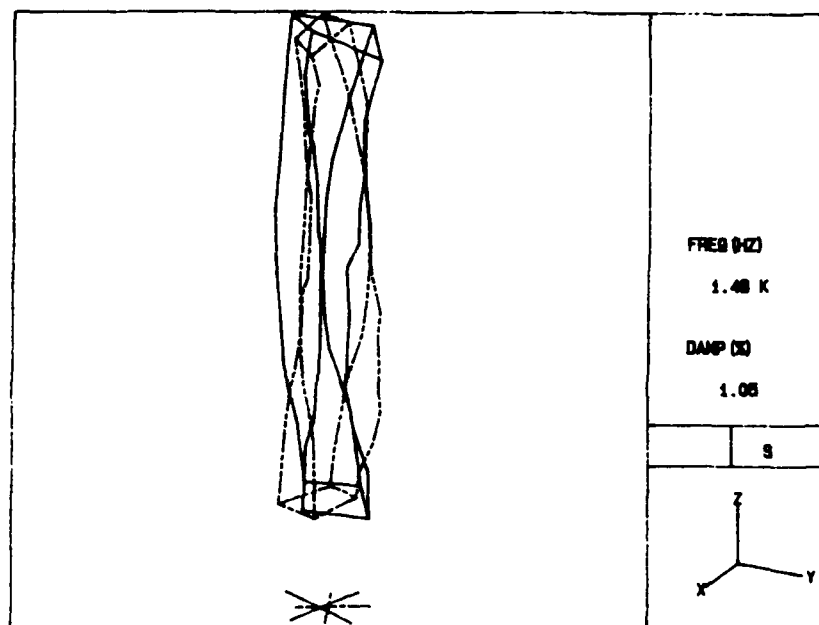


Figure A.20: Mode shape no.5 of Z-carriage as obtained by test

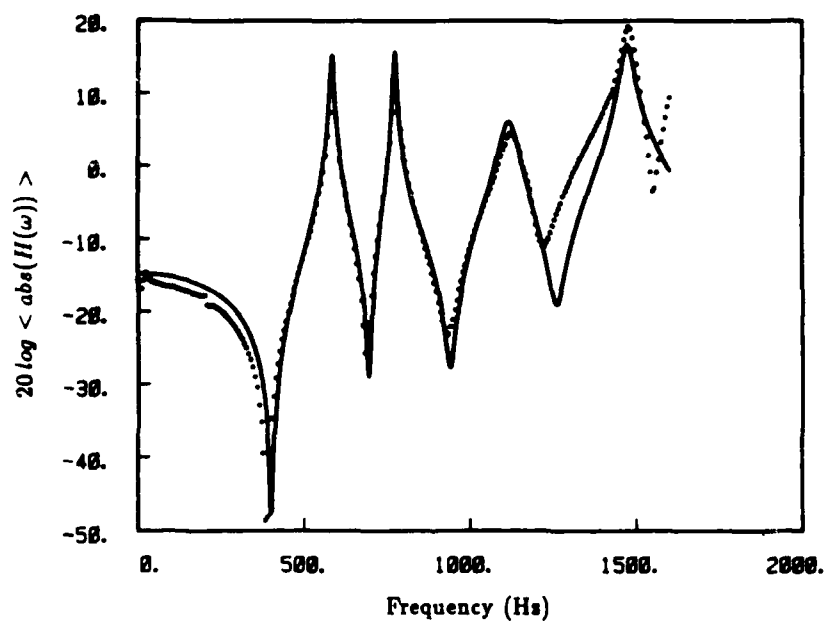


Figure A.21: Drive-point transfer function of Z-carriage

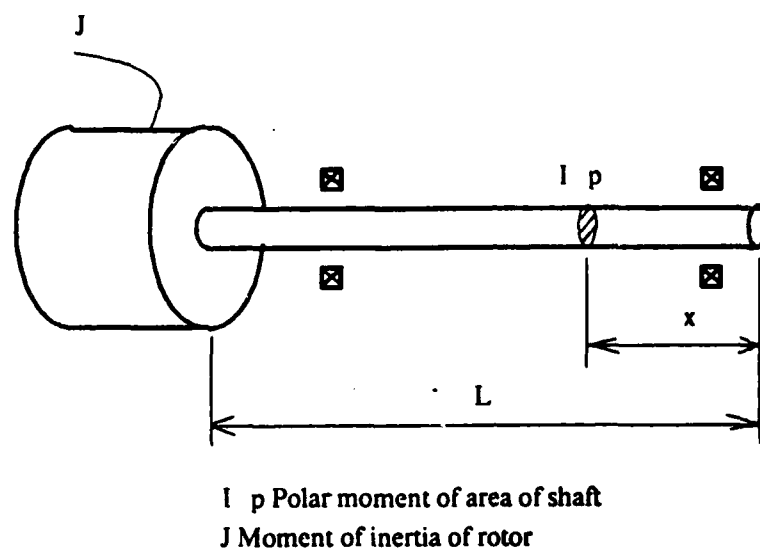


Figure A.22: Model of motor-rotor and lead-screw

The results for both lead screws were given in Table 2.3. The Z-carriage motor MZ with its short shaft and pinion is essentially rigid, so we considered only its rigid body mode in torsion.

## A.5 Modal Matrices for Data Input to Mathematical Model

The modal matrices to be used in the mathematical model are obtained from the mode shapes just shown. To get these data files into the computer, we transfer data from the analyzer through a GPIB interface by means of a computer program shown in Table A.2.

The modal matrices are formed from these data files by properly scaling them in order to normalize the eigenvectors. If the correct drive-point mode-shape value has been obtained by curve-fitting the drive-point trans-

Table A.2: Computer programs to transmit data, back and forth, between a pdp11/44 computer and an HP analyzer.

```

C TRAMOD.FTN
C*****
C
C PROGRAM TO TRANSFER HP5423A MODAL DATA TO THE
C PDP-11/44 VIA THE NATIONAL INSTRUMENTS GPIB11-1 INTERFACE.
C
C DATA IS TRANSFERRED IN ASCII BY A 501.4.2 SAVE COMMAND
C
C THE OUTPUT FILE IS FORMATTED WITH 1 VALUE PER RECORD (E15.7)
C
C NOTE: THE IB: HANDLER USES RSX CHANNEL 1
C
C SEE CHAPTER 3 OF VOL. 3 "USING HP-IB" (5423A)
C
C*****
C
C BYTE BDATA(630), BSAVE(10), FILNAM(20),CSAVE(96)
C REAL MDATA(999)
C INTEGER*4 ASAVE(3)
C
C 501.4.2SA IS THE SAVE TO CONTROLLER COMMAND
C 10 IS THE DECIMAL VALUE OF THE LF TERMINATOR.
C
C DATA BSAVE / '5','0','1',' ','4',' ','2','S','A',10/
C DATA IWR,IRE,ICL,ITR,IRM,ILO,IPO,ICO,IPC,IDE,IFI
C 1 /0, 1, 2, 3, 4, 5, 6, 7, 8, 9, 10/
C DATA IHP, ITA, ILI /"4, "104, "44/
C
C TELL THE OPERATOR TO PREPARE THE INTERFACE
C
C TYPE *, 'TRAMOD- HP5423A to PDP-11/44 data transfer program.'
C TYPE *, '
C TYPE *, '1. Connect the HP-IB cable from the PDP-11totheHP.'
C TYPE *, '2. Set the HP back panel switch to "ADDRESSABLEONLY".'
C 5 TYPE *, '3. Get measurement data on the active trace of the HP.'
C TYPE *, '4. Enter 0 to stop or 1 to continue : '
C ACCEPT *, J
C IF(J.EQ. 0) GO TO 1000
C TYPE *, ' 5. ENTER MODE, 1ST DOF, AND LAST DOF: ONE AT A TIME'
C ACCEPT *, ASAVE(1)
C ACCEPT *, ASAVE(2)
C ACCEPT *, ASAVE(3)
C NWRDS=ASAVE(3)-ASAVE(2)+1

```

Table A.2: continued

```
C
C FIRST CLEAR THE BUS
C
10 TYPE *, ' Initializing ...'
J = IBUP(ICL,-1)
IF( J.NE. 1)TYPE *, ' BUS CLEAR FAILED, ERROR=',J
C
C MAKE SURE THAT ANALYZER IS DEFINED AND ON THE BUS.
C
J = IBUP( IDE, IHP, ITA, ILI, 0, 0, 0, 0)
IF( J.NE. 1)TYPE *, ' HP DEFINE FAILED, ERROR=',J
J = IBUP( ICL, IHP)
IF( J.EQ. 1)GO TO 20
C
15 TYPE *, ' TRY AGAIN ? 0=NO, STOP; 1=YES :'
ACCEPT *,J
IF(J.EQ. 0) STOP
GO TO 10
C
C ALL SET, SEND 501,4,2 SAVE COMMAND
C
20 ILEN = 10
J = IBUP( IWR, IHP, BSAVE(1), ILEN)
IF(J.EQ. ILEN)GO TO 30
C
C ERROR
C
25 TYPE *, ' SAVE COMMAND FAILED, REC=',J, ' SENT=',ILEN
C
C SERIAL POLL TO GET SDA SRQ
C
J = IBUP( IPO, IHP)
TYPE *, ' ANALYZER SRQ = ',J
GOTO 15
C
C START READING HEADER (3 VARIABLES)
C
C THIS POLL IS NEEDED WHEN CONTROLLER SENDS SAVE COMMAND
C THE PROGRAM WAITS UNTIL THE ANALYZER IS READY (SRQ=96)
C
30 ISAV = 91
DO 35 I = 1, 2000
J = IBUP(IPO, IHP)
IF(J.EQ. ISAV)GO TO 38
```

Table A.2: continued

```
35 CONTINUE
TYPE *, ' TIMEOUT ON SAVSRQ, HP SRQ =',J
GO TO 25
C
38 ILEN = 32
IOF = 1
ILAN=96
ENCODE(ILAN,891,CSAVE(1))ASAVE(1),ASAVE(2),ASAVE(3)
891 FORMAT(3I5)
J=IBUP(IWR,IHP,CSAVE(1),ILAN)
C
C NOW READ IN NWRDS OF (REAL) DATA TO MDATA
C USE BDATA(17-33) AS A BUFFER
C
999 FORMAT(E14.4)
ILEN = 32
DO 50 I = 1, NWRDS
J = IBUP( IRE, IHP, BDATA(17), ILEN)
DECODE( ILEN-2, 999, BDATA(17) )MDATA(I)
TYPE *,MDATA(I)
50 CONTINUE
C
C STORE ON DISK FILE IN ASCII (2 VALUES / RECORD)
C
60 TYPE 996
996 FORMAT(' Enter filename for storage :',%)
ACCEPT 995,FILNAM
995 FORMAT(20A1)
FILNAM(20) = 0
C
OPEN( UNIT=2, NAME=FILNAM, TYPE='NEW', ERR=60)
C
WRITE(2,994) (MDATA(I),I=1,NWRDS)
994 FORMAT(E15.7)
CLOSE(UNIT=2)
TYPE 997,FILNAM
997 FORMAT(1X,'Ascii data and header stored in "',20A1,'"')
GO TO 5
1000 STOP
END
```

Table A.2: continued

```

C*****
C TRARES2.FTN
C PROGRAM TO TRANSFER HP5423A RESIDUE DATA FROM THE
C PDP-11/44 VIA THE NATIONAL INSTRUMENTS GPIB11-1 INTERFACE.
C
C DATA IS TRANSFERRED IN ASCII BY A 504,1 RECALL COMMAND
C
C THE INPUT FILE SHOULD BE FORMATTED WITH 1 VALUE PER RECORD (E15.7)
C
C THE PROGRAM TAKES THE 40 VARIABLE HEADER FROM THE END OF THE FILE
C AND SENDS IT FIRST.
C
C NOTE: THE IB: HANDLER USES RSX LOGICAL UNIT 1
C SEE THE NATIONAL INSTRUMENTS "GPIB11 SOFTWARE REFERENCE MANUAL"
C FOR INFORMATION ON USING THE BUS FROM FORTRAN OR ASSEMBLER
C
C SEE CHAPTER 3 OF VOL. 3 "USING HP-IB" (5423A)
C FOR THE SAVE/RECALL DATA AND HEADER FORMATS
C
C*****
C
C BYTE BDATA(630), BRCL(10), FILNAM(20),CSAVE(96)
C REAL MDATA(700)
C INTEGER*4 ASAVE(3)
C
C 504.1RA IS THE RECALL FROM CONTROLLER COMMAND
C 10 IS THE DECIMAL VALUE OF THE LF TERMINATOR.
C
C DATA BRCL / '5','0','1','','4','','1','R','A',10/
C
C INSTRUMENT BUS UTILITY PROGRAM (IBUP) FUNCTION CODES
C
C DATA IWR,IJE,IJL,ITR,IRM,ILO,IPO,ICO,IPC,IDE,IFI
C 1 /0, 1, 2, 3, 4, 5, 6, 7, 8, 9, 10/
C
C DATA IHP, ITA, ILI /"4, "104, "44/
C
C TELL THE OPERATOR TO PREPARE THE INTERFACE
C
C
C TYPE *, ' TRARES2- HP5423A from PDP-11/44 data transferprogram.'
C TYPE *, '
C TYPE *, '1. Connect the HP-IB cable from the PDP-11 to theHP.'

```

Table A.2: continued

```
TYPE *, '2. Set the HP back panel switch to "ADDRESSABLEONLY".'
10 TYPE *, '3. Enter 0 to stop or 1 to continue : '
ACCEPT *, J
IF(J .EQ. 0) GO TO 1000
TYPE *, ' 4. ENTER MODE, 1ST MEAS AND LAST MEAS [MAX MEAS+4IF'
TYPE *, 'MODE.NE.0], [(MAX MEAS+1)*4 IF MODE.EQ.0], ONE BY ONE'
ACCEPT *, ASAVE(1)
ACCEPT *, ASAVE(2)
ACCEPT *, ASAVE(3)
NWRDS=ASAVE(3)-ASAVE(2)+1
C
C FIRST CLEAR THE BUS
C
20 TYPE *, ' Initialising ...'
J = IBUP(ICL,-1)
IF( J .NE. 1)TYPE *, ' BUS CLEAR FAILED, ERROR=', J
C
C MAKE SURE THAT ANALYZER IS DEFINED AND ON THE BUS.
C
J = IBUP( IDE, IHP, ITA, ILI, 0, 0, 0, 0)
IF( J .NE. 1)TYPE *, ' HP DEFINE FAILED, ERROR=', J
J = IBUP( ICL, IHP)
IF( J .EQ. 1)GO TO 40
C
30 TYPE *, ' TRY AGAIN ? 0=NO, STOP; 1=YES : '
ACCEPT *, J
IF(J .EQ. 0)GO TO 1000
GO TO 20
C
C GET NAME OF ASCH FILE (1 VALUE / RECORD)
C
40 TYPE 999
999 FORMAT(' Enter filename for transfer (0=quit) :', $)
ACCEPT 998, FILNAM
998 FORMAT(20A1)
IT = FILNAM(1)
IF(IT .EQ. 48) GO TO 1000
FILNAM(20) = 0
C
C GET NUMBER OF DATA VALUES TO SEND
C
50 TYPE 997
```



Table A.2: continued

```
997 FORMAT(' Enter number of data values to be sent -',/,
1' 512 for trans or time, 256 for coh :', $)
ACCEPT *, NVAL
C
C READ DATA AND HEADER FROM FILE
C
D DO 45 I=1,630
D 45 BDATA(I) = 0
OPEN( UNIT=2, NAME=FILNAM, TYPE='OLD', ERR=40)
C
READ(2,996) (MDATA(I),I=1,NVAL)
996 FORMAT(E15.7)
CLOSE(UNIT=2)
C
C CHECK THAT NWRDS IN HEADER (VARIABLE 3) = 2 * NVAL
C THE ENCODE ROUTINE TRANSLATES FROM DEC INTERNAL FORM TO ASCII
C THE DECODE ROUTINE TRANSLATES FROM ASCII TO DEC INTERNAL FORM
C THE LAST TWO CHARACTERS ARE CR,LF WHICH ARE NOT DECODED.
C
C ILEN = 16
C IOF = ILEN * 2 + 1
C DECODE(ILEN-2, 995, BDATA(IOF) ) BUF
C995 FORMAT(E14.4)
C NWRDS = BUF
C IF(NWRDS.EQ. 2*NVAL) GO TO 60
C TYPE *, '** ERROR, NVAL DISAGREES WITH HEADER'
C GO TO 60
C
C ALL SET, SEND 501,4,1 RECALL COMMAND
C
60 ILEN = 10
TYPE *, ' Sending 501,1 recall command...'
J = IBUP( IWR, IHP, DRCL(1), ILEN)
IF(J.EQ. ILEN)GO TO 80
C
C ERROR
C
70 TYPE *, ' RECALL COMMAND FAILED, REC=',J,' SENT=',ILEN
C
C SERIAL POLL TO GET SDA SRQ
C
J = IBUP( IPO, IHP)
```

Table A.2: continued

```
TYPE *, 'ANALYZER SRQ = ', J
GO TO 30
C
C THIS POLL IS NEEDED WHEN CONTROLLER SENDS RECALL COMMAND
C THE PROGRAM WAITS UNTIL THE ANALYZER IS READY (SRQ=121)
C
80 IRCL = 121
DO 90 I = 1, 2000
J = IBUP(IPO, IHP)
IF(J.EQ. IRCL)GO TO 100
90 CONTINUE
TYPE *, 'TIMEOUT ON RECALL SRQ, HP SRQ = ', J
GO TO 30
C
C START SENDING HEADER (3 VARIABLES)
C
100 CONTINUE
TYPE *, ' Sending measurement header...'
ILEN=32
IOF=1
ILAN=96
ENCODE(ILAN,891,CSAVE(1))ASAVE(1),ASAVE(2),ASAVE(3)
891 FORMAT(3I5)
J=IBUP(IWR,IHP,CSAVE(1),ILAN)
C ILEN = 16
C IOF = 1
C J = IBUP( IWR, IHP, BDATA(IOF), ILEN)
C IF(J.NE. ILAN)TYPE *, ' FIRST VARIABLE TRANSMIT FAILED, J=', J
C
C SEND THE REST OF THE HEADER (VARS 2-37)
C
C DO 110 I = 2, 37
C IOF = IOF + ILEN
C TYPE 333.(BDATA(IOF+J-1),J=1,ILEN)
333 FORMAT(22A1)
C J = IBUP( IWR, IHP, BDATA(IOF), ILEN)
110 CONTINUE
C
C LAST THREE VARS ARE ASCII
C
C IOF = IOF + ILEN
C ILEN = 8
```

Table A.2: continued

```
C TYPE 333,(BDATA(IOF+J-1),J=1,ILEN)
C J = IBUP( IWR, IHP, BDATA(IOF), ILEN) !INPUT TRANSDUCER MODEL
C IOF = IOF + ILEN
C TYPE 333,(BDATA(IOF+J-1),J=1,ILEN)
C J = IBUP( IWR, IHP, BDATA(IOF), ILEN) !OUTPUT TRANSD.
C IOF = IOF + ILEN
C ILEN = 22
C TYPE 333,(BDATA(IOF+J-1),J=1,ILEN)
C J = IBUP( IWR, IHP, BDATA(IOF), ILEN) !MEAS. TITLE 20 CHARS.
C TYPE 994,(BDATA(IOF+I-1),I=1,20),NVAL
994 FORMAT(1X,' Title= ',20A1,' ',/, ' Sending',I4,' datavalues.')
C
C NOW SEND OUT NVAL OF (REAL) DATA TO THE ANALYZER
C USE BDATA(17-32) AS A BUFFER
C FINISH EACH VARIABLE WITH CR,LF FOR TOTAL OF 16 BYTES / VARIABLE
C
BDATA(31) = 13
BDATA(32) = 10
ILEN = 16
993 FORMAT(E14.7)
DO 120 I = 1, NVAL
ENCODE( ILEN-2, 993, BDATA(17) )MDATA(I)
TYPE *,MDATA(I)
J = IBUP( IWR, IHP, BDATA(17), ILEN)
120 CONTINUE
TYPE *, ' Operation finished.'
GO TO 10
1000 CONTINUE
STOP
END
```

fer function, then we scale the eigenvector by pivoting on the current drive-point mode-shape value. If the normalization procedure is based on the mass distribution of the test points of the component, then we determine  $C$ , the scaling factor, directly.

Each robot component was tested on a number of points which include the points of connection to other components. These test points are marked all over the contour of each component in order to see how the mode shapes are. For data input to the mathematical model, we only need the points of connection.

## A.6 Mode Shape Data for Complete Robot, Experimental and Predicted Results

The robot was tested for the configuration shown in Figure 4.1, that is, with the X-carriage and Y-carriage in the middle and the Z-carriage down. The mode shapes in the frequency bandwidth of 0 to 200 Hz, as obtained by experimental test using a shaker, are shown in the top part of Figures A.23-A.39.

For this same configuration, we have run the mathematical model to predict the mode shapes of the robot; the synthesized mode shapes are shown in the bottom part of Figures A.23- A.39. A comparison of natural frequencies as well as modal damping factors can be seen in Table A.3.

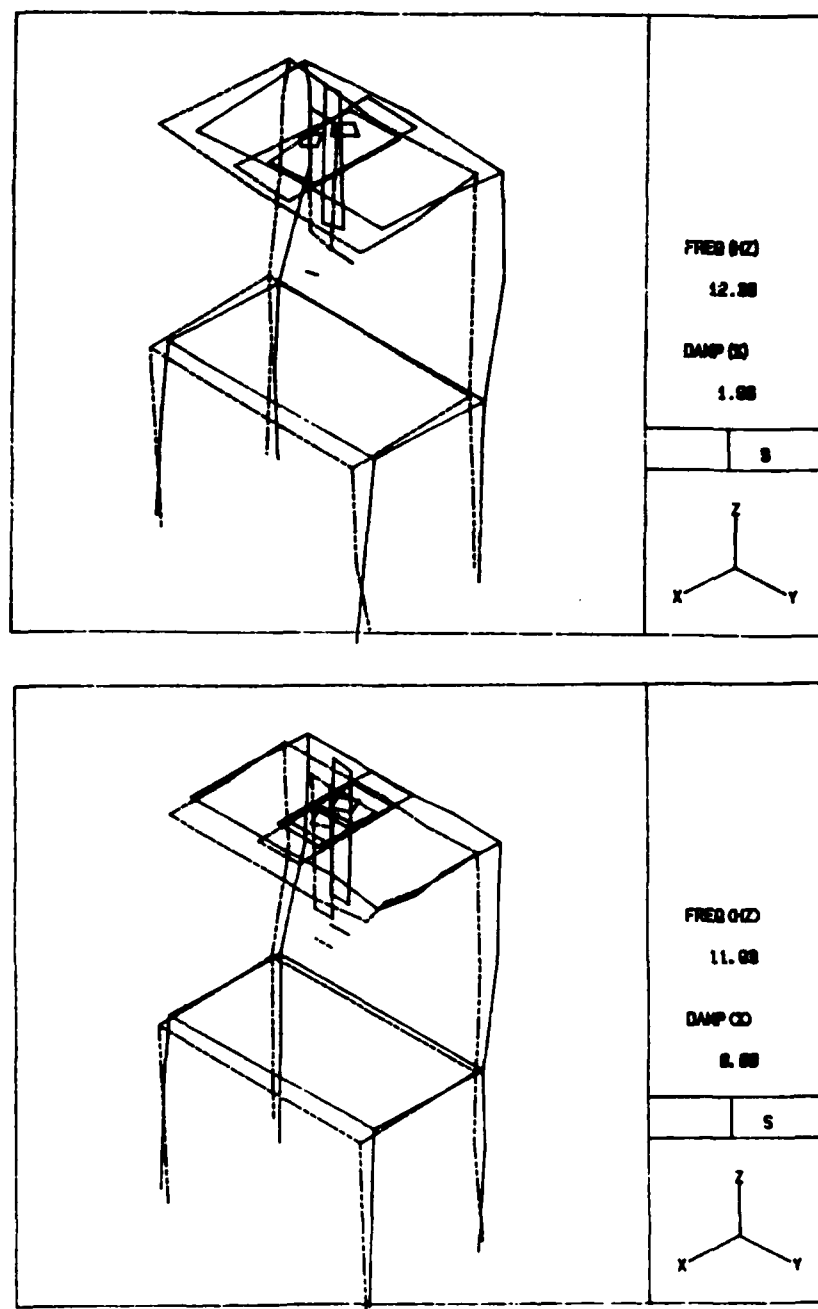


Figure A.23: mode shape no.1 of complete robot as obtained by test(top) and by synthesis(bottom)

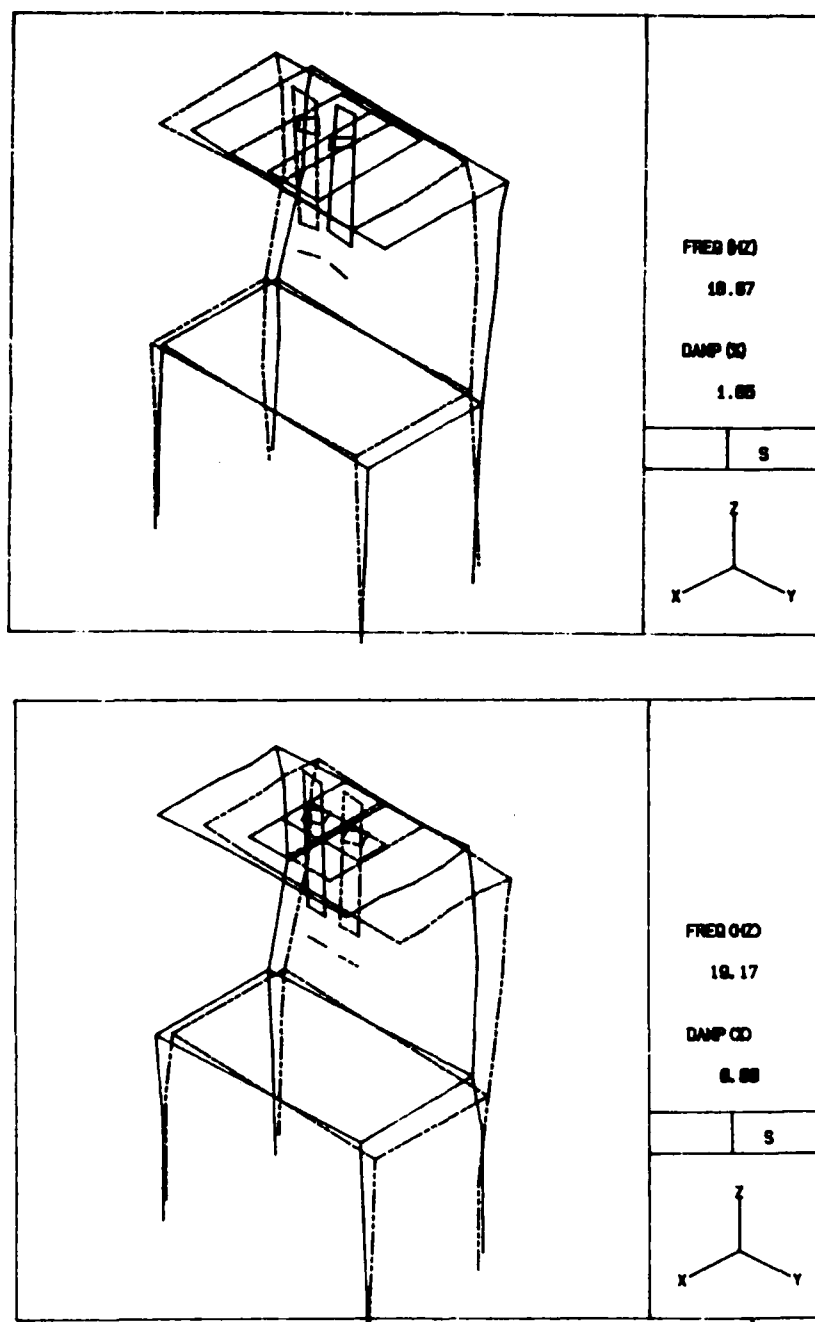


Figure A.24: mode shape no.2 of complete robot as obtained by test(top) and by synthesis(bottom)

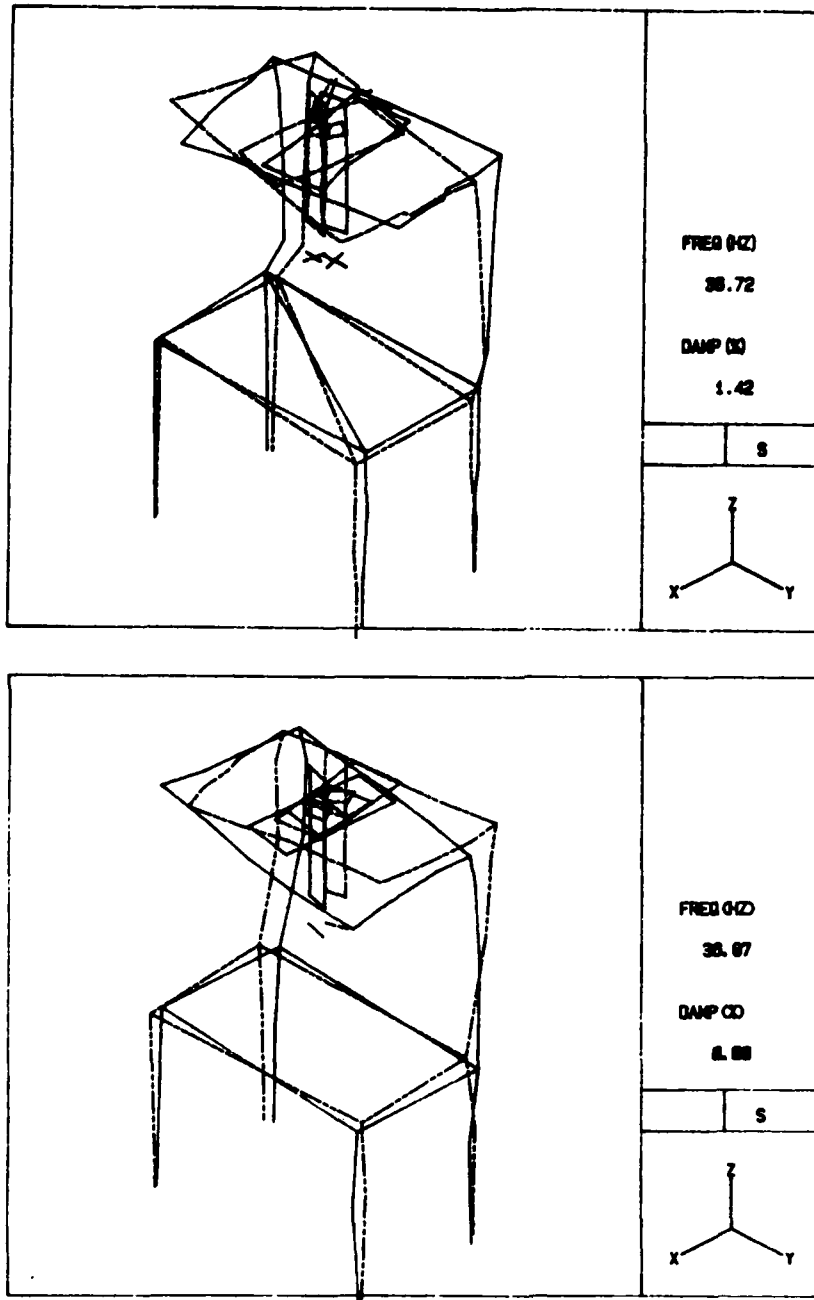


Figure A.25: mode shape no.3 of complete robot as obtained by test(top)  
and by synthesis(bottom)

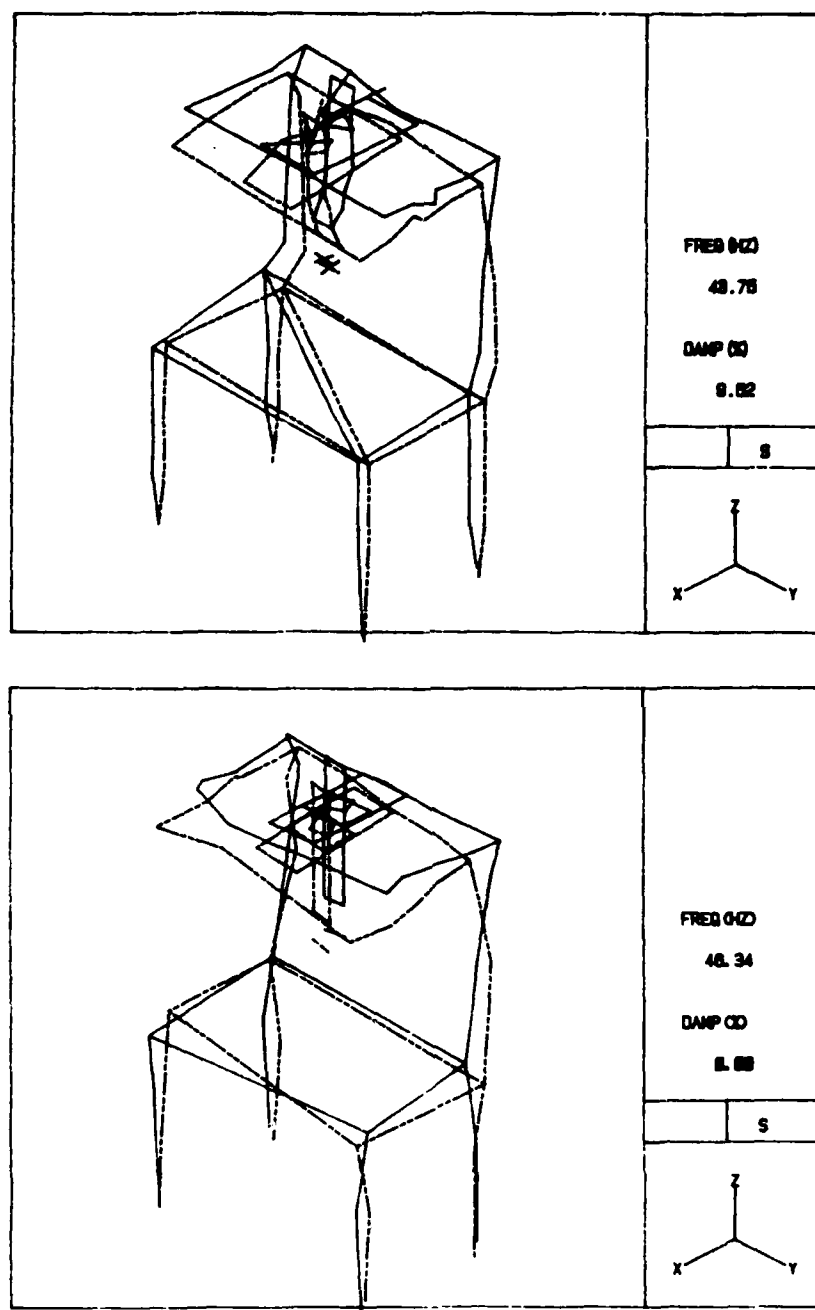


Figure A.26: mode shape no.4 of complete robot as obtained by test(top) and by synthesis(bottom)



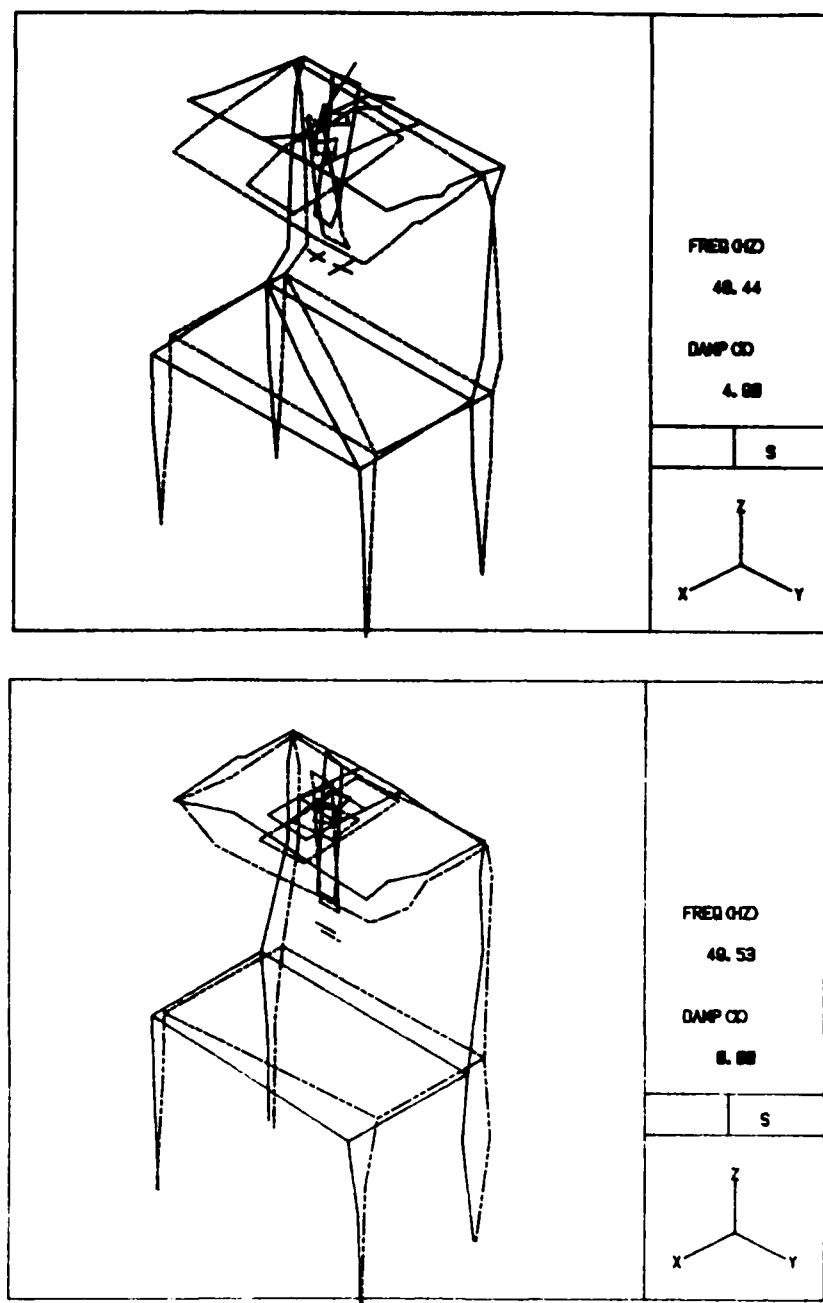


Figure A.27: mode shape no.5 of complete robot as obtained by test(top) and by synthesis(bottom)

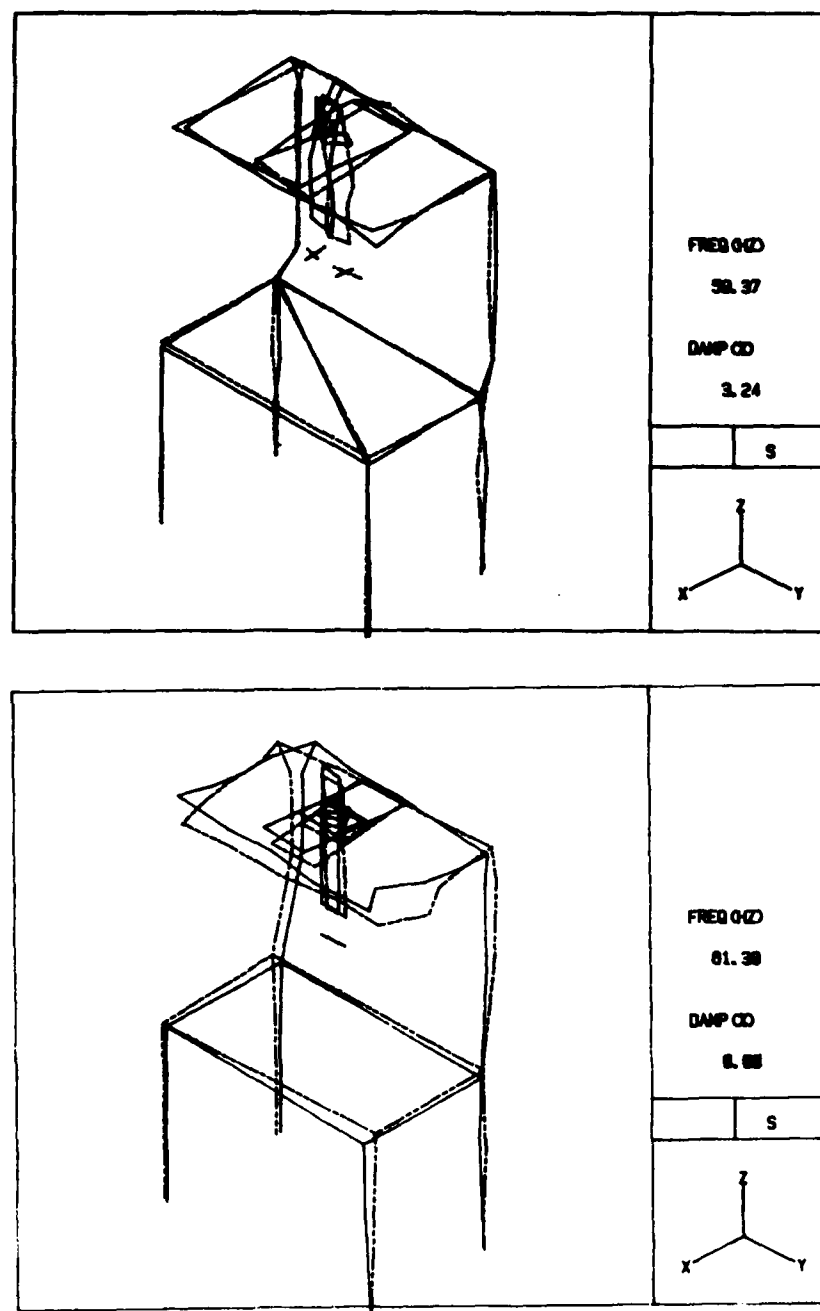


Figure A.28: mode shape no.6 of complete robot as obtained by test(top)  
and by synthesis(bottom)

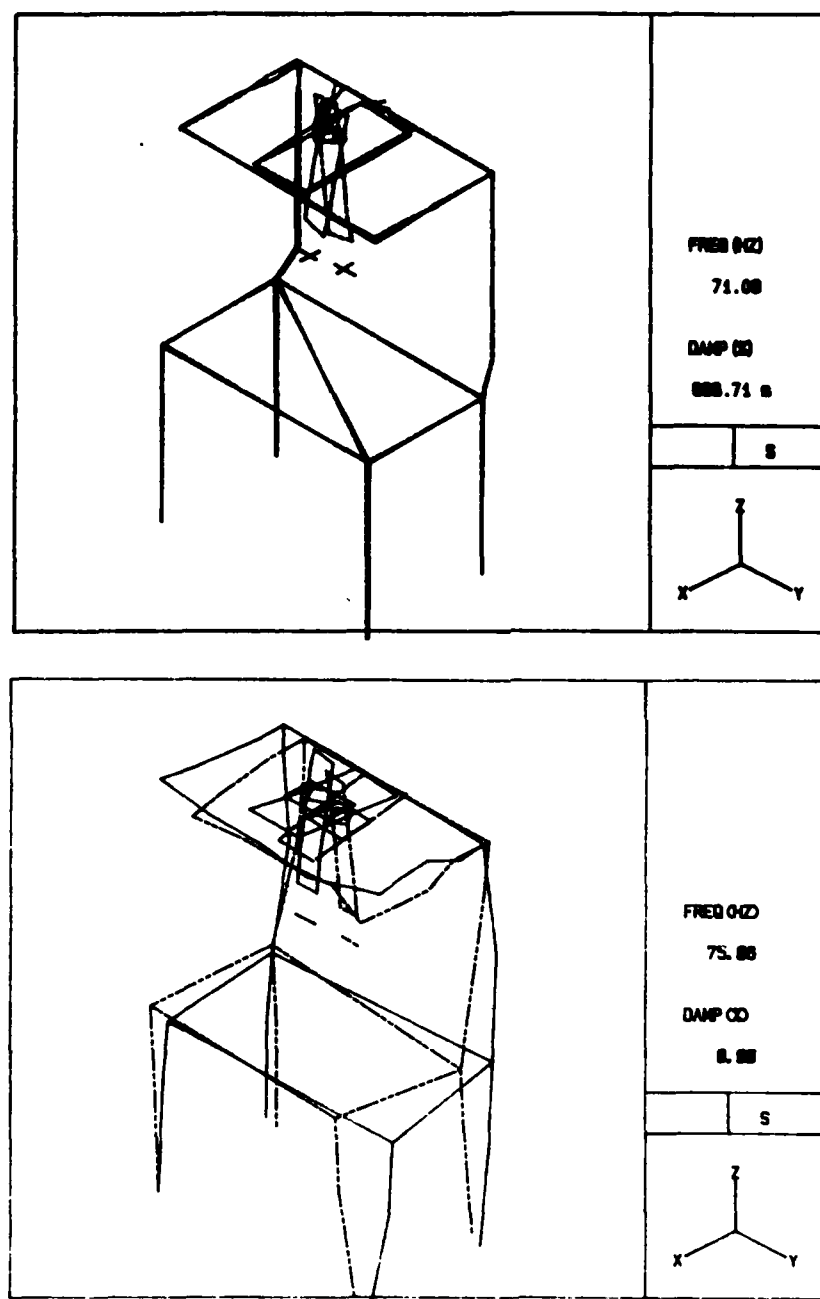


Figure A.29: mode shape no.7 of complete robot as obtained by test(top) and by synthesis(bottom)

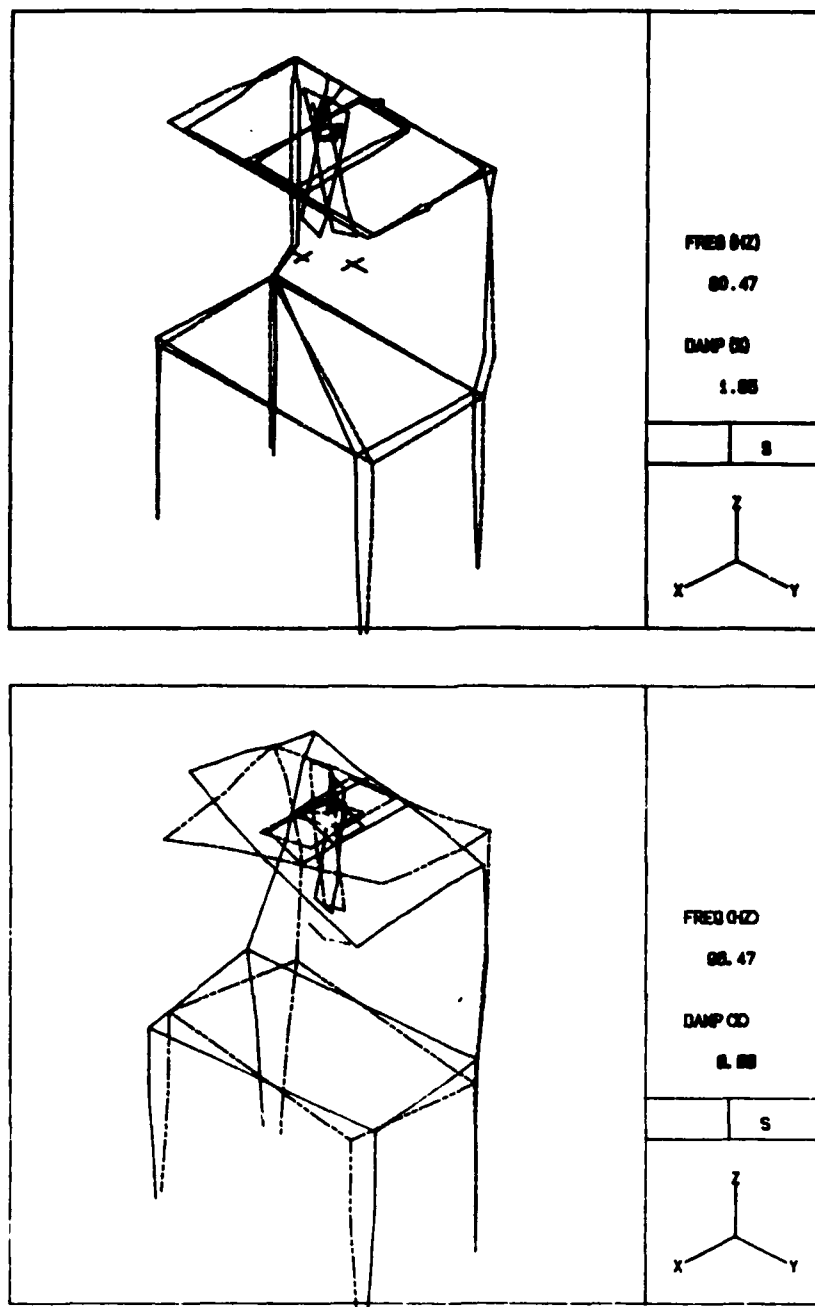


Figure A.30: mode shape no.8 of complete robot as obtained by test(top) and by synthesis(bottom)

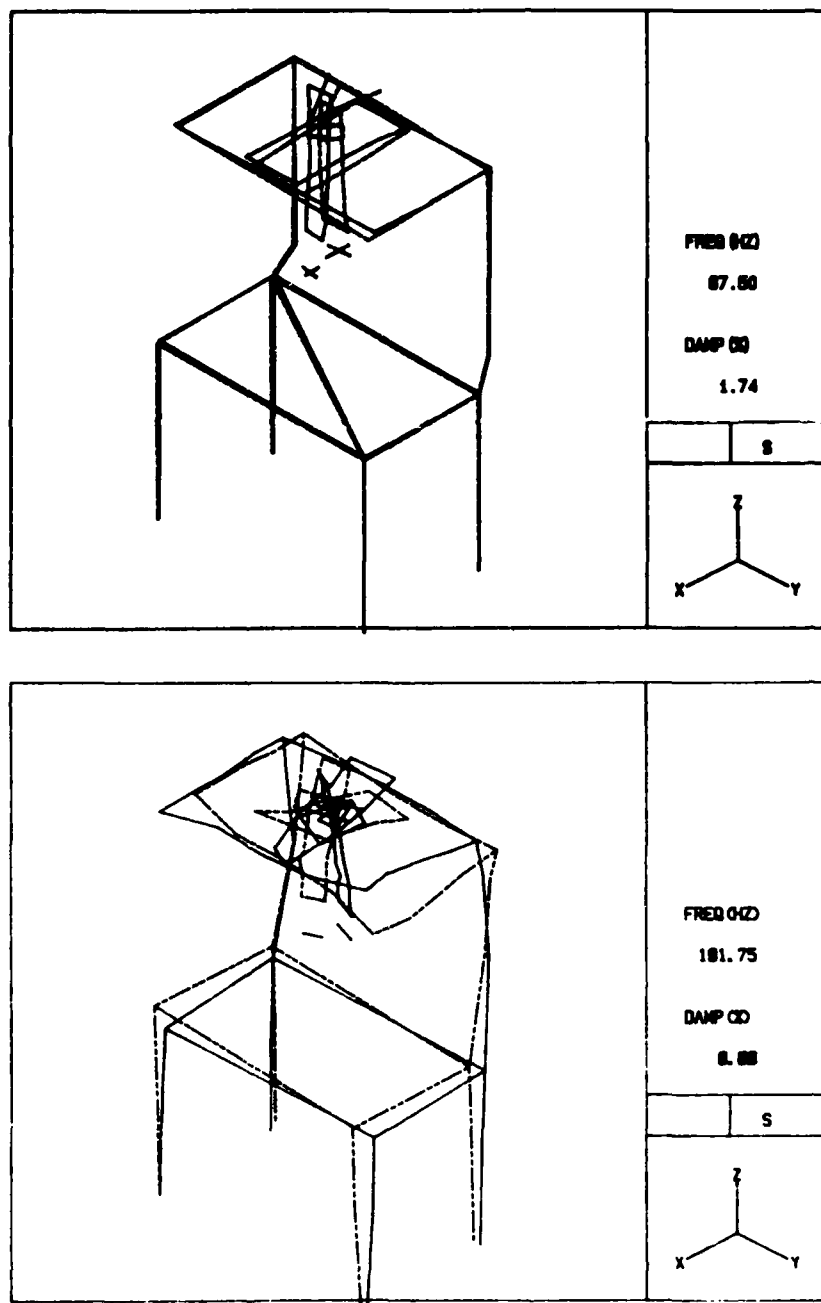


Figure A.31: mode shape no.9 of complete robot as obtained by test(top) and by synthesis(bottom)

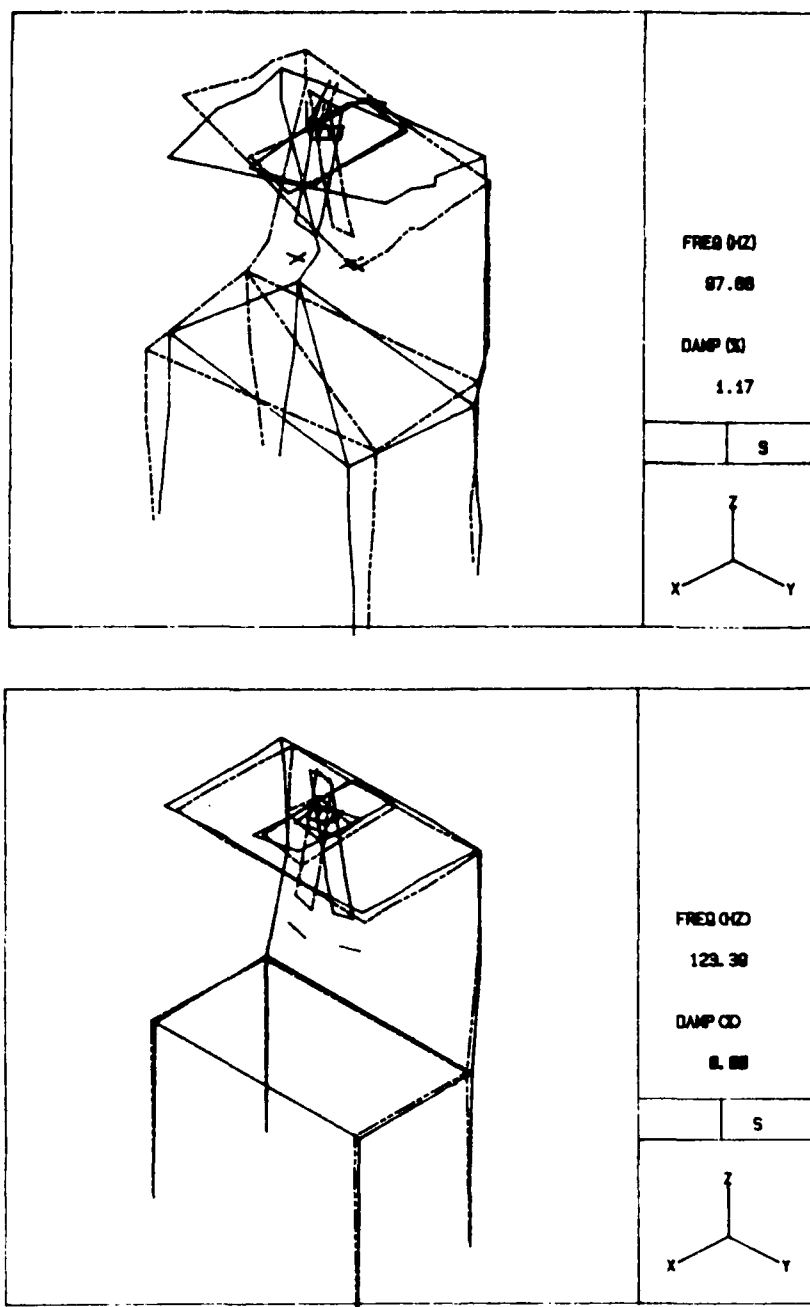


Figure A.32: mode shape no.10 of complete robot as obtained by test(top) and by synthesis(bottom)

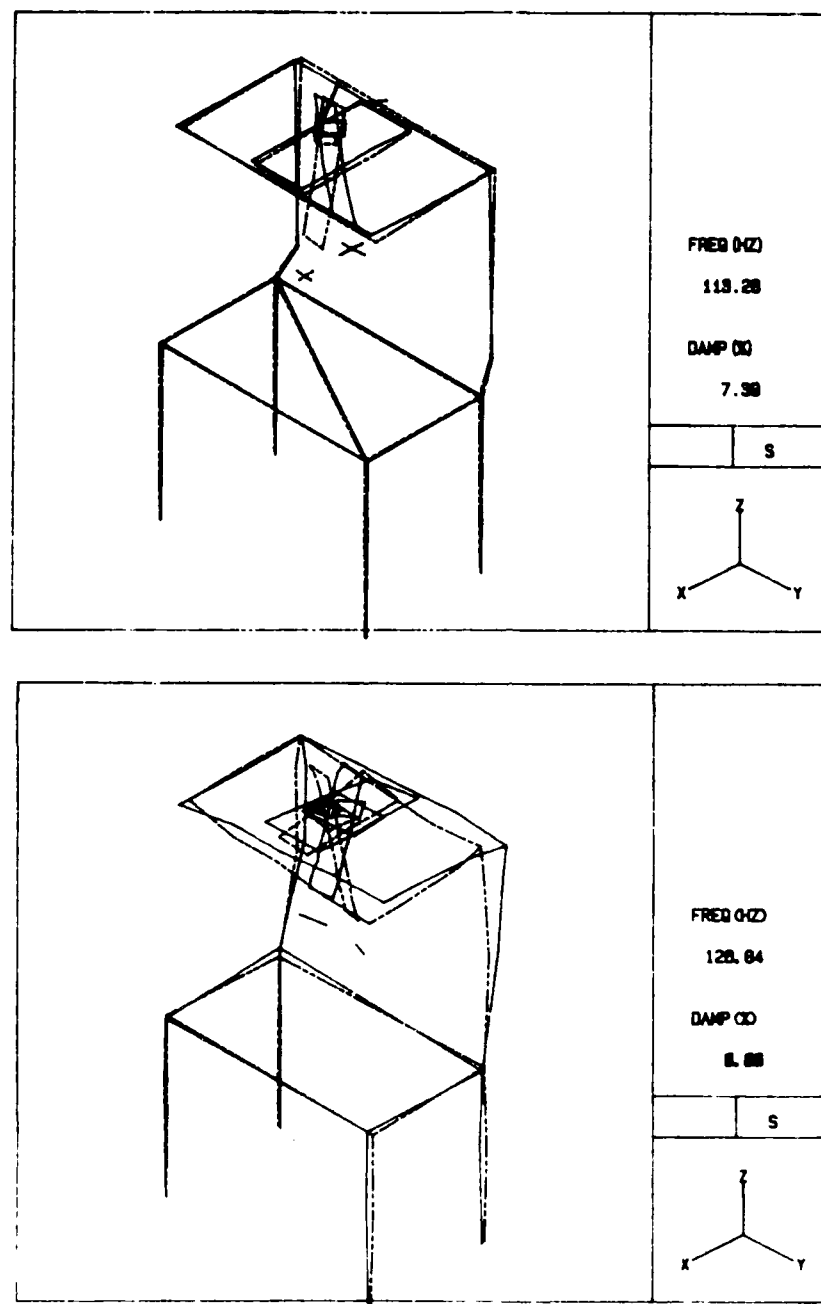


Figure A.33: mode shape no.11 of complete robot as obtained by test(top) and by synthesis(bottom)

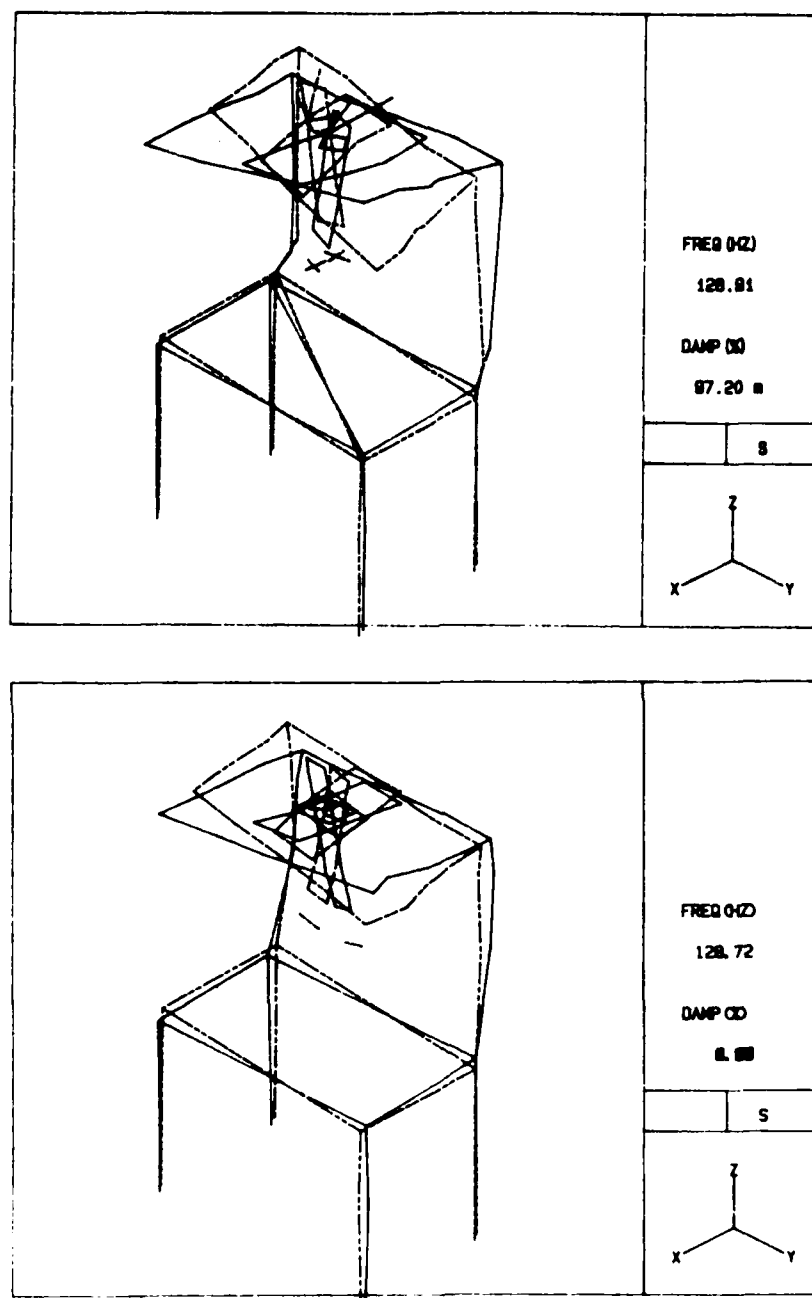


Figure A.34: mode shape no.12 of complete robot as obtained by test(top)  
and by synthesis(bottom)



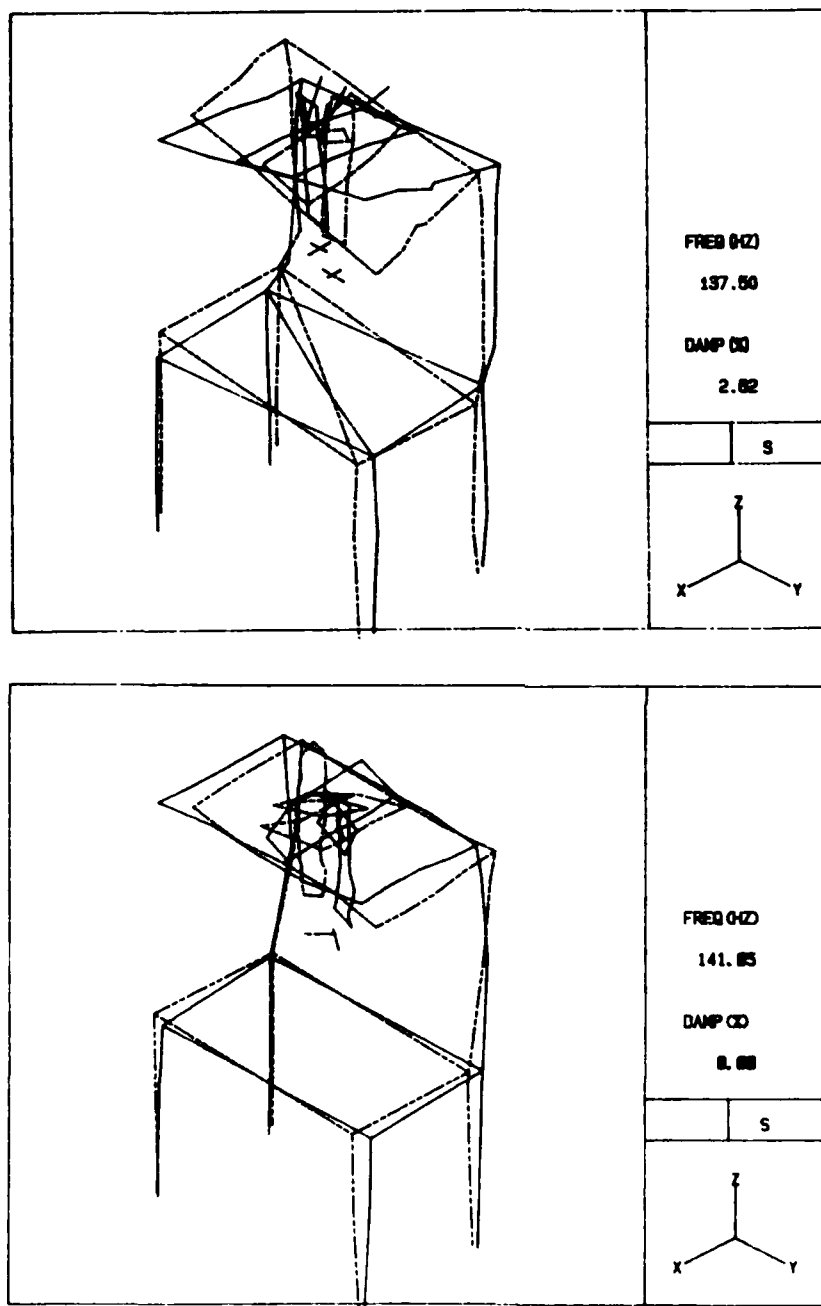


Figure A.35: mode shape no.13 of complete robot as obtained by test(top)  
and by synthesis(bottom)

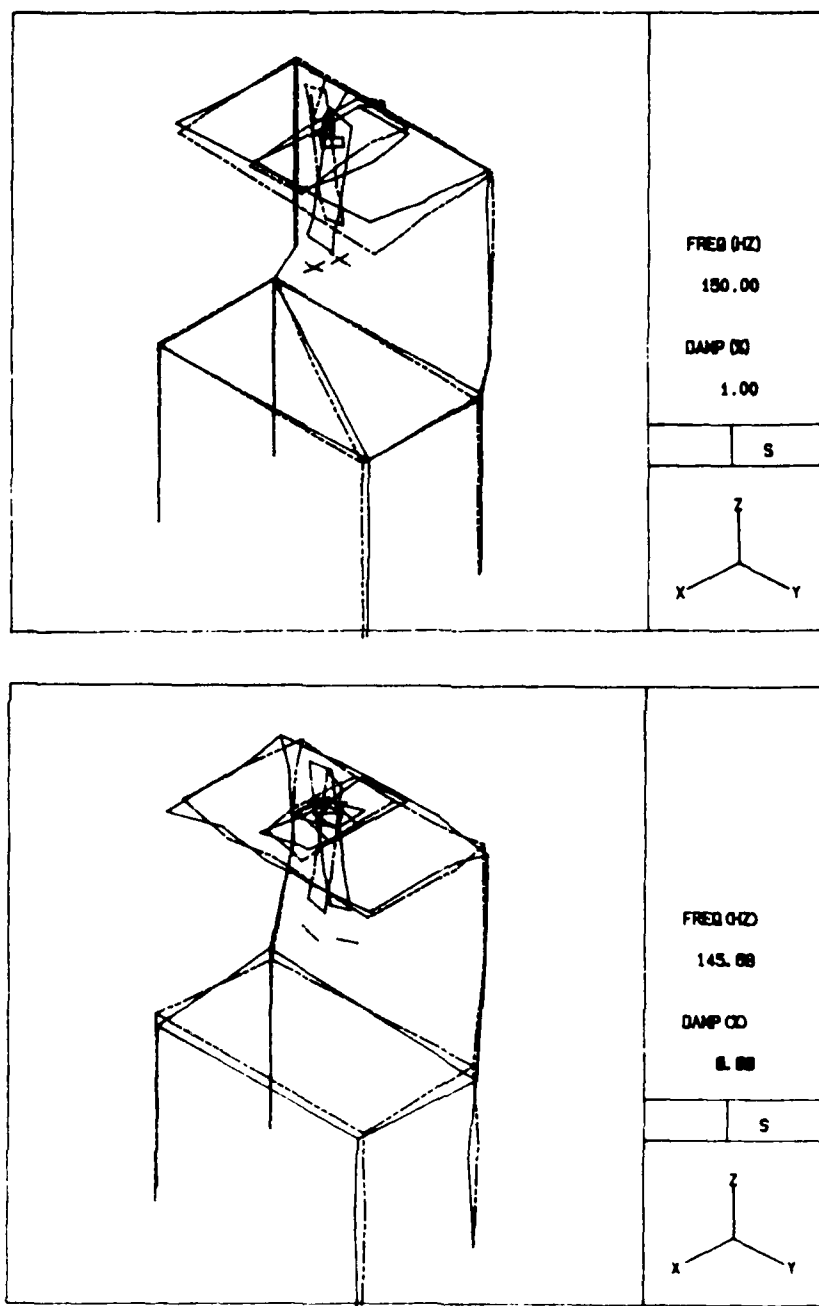


Figure A.36: mode shape no.14 of complete robot as obtained by test(top) and by synthesis(bottom)

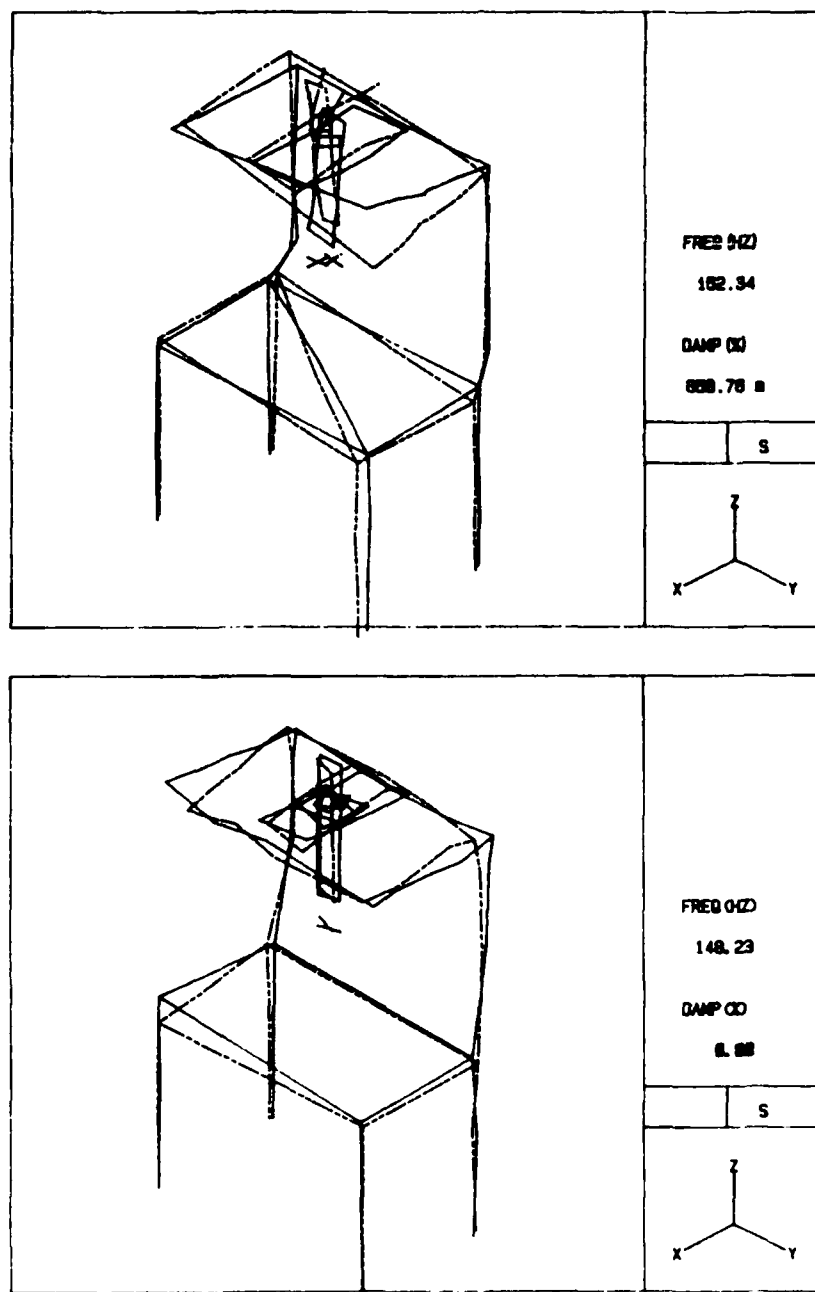


Figure A.37: mode shape no.15 of complete robot as obtained by test(top) and by synthesis(bottom)

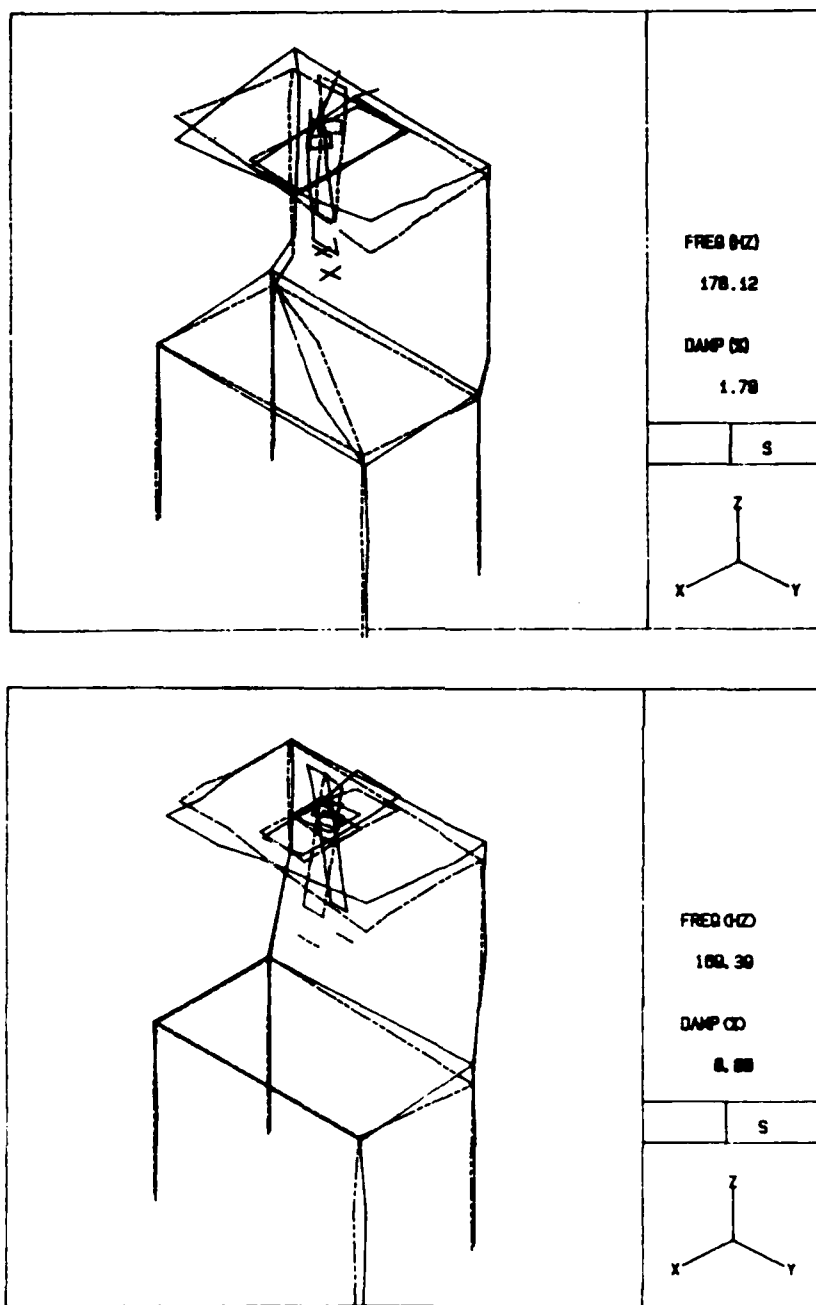


Figure A.38: mode shape no.16 of complete robot as obtained by test(top) and by synthesis(bottom)

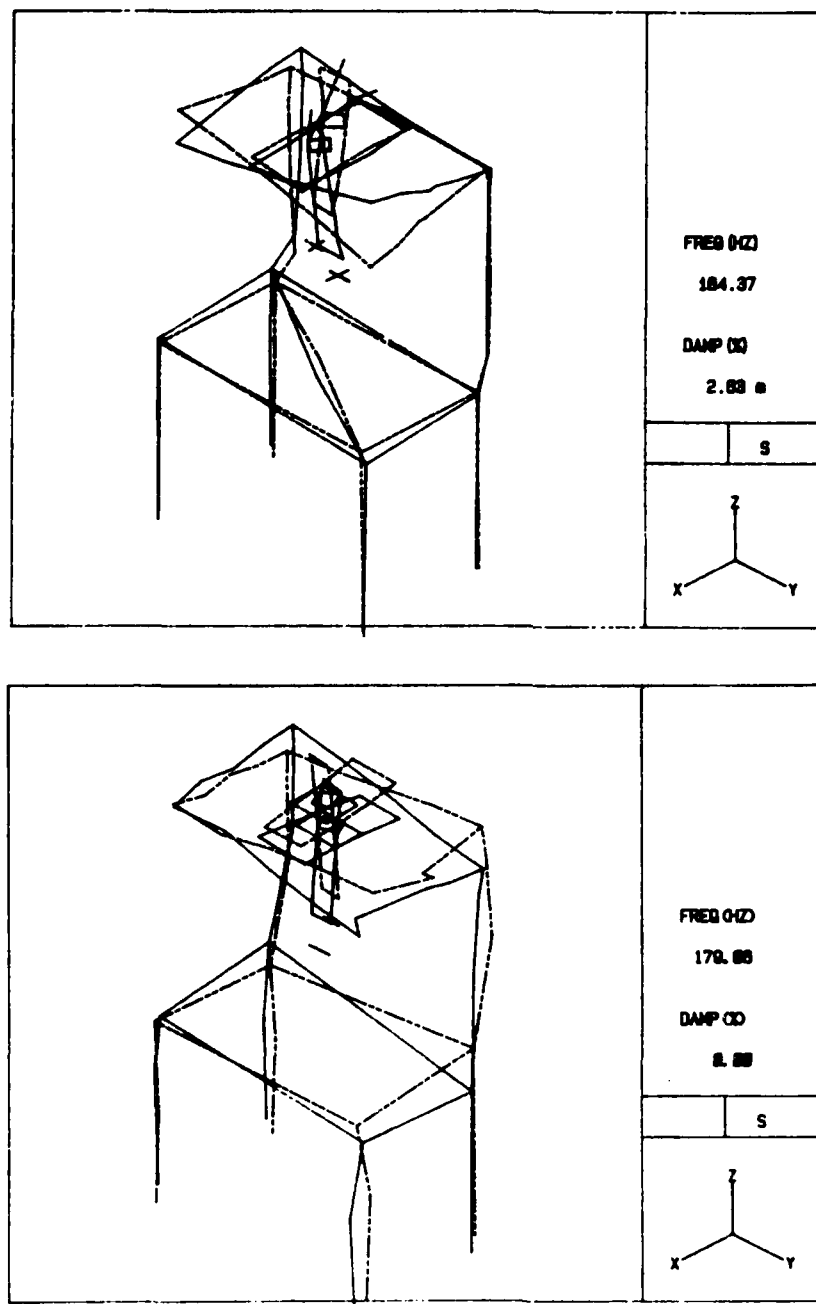


Figure A.39: mode shape no.17 of complete robot as obtained by test(top) and by synthesis(bottom)

Mode No.	Measured		Predicted	
	$f_n$ (Hz)	$\zeta_n$ (%)	$f_n$ (Hz)	$\zeta_n$ (%)
1	12.36	1.98	11.93	1.45
2	18.85	1.65	19.17	1.45
3	36.36	1.42	36.87	0.78
4	42.83	9.52	46.34	3.30
5	47.83	4.90	49.53	2.54
6	60.51	3.24	61.38	1.45
7	70.72	0.89	75.06	1.82
8	81.47	1.95	96.47	0.63
9	86.67	1.74	101.75	1.41
10	97.70	1.17	123.39	1.30
11	112.52	7.39	126.84	1.06
12	126.27	0.10	128.72	0.75
13	139.43	2.62	141.05	1.16
14	149.85	1.00	145.68	2.86
15	152.34	0.66	148.23	2.76
16	178.12	1.79	169.39	1.04
17	184.37	0.01	179.06	1.11

Table A.3: Comparison of natural frequencies and modal damping factors

## Appendix B

# VIBRATION OF MOVING ROBOT

This appendix describes the method of analysis employed in the study of robot vibrations during motion, method which has been used in Chapter 3 to do the simulations.

### B.1 Methods of Analysis

After briefly mentioning the case of prescribed rigid body motions which provides a simple approach to the problem, we then discuss in some detail the procedures that can be used for the case when the motor-rotor vibration is specified.

#### B.1.1 Prescribed Rigid Body Motion

As was discussed in Chapter 3, one of the simplest approaches to the problem of predicting the robot vibrations caused by its motion is to prescribe how a particular substructure is moving (as a rigid body) regardless of the input required to cause that motion, thus leaving out the effects of the robot

control system. In order for this procedure to be simple we can assume for a moment that the substructures are rigid and calculate the forces exerted at the connection points; forces which would produce that specified motion of the center of gravity of the substructure under the presence of friction and gravity. This procedure, although a rough approximation leads to a relatively fast computer model.

### B.1.2 Prescribed Motor-Rotor Vibration

The motor-rotor motion can be easily determined experimentally from encoder data, and this motion, including vibration, may be used as input to the mathematical model. We drive the mathematical model using this prescribed motor-rotor vibration while ignoring the forcing function exerted by the amplifier-motor combination. The procedure developed for this purpose had to be restricted to the available data, that is, to the use of modal parameters only. Two suitable techniques for this analysis are described in what follows.

#### Frequency-Domain Technique

There is a very powerful technique for this application which works in the frequency domain through the use of Fourier transforms, unfortunately it is only valid for time-invariant systems. This can be briefly described as follows: Consider a flexible system as shown in Figure B.1 where a force  $f_p(t)$  is applied at the point P producing a vibration  $x_p(t)$ . Suppose we know  $x_p(t)$  and the transfer function

$$H_{pp}(\omega) = \frac{X_p(\omega)}{F_p(\omega)} \quad (B.50)$$



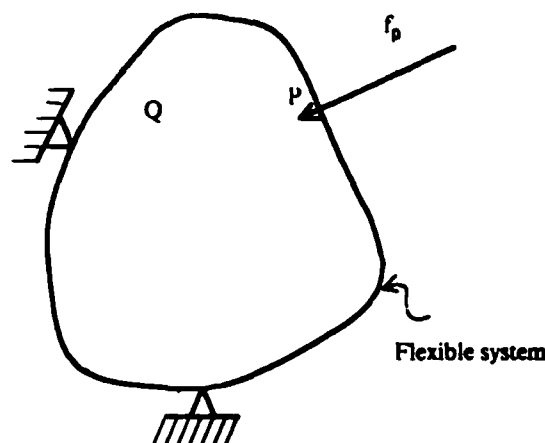


Figure B.1: Flexible system

which may be synthesized from the modal parameters as follows:

$$H_{pp}(\omega) = \sum_{i=1}^n \frac{(\phi_p^{(i)})^2}{-\omega^2 + \omega_i^2 + 2j\zeta_i\omega_i\omega} \quad (B.51)$$

Then, by taking the Fourier transform of  $x_p(t)$  to get  $X_p(\omega)$  we can calculate  $F_p(\omega)$ , and after taking the inverse Fourier transform we can get  $f_p(t)$ . With  $f_p(t)$  known, we can then integrate the equations of motion

$$\{\ddot{p}\} + [2\zeta_n\omega_n]\{\dot{p}\} + [\omega_n^2]\{p\} = [\phi]^t\{f\} \quad (B.52)$$

to get the vibration at any point of the structure by means of  $\{x_Q\} = [\phi_Q]\{p\}$ .

Another procedure which may be faster to apply consists of the following. Assume that we also know  $H_{PQ}(\omega)$  as indicated below, and we wish to calculate  $x_Q(t)$ .

$$H_{PQ}(\omega) = \sum_{i=1}^n \frac{\phi_p^{(i)}\phi_Q^{(i)}}{-\omega^2 + \omega_i^2 + 2j\zeta_i\omega_i\omega} \quad (B.53)$$

Then

$$H_{PQ}(\omega) = \frac{X_Q(\omega)}{F_p(\omega)} \quad (B.54)$$

Solving for  $F_p(\omega)$  in equation B.50 and B.54 we can then equate both expressions to get:

$$X_Q(\omega) = \frac{H_{PQ}(\omega)}{H_{PP}(\omega)} X_P(\omega) \quad (B.55)$$

Then we calculate  $x_Q(t)$  from equation B.55 by inverse transforming  $X_Q(\omega)$ , all without explicitly calculating the force  $f_P(t)$ .

One source of error in this process may come from the use of the FFT which assumes that the function  $x_P(t)$  is periodic, but in this case of robot motions there is a start point. This start condition is normally taken into account by extending the time history back from time zero, that is:

$$x_P(t) = \begin{cases} 0 & \text{for } t < 0 \\ x_P(t) & \text{for } t > 0 \end{cases} \quad (B.56)$$

and giving enough span to get good approximation.

Even though this technique was not applied to the study of the robot vibrations, it could be used to get approximate results if we considered average values for the transfer functions involved.

### Time-Domain technique

A time-domain technique which can be of more general application is the following:

Consider the same system of Figure B.1 where we ultimately want to determine the vibration  $x(t)$  at any point by knowing  $x_P(t)$  but not  $f_P(t)$ . The system can be described by the truncated system of uncoupled equations B.52. Since there is only one external force  $f_P(t)$  acting on the system, we can express the modal force as

$$\{c\}'\{f\} = \{a\}'\{f_P\} \quad (B.57)$$

where  $\{a\}$  is formed by the modal matrix evaluated at point  $P$  in the direction of the force.

In addition to the  $n$  equations of B.52, we have another condition to be satisfied:

$$\{x_P\} = [\phi_P]\{p\} = \{a\}^t\{p\} \quad (B.58)$$

So, we have  $n + 1$  equations and  $n + 1$  unknowns, those are  $\{p\}$  and  $f_P$ .

Assuming that  $a_i \neq 0$  for all  $i$  we can eliminate from equation B.52  $f_P$  by combining the  $n$  equations to get  $n - 1$  equations as follows:

- multiply 1st equation by  $\frac{1}{a_1}$  :  $\frac{1}{a_1}\ddot{p}_1 + \frac{2}{a_1}\zeta_1\omega_1\dot{p}_1 + \frac{1}{a_1}\omega_1^2 p_1 = f_P$ .
- multiply  $i + 1$ th equation by  $\frac{1}{a_{i+1}}$  :

$$\frac{1}{a_{i+1}}\ddot{p}_{i+1} + \frac{2}{a_{i+1}}\zeta_{i+1}\omega_{i+1}\dot{p}_{i+1} + \frac{1}{a_{i+1}}\omega_{i+1}^2 p_{i+1} = f_P.$$

Subtract to get the  $i$ th new equation without the term in  $f_P$ . Then we

get  $n - 1$  equations for the  $n$  variables  $p_i$

$$\begin{aligned}
 & \begin{bmatrix} \frac{1}{a_1} & -\frac{1}{a_2} & 0 & 0 & \dots & 0 \\ \frac{1}{a_1} & 0 & -\frac{1}{a_3} & 0 & \dots & 0 \\ \vdots & \vdots & \vdots & \vdots & \ddots & \vdots \\ \frac{1}{a_1} & 0 & 0 & 0 & \dots & -\frac{1}{a_n} \\ a_1 & a_2 & a_3 & a_4 & \dots & a_n \end{bmatrix} \begin{Bmatrix} \ddot{p}_1 \\ \ddot{p}_2 \\ \vdots \\ \ddot{p}_n \end{Bmatrix} + \\
 & \begin{bmatrix} \frac{2\zeta_1\omega_1}{a_1} & -\frac{2\zeta_1\omega_1}{a_2} & 0 & 0 & \dots & 0 \\ \frac{2\zeta_1\omega_1}{a_1} & 0 & -\frac{2\zeta_3\omega_3}{a_3} & 0 & \dots & 0 \\ \vdots & \vdots & \vdots & \vdots & \ddots & \vdots \\ \frac{2\zeta_1\omega_1}{a_1} & 0 & 0 & 0 & \dots & -\frac{2\zeta_n\omega_n}{a_n} \\ 0 & 0 & 0 & 0 & \dots & 0 \end{bmatrix} \begin{Bmatrix} \dot{p}_1 \\ \dot{p}_2 \\ \vdots \\ \dot{p}_n \end{Bmatrix} \\
 & + \begin{bmatrix} \frac{\omega_1^2}{a_1} & -\frac{\omega_1^2}{a_2} & 0 & 0 & \dots & 0 \\ \frac{\omega_1^2}{a_1} & 0 & -\frac{\omega_3^2}{a_3} & 0 & \dots & 0 \\ \vdots & \vdots & \vdots & \vdots & \ddots & \vdots \\ \frac{\omega_1^2}{a_1} & 0 & 0 & 0 & \dots & -\frac{\omega_n^2}{a_n} \\ 0 & 0 & 0 & 0 & \dots & 0 \end{bmatrix} \begin{Bmatrix} p_1 \\ p_2 \\ \vdots \\ p_n \end{Bmatrix} = \begin{Bmatrix} 0 \\ 0 \\ \vdots \\ \ddot{x}_P \end{Bmatrix} \quad (B.59)
 \end{aligned}$$

Now we can apply equation B.58 to add another equation (or row) in such a way that the mass matrix remains non-singular, that is, by differentiating equation B.58 twice with respect to time:

$$\{\ddot{x}_P\} = [\phi_P]\{\ddot{p}\} = \{a\}^t\{\ddot{p}\} \quad (B.60)$$

so, the  $n$ th equation of B.59 after the addition would contain  $\{a\}$  in the mass matrix and the corresponding forcing function would be  $\{\ddot{x}_P\}$ . Therefore, starting with a coupled system of equations given by equation B.52 and equation B.58, we end up with a coupled system of equations which is driven by the prescribed motion  $x_P(t)$ , and which can be integrated directly to determine  $\{p\}$  and ultimately  $\{x\}$ .

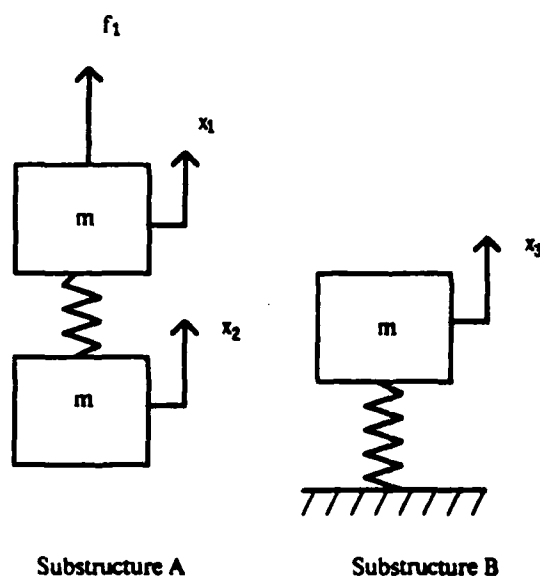


Figure B.2: Two substructures A,B

One important observation regarding the application of this method is that the differentiation of  $x_P$  with respect to time assumes that  $\dot{\phi}_{ij} = 0$ . This is strictly correct for a time-invariant system, but only approximately valid for a slowly-varying system. For the general case we would have to include terms in  $\dot{\phi}_{ij}$  and  $\ddot{\phi}_{ij}$  in the equations of motion.

### APPLICATION TO A SIMPLE CASE

In order to evaluate these methods, we consider a simple case which can illustrate with detail what we have applied to the study of the cartesian robot. To make it more similar to the robot case, we include a connection of two substructures.

The problem is defined as follows. Consider the two substructures, A and B, as shown in Figure B.2. Given  $x_1(t)$  of the assembled system, find  $x_2(t)$  of the same assembled system for two different cases:

- Impulse response.
- Step response.

### Synthesis of Modal Data for Assembled System

Substructure A has the following modal parameters:

$$[\omega_A^2] = \begin{bmatrix} 0 & 0 \\ 0 & \frac{2k_A}{m} \end{bmatrix}, [\phi_A] = \begin{bmatrix} \frac{1}{\sqrt{2m}} & \frac{1}{\sqrt{2m}} \\ \frac{1}{\sqrt{2m}} & -\frac{1}{\sqrt{2m}} \end{bmatrix}, \{f_A\} = \begin{Bmatrix} f_1 \\ 0 \end{Bmatrix} \quad (B.61)$$

Substructure B has

$$[\omega_B^2] = \frac{k_B}{m}, [\phi_B] = \frac{1}{\sqrt{m}}, \{f_B\} = 0 \quad (B.62)$$

The uncoupled equations before assembly are given by

$$\begin{aligned} \{\ddot{p}_A\} + [\omega_A^2]\{p_A\} &= [\phi_A]^T \{f_A\} = \begin{Bmatrix} \frac{f_1}{\sqrt{2m}} \\ \frac{f_1}{\sqrt{2m}} \end{Bmatrix} \\ \{\ddot{p}_B\} + [\omega_B^2]\{p_B\} &= [\phi_B]^T \{f_B\} = \{0\} \end{aligned} \quad (B.63)$$

The compatibility condition requires that

$$\{x_2\} = \{x_3\}, \text{ or } [\phi_A]\{p_A\} = [\phi_B]\{p_B\} \quad (B.64)$$

Choosing  $p_B$  as the generalized coordinate to be eliminated, we get

$$\{p_B\} = [\phi_B]^{-1}[\phi_A]\{p_A\} = \begin{bmatrix} \frac{1}{\sqrt{2}} & -\frac{1}{\sqrt{2}} \end{bmatrix} \{p_A\} \quad (B.65)$$

Then, the transformation matrix  $T$  as defined by formula 2.7 becomes

$$[T] = \begin{bmatrix} 1 & 0 \\ 0 & 1 \\ \frac{1}{\sqrt{2}} & -\frac{1}{\sqrt{2}} \end{bmatrix}, \text{ for the case } \begin{cases} q_1 = p_{A_1} \\ q_2 = p_{A_2} \end{cases} \quad (B.66)$$

The assembled system is obtained by

$$[m] = [T]^T [T], [k] = [T]^T [\omega^2] [T], \{F\} = [T]^T [\phi]^T \{f\} \quad (B.67)$$

. Substituting the previously obtained values, we get:

$$\begin{bmatrix} \frac{3}{2} & -\frac{1}{2} \\ -\frac{1}{2} & \frac{3}{2} \end{bmatrix} \begin{Bmatrix} \ddot{q}_1 \\ \ddot{q}_2 \end{Bmatrix} + \begin{bmatrix} \frac{k_D}{2} & -\frac{k_D}{2} \\ -\frac{k_D}{2} & 2k_A + \frac{k_D}{2} \end{bmatrix} \begin{Bmatrix} q_1 \\ q_2 \end{Bmatrix} = \begin{Bmatrix} \frac{f_1}{\sqrt{2m}} \\ \frac{f_1}{\sqrt{2m}} \end{Bmatrix} \quad (B.68)$$

. This assembled system has the eigenvalues

$$\omega_{1,2}^2 = \frac{1}{4} \left[ \frac{3k_A + k_D}{m} \pm \sqrt{\frac{9k_A^2 - 2k_A k_D + k_D^2}{m^2}} \right] \quad (B.69)$$

and the eigenvectors

$$[\phi] = \begin{bmatrix} \phi_{11} & \phi_{12} \\ \phi_{21} & \phi_{22} \end{bmatrix} \quad (B.70)$$

This can be verified to be exactly correct for the resulting system shown in Figure B.3.

### Analysis by Frequency-Domain Technique

In order to get the response at  $x_2$  given the response at  $x_1$ , we can apply the frequency-domain technique described above. First we decouple the system of equations given by B.68 to get

$$\begin{bmatrix} 1 & 0 \\ 0 & 1 \end{bmatrix} \begin{Bmatrix} \ddot{r}_1 \\ \ddot{r}_2 \end{Bmatrix} + \begin{bmatrix} \omega_1^2 & 0 \\ 0 & \omega_2^2 \end{bmatrix} \begin{Bmatrix} r_1 \\ r_2 \end{Bmatrix} = \begin{Bmatrix} (\phi_{11} + \phi_{21}) \frac{f_1}{\sqrt{2m}} \\ (\phi_{12} + \phi_{22}) \frac{f_1}{\sqrt{2m}} \end{Bmatrix} \quad (B.71)$$

. The transfer function at point  $x_1$  is

$$H_{11}(\omega) = \frac{\phi_{11}^2}{\omega_1^2 - \omega^2} + \frac{\phi_{12}^2}{\omega_2^2 - \omega^2} \quad (B.72)$$

So, by applying equation B.72 we can obtain  $F_1(\omega)$  and from there  $f_1(t)$ . Integrating equations B.68 we can determine  $x_1(t)$  as shown below, or we can use  $H_{12}$  in combination with  $H_{11}$  in formula B.55 to get  $X_2(\omega)$  directly, and from it  $x_2(t)$ .

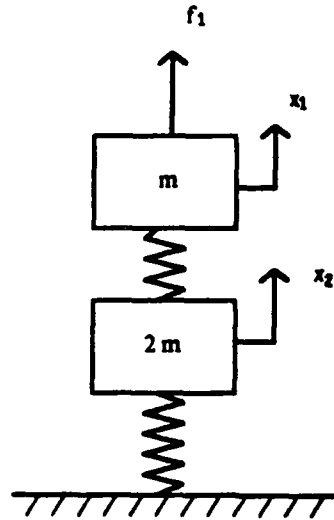


Figure B.3: Assembled A-B

### Analysis by Time-Domain Technique

The prescribed vibration  $x_1(t)$  is related to the variables  $q$  by

$$x_1 = [\phi_1]\{q\} = \left\{ \frac{1}{\sqrt{2m}} \quad \frac{1}{\sqrt{2m}} \right\} \begin{Bmatrix} q_1 \\ q_2 \end{Bmatrix} \quad (B.73)$$

. First we eliminate  $f_1$  from equation B.68 by subtracting the first row from the 2nd to get

$$\begin{bmatrix} -2 & 2 \end{bmatrix} \begin{Bmatrix} \ddot{q}_1 \\ \ddot{q}_2 \end{Bmatrix} + \begin{bmatrix} -k_B & 2k_A + k_B \end{bmatrix} \begin{Bmatrix} q_1 \\ q_2 \end{Bmatrix} = 0 \quad (B.74)$$

. Differentiating equation B.73 twice with respect to time, and adding that equation to B.74 we get

$$\begin{bmatrix} -2 & 2 \\ \frac{1}{\sqrt{2m}} & \frac{1}{\sqrt{2m}} \end{bmatrix} \begin{Bmatrix} \ddot{q}_1 \\ \ddot{q}_2 \end{Bmatrix} + \begin{bmatrix} -k_B & 2k_A + k_B \\ 0 & 0 \end{bmatrix} \begin{Bmatrix} q_1 \\ q_2 \end{Bmatrix} = \begin{Bmatrix} 0 \\ \ddot{x}_1 \end{Bmatrix} \quad (B.75)$$



These equations B.75 can be integrated directly to get  $q_1(t)$  and  $q_2(t)$  to then get

$$x_2(t) = \{\phi_2\}\{q\} = \phi_{21}q_1 + \phi_{22}q_2 \quad (B.76)$$

An alternative way to arrive at the differential equation driven by the prescribed motion  $x_1$  consists of eliminating one of the  $q_i$ , say  $q_2$  from equation B.73, and substitute in equation B.75 to get a single equation

$$\ddot{q}_1 + \frac{k_A + k_B}{2m}q_1 = \frac{\sqrt{2m}}{2}\ddot{x}_1 + \frac{\sqrt{2m}}{4m}(2k_A + k_B)x_1 \quad (B.77)$$

### Results

Two kinds of inputs or prescribed motions at  $x_1$  can be employed now. The impulse response is given by

$$x_2(t) = \frac{\phi_{22}^2}{\omega_2} \sin(\omega_2 t) + \frac{\phi_{21}^2}{\omega_1} \sin(\omega_1 t) \quad (B.78)$$

and the step response by

$$x_2(t) = \frac{\phi_{21}^2}{\omega_1^2}(1 - \cos(\omega_1 t)) + \frac{\phi_{22}^2}{\omega_2^2}(1 - \cos(\omega_2 t)) \quad (B.79)$$

The corresponding responses at  $x_2$  as given by the first method are shown in Figure B.4 and Figure B.5, where the calculated response is the top plot and the expected response  $x_2(t)$  is shown for comparison at the bottom. Both results, the calculated and the expected, are very similar.

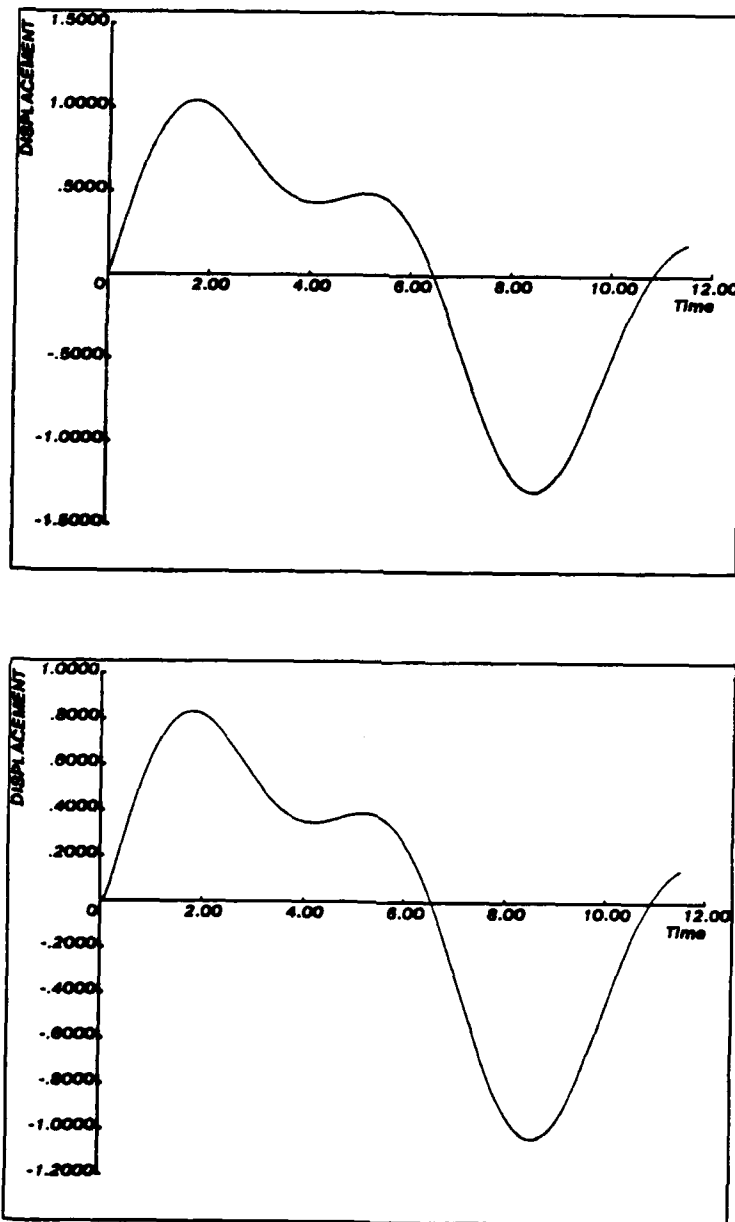


Figure B.4: Response at  $x_2$  to impulse-response input at  $x_1$ , calculated (top) and expected (bottom)

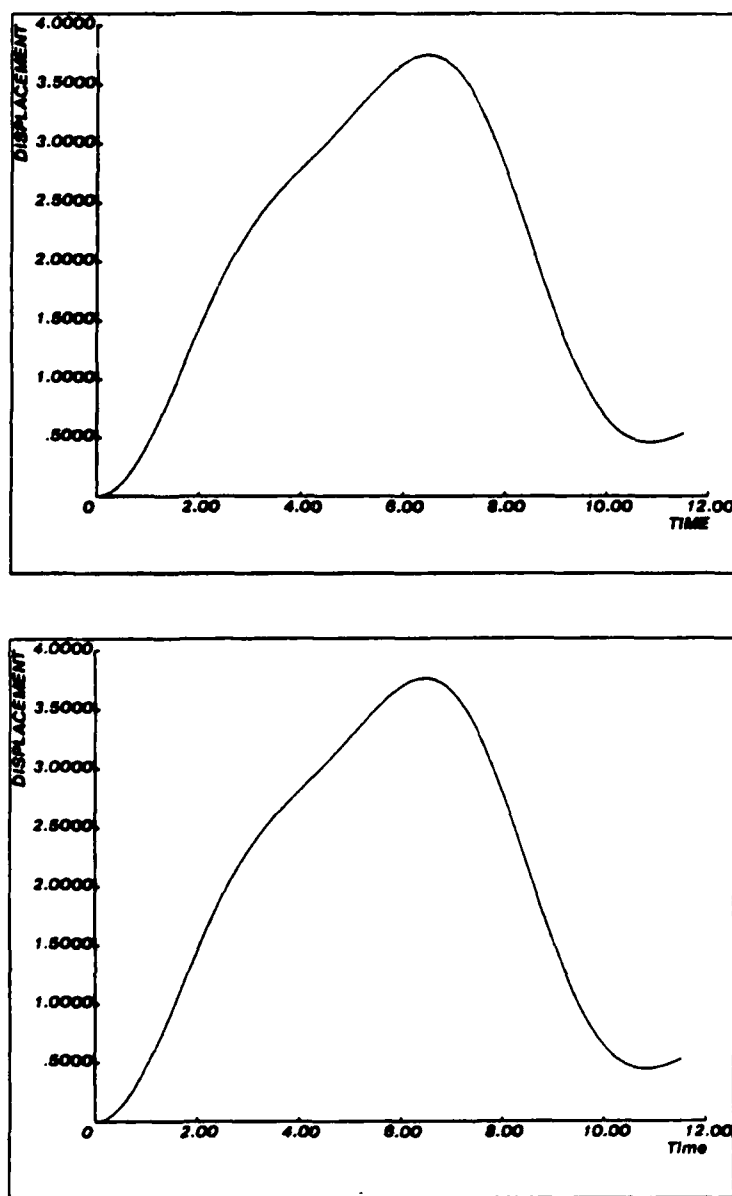


Figure B.5: Response at  $x_2$  to step-response input at  $x_1$ , calculated (top) and expected (bottom)

## Appendix C

# PRELIMINARY STUDY OF VIBRATIONS OF A GEOMETRICALLY NONLINEAR SYSTEM

### C.1 Preliminary Vibration Analysis

Before we started doing the analysis of the cartesian robot, we were involved in the study of the vibration characteristics of a four-bar linkage with elastic input and output shafts which presented some common characteristics with the cartesian robot, and from whose analysis we could get insights into the problem of position-dependent systems. The experience obtained in the preliminary study facilitated the development of a procedure to analyze the robot vibrations, and that is why we dedicate this Appendix to its presentation.

The system consists of a crank-rocker mechanism with flexible input and output shafts (see Figure C.1). The input shaft transmits power from

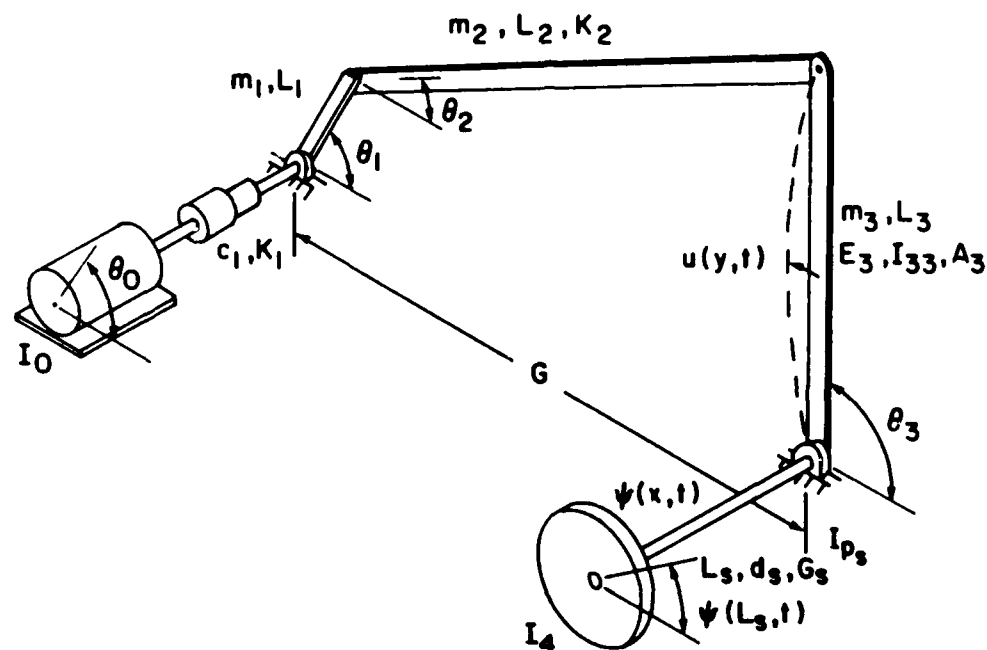


Figure C.1: Continuous parameter model of the system

an ideal motor, represented by its rotor inertia  $I_0$ , to the crank. The input shaft stiffness is normally high as is the first natural torsional frequency of the shaft considered in isolation. Also the shaft inertia is usually quite small as compared to that of the rotor. Therefore, the shaft may be modeled as a linear torsional spring and viscous damper with spring and damping coefficients  $K_1$  and  $C_1$ .

For this study the crank and connecting rod are assumed to be short and their natural frequencies in bending, considered as isolated beams are assumed high when compared with the length and bending natural frequency of the rocker. Therefore the input link is considered to be a rigid link of mass  $m_1$  and inertia  $I_1$  and the coupler link is modeled as a link of mass  $m_2$  inertia  $I_2$ , and axial stiffness  $K_2$ . The rocker is a long uniform member; it has mass  $m_3$ , and elasticity in bending only. The output shaft is rigidly attached to the rocker, and is perpendicular to the rocker's plane of motion. It is a uniform circular shaft of length  $L_4$ , diameter  $d_4$ , polar

moment of inertia  $I_{ps}$ , density  $\rho_s$ , and shear modulus  $G_s$ . At the end of the shaft there is a system load represented as an inertia  $I_4$ .

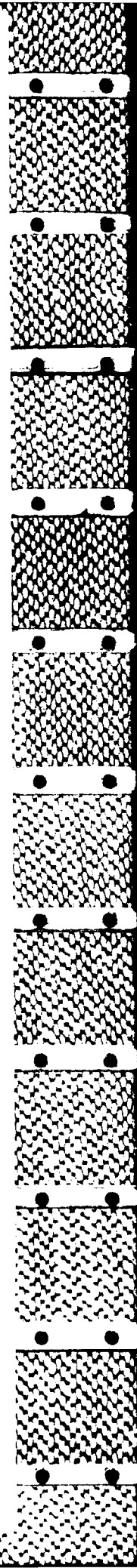
Before proceeding to derive the equations, we should point out the similarities and differences with the robot problem:

- For a given configuration of these systems, the modal characteristics can be calculated by one of several methods, and these modal parameters may be different from those corresponding to another configuration, that is, by changing relative positions the boundary conditions of some elements may change, or the relative inertias and stiffnesses may vary. This is true for both systems, and as we will see later, the method to obtain the modal parameters has to be chosen according to the system complexity, and the more complex the system, the simpler the method ought to be in order to be able to solve the resulting differential equations.
- The four-bar linkage problem consists of finding steady-state solutions and the cyclic variation of the system coefficients is fast as compared to the vibration which takes place superposed on the rigid body motion. On the other hand, the cartesian robot problem concerns finding transient vibrations which occur during motion of the carriages; this system can be modeled as a slowly varying one, that is, the system coefficients vary slowly as compared to the vibrations. In both cases, the solution involves integration of a system of differential equations with variable coefficients.

## C.2 Introduction

Many authors have studied the vibration of four-bar linkages with one or more elastic links. In 1972, Erdman, Sandor and Oakberg [21] reported

using Finite Element methods to study an elastic linkage. In their analysis they considered effects of input speed fluctuations. In 1973, Imam, Sandor and Kramer [42] applied quasi-static structural techniques to this problem; they included in their analysis the rate of change of eigenvalues and eigenvectors to reduce the computer time. In 1973, Sadler and Sandor [68] analyzed a linkage with rigid crank and elastic coupler links using Euler-Bernoulli theory for beams; to solve the equations they used the difference approximation and Taylor expansions. The same authors in 1974 [69] analyzed a crank-rocker mechanism with rotational inertia in the output. They modeled the crank link as a cantilever beam and the coupler and rocker links as simply supported beams. Sutherland [74], in 1976 assumed sinusoidal mode shapes for the elastic links in order to model their behavior; he applied both analytical and numerical methods to solve the equations. For all of these analyses, the input link is assumed to be driven directly by the motor; for many cases, input link angular velocity is considered constant and there are no loads assumed to be acting on the system except the inertia loads of the links. In fact however, most linkages in use are driven through input shafts which are not rigid and motions of interest are often those of inertias being driven by shafts connected to the output or rocker link. Examples are found in industrial sewing machines, paper making machines, packaging machines, and others. Often the frequencies of the first torsional resonances of the input and output shafts are near the bending frequencies of the links. As a result, the resonances of the system are coupled and cannot be evaluated correctly unless the characteristics of the input and output shafts are taken into consideration. In 1978, Sanders and Tesar [70] performed an analytical and experimental study of linkages with transverse coupler link vibrations which are uncoupled with the vibrations of the rest of the system. They recommend relatively robust



mechanisms for high speed linkages. However, robust mechanisms carry weight penalties which are unacceptable in many applications. As demand for faster systems is increasing and because vibration is the phenomenon which most often limits the speed at which a high-speed mechanism can operate, it is important to develop tools for predicting frequency response for mechanisms consisting of flexible linkages and elastic input and output shafts. To date only a few authors have included in their models the effects of flexibility in the system input and output shafts or the effects of inertial loads on the ends of these shafts. In 1967, Capellen [13] considered input and output shafts but did not account for any elasticity in the linkage itself. In 1977, Kohli, Hunter and Sandor [50] included the elastic effects of supports and input and output shafts on the vibration of an elastic linkage; they applied fourier series representations to model the deflections of the links. In this paper we consider the case in which a four-bar linkage with an elastic rocker or output link is driven by a motor through a flexible input shaft and drives, through connection to the rocker link, a flexible output shaft which in turn drives an inertial load.(Figure C.1).

Starting with a continuous parameter model of the system, the behavior of the rocker-beam is analyzed, and from these results a lumped parameter model is constructed. Then the equations of motion are linearized to get a system of differential equations with periodic coefficients. Finally a dimensional analysis leads to a procedure for design of such linkages whose resonances do not match frequencies of system energy input.



### C.3 Description of the Continuous Parameter Model

Figure C.1 shows a crank-rocker mechanism with flexible input and output shafts. Two discrete and two continuous generalized coordinates are required to describe this system. They are the following:

- $\theta_0$  , the angular position of the motor rotor
- $\theta_1$  , the angular position of the input link
- $u(y, t)$  , the displacement from static equilibrium of all points on the rocker
- $\phi(x, t)$  , the torsional displacement from static equilibrium of all points on the output shaft.

We shall derive the equations of motion of this continuous system for discrete configurations; that is, for small motions about a given position of the crank; using the energy Method [20].

#### C.3.1 Kinetic co-energies

The system elements have the following kinetic co-energies:

- Output shaft:  $T_1^* = \frac{1}{2} \int_0^{L_3} \rho_s I_{\rho_s} \left( \frac{\partial \psi}{\partial t} \right)^2 dx$
- Inertia  $I_4$  :  $T_2^* = \frac{1}{2} I_4 \left( \frac{\partial \psi}{\partial t} \right)_L^2$
- Rocker:  $T_3^* = \frac{1}{2} \int_0^{L_3} \rho_3 A_3 \left( \frac{\partial u}{\partial t} \right)^2 dy$
- Crank:  $T_4^* = \frac{1}{2} I_1 \dot{\theta}_1^2$
- Motor inertia:  $T_5^* = \frac{1}{2} I_0 \dot{\theta}_0^2$

- Coupler:  $T_6^* = \frac{1}{2} A \dot{\theta}_0^2$ , where

$A = I_{2,y} i_2^2 + m_2 (L_1^2 + \frac{L_2^2}{4} i_2^2 + L_1 L_2 i_2 \cos(\theta_1 - \theta_2))$  where  $i_2$  and  $i_3$  (used later) are the angular velocity ratios as defined by Paul [60].

$$i_2 = \frac{\dot{\theta}_2}{\dot{\theta}_1} = \frac{L_1 \sin(\theta_3 - \theta_1)}{L_2 \sin(\theta_4 - \theta_3)}$$

$$i_3 = \frac{\dot{\theta}_3}{\dot{\theta}_1} = \frac{L_1 \sin(\theta_2 - \theta_1)}{L_3 \sin(\theta_2 - \theta_3)}$$

- Total kinetic energy:  $T^* = T_1^* + T_2^* + \dots + T_6^*$

### C.3.2 Potential Energies

The system elements have the following potential energies:

- Output shaft:  $V_1 = \frac{1}{2} \int_0^{L_3} G_s I_{\rho_s} \left( \frac{\partial \psi}{\partial x} \right)^2 dx$
- Rocker:  $V_2 = \frac{1}{2} \int_0^{L_3} E_3 I_{33} \left( \frac{\partial^2 u}{\partial y^2} \right)^2 dy$
- Input shaft:  $V_3 = \frac{1}{2} K_1 (\theta_1 - \theta_0)^2$
- Coupler axial spring:  $V_4 = \frac{1}{2} K_2 (N_1 L_1 \theta_1 - N_2 u_L)^2$ , where  
 $N_1 = \sin(\theta_1 - \theta_2)$  and  $N_2 = \sin(\theta_3 - \theta_2)$  are the factors that project the displacements at the ends of the coupler in the direction of the coupler, and  
 $u_L = u(L, t)$ .
- Total potential energy :  $V = V_1 + V_2 + V_3 + V_4$

### C.3.3 Generalized Forces

Variation of virtual work is  $\delta W = T_0 \delta \theta_0 - C_1 \dot{\theta}_1 \delta \theta_1 - C_2 \left( \frac{\partial \psi}{\partial t} \right)_{x=0} \delta \psi_0$ .

Then  $Z_{\theta_0} = \frac{\delta W}{\delta \theta_0} = T_0$ ,  $Z_{\theta_1} = -C_1 \dot{\theta}_1$ ,  $Z_{\psi_0} = -C_2 \left( \frac{\partial \psi}{\partial t} \right)_{x=0}$

Using Hamilton's principle [20] we obtain:

$$\delta I = \int_{t_1}^{t_2} (\delta L + \sum_{j=1}^m Z_j \delta \xi_j) dt, \quad L = T^* - V$$

Substitution of above expressions for  $T$  and  $V$  into the expression for the Variational indicator and then integration by parts both timewise and spacewise produces the equations of motion and boundary conditions at the vanishing of the Variational indicator for arbitrary variations of the generalized coordinates. These are as follows:

$$\rho_s \frac{\partial^2 \psi}{\partial t^2} + G_s \frac{\partial^2 \psi}{\partial x^2} = 0 \text{ in } 0 < x < L_s$$

$$\rho_3 A_3 \frac{\partial^2 u}{\partial t^2} + E_3 I_{33} \frac{\partial^4 u}{\partial y^4} = 0 \text{ in } 0 < y < L_3$$

$$I_4 \frac{\partial^2 \psi}{\partial t^2} + G_s I_{\rho_s} \frac{\partial \psi}{\partial x} = 0 \text{ at } x = L_s$$

$$G_s I_{\rho_s} \frac{\partial \psi}{\partial x} \Big|_{x=0} - C_2 \frac{\partial \psi}{\partial t} \Big|_{x=0} + E_3 I_{33} \left( \frac{\partial^2 u}{\partial y^2} \right) \Big|_{y=0} = 0 \text{ at } x = 0, y = 0$$

$$\frac{\partial^2 u}{\partial y^2} = 0 \text{ at } y = L_3$$

$$(I_1 + A) \ddot{\theta}_1 + C_1 \dot{\theta}_1 + K_1(\theta_1 - \theta_0) + K_2 N_1 L_1 (N_1 L_1 \theta_1 - N_2 u_L) = 0, \\ \text{at } \theta_1$$

$$I_0 \ddot{\theta}_0 + K_1(\theta_0 - \theta_1) = 0 \text{ at } \theta_0$$

$$E_3 I_{33} \frac{\partial^3 u}{\partial y^3} + K_2 N_2 (N_1 L_1 \theta_1 - N_2 u_L) = 0 \text{ at } y = L_3$$

For this derivation the equation of motion for  $\theta_1$  has been linearized by considering small motions about a given configuration. To solve the eigenvalue problem, we put temporarily  $C_1 = C_2 = 0$ ,  $T_0 = 0$  and try solutions of the form:

$$\psi(x, t) = a_n(x) \sin(\omega_n t + \phi)$$

$$u(y, t) = b_n(y) \sin(\omega_n t + \phi)$$

$$\theta_1(t) = \hat{\theta}_1 \sin(\omega_n t + \phi)$$

$$\theta_0(t) = \hat{\theta}_0 \sin(\omega_n t + \phi)$$

The substitution of these solutions into the above equations gives:

$$\rho_s \omega_n^2 a_n(x) + G_s \frac{\partial^2 a_n}{\partial x^2} = 0, \text{ in } 0 < x < L_s \quad (C.80)$$

$$-\rho_3 A_3 \omega_n^2 b_n(x) + E_3 I_{33} \frac{\partial^4 b_n(y)}{\partial y^4} = 0, \text{ in } 0 < y < L_3 \quad (C.81)$$

$$-\omega_n^2 (I_1 + A) \hat{\theta}_1 + K_1 (\hat{\theta}_1 - \hat{\theta}_0) + K_2 N_1^2 L_1^2 \hat{\theta}_1 - K_2 N_1 N_2 L_1 b_n(L) = 0, \text{ at } \theta_1 \quad (C.82)$$

$$-I_0 \omega_n^2 \hat{\theta}_0 + K_1 (\hat{\theta}_0 - \hat{\theta}_1) = 0, \text{ at } \theta_0 \quad (C.83)$$

$$G_s I_{\rho_s} \frac{\partial a_n}{\partial x} - I_4 \omega_n^2 a_n = 0, \text{ at } x = L_s \quad (C.84)$$

$$G_s I_{\rho_s} \frac{\partial a_n}{\partial x} + E_3 I_{33} \frac{\partial^2 b_n(y)}{\partial y^2} = 0, \text{ at } x = 0, y = 0 \quad (C.85)$$

$$\frac{\partial^2 b_n(y)}{\partial y^2} = 0, \text{ at } y = L_3 \quad (C.86)$$

$$-E_3 I_{33} \frac{\partial^3 b_n}{\partial y^3} + K_2 N_2^2 b_n(y) - K_2 N_1 N_2 L_1 \hat{\theta}_1 = 0, \text{ at } y = L_3 \quad (C.87)$$

Also from geometry:  $b_n(0) = 0$ , and  $a_n(0) = \left(\frac{db_n}{dy}\right)_{y=0}$

From (1) we get:

$$a_n(x) = C_1 \sin \frac{\omega_n x}{\sqrt{\frac{G_s}{\rho_s}}} + C_2 \cos \frac{\omega_n x}{\sqrt{\frac{G_s}{\rho_s}}}$$

From (2) we get:

$$b_n(y) = C_3 \sin \beta y + C_4 \cos \beta y + C_5 \sinh \beta y + C_6 \cosh \beta y$$

where  $\beta = \left(\frac{\rho_3 A_3 \omega_n^2}{E_3 I_{33}}\right)^{1/4}$

After some manipulations in order to eliminate the constants  $C_1$  through  $C_6$ ,  $\hat{\theta}_1$  and  $\hat{\theta}_0$  we can get the transcendental equation:

$$Z_1 = Z_2 \quad (C.88)$$

where

$$Z_1 = \frac{-\beta U \left( \frac{1}{2 \sin \beta L_3} + \frac{1}{2 \sinh \beta L_3} \right)}{\beta (\cot \beta L_3 - \coth \beta L_3) + 2\beta^2 \frac{E_3 I_{33}}{G_s I_{\rho_s}} \frac{\sqrt{G_s / \rho_s}}{\omega_n} \left[ \frac{G_s I_{\rho_s} \sqrt{G_s / \rho_s} \cos \left( \frac{\omega_n L_s}{\sqrt{G_s / \rho_s}} \right) - I_4 \omega_n \sin \left( \frac{\omega_n L_s}{\sqrt{G_s / \rho_s}} \right)}{G_s I_{\rho_s} \sqrt{G_s / \rho_s} \sin \left( \frac{\omega_n L_s}{\sqrt{G_s / \rho_s}} \right) + I_4 \omega_n \cos \left( \frac{\omega_n L_s}{\sqrt{G_s / \rho_s}} \right)} \right]}$$

and

$$Z_2 = \frac{\frac{U}{E_3 I_{33}} K_2 N_2^2 - \frac{N_1 N_2 L_1}{E_3 I_{33}} \frac{K_2}{K_1} (K_1 - I_0 \omega_n^2) + \beta^3 \frac{U}{2} (\cot \beta L_3 - \coth \beta L_3)}{-\beta^3 (\cot \beta L_3 \cos \beta L_3 + \sin \beta L_3 + \coth \beta L_3 \cosh \beta L_3 - \sinh \beta L_3)}$$

with

$$U = \frac{-K_1 + [-\omega_n^2(I_1 + A) + K_1 + K_2 N_1^2 L_1^2] \left( \frac{K_1}{K_1} \frac{I_n \omega_n^2}{K_1} \right)}{K_2 N_1 N_2 L_1}$$

From equation C.88 we can obtain an infinite set of eigenvalues which consists of a subset reflecting rocker bending, a subset reflecting shaft torsional vibration and a subset reflecting lumped parameter vibration modes. The behavior of the rocker is particularly important because one of its eigenvalues may be at or near the system energy input frequency for some system configurations and the magnitudes of its eigenvalues depend on all the parameters of the system. For example, if the stiffness of the input shaft is large and  $I_0$  (motor inertia) is large, the rocker tends to behave as a beam whose upper end is pinned, whereas if the input shaft stiffness is small, the rocker tends to behave as a free-end beam. Additionally, if both the stiffness of the output shaft and the output inertia  $I_4$  are large, then near the fixed bearing the rocker tends to behave as a clamped-end beam while if this stiffness is small, it behaves as a pinned-end beam. To illustrate this behavior we define a parameter  $a$  as follows:

$$\omega_{1,bending} = a^2 \sqrt{\frac{E_3 I_{33}}{\rho_3 A_3 L_3^4}}$$

where  $a$  depends on the boundary conditions. Values of  $a$  for typical boundary conditions are as follows [29]:

- hinged-clamped  $a = 3.91$
- hinged-hinged  $a = \pi$
- cantilever  $a = 1.87$
- free-hinged  $a = 0$ .

After solving the eigenvalue problem for several values of  $K_1$  and  $K_2$  for fixed  $K_3$  we obtain the behavior of  $a$  vs  $K_1$  for the two values of  $K_2$  (see

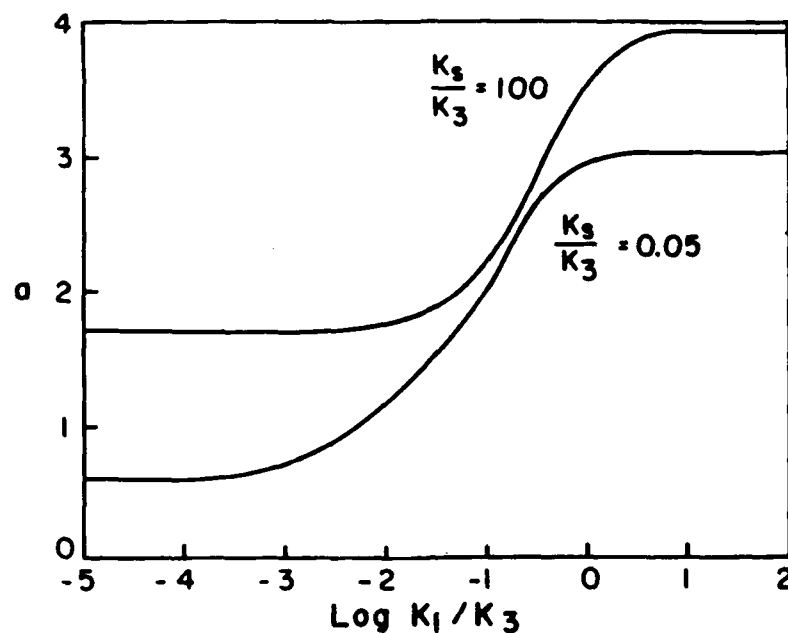


Figure C.2: Behavior of  $a$  vs.  $K_1$  for various values of  $K_3$ .

Figure C.2). Note that in the case where both input and output shafts are soft,  $a$  for the rocker takes a value (zero) appropriate for a beam hinged or pinned at its base and free at the coupler end. When both shafts are stiff, the value of  $a$  is that of a beam clamped at the base and hinged at the other end. For a soft input and stiff output shaft, the value of  $a$  is that of a cantilever, while for a stiff input and a soft output shaft  $a$  has the value fitting a hinged-hinged beam.

#### C.4 Description of Simplified Models

For most actual systems, the motor inertia is very high compared to the inertias of each link of the mechanism and the input shaft is short and therefore very stiff. Existence of these conditions implies that the rocker will behave near the rocker-coupler joint as a pinned beam. Based on this implication, a bending deformation pattern for the rocker can be assumed

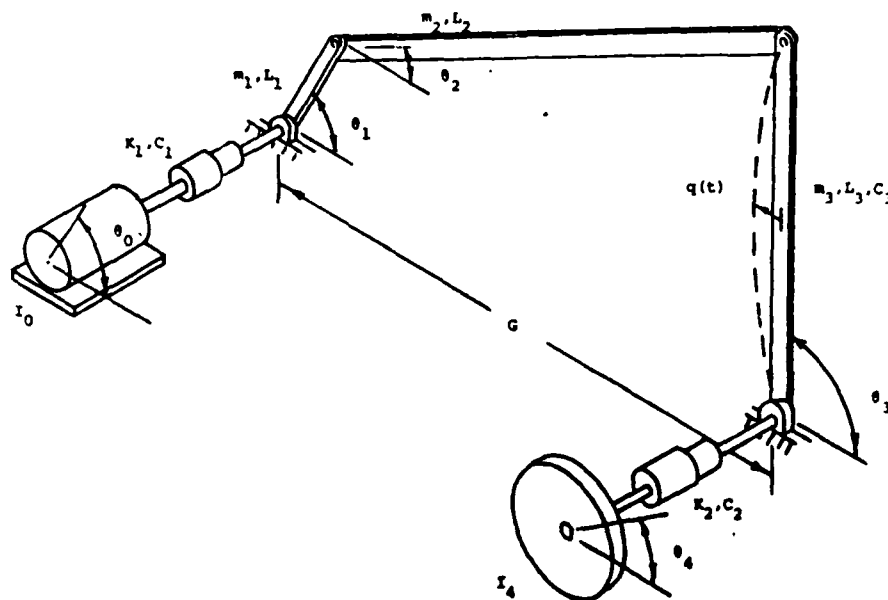


Figure C.3: Lumped parameter model of the system

and a much simpler system model, described by a set of ordinary differential equations, can then be developed. Validity of this assumption, for a specific system can be checked by comparing results of this simplified analysis to those obtained from the analysis of the more precise continuous model. From the simple model, a finite number of eigenvalues and mode shapes will be obtained. For most problems, only a finite range of eigenvalues is of interest and so the loss of higher eigenvalues is not a serious limitation, and the simplified system equations are much easier to solve than are those for the continuous model. For the case of a large motor inertia and a stiff input shaft, the vibration induced deflection pattern of the rocker link can be assumed to be sinusoidal.

$$u(y, t) = q(t) \sin \frac{\pi y}{L_3}$$

For this case, a nondimensional generalized coordinate  $z = q/L_3$  is chosen. The output shaft is modeled as a massless spring  $K_s$ . Figure C.3 shows

this simplified model. The Lagrangian for this system is as follows:

$$\begin{aligned}
 L = & \frac{1}{2} \dot{\theta}_1^2 [I_1 + I_{2_0} i_2^2 + m_2 (L_1^2 + \frac{L_1^2}{4} i_2^2 + L_1 L_2 i_2 \cos(\theta_1 - \theta_2))] + \\
 & \frac{1}{2} I_0 \dot{\theta}_0^2 + \frac{1}{2} I_4 \dot{\theta}_4^2 + \frac{1}{2} m_3 (\frac{L_3^2}{3} i_3^2 \dot{\theta}_1^2 + \frac{L_3^2}{2} \dot{z}^2 + \frac{2L_3^2}{\pi} i_3 \dot{\theta}_1 \dot{z}) \\
 & - \frac{1}{2} K_1 (\theta_1 - \theta_0)^2 - \frac{1}{2} K_s (\theta_4 - \theta_3 - \pi z)^2 - \frac{\pi^4}{4} \frac{E_3 I_{33}}{L_3} z^2
 \end{aligned} \quad (C.89)$$

where  $\pi z$ , the slope of the rocker beam near the fixed bearing relative to its position at static equilibrium, is considered approximately equal to the angle made by a tangent to the beam at the fixed bearing with respect to the position of the beam in static equilibrium. From the Lagrangian we can derive equations of motion which are nonlinear ordinary differential equations. Note that the term in  $m_3$  is the kinetic energy of the beam and is obtained by

$$KE = \frac{1}{2} \rho_3 A_3 \int_0^{L_3} v^2 dy$$

, where

$$v = \dot{\theta}_3 y + \dot{z} L_3 \sin \frac{\pi y}{L_3}$$

and the term in  $z$  is the potential energy of the beam and is obtained by

$$V = \frac{1}{2} E_3 I_{33} \int_0^{L_3} \left[ \frac{\partial^2}{\partial y^2} (z L_3 \sin \frac{\pi y}{L_3}) \right]^2 dy$$

To obtain a more precise but still a simple set of system equations, we can, instead of taking  $z L_3 \sin(\frac{\pi y}{L_3})$  as the first natural mode of the beam, take the actual mode shape obtained from the continuous parameter model discussed above, then

$$b_1(y, t) = z L_3 [C_3 \sin \beta y + C_4 \cos \beta y + C_5 \sinh \beta y + C_6 \cosh \beta y]$$

where  $C_3, C_4, C_5$  and  $C_6$  are determined for a particular case from the continuous model. The kinetic and potential energies then become:

$$\begin{aligned}
 KE &= \frac{1}{2} m_3 (\frac{L_3^2}{3} \dot{\theta}_3^2 + f_1 \dot{z}^2 + f_2 \dot{\theta}_3 \dot{z}) \\
 V &= \frac{1}{2} \frac{E_3 I_{33}}{L_3} f_3 z^2
 \end{aligned}$$



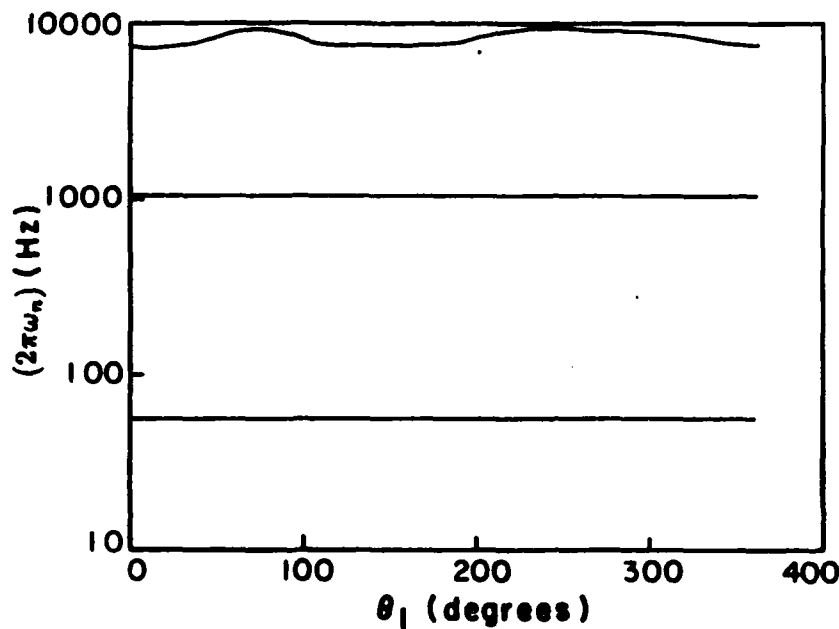


Figure C.4: Variation of three natural frequencies with crank position for quasi-static case

where  $f_1, f_2, f_3$  are constants derived for the particular case. When these energies are incorporated into the Lagrangian (10), we obtain equations of motion, this time by use of Lagrange's equations, which more precisely describe the bending motion of the link, (see equation(11) which for  $\omega = 0$  gives the quasi-static case.) For a given linkage configuration we linearize the equations of motion and since the coefficients are constant we can form and solve the eigenvalue problem. When this solution is obtained for various configurations we can determine the variation of the system eigenvalues in one cycle of the crank as a function of crank angle. Figure C.4 shows how the eigenvalues change for discrete crank positions. Shown are results for the continuous model. Results obtained from the lumped mass models are very similar. To obtain values for these eigenvalues, we have used the system parameters calculated from drawings of a linkage which is part of an industrial sewing machine that has presented its manufacturer with a

serious vibration problem during high speed operation.

This system exhibited a strong vibration at 400 Hz with the crank speed at 100 Hz, illustrating that even for a small ratio of crank length to ground link length, 0.13 in this case, the geometric nonlinearity brought about an important parametric excitation. Values of the chosen system parameters are shown in table C.1.

The lumped parameter system has four generalized coordinates and has therefore four eigenvalues, one of which is zero. Note that for the frequency range of interest (0-1000 Hz) the eigenvalues are nearly constant around the cycle and this allows us to consider  $f_1, f_2, f_3$  to be constants.

### C.5 Comparison of the Continuous and Lumped Mass Models

In order to illustrate the comparison of the eigenvalues obtained from the lumped parameter models with the ones obtained from the continuous parameter model which are known to be more precise, we have solved each eigenvalue problem for various system parameters with the crank position fixed at 90 degrees. These results are shown in figure C.5 and Figure C.6. Differences in the first eigenvalues are seen to be small for a wide range of input shaft stiffnesses for two choices of output shaft stiffnesses. Maximum difference is 5 % of the peak value.

### C.6 Linearized System Vibration for Steady Motor Rotation

In order to linearize the equations of motion we assume that the motor rotates at constant speed and that a small amplitude vibration can be

$L_1 = .02m$	$m_1 = 4.08341E - 2 \text{ Kg}$
$L_2 = .035m$	$m_2 = 2.69775E - 2 \text{ Kg}$
$L_3 = .150m$	$m_3 = 1.70105E - 2 \text{ Kg}$
$G = .155m$	$I_0 = 2.82528E - 1 \text{ Kg} - m^2$
$I_{33} = 9.037E - 12m^4$	$I_1 = 5.12082E - 6 \text{ Kg} - m^2$
$E_3 = 2.0601E11 \text{ N/m}^2$	$I_2 = 2.7468E - 6 \text{ Kg} - m^2$
$K_1 = 5258 \text{ N-m/rad}$	$I_3 = 1.2753E - 4 \text{ Kg} - m^2$
$K_s = 202 \text{ N-m/rad}$	$I_4 = 1.56E - 3 \text{ Kg} - m^2$

Table C.1: Data of a Particular Mechanism

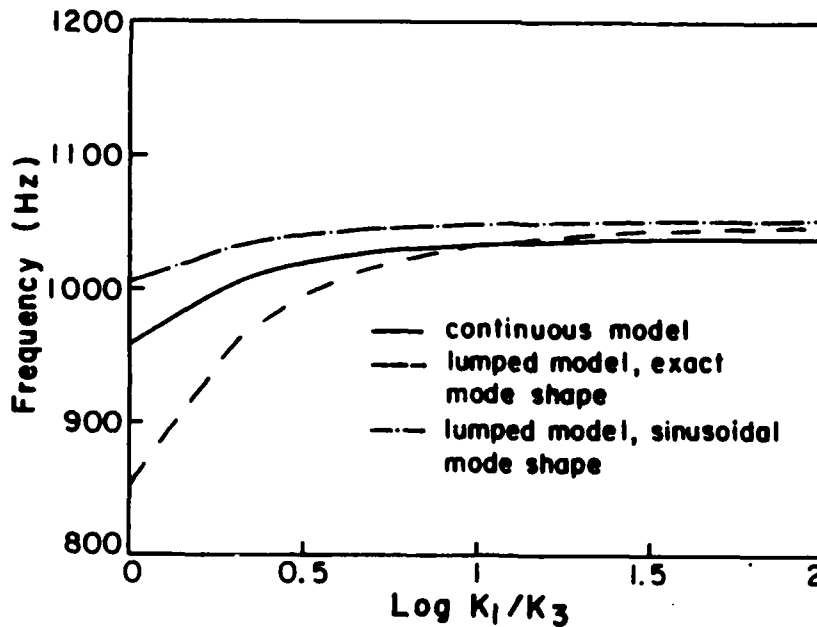


Figure C.5: Comparison of behavior of first natural frequency in bending obtained from the continuous and the lumped models. Case of  $\frac{K_4}{K_3} = 0.1$

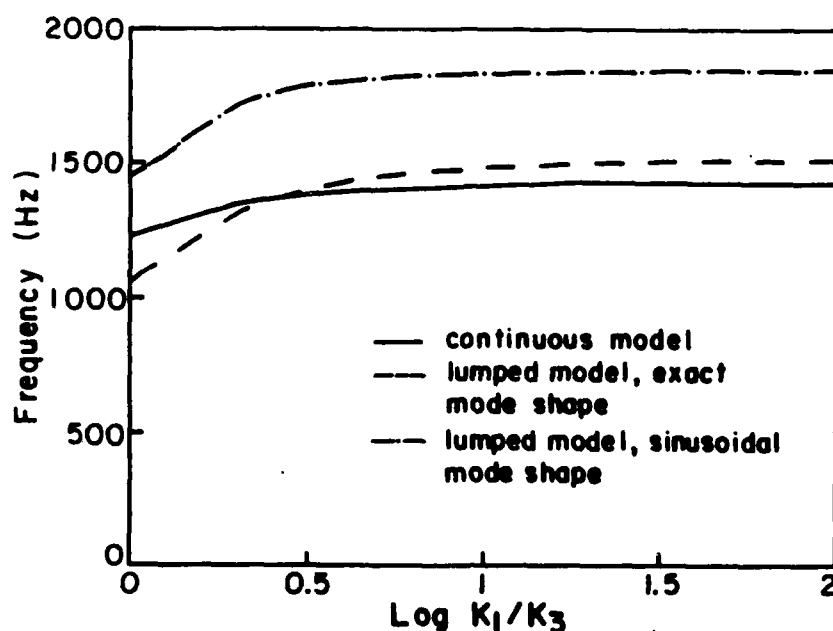


Figure C.6: Comparison of behavior of first natural frequency in bending obtained from the continuous and the lumped models. Case of  $\frac{K_1}{K_3} = 10$ .

superimposed on the rigid body motion. Then we can obtain a system of linear differential equations with periodic coefficients. To do this we define a new generalized coordinate  $\psi_1$  which will replace  $\theta_0$  and  $\theta_1$ , thus reducing the number of degrees of freedom to three, as follows:

$$\psi_1 = \theta_1 - \theta_0, \quad \theta_1 = \psi_1 + \omega t$$

where  $\omega$  is the angular velocity of the motor and  $t$  is the time. To first order approximation

$$\bar{\theta}_3 = \theta_3 + i_3 \psi_1$$

where  $\theta_3$  is the rocker position for rigid body motion and  $\bar{\theta}_3$  is the corrected value. Also

$$\dot{\theta}_1 = \dot{\psi}_1 + \omega,$$

$$\bar{\theta}_1 = \bar{\psi}_1,$$

$$\dot{\bar{\theta}}_3 = i_3 \omega + i_3 \dot{\psi}_1$$

The equations of motion obtained from this system can be linearized as follows:

$$\psi_1 = \delta\psi_1 \text{ (already small)}$$

$$z = \delta z \text{ (already small)}$$

$$\theta_4 = \theta_3 + \delta\theta_4$$

These equations then are :

$$\begin{aligned} & \begin{bmatrix} A & 0 & \frac{1}{2}m_3L_3^2i_3 \\ 0 & I_4 & 0 \\ \frac{1}{2}m_3L_3^2i_3 & 0 & f_1m_3L_3^2 \end{bmatrix} \begin{Bmatrix} \delta\psi_1 \\ \delta\theta_4 \\ \delta z \end{Bmatrix} + \\ & \begin{bmatrix} [A'\omega + C_1 - C_2i_3^2 & -C_2i_3 & TC_2i_3 \\ -C_2i_3 & C_2 & -TC_2 \\ TC_2i_3 & -TC_2 & T^2C_2 + C_3] \end{bmatrix} \begin{Bmatrix} \dot{\delta\psi}_1 \\ \dot{\delta\theta}_4 \\ \dot{\delta z} \end{Bmatrix} + \\ & \begin{bmatrix} K_1 + K_2i_3^2 & -K_2i_3 & TK_2i_3 \\ -K_2i_3 & K_2 & -TK_2 \\ TK_2i_3 & -TK_2 & T^2K_2 + f_3\frac{E_1I_{11}}{L_3} \end{bmatrix} \begin{Bmatrix} \delta\psi_1 \\ \delta\theta_4 \\ \delta z \end{Bmatrix} = \\ & \begin{Bmatrix} -\frac{A'}{2}\omega^2 - C_2i_3^2\omega \\ -I_4K_3'\omega^2 + C_2i_3\omega \\ -\frac{1}{2}m_3L_3^2K_3'\omega^2 - C_2i_3\omega \end{Bmatrix} \end{aligned} \quad (C.90)$$

where

- $A = I_1 + I_{2c}i_2^2 + m_2[L_1^2 + \frac{1}{4}L_2^2i_2^2 + L_1L_2i_2 \cos(\theta_1 - \theta_2)]$
- $T = a(C_3 + C_3)$ , obtained from mode shape(continuous model)
- $K_3' = \frac{1}{\omega} \frac{dK_3}{d\omega}$

These equations (11) can be integrated numerically to get the steady state response and determine the amplitudes of vibration and the frequency content.

Because the process of numerical integration can be expensive in terms of computer time, it is helpful to perform a dimensional analysis before

integrating. Then each numerical solution will apply to a family of mechanisms. Define the nondimensional parameters:

$$K_3 = \frac{E_3 I_{33}}{L_3}, \quad D_1 = \frac{C_1}{2\sqrt{K_1 i_{10}}},$$

$$D_2 = \frac{C_2}{2\sqrt{K_2 i_4}}, \quad D_3 = \frac{C_3}{2\sqrt{K_3 i_3}}$$

and the following parameters with dimensions of frequency:

$$\Omega_0 = \sqrt{\frac{K_1}{I_0}}, \quad \Omega_1 = \sqrt{\frac{K_1}{m_3 L_3^2}}, \quad \Omega_3 = \sqrt{\frac{K_3}{m_3 L_3^2}}$$

$$\Omega_4 = \sqrt{\frac{K_2}{I_4}}, \quad \Omega_5 = \sqrt{\frac{K_2}{I_1}}, \quad \Omega_6 = \sqrt{\frac{K_2}{I_{2c9}} + \frac{1}{2} m_2 L_2^2}$$

$$\Omega_7 = \sqrt{\frac{K_2}{m_2 L_1 L_2}}, \quad \Omega_8 = \sqrt{\frac{K_2}{m_2 L_1^2}}, \quad \Omega_{10} = \sqrt{\frac{K_3}{m_3 L_3^2}}$$

Define also a dimensionless time  $\hat{t} = \Omega_4 t$ . Then,

$$\dot{\delta\psi}_1 = \Omega_4 \dot{\delta\psi}_1, \quad \ddot{\delta\psi}_1 = \Omega_4^2 \ddot{\delta\psi}_1$$

The equations of motion (11) become after some manipulations:

$$\begin{aligned} & \begin{bmatrix} \hat{A} & 0 & \frac{I_2}{2} i_3 \\ 0 & (\frac{\Omega_1}{\Omega_4})^2 & 0 \\ \frac{I_2}{2} i_3 & 0 & f_1 \end{bmatrix} \begin{bmatrix} \delta\bar{\psi}_1 \\ \delta\bar{\theta}_4 \\ \delta\bar{z} \end{bmatrix} + \\ & \begin{bmatrix} [\hat{A} \frac{\omega}{\Omega_4} + 2D_1 \frac{\Omega_1}{\Omega_0} \frac{\Omega_1}{\Omega_4} - 2i_3^2 D_2 (\frac{\Omega_1}{\Omega_4})^2] & -2i_3 D_2 (\frac{\Omega_1}{\Omega_4})^2 & 2Ti_3 D_2 (\frac{\Omega_1}{\Omega_4})^2 \\ -2i_3 D_2 (\frac{\Omega_1}{\Omega_4})^2 & 2D_2 (\frac{\Omega_1}{\Omega_4})^2 & -2TD_2 (\frac{\Omega_1}{\Omega_4})^2 \\ 2Ti_3 D_2 (\frac{\Omega_1}{\Omega_4})^2 & -2i_3 D_2 (\frac{\Omega_1}{\Omega_4})^2 & 2T^2 D_2 (\frac{\Omega_1}{\Omega_4})^2 + \frac{2}{\sqrt{3}} D_3 \frac{\Omega_1}{\Omega_4} \end{bmatrix} \begin{bmatrix} \delta\dot{\psi}_1 \\ \delta\dot{\theta}_4 \\ \delta\dot{z} \end{bmatrix} \\ & + \begin{bmatrix} (\frac{\Omega_1}{\Omega_4}) + i_3 (\frac{\Omega_1}{\Omega_4})^2 & -i_3 (\frac{\Omega_1}{\Omega_4})^2 & Ti_3 (\frac{\Omega_1}{\Omega_4})^2 \\ -i_3 (\frac{\Omega_1}{\Omega_4})^2 & (\frac{\Omega_1}{\Omega_4})^2 & -T (\frac{\Omega_1}{\Omega_4})^2 \\ Ti_3 (\frac{\Omega_1}{\Omega_4})^2 & -T (\frac{\Omega_1}{\Omega_4})^2 & [T^2 (\frac{\Omega_1}{\Omega_4})^2 + f_3 (\frac{\Omega_1}{\Omega_4})^2] \end{bmatrix} \begin{bmatrix} \delta\psi_1 \\ \delta\theta_4 \\ \delta z \end{bmatrix} = \\ & \begin{bmatrix} -\frac{\lambda'}{2} (\frac{\omega}{\Omega_4})^2 - 2i_3^2 D_2 (\frac{\Omega_1}{\Omega_4})^2 (\frac{\omega}{\Omega_4}) \\ -(\frac{\Omega_1}{\Omega_4})^2 K_3' (\frac{\omega}{\Omega_4})^2 + 2i_3 D_2 (\frac{\Omega_1}{\Omega_4})^2 (\frac{\omega}{\Omega_4}) \\ -\frac{f_2}{2} K_3' (\frac{\omega}{\Omega_4})^2 - 2i_3 D_2 (\frac{\Omega_1}{\Omega_4})^2 (\frac{\omega}{\Omega_4}) \end{bmatrix} \end{aligned} \quad (C.91)$$

where

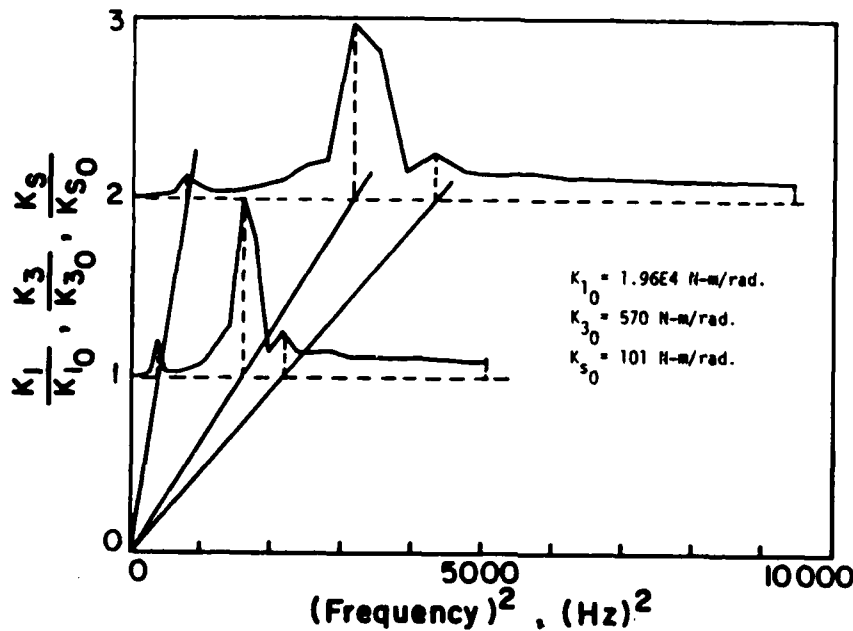


Figure C.7: Frequency response of two members of a family of mechanisms. The original data corresponds to ordinate 2

- $\hat{A} = \left(\frac{\Omega_3}{\Omega_6}\right)^2 + i_2^2 \left(\frac{\Omega_3}{\Omega_6}\right)^2 + \left(\frac{\Omega_3}{\Omega_6}\right)^2 + \left(\frac{\Omega_3}{\Omega_7}\right)^2 i_2 \cos(\theta_1 - \theta_2) + \frac{i_2^2}{3}$
- $T = a(C'_3 + C_5)$ , obtained from mode shape(continuous model)
- $K'_3 = \frac{1}{\omega} \frac{d\hat{A}}{dt}$

From these equations (12) we can observe clearly the consequences of dynamic similarity [64]. If for example the system has a small value for the damping ratio as most mechanisms do, then changing all the stiffnesses proportionally, or all the inertias proportionally will not change the dynamic response expressed in nondimensional variables. Therefore, all the systems that have the same ratio of  $\frac{K_1}{K_s}, \frac{K_3}{K_s}, \frac{I_0}{I_s}, \frac{I_1}{I_s}, \frac{I_{2cg}}{I_s}, \frac{I_3}{I_s}$  belong to a family whose dynamic response is unique. By translating the results from the nondimensional space to a dimensional space, we can produce the following graph.(See figure C.7).

This figure shows the frequency response for two members of the family. Each data point represents an angular displacement of the inertial mass on the output shaft as determined from a numerical integration with respect to its expected position for rigid body motion during operation at the given motor angular velocity. The angular displacement is an RMS displacement measured at 256 points during six cycles of the input crank after the system had reached equilibrium. For the two members of the family shown, all system stiffnesses differ by a factor of 2; damping ratios and inertias for both are the same. From the figure we see that if amplitudes are plotted vs  $\omega^2$ , points of constant response amplitude for the two family members occur at frequencies which lie on a straight line emanating from the origin. This is as expected on the basis of the system equations (12) and of dynamic similarity [64]. After the frequency response for one member of the family is obtained, these results can be extended to any other member simply by scaling the frequency axis appropriately. Having performed this analysis for a family from which a designer expects to pick a member, and having determined from design considerations the frequencies (driving frequency for example) at which energy will be introduced into the system, the designer can now pick a member of the family whose frequency response at the known input frequencies is low.

## C.7 Summary

Analysis of a four-bar linkage system with flexible input and output shafts has shown that for typical system parameters, the flexibility in the driving and driven shafts have a significant influence on the system response. Quasi-static response has been reported for a continuous parameter system model, and this response has been compared to that obtained for much



simpler lumped parameter system models. For wide ranges of system parameters, the lumped system responses are similar to those obtained from the more precise continuous system model. Values for first and second system natural frequencies are shown to vary only slightly with changes in system geometry. Two sets of nondimensionalized lumped parameter model system equations, one assuming sinusoidal mode shape for the rocker link and one using for rocker link mode shapes the shapes determined from the quasi-static analysis of the continuous model, have been integrated numerically to establish dynamic system response. Resulting plots of RMS displacement of the output shaft about its calculated rigid body motion position vs. frequency of the input shaft rotation can be examined, and from these results, and on the basis of dynamic similarity, design parameters for the system can be chosen so as to minimize RMS response at frequencies to which the system is likely to be subjected.